Maria Teresa Gonçalves Lobato de Almeida

PhD in Advanced Manufacturing Technology

Design and Fabrication of a Device for Three-Dimensional Neuronal Development

Thesis submitted to the University of Nottingham for the degree of Doctor of Philosophy



University of Nottingham
UK | CHINA | MALAYSIA

October, 2019

Abstract

The assessment of axonal growth improves our knowledge of neurological disorders, such as Alzheimer's disease (AD). Currently, axonal growth is being assessed with compartmentalised two-dimensional (2D) cell culture devices; where is possible to study and treat the neuron cell counterparts (i.e. axons) individually. However, 2D cell culture models fail in recreating the traits displayed as *in vivo* environment. Therefore, a novel three-dimensional (3D) compartmentalised cell culture device has been developed to allow the assessment of axonal growth in three dimensions within a more relevant cell environment.

The main feature of the new 3D compartmentalised prototype device consists of a physical barrier (i.e. membrane), which facilitates the isolation of axonal cellular material, by allowing only the passage of axons between the two compartments. The materials and manufacturing techniques were selected to achieve the design requirements: having such as transparency, biocompatibility and low-cost. The design of the device consists of sealing two polydimethylsiloxane (PDMS) blocks to a polycarbonate membrane. The PDMS blocks, manufactured using soft-lithography, are sealed to a polycarbonate membrane with silicone double adhesive transfer tape. As each PDMS block incorporates one compartment, the membrane allows the passage of axons between compartments without their cell bodies.

Matrigel and Agarose are two natural hydrogels that mimic the extracellular matrix (ECM) environment. Primary cortical neurons were mixed in pre-gel solutions and platted in one compartment of the new device. The neurons started to develop with their axons crossing to the other compartment. A comparison between neuron morphology and cell survival in 2D and 3D environments were achieved for up to 7 days *in vitro* (DIV). The results show that neurons growing in Matrigel form a pyramidal shape, which is closer to the morphology found *in vivo*. While Agarose neuron cultures, presented more rounded neurons with a shorter axons. This confirms that neuron development is different in hydrogel (a 3D environment) than in media (a 2D environment). In addition, it was found that using a high plating density (3.75×10^6 cells/ml) of cells in a lower concentration of Matrigel (5 mg/ml) is the optimal solution for cell survival.

Matrigel was also shown to be the best host for culturing neurons in 3D, since they presented a similar cell survival to the 2D neuron cultures. Neurons laden Matrigel showed 79% cell survival at 7 DIV, whereas neurons laden Agarose shown over 50% cell survival, and for 2D neuron cultures this was 75%.

The new 3D compartmentalised device was characterised and validated by fluidic isolation. Isolating axons from their cell bodies and keeping neurons alive and healthy during the time of culture. The fluidic isolation is achieved by applying a volume difference between two compartments, which prevents the passage of a molecule from the lower volume compartment to the higher volume compartment. The length of time a molecule is isolated in one compartment was determined by the fluorescein diffusion profile for two different hydrogel types tested: Agarose and Matrigel. Results showed that the new device was able to isolate the fluorescein in one compartment for 25 minutes in Agarose and for 8 minutes in Matrigel.

The device was validated showing 3D axonal isolation. Neurons were cultured in Matrigel, platted in the new 3D device and the axonal growth was assessed in three dimensions after 2 DIV. The new device provides the ability to conduct fast biological experiments. As this 3D device is manufactured using rapid prototyping techniques, it is simple and cost-effective to be used in most biological laboratories. Finally, the proof of concept was successfully achieved, a new device provides 3D axonal isolation, which provides more realistic experimental results.

Acknowledgements

This work would not have been possible without the help, care and support of a few people, which I could not fail to express my sincere thanks to.

Firstly, sincere thanks to my supervisors, Dr. Joel Segal for always being there when I needed; Dr. Federico Dajas-Bailador for the sharing of knowledge and; to Dr. Tomas Bellamy for counsel and support.

Thanks is also given to Dr. Raquel Ribeiro, Dr. Hala S. Dhowre, Dr. Solomon Idinyang, Dr. Cristiano Lucci, Khalid Al Mughairi and Dr. Andrew Gleadall, for the support and valuable contributions given. I would also like to thank my colleagues in the Medical School and Faculty of Engineering, for their friendship during my three years in Nottingham. With special thanks, for their care, friendship and assistance, to Lizzie Radley, Jan Warsffman, and Richard Evans.

Finally, inexpressible thanks goes to my grandmother Silvina, without whom I would not have achieved what I have today. With huge thanks to my mother and siblings.

Publications in preparation from this PhD research:

- Review – “Manufacturing Techniques applied to Neuronal Microfluidic Devices”
- Journal Paper – “Three-dimensional Axonal Isolation in a New Compartmentalised Cell Culture Device”

Table of Contents

Abstract iv
Acknowledgements vi
Publications in preparation from this PhD research: vii
Acronyms, abbreviations and Symbols xi
List of Figures xii
List of Tables xx
Chapter 1 Introduction 1
1.1 Motivation – Executive Summary 1
1.2 Aims and Objectives 2
1.3 Thesis Structure 3
Chapter 2 Literature Review 6
2.1 Neuronal Development 6
2.1.1 Neuron Polarity *in vivo* 8
2.1.2 Neuron development *in vitro* 10
2.1.3 Extracellular Matrix 12
2.1.4 2D versus 3D Neuronal Cultures 13
2.1.5 Hydrogels 22
2.2 Manufacturing and Rapid prototyping Techniques 36
2.2.1 Materials 45
2.2.2 Soft-lithography 46
2.2.3 Xurography 47
2.3 Rheology 49
2.4 *In Vitro* Neuron Culture Devices for Axon Isolation 52
2.5 Summary 55
2.6 Knowledge Gap 56
Chapter 3 Methodology 62
3.1 Microfluidic devices Fabrication 62
3.1.1 Design 62
3.1.2 Soft-Lithography 63
3.1.3 Xurography 63
3.1.4 Materials cleaning 64
3.1.5 Reversible sealing 64
3.2 Leakage Tests 64
3.3 Diffusion Profiles of the Devices 65
3.3.1 Fluorescein Solution 65
3.3.2 Diffusion Profiles in XONA device for 2D conditions 66

3.3.3 Diffusion Profiles in XONA device for 3D conditions 66
3.3.4 Diffusion Profiles in the new device for 3D conditions 68
3.3.5 Image Analysis 69
3.4 Rheology 70
3.5 Cell culture of cortical neurons 71
3.5.1 Ethics 71
3.5.2 Dissociation 71
3.5.3 Cell plating 71
3.5.4 Cell Staining 73
3.5.5 Statistical Analysis 74
Chapter 4 2D and 3D Neuronal Cell Culture 78
4.1 Introduction 78
4.2 2D and 3D neuronal cultures 79
4.2.1 Neuronal Density 79
4.2.2 Neuronal Morphology 83
4.2.3 Assessment of cell functionality using fluorescence techniques 88
4.2.1 Neuronal Viability 92
4.3 Mechanical properties of Matrigel and Agarose Matrices 99
4.4 Discussion 101
4.5 Conclusions of this Chapter 104
Chapter 5 Design and fabrication of the new 3D device 106
5.1 Introduction 106
5.2 Design of the Device 107
5.2.1 Design Choices during Fabrication 114
5.2.2 Device Fabrication 117
5.3 Cell Culture Device Characterisation 118
5.3.1 Leakage tests 119
5.3.2 Diffusion Profiles on XONA devices 121
5.3.3 Diffusion Profiles in the New Device 127
5.4 Discussion 128
5.5 Conclusions 132
Chapter 6 Neuronal Culture Assessment within new 3D Cell culture devices 133
6.1 Introduction 133
6.2 3D Axonal Isolation 133
6.3 Discussion 141
6.4 Conclusions and Questions addressed 143
Chapter 7 Conclusions and Future work 144

7.1 Conclusions 144
Chapter 8 References 147
Chapter 9 Appendices 183
9.1 Appendix 1 183
9.2 Appendix 2 184
9.3 Appendix 3 185
9.4 Appendix 4 185
9.5 Appendix 5 186
9.6 Appendix 6 190
9.7 Appendix 7 191

Acronyms, abbreviations and Symbols

AD – Alzheimer's disease

AM – Acetoxymethyl

CNS – Central Nervous System

DIV – Days in Vitro

DI – Deionised water

ECM – Extracellular Matrix

ICC – Immunocytochemistry

PBS – Phosphate buffered Saline

PC – Polycarbonate

PDMS – Polydimethylsiloxane

PI – Propidium Iodide

PMMA – Polymethylmethacrylene

3D – Three-Dimensional

2D – Two-Dimensional

List of Figures

Figure 1 – Diagram showing the thesis' structure and organisation**.....5**

Figure 2 – Schematic representation of a neuron cell, indicating the main parts of the neuron.**.....7**

Figure 3 – Neuronal polarisation in vivo for pyramidal neurons of the cortex. The radial glial cells (1) undergo asymmetric cell division and generate a new-born neurons (2). The post-mitotic neurons undergoes through a multipolar transition forming the immature neurites (3). One of these neurites extends to become the axon (4) and the cell body migrates to the cortical plate. The remaining neurites become dendrites forming pyramidal neuron (5). **.....10**

Figure 4 – Stages of neuron morphology from embryonic to mature state. Initially the neuronal cell is spherical and it starts to appear sprouts of filopodia and lamellipodia (a). Then, the immature neurites start to expand (b) and one neurite starts to grow to become an axon (c). The axon is formed and the remaining neurites form dendrites (d). **.....11**

Figure 5 – The extracellular matrix (ECM) components and their influence in the cell structure. The ECM consists in proteins, such as laminin and fibronectin, that allow the neuron growth cone components (e.g. actin) to adhere to and to move through the ECM by linking to a cell receptor known as Integrin. The ECM has collagen, which are responsible for the maintenance of the mechanical structure of ECM. Another component of ECM is known as proteoglycan, proteins connected to polysaccharide chains, which are responsible for the gel-like structure of ECM and affecting cells by binding to several cell membrane proteins.**.....12**

Figure 6 – Scheme showing 2D cell cultures procedure. The substrates, such as glass coverslips and the plastic surfaces (polysterene) of the petridishes, where cells are going to grow need to be clean and sterile. These substrates are coated with matrix proteins to allow the cell adhesion to the substrates. Then, the cells are platted, developed and their functional behaviour may be assessed using the following techniques: cell viability assay, immunocytochemistry, PCR, electrophysiology and calcium imaging. Neurons can be cultured in microfluidic devices, which consist normally in the sealing of the microfluidic device to glass or plastic surfaces. In contrary to the standard 2D cell cultures, the microfluidic devices provide the researchers the axonal/dendritic length measurement and all the other assays to characterise cell functional behaviour. **.....15**

Figure 7 – Diagram showing the polymeric chain highly negatively charged after being in contact with water (a) and the water molecule with its oxygen and hydrogen atoms charged after being attracted to the chain (b). **.....23**

Figure 8 – Scheme with examples of natural and synthetic hydrogels, with the respective advantages and disadvantages. **25**

Figure 9 – Schematic of hydrogel technique for cell culture. Cells in suspension (a) are added to a hydrogel material in a liquid state (b). After mixing cells in hydrogel, the solution is added to the cell culture system and the matrix is cross linked in order to immobilise cells in a 3D matrix, where they start to develop (c). **31**

Figure 10 – Scheme showing 3D cell cultures procedure. The substrates, such as glass coverslips and the plastic surfaces (polysterene) of the petridishes, where cells are going to grow need to be clean and sterile. The cells are platted within a 3D matrix and cells develop. The functional behaviour of cells in 3D may be assessed using the following techniques: cell viability assay, immunocytochemistry, PCR, electrophysiology and calcium imaging. **34**

Figure 11 - Scheme with the requirements for the device that is proposed to develop in this work. **38**

Figure 12 – Schematic of the soft-lithography process, with the replication of a pattern from a mould. Typically, for biological devices, replicas are made of PDMS, which are poured on the mould, cured and removed. **47**

Figure 13 – Scheme of Xurography technique, which consists in designing the features desired in a CAD software connected to the cutting plotter. The blade cuts the film to replicate the design drawn in the CAD design. Later the film that was cut is collected and incorporated into the device. **48**

Figure 14 – The linear viscoelastic region of a sample measured using a rheometer, where the storage modulus and the viscous modulus are plotted as a function of the strain. The linear viscoelastic region is determined by the strain dependence of the G' and G'' moduli. **50**

Figure 15 – Rheological frequency sweep tests for materials showing the storage modulus (G') and the loss modulus (G''). **51**

Figure 16 – Schematic design of microfluidic cell culture devices for axon isolation. a) Top view of the compartmentalised XONA device, showing the soma compartment where the neurons are seeded. The cells begin to polarize and its neurites grow. The axons cross to the axon side through the microgrooves. b) Section view: fluidic isolation of cell bodies from the soma side is achieved by applying an asymmetric media volume (hydrostatic pressure) between the two sides. **54**

Figure 17 – Diagram showing why axonal isolation is important and why cells should be studied in 3D. **60**

Figure 18 – Schematic of axonal isolation in a 2D environment (left) and in a 3D environment (right), where neuron development is represented in blue. In the 2D

culture, neurons have a limited growth with a flattened shape attached to the surface, whereas for the 3D culture neurons are unrestricted with axonal isolation possible in 3D**. 62**

Figure 19 – Schematic representation of the process of the soft-lithography. A mould containing desired features (a) is used to replicate those features onto PDMS. Replicas are made of PDMS, which is first poured onto a mould (b) and then cured for 3 hours at 70° C (c). After curing, the PDMS is removed by peeling it off from the mould. **.....63**

Figure 20 – PDMS block is sealed to double adhesive tape (a). The opposite side of the tape is sealed to the membrane (b). The other side of the membrane is sealed to tape (c) and the free side of tape is sealed to other PDMS block (d)**. 65**

Figure 21 – Schematic representation of methodology used to determine the diffusion profiles in XONA devices for 2D environment conditions.**.....66**

Figure 22 – Schematic representation of the methodology used to determine the diffusion profiles in XONA devices for 3D conditions. First step, Matrigel to the device in pre-gel solution. Second, the gel is formed by placing the device in the incubator, following the addition of fluorescein and PBS to the device**.....67**

Figure 23 – Schematic representation of the methodology used to determine the diffusion profiles in the new 3D device. First step, a pre-gel solutions of Agarose or Matrigel was introduced in the device. Second, the gel is formed by placing in the incubator, following the addition of fluorescein and PBS to the device.**.....68**

Figure 24 – Schematic representation of the regions of interest in the axon side (blue dotted lines) and soma side (green dotted lines) in the XONA device (a) and in the new device (b). **.....70**

Figure 25 – Representative phase contrast images (10x) of neurons cultured in both 2D growth media and Matrigel after two days in vitro. **.....81**

Figure 26 – Representative phase contrast images of neurons cultured in both 2D growth media and Matrigel after four days in vitro. **.....82**

Figure 27 – Representative phase contrast images 20x of primary cortical neurons in 0.5% (v/v) Agarose and 5 mg/ml Matrigel acquired at DIV 0, 2, 5 and 7, to evaluate their morphology.**.....85**

Figure 28 – Diagram of phase contrast images of neurons growing in 3D Matrigel in different dimensions, 10 days after plating achieving a gel thickness of 210 µm. It is possible to visualise neurons growing at a 3D structure. **.....86**

Figure 29 – Phase contrast images of a 3D Matrigel matrix with neurons cultured in 10 DIV, in the same position with different Z plan.**.....87**

Figure 30 – Trial of immunocytochemistry in primary cortical neurons within Matrigel matrix at a concentration of 5 mg/ml. Where the matrix was still depolymerised and it was not possible to visualise the neuron cell networks in 3D, even because cells were also washed away with some part of the part of the matrix. Neurons were fixed with 2% paraformaldehyde and stained with DAPI to label the nucleus and to stained with βIII-Tubulin. Imaged in a widefield fluorescence microscope with 10x. **..... 89**

Figure 31 – Confocal image of neurons growing within Matrigel labelled with Calcein AM at DIV2. Scale bar 50 µm. **..... 90**

Figure 32 – Images of labelling neurons in 3D with Calcein AM, where neurons are labelled with green at DIV 2 at 10x with a widefield microscope. **..... 91**

Figure 33 – Representative images of live/dead assay in 2D neuron cultures at 2DIV (a), 5 DIV (b) and 7 DIV (c). The percentage of living cells for DIV 2, 5 and 7. The data shown mean± SEM (n=3). **..... 93**

Figure 34 – Representative images of live/dead assay in 2D neuron cultures at 7 DIV at 20x. **..... 93**

Figure 35 – Neuronal survival assessed at DIV 2, 5 and 7, in Matrigel and in Agarose. Live cells were labelled with Calcein AM (shown in green) and the dead cells stained with Propidium Iodide (shown in red). The percentage of living cells is shown at DIV 2 (g), DIV 5 (h) and at DIV 7 (i). The data shown mean± SEM (n=3), using one way-ANOVA with Tukey's test (c), with ** $p < 0.01$ and with *** $p < 0.001$. Images were deconvoluted with Huygens Software. **..... 94**

Figure 36 – Deconvoluted imaged of live/dead assay in neurons laden Matrigel (5 mg/mL) within 2DIV, neurons are labelled with Calcein AM (live cells) and P.I. (dead cells). Huygens was the software used to remove background. **..... 95**

Figure 37 – Deconvoluted imaged of live/dead assay in neurons laden Agarose (0.5%) within 2DIV, neurons are labelled with Calcein AM (live cells) and P.I. (dead cells). Huygens was the software used to remove background. **..... 95**

Figure 38 – Deconvoluted imaged of live/dead assay in neurons laden Matrigel (5 mg/mL) within 5DIV, neurons are labelled with Calcein AM (live cells) and P.I. (dead cells). Huygens was the software used to remove background. **..... 96**

Figure 39 – Deconvoluted imaged of live/dead assay in neurons laden Agarose (0.5%) within 5DIV, neurons are labelled with Calcein AM (live cells) and P.I. (dead cells). Huygens was the software used to remove background. **..... 96**

Figure 40 – Deconvoluted imaged of live/dead assay in neurons laden Matrigel (5 mg/mL) within 7DIV, neurons are labelled with Calcein AM (live cells) and P.I. (dead cells). Huygens was the software used to remove background. **..... 97**

Figure 41 – Deconvoluted imaged of live/dead assay in neurons laden Agarose (0.5%) within 7DIV, neurons are labelled with Calcein AM (live cells) and P.I. (dead cells). Huygens was the software used to remove background. **.....97**

Figure 42 – The percentage of viable cells assessed as a function of cell culture environment (2D culture, Matrigel culture, Agarose culture) at DIV 2, 5, 7. The data shows mean ± SEM (n=3). One way NOVA with Tukey's test where ** $p < 0.01$ and *** $p < 0.001$.**.....99**

Figure 43 – Strain sweeps amplitude results for Matrigel (a) and Agarose (b) matrices to obtain the linear-viscoelastic limit, which is determined with respect to the strain. The strain sweeps were carried out with a fixed frequency of 1 Hz. Frequency sweeps results for Agarose (c) and in Matrigel (d) at 1% strain. Both oscillation tests were repeated three times**.....100**

Figure 44 – Illustration of axonal isolation from cell bodies by a polycarbonate membrane with a pore diameter of 5 µm. Axons are isolated in 3D within the hydrogel, which provides the mechanical and biochemical host environment. **.....106**

Figure 45 – Image of the design to transmit to a master mould by photolithography technique. After which, the master is employed in soft-lithography to get bulk layers of PDMS with these features. This design allows the fabrication of 6 bulk layers of PDMS that are later sealed one on top of the other. **.....108**

Figure 46 – Two different proposed techniques to build the 3D physical barrier for axon isolation (200 µm x 200 µm x 200 µm), which holes spaced at 20 µm intervals with 5 µm diameter: a) barrier fabricated with microgrooves; b) barrier fabrication by layers, where each layer forms the microgrooves.**.....109**

Figure 47 – SEM image of a barrier structure made of Ormocer material by two-photon polymerization. **.....109**

Figure 48 – Layer-by-layer of two XONA devices with neurons laden matrigel (a). Cells did settle in the direction of the surface. There is no force that will make then go inside the cell culture chamber from the top XONA device. After 1 DIV cells were dead.**.....111**

Figure 49 – 3D device (22 x 22 x 10 mm) consisting in two holes: one on top that is a reservoir (5 mm in diameter) and a second hole that corresponds to the channel (10 x 7 x 3 mm). The device consists of two PDMS blocks connected to each other, forming a long channel divided by a polycarbonate membrane (a). Adhesive tape is used to seal the two PDMS blocks either side of the polycarbonate membrane, resulting in the configured platform: PDMS block–tape-membrane-tape-PDMS block. The underside of the platform is sealed to the glass substrate with a reversible bonding (b). **.....113**

Figure 50 – Strategies to develop a lateral hole in the reservoir's block and how to ensure a smooth flat surface (a, b, c, d). **114**

Figure 51 – PDMS blocks extracted from the moulds. a) Simple PDMS block, with two punches made, one for the lateral hole and the other for the reservoir (Figure 50a); b) PDMS reservoir with a lateral hole made from a cubic form located next to the mould (Figure 50b); c) A lateral hole fabricated in the middle of one of the PDMS faces (Figure 50c); d) PDMS block with a channel along its surface (Figure 50d). **116**

Figure 52 – Strategy used to fabricate PDMS blocks: a) PDMS block casted from the mould; b) reservoir punch in the PDMS block. **116**

Figure 53 – Following the proposed strategy, two one compartment PDMS block are sealed by double adhesive tape (a). One side of the tape is sealed to the membrane (b), and the other side of the membrane is sealed to other tape (c), which is sealed to the second compartment (d). **117**

Figure 54 – Flow characterisation experiments to test the proposed sealing method (a) showing a perfect seal (b) between XONA devices and the glass substrate in the beginning of the experiment (left side) and after 2 hours of experiment (right side). The white area corresponds to the axon side, where Fluorescein is placed, whereas the black area corresponds to the soma side, which is not filled with Fluorescein. Example of sealing issues within the new device (c – left hand image), showing no isolation between cells and a good sealing in the new device (c – right hand image), where cells are isolated in one compartment. **120**

Figure 55 – Leakage test in the new cell culture device showing no leakage after top up. First, one side of the device was topped up with Ponceau dye (red) (a) and the other side was filled with Coomassie dye (blue) (b). No fluidic leakage was visible in the device, proving the device was successfully sealed. **121**

Figure 56 – 2D Diffusion profiles in the XONA device. a) The devices were filled with 160 µl of PBS solution added to the soma compartment and 100 µl of fluorescein (1 µM) in the axonal compartment. Square in red represent the area of image acquisition. b) Fluorescence intensity values are plotted as a function of time, where images were taken every 15 minutes over a 15 hours period. The fluorescence intensity was normalised to the maximum intensity value recorded. All trials were repeated three times. **123**

Figure 57 – 3D Diffusion profiles in the XONA device. a) For the 3D conditions the devices were filled with 160 µl of Matrigel (5 mg/ml) added to the soma compartment and 100 µl added to the axonal compartment. After filling the devices with Matrigel, they were placed inside the incubator at 37°C for 30 minutes. After which, 160 µl of PBS was added to the soma compartment and 100 µl of fluorescein (1 µM) to the axonal compartment. Squares in red represents the area of image acquisition. b) The

fluorescence intensity values are plotted as a function of time, where images were taken every 15 minutes for a 48 hour period. The fluorescence intensity was normalised to the maximum intensity value recorded. All trials were repeated three times. **.....125**

Figure 58 - Diffusion profiles for Matrigel within the XONA device at 24 hours. The micrograph images have coloured lines, which corresponds to the fluorescein intensity values in different directions. Each line is plotted as a function of the x position.**.....126**

Figure 59 – 3D Diffusion profiles in the new cell culture device. a) For each device, the soma side was filled with 250 µl of pre-gel solution (0.5% Agarose or 5 mg/ml Matrigel), while the axon side had 200 µl of pre-gel solution. After forming a gel, 200 µl of PBS was added to the soma side and 50 µl of fluorescein (1 µM; 400 Da) to the axonal side. The squares in red represent the area of image acquisition. Diffusion profiles in the new device obtained for both the Agarose (b) and Matrigel (c) matrices. Fluorescence intensity values are plotted as a function of time. The images are taken every 2 seconds over a 1 hour period. The fluorescence intensity is normalised to the maximum intensity value, with each experiment repeated three times.**.....128**

Figure 60 – Bright Field images of axons starting to cross the membrane at 2DIV.**.135**

Figure 61 – Phase contrast images showing axons growing in 3D after 4 days in culture. Each frame is taken at a distance of 6 µm between each other in the z-stack. **.....136**

Figure 62 – Representative phase contrast image of isolated axons from their cell bodies in Matrigel within the new device at 4 days in culture. Each image is separated by 10 µm distance between each other in the stack. Higher magnification images are shown in Appendix 7. **.....137**

Figure 63 – Representative phase contrast image of axons crossing the membrane at DIV 4.**.....138**

Figure 64 – Representative phase contrast image of axons crossing the membrane without cell bodies at DIV 4. **.....138**

Figure 65 – Percentage of axonal growth at t=0 (a) and measurement of axonal growth rate (b) in the XONA device. The data was normalised to the mean value at DIV 5, with an axonal growth of 1.54 µM per day. The data show mean ± SEM (n=3). **.....139**

Figure 66 – Percentage of axonal growth at t=0 (a) and measurement of axonal growth rate (b) in the new 3D device. The data was normalised to the mean value at DIV2, with an axonal growth rate of 1.74 µM per day. The data shown mean ± SEM (n=3). **.....139**

Figure 67 – Representative confocal image of axons isolated in the new 3D device at DIV 5. The line in blue represents a membrane. **141**

Figure 68 – Schematic representation of the new device with axons shown in blue and astrocytes shown in orange growing in a 3D environment. **146**

Figure 69 – The novelty of the project, as no one has never considered to isolate axons from cell bodies in 3D, with different Z-coordinates, which mimics the brain cytoarchitecture. As expressed above in neuronal development, the ability to isolate the axons allow to study the proteins that regulate the mechanisms for axonal regeneration. **146**

Figure 68 – Schematic representation of the vector diagram showing the components G' and G'', which result vector is the shear modulus G. **183**

Figure 69 – Setup of Matrigel manipulation, where media, Matrigel and well plates and devices, are placed in a recipient filled with ice. **185**

Figure 70 – Fluorescence intensity for 3D conditions in XONA devices at 4 hours. **186**

Figure 71 – Fluorescence intensity for 3D conditions in XONA devices at 20 hours. **187**

Figure 72 – Fluorescence intensity for 3D conditions in XONA devices at 24 hours. **188**

Figure 73 – Fluorescence intensity for 3D conditions in XONA devices at 48 hours**.** **189**

Figure 74 – Flow curves of agarose 1%, 0.75%, 0.5% (a) and Matrigel at 8 mg/ml and 5 mg/ml (b) at a constant temperature of 37°C. **190**

Figure 75 – Phase contrast images showing 3D axonal isolation, where axons are isolated growing in 3D. **191**

Figure 76 – Continuation of the image from Figure 57**.** **192**

List of Tables

Table 1 – Summary of main techniques applied in the development of medical devices, as well as associated resolution and the materials typically used**.** ... **39**
Table 2 – Range of wavelengths for the respective lithography technique. **... 41**
Table 3 – List of the materials used in this PhD work. **76**
Table 4 – List of the equipment used in this PhD work. **77**
Table 5 – List of the software used in this PhD work. **77**
Table 6 – Different cell and Matrigel concentrations were investigated. The respective concentrations of cells were applied in media and in Matrigel to compare neurites survival and polarisation between 2D and 3D environments. **80**
Table 7 – Volumes of gel inserted in the axon and soma compartment within Agarose..... **122**

Chapter 1 Introduction

1.1 Motivation – Executive Summary

Research on neural development is of great importance to improve the understanding of brain function and human illness. The role of neuronal connectivity has been intensively investigated from the embryonic up to mature state; in response to biological, chemical and physical cues and cell malfunction (Yamamoto, Tamada and Murakami, 2002; Yu, Leipzig and Shoichet, 2008; Millet and Gillette, 2012b). Any disruption on neuronal connectivity can lead to nervous system dysfunction and disease, such as Alzheimer's and Parkinson's disease or spinal cord injury (Millet and Gillette, 2012b). Much of the current knowledge regarding neuronal cells comes from conventional two-dimensional (2D) cultures, where cells are seeded onto flat, stiff materials (e.g. glass), forming a flattened cell shape and morphology that leads to abnormal polarisation and an altered response to pharmaceutical reagents (Caliari and Burdick, 2016; Langhans, 2018). This in turn causes a loss in the cells' phenotype, making the culture and analysis of nervous system cells in three-dimensional (3D) environments an important area of research (Antoni *et al.*, 2015; Caliari and Burdick, 2016). The advantage of native cells grown in 3D is that they can receive signals from all their surroundings. For cells developed in 2D, only one side is exposed to biochemical cues (Millet and Gillette, 2012a; Edmondson *et al.*, 2014). Hydrogels are now being used to provide this 3D microenvironment, being able to better mimic the extracellular matrix (ECM) native elements (Mark W Tibbitt and Anseth, 2009; Geckil *et al.*, 2011).

Over the years, many research groups have exploited compartmentalised devices with interconnected microgrooves to specifically grow axons separated from the cell bodies into fluidically isolated compartments, thus enabling biochemical and functional analyses of pure axonal processes (Taylor *et al.*, 2005; Hengst *et al.*, 2009; Dajas-bailador *et al.*, 2012, 2014a, 2014b; Blizzard *et al.*, 2015; Briese *et al.*, 2015; Reginensi *et al.*, 2015; Yao *et al.*, 2015; Zhang *et al.*, 2015; Cosker *et al.*, 2016; Kneynsberg *et al.*, 2016; Yap *et al.*, 2017; Ohtake *et al.*, 2018; Jia *et al.*, 2018; Zheng *et al.*, 2019; Lucci *et al.*, 2020). In addition, compartmentalised devices allow a fine control over the neuron microenvironments, the study of their connectivity with other cells and/or their response to cues (such as axon guidance molecules and signalling cues) in specific subcellular regions providing also the opportunity to study local processes relevant for axon development, synapse formation and regulation, and axonal/synapse degeneration (Taylor *et al.*, 2005; Hengst *et al.*, 2009; Millet and Gillette, 2012a; Virlogeux *et al.*, 2018).

Although a wide selection of compartmentalised chambers for 2D neuronal cell culture are now currently available, an effective counterpart device that allows to mimic a 3D neuronal environment is still largely missing. Work presented in this thesis aims at developing a new 3D compartmentalised device, fabricated and tested with a 3D structure, to allow a more representative modelling of the *in vivo* environment. Using such new device, with new capabilities, will make it possible to observe the cellular interactions and investigate their function in a more “biologically relevant” microenvironment; helping to drive neurological research. For example, investigating cell-cell interaction and the transmission of information between different cell types.

1.2 Aims and Objectives

This project aims to answer the following research questions: *Would it be possible to design and manufacture a new cell culture device that could became the bridge between conventional cultures and the complex in vivo environment, allowing for compartmentalisation of axons and cell bodies in a 3D microenvironment? How easy will it be to fabricate a barrier for the isolation of axons? Will it be possible to assess the viability of cells in this new cell culture device coupled with a 3D barrier?*

In order to achieve this aim, this project has the following objectives:

- Establish the protocols for the culture and characterisation of cells growing in a 3D configuration. Investigating the cell morphology and neuron viability in both cell culture methods (i.e. 2D and 3D).

- Characterise the biomaterials used to host neuronal cells, providing the mechanical structure for them to grow as would in the native tissue. Measure the stiffness of the biomaterial and evaluating its viscosity.

- Design a device as a first approach to allow axonal isolation in three dimensions, incorporating features for axon growth and isolation, as well as being made from transparent, portable and biocompatible materials. It must be easy to fabricate using inexpensive and rapid prototyping techniques.

- Establish for how long compartmentalised isolation of a soluble molecule can be achieved within existing and new devices. Confirm the maximum achievable duration for fluidically isolated cell experiments (i.e. for the testing of local drug treatments).

- Provide a new method to study axonal function in a fluidically isolated condition, making it closer to the environment in the native tissue. The ability to isolate axons in a 3D environment will provide neuroscientists with new possibilities to obtain results closer to the reality of neuronal networks *in vivo*.

1.3 Thesis Structure

The thesis structure, as presented in **Figure 1**, is as follows:

- Chapter 1 describes the motivation of the project and the aim and objectives of the research.

- Chapter 2 provides a brief introduction to neuronal morphology and function; including previous studies; materials; manufacturing processes and a description of the relevant neuronal characterisation techniques employed.

- Chapter 3 includes the methods used to address the questions of this PhD thesis, including fabrication techniques used to build the devices, mechanical tests carried-out (methods to ensure fluidic isolation inside the devices), cell culture characterisation techniques, both in 2D and 3D environments.

- Chapter 4 contains details about the neurons' survival, morphology and differentiation in normal culture dishes for both environments (2D and 3D). It provides a comparison between neurons growing within 2D and 3D environments and a comparison of neuron behaviour between two different 3D environments (neuron laden agarose and neuron laden Matrigel).

- Chapter 5 reports the design of the newly developed device, manufacturing techniques employed and the respective protocols for how to fabricate the new 3D prototype devices for isolation of axons. The chapter includes the strategies, methods and challenges found in fabricating the devices.

- Chapter 6 describes the 3D axon isolation devices and how to analyse neurons for validation of the device.

- Chapter 7, indicates the overall discussion, conclusions made from this PhD, the relevance in the field of study and future applications.

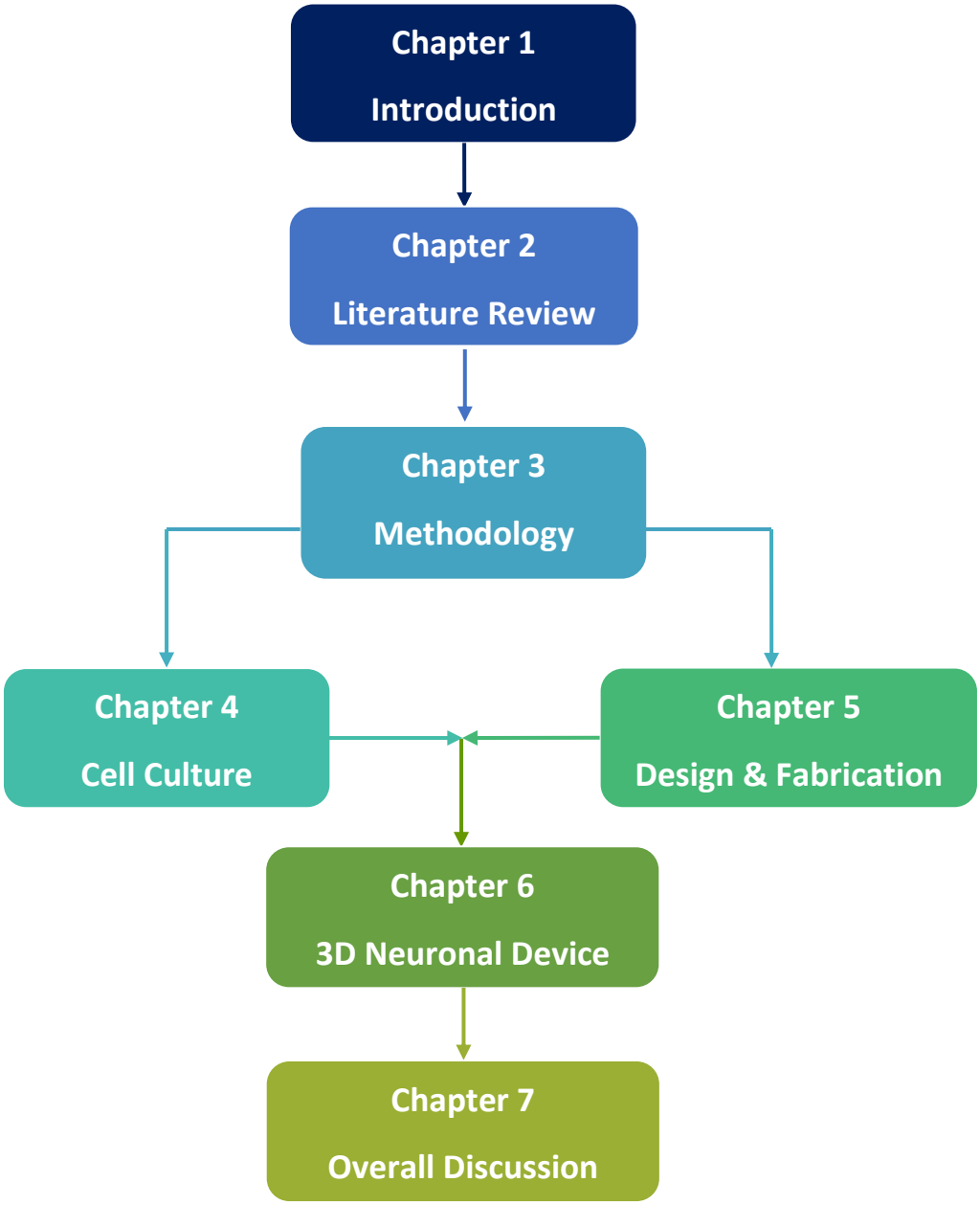


Figure 1 – Diagram showing the thesis' structure and organisation.

Chapter 2 Literature Review

2.1 Neuronal Development

The nervous system consists of a complex network of neurons and non-neuronal glia cells, which is responsible for controlling activities such as emotion, thinking and behaviour of humans (Wang *et al.*, 2009; Price *et al.*, 2011). The process behind the making of the nervous system is known as neuronal development and that occurs during the embryonic phase up to after birth (Wang *et al.*, 2009; Price *et al.*, 2011). Neurons are responsible for the transmission of information within the brain and are composed of a cell body, dendrites and usually a single axon, as shown in **Figure 2**. The dendrites are highly branched neurites, allowing morphological diversification of the receptive area of a neuron and maximizing the communication between cells (Price *et al.*, 2011; Parekh and Ascoli, 2013; Budday, Steinmann and Kuhl, 2015). They receive the incoming signals and re-transmit them to the cell body, whilst, the axons transmit the signals and communicate with other targets *via* the thousands of connections between neurons, thus leading to the formation of a highly interconnected nervous system. (Debanne, 2004; Taylor *et al.*, 2005; Park *et al.*, 2006, 2009; Bae *et al.*, 2010; Price *et al.*, 2011; Millet and Gillette, 2012b; Lewandowska *et al.*, 2015).

Non-neuronal glia cells are the second most abundant type of cells in our central nervous system (CNS). These type of cells are crucial during development, as they are involved in the regulation of synaptic functional mechanisms (Shi *et al.*, 2013), neurons excitability (i.e. in pain processes), neuronal migration, neurite outgrowth and communication between cells. Co-cultures of glia and neuron cells are important to develop biological models to study cellular behaviour (Millet and Gillette, 2012a).

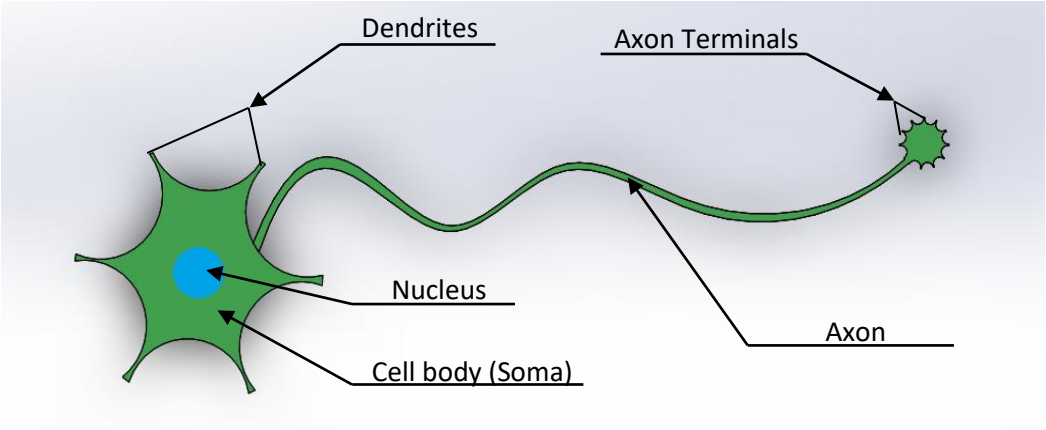


Figure 2 – Schematic representation of a neuron cell, indicating the main parts of the neuron.

When the axons are damaged, a breakage of information occurs between neurons. In the CNS, once axons are degenerated, they are unable to regenerate successfully, and any pathological processes affecting their function and viability could lead to impairment of connectivity and ultimately neuron death (Lingor *et al.*, 2012; Li and Chen, 2016; Hilton and Bradke, 2017). The axons from the central nervous system fail to regenerate due to the limited axonal growth capacity present once maturity is achieved (Debanne, 2004; Taylor *et al.*, 2005; Park *et al.*, 2006; Chiu, Alqadah and Chang, 2014; Haggerty, Marlow and Oudega, 2016). In this context, axonal damage becomes a critical part of the etiology of neurodegenerative diseases, such as Alzheimer's and Parkinson's disease (Amor *et al.*, 2010; Lingor *et al.*, 2012; Hussain *et al.*, 2018). Therefore, it is important to continue investigating new treatments, as well as the development of new methodologies to improve axonal function studies. The development of methods to study specific molecular and signalling events in axons are extremely important to study axon biology. Consequently, finding ways to physically and functionally separate the axons from their soma (cell bodies) becomes crucial to depict cellular processes into a specific sub-cellular compartment. A physical structure (barrier in the microfluidic device) must allow only the passage of axons through smaller features than 10 µm, since the size of cell bodies can range from 10 µm up to 100 µm. However, an axon can achieve one meter in length and 0.1 - 0.2 µm in diameter (Debanne, 2004; Price *et al.*, 2011; Lewandowska *et al.*, 2015).

2.1.1 Neuron Polarity *in vivo*

Neurons are the most complex and specialised cells within our body. As said above, with their long axon and dendrites, they can form an intricate network with hundreds of millions of connections known as synapses. Even if neurons in the mammalian brain are not a homogenous entity, coming in different types and having different morphological and functional properties, they all have to break the symmetry, and to polarise into distinct functional domains, which are normally defined as the axon and the somatodendritic (Dotti, Sullivan and Banker, 1988). In the mammalian cortex, most of neurons are the excitatory type, and in this thesis, I will mostly discuss this population of cells.

During neuronal development, neural stem cells (NSCs) generate most of cell types in the cortex, including excitatory neurons, astrocytes and oligodendrocytes (Gallo and Deneen, 2014). These stem cells undergo a series of symmetric divisions in order to self-renew and increase their number, until, with the onset of neurogenesis, they start producing post-mitotic neurons. Depending on the cortical layer location and type of projection, morphology of excitatory neurons can vary. However, many excitatory neurons resemble so-called “pyramidal cells” and migrate through the developing cortex. The cells migrate from the proliferative region, known as ventricular zone, up to a thick layer called cortical plate (Arimura and Kaibuchi, 2007; Price *et al.*, 2011). The cells in the ventricular zone that have processes along the developing cortex are known as radial glia, as seen in **Figure 3**. The radial glia divides to generate new-born neurons and guide them during the migration process, which results from the response of neuronal cells to environmental cues. Besides, the neurons undergo polarisation, which is the process that refers to the differentiation of neurites into dendrites and axon, while they migrate (Arimura and Kaibuchi, 2007; Price *et al.*, 2011).

In fact, during migration, neuron goes through a multipolar transition, where neurites start to appear from the soma. After this phase the neuron initiates radial translocation along a radial glial process and leaves behind a trailing process which elongates tangentially in the intermediate zone. The cell body continues to translocate toward the cortical plate and its final destination, whilst the axon rapidly elongates and the leading process gives rise to the dendrite which initiates local branching in the marginal zone just above the cortical plate. (Arimura and Kaibuchi, 2007; Anthony P Barnes and Polleux, 2009; Price *et al.*, 2011).

The neuron polarisation is essential for neuronal function, and for the axon to acquire its identity and to be able to transmit information to post-synaptic target and establish neuronal networks (Arimura and Kaibuchi, 2007; Anthony P. Barnes and Polleux, 2009; Polleux and Snider, 2010).

After axon specification, growth represents another important process of axon development, and is directly linked to axon guidance towards post-synaptic targets (Stoeckli, 2018). Axons grow at their tips *via* the growth cone, a highly dynamic structure capable of sensing and integrating several signals that, by converging on cytoskeletal dynamics, eventually lead the axons to their targets (Lowery and Vactor, 2009). Growth cones can detect extracellular signals through an actin-rich and highly dynamic membrane-limited structures called filopodia. Their surface membranes are enriched of receptors for the molecules that serve as directional cues for the axon. The processes of elongation is then generated by the coordinated action of both actin and microtubule dynamics (Price *et al.*, 2011). Among the signals released in the extracellular space that can influence growth, the most important is the Transforming Growth Factor beta (TGF-β), which is released in the ventricular zone and can promotes the axon growth during the development of cortical neurons (Yi *et al.*, 2010). It is worth noting that any extracellular signal uptaken by the cells, can then influence intracellular pathways that in turn impinge on microtubule and actin dynamics (Hur *et al.*, 2011).

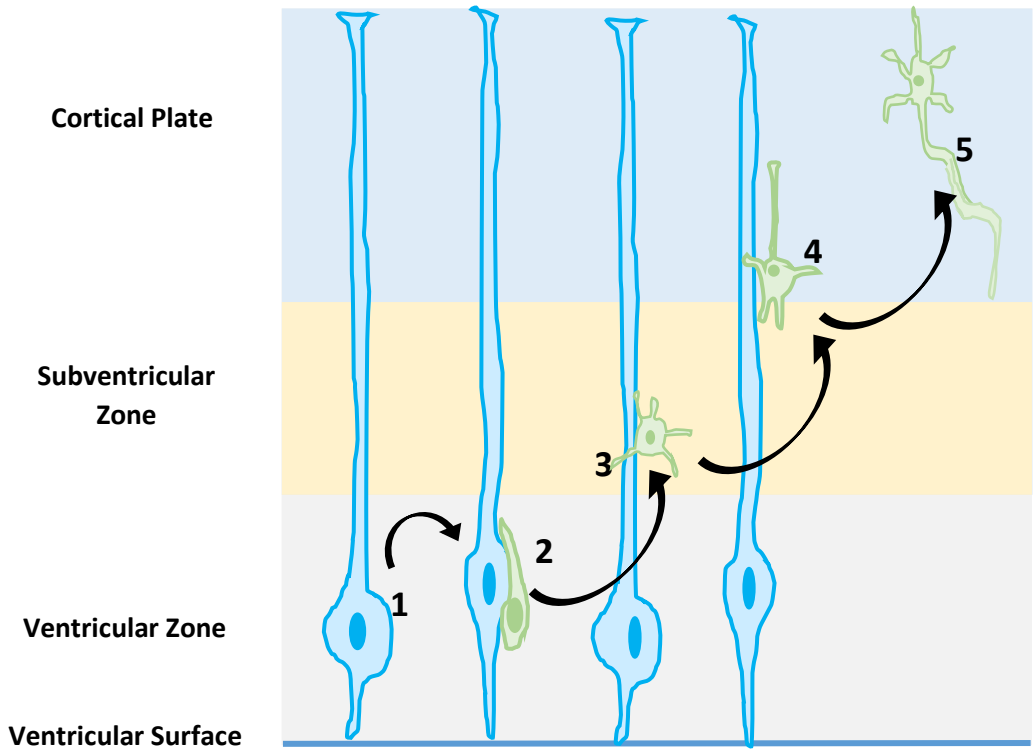


Figure 3 – Neuronal polarisation *in vivo* for pyramidal neurons of the cortex. The radial glial cells (1) undergo asymmetric cell division and generate a new-born neurons (2). The post-mitotic neurons undergoes through a multipolar transition forming the immature neurites (3). One of these neurites extends to become the axon (4) and the cell body migrates to the cortical plate. The remaining neurites become dendrites forming pyramidal neuron (5).

2.1.2 Neuron development *in vitro*

After dissociation of neuronal cells (separated from *in vivo* tissue), neurons are plated using *in vitro* culture techniques and start to develop and polarise, despite being outside of their native three-dimensional (3D) environment. The processes of morphological changes during neuronal polarisation are shown in **Figure 4** (Arimura and Kaibuchi, 2007; Polleux and Snider, 2010). Initially, after neurons are plated, they have a spherical morphology (**Figure 4a**) and after a few hours, cells start projecting immature neurites (**Figure 4b**). After 36 hours one neurite start extending more than others and will become the future axon (**Figure 4c**), and after 7 days of plating, the axon terminals of the neurons start to develop into synapses (**Figure 4d**).

After 14 days in culture, neurons are fully mature and can potentially establish a fully active neuronal network (Arimura and Kaibuchi, 2007; Namba *et al.*, 2015). The fact that dissociated cortical neurons *in vitro* are still able to break the symmetry and to polarise even if they are outside their physiological environment and in absence of the aforementioned extracellular cues, it suggests that axon specification is also an intrinsic mechanism regulated by intracellular signalling cascades. In fact, over-expression and downregulation studies of candidate genes involved in polarity have revealed over the years an intricate and complex network of signalling molecules that orchestrate the formation of the axonal domain (Takano, Funahashi and Kaibuchi, 2019).

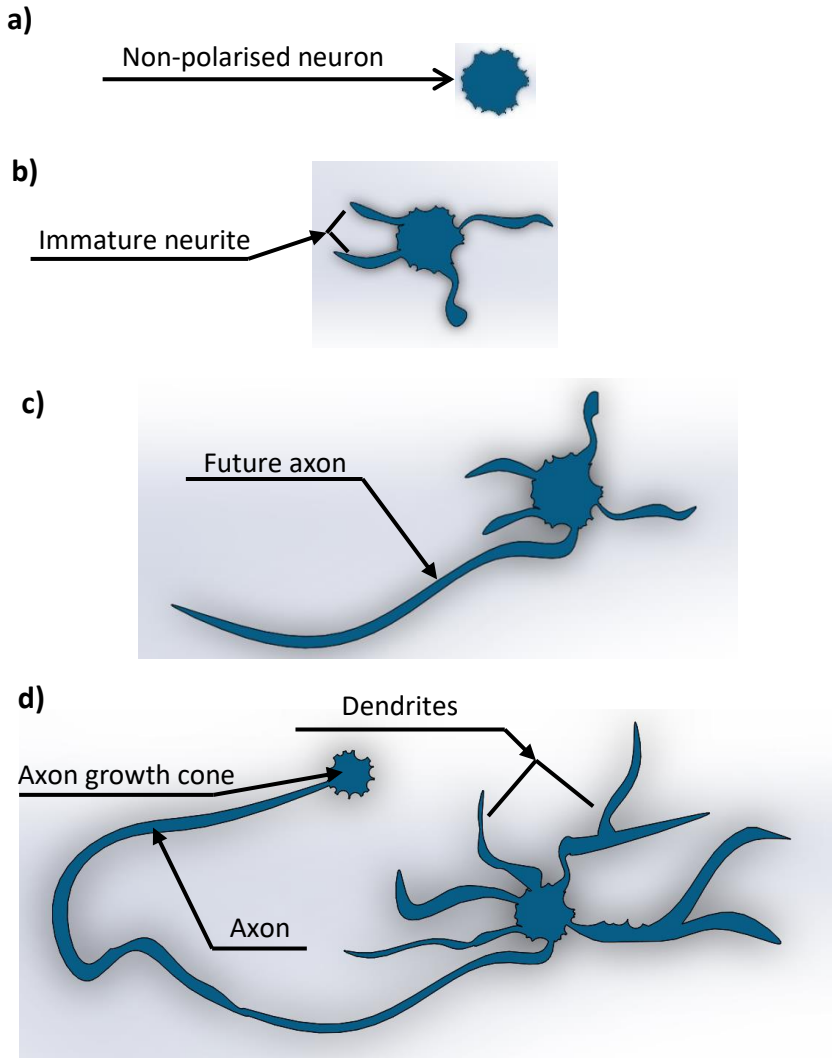


Figure 4 – Stages of neuron morphology from embryonic to mature state. Initially the neuronal cell is spherical and it starts to appear sprouts of filopodia and lamellipodia (**a**). Then, the immature neurites start to expand (**b**) and one neurite starts to grow to become an axon (**c**). The axon is formed and the remaining neurites form dendrites (**d**).

2.1.3 Extracellular Matrix

Neuronal cells are contained in a soft and flexible matrix, being part of the white and gray matter, known as extracellular matrix (ECM) (Bae *et al.*, 2010). In particular, ECM mediates the axon guidance and growth in our neuronal system (Haggerty, Marlow and Oudega, 2016). The ECM is in constant change, being remodelled several times during tissue development, from the embryonic to its mature stage (Rozario and Desimone, 2010). ECM is composed by proteins, water, polysaccharides, and cellular components within its structure (Frantz *et al.*, 2010), as well ECM receptors, like integrins, as seen in **Figure 5**.

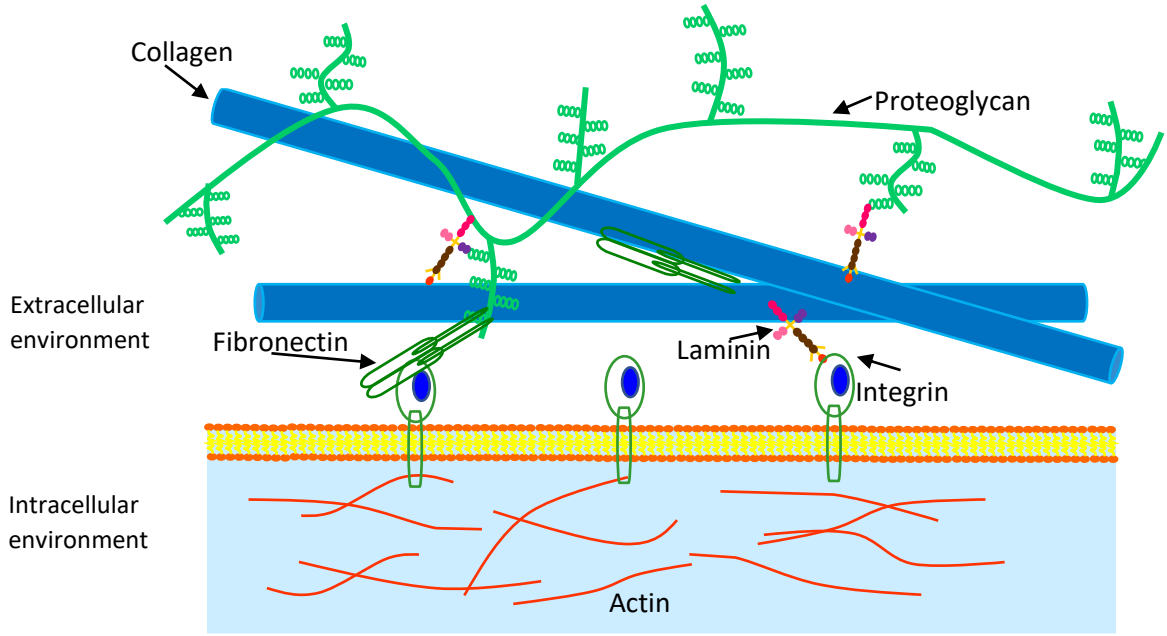


Figure 5 – The extracellular matrix (ECM) components and their influence in the cell structure. The ECM consists in proteins, such as laminin and fibronectin, that allow the neuron growth cone components (e.g. actin) to adhere to and to move through the ECM by linking to a cell receptor known as Integrin. The ECM has collagen, which are responsible for the maintenance of the mechanical structure of ECM. Another component of ECM is known as proteoglycan, proteins connected to polysaccharide chains, which are responsible for the gel-like structure of ECM and affecting cells by binding to several cell membrane proteins.

Two main groups of macromolecules that compose the ECM are the proteoglycans and the fibrous proteins, such as collagens, fibronectins and laminins (Ruoslahti, 1996; Frantz *et al.*, 2010). Proteoglycans are proteins with important role in cell surfaces, regulation of cell adhesion and growth factors, on neurite growth, in the architecture and offer resistance to compressive forces involved in ECM structure (Ruoslahti, 1996; Griffith and Swartz, 2006). Fibrous proteins, such as fibronectins, are involved in cell adhesion and migration, having a role in repairing damage tissues (Haggerty, Marlow and Oudega, 2016). For example, Laminins are involved in cell growth and they act as guidance molecules for axon growth (Ruoslahti, 1996). Besides, laminins modulate the interaction between cells and substrate (Saneinejad and Shoichet, 1998). Integrins, another component of the ECM, are responsible for the cytoskeleton adhesion to the ECM (Gullberg and Ekblom, 1995; Frantz *et al.*, 2010; Schmidt and Friedl, 2010).

The ECM is important for cell culture studies, since it provides structure; transduces the mechanical and chemical signals (Rozario and Desimone, 2010); has significant influence on cell interactions; and on the changes in morphogenetic processes (Saneinejad and Shoichet, 1998; Frantz *et al.*, 2010). However, most studies of neuronal cultures to date have been carried out in relatively simple 2D environments, with little attempt to model the complexity of ECM and 3D contexts.

2.1.4 2D versus 3D Neuronal Cultures

A vast amount of *in vitro* studies are based on two-dimensional (2D) cell culture methods and despite the undoubted contributions given by these studies in neuron function and development, cells growing in two dimensions present a cell morphology that might not reflect a physiological phenotype (Yamada and Cukierman, 2007; Edmondson *et al.*, 2014; Watson *et al.*, 2017). In 2D cell culture models, cells are normally cultured onto hard substrates, such as plastic or glass surface. Neuron cells adhere to the rigid surface and grow in two dimensions, resulting in non-physiological cell morphology (Griffith and Swartz, 2006; Edmondson *et al.*, 2014; Virlogeux *et al.*, 2018). When cells grow in two dimensions, there is a loss of phenotype due to the relative lack of cell-matrix interactions, which leads to altered cell behaviour; such as gene expression and growth features (Antoni *et al.*, 2015; Duval *et al.*, 2017).

When cells lose their phenotype, they promote a lack of compatibility with *in vivo* systems. The interaction between cells occurs on its edges receiving biochemical signals on only one side, since most of the cell is in contact with the surface. As a result, cells in 2D cultures do not grow in the same way to those in our body (Duval *et al.*, 2017; Watson *et al.*, 2017).

In 2D neuronal cultures, neurons are cultured on flat substrates, which are glass substrates or polyethelene substrates. The substrates and microfluidic devices are cleaned, sterilised and coated with matrix proteins. The coating of substrates allows the adhesion of the neuron cells to the substrates. Normally, to promote the neuronal cell adhesion to the substrates, researchers have been using poly-D-lysine (Kos *et al.*, 2016; Kamande *et al.*, 2019), poly-L-lysine (Yap *et al.*, 2017; Zheng *et al.*, 2019), laminin (Gumy *et al.*, 2011; Bigler *et al.*, 2017) or Poly-L-Ornithine (Paranjape *et al.*, 2019; Lucci *et al.*, 2020). In 2D, cells need the protein coating to adhere and to develop onto the substrates.

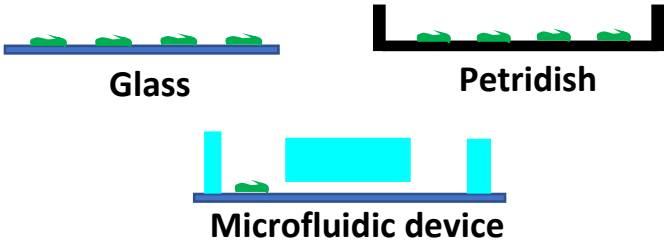
As the cells grow, their functional behaviour can assessed by employing different assays, such live/dead assays (to characterise cell viability), immunocytochemistry (to identify parts of the cells or their components (e.g. organelles, proteins), axonal length measurements (to determine the influence of any compound in axonal growth; this experiment is only allowed in 2D cultures within microfluidic devices) and calcium imaging and electrophysiology (to understand how cells communicate between each other), see **Figure 6**.

1. Clean the surfaces with Ethanol

2. Coat the surfaces with matrix protein of choice

(e.g. Poly-L-Ornithine or Poly-L-Lysine)

3. Culture of cells onto the substrates



4. Characterisation of the functional behaviour of cells

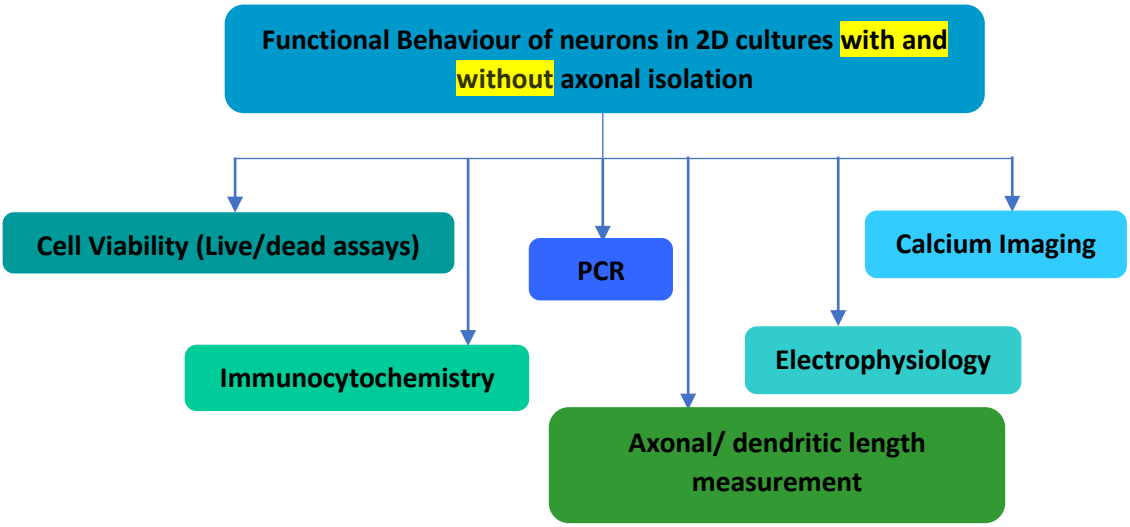


Figure 6 – Scheme showing 2D cell cultures procedure. The substrates, such as glass coverslips and the plastic surfaces (polysterene) of the petridishes, where cells are going to grow need to be clean and sterile. These substrates are coated with matrix proteins to allow the cell adhesion to the substrates. Then, the cells are platted, developed and their functional behaviour may be assessed using the following techniques: cell viability assay, immunocytochemistry, PCR, electrophysiology and calcium imaging. Neurons can be cultured in microfluidic devices, which consist normally in the sealing of the microfluidic device to glass or plastic surfaces. In contrary to the standard 2D cell cultures, the microfluidic devices provide the researchers the axonal/dendritic length measurement and all the other assays to characterise cell functional behaviour.

As said above, once cells are in culture, one of the first cell functional experiment to be performed is the characterization of the cell viability using the live-dead assays. These assays consist in observing cells that are labelled with dyes (Burry, 2010; Murphy and Davidson, 2012). The labelling of cells with live cell dyes allows the imaging of living and dead cells, providing a range of tools to investigate several cellular process under the microscope (Manuscript, Live and Imaging, 2015)(Murphy and Davidson, 2012). The cell viability tests for 2D cell cultures and 3D cell cultures haven been reported using two dyes, one for live cells and other for dead cells (Connor et al., 2001; Taylor et al., 2003; Xu et al., 2009; Dermutz et al., 2017; Morelli et al., 2019). Calcein acetoxymethyl (AM) is one of the most commonly used dyes that can be retained in the cell cytoplasm, labelling the live cells, whereas, Propidium Iodide (P.I.) is a dye used to label dead cells (Murphy and Davidson, 2012).

The use of primary cortical neurons in compartmentalised culture provides an opportunity for the study of cellular mechanisms with great spatiotemporal detail. In fact, in this system axons are allowed to extend and cross the microgrooves to the axonal channel. Even after 8 days of culture, only axonal projections have grown long enough to extend through microgrooves into the opposite side of the channel. This is demonstrated by the fact that, at this stage of culture, dendritic staining with MAP2 was restricted solely to the somatodendritic compartment of microfluidic chambers (Lucci *et al.*, 2020).

Moreover, average dendritic length at this stage of culture, as demonstrated by Lucci and colleagues, it is 91.53±2.7 μm, significantly shorter than the 150 μm long microgrooves of the chambers (Lucci et al 2020). Conversely, in a normal dish, axons grow stochastically in any direction and without physical guidance. In order to better regulate the growth patterns and dynamics, some researchers have employed the “stripe assay”, which consists in coating onto the surfaces patterns of repulsive (e.g. Fibronectin Leucine Rich Transmembrane Protein 2) and attractive (e.g. poly-L-lysine/laminin) molecules to control the axonal guidance (Vahidi *et al.*, 2008; Yamagishi *et al.*, 2016). However, by using this approach it is not possible to study the local influence of a compound into a specific neuronal compartments (i.e. axon).Therefore, microfluidic devices were developed to allow a directed growth, and considering the possibility to have fluidic isolation, they also allow the investigation of specific axonal events (Taylor *et al.*, 2003, 2005).

For example, Walker et al. (Walker *et al.*, 2018) treated axons with Aβ1-42 protein, using 2D neuron cultures in compartmentalised chambers, to identify the protein synthesis in axon degeneration. The addition of Aβ1-42 protein to the axon compartment induced a fast and localised protein synthesis in the axon as a cell-response. The axonal synthetized transcripts promoted then a retrograde signalling complex from axon to the nucleus that led to degeneration (Walker *et al.*, 2018). Another possibility that can be exploited by using microfluidic devices, it is isolate and identify axonal mRNAs associated with specific cellular processes such as axonal guidance, regeneration and injury (Bigler *et al.*, 2017).

In fact, it was reported that the identification of mRNAs that promote axonal survival using this microfluidic devices (Cosker *et al.*, 2016). Another example of using microfluidic devices, where axons are isolated from their cell bodies was reported by *Blizzard et al.* (Blizzard *et al.*, 2015). Here, it was investigated the cell bodies under similar conditions to the neuromuscular junction degeneration of a motor neurologic disease. Using compartmentalised devices it was possible to identify the RNAs composition on motor neurons, identifying specifically the composition of RNAs on the axons and on the soma (Briese *et al.*, 2015). Using microfluidic devices, axons can be studied individually, which allowed the investigation of the regulation mechanism involved in axonal growth by the protein JIP1-AKT (Dajas-bailador *et al.*, 2014b). These microfluidic devices were also used to investigate the anterograde axonal transport of the Herpes virus and how it spreads from the axons (Diefenbach *et al.*, 2016). In this way, it was possible to investigate the tau pathology propagation between cells by seeding cells with tau in one compartment and healthy neurons in the other compartment. (Calafate *et al.*, 2015). All these advances were possible by involving the separation between axons and soma, studying the onset neurologic disorders, axonal transport, axonal regeneration, etc. (Dajas-bailador *et al.*, 2014b; Blizzard *et al.*, 2015; Lewandowska *et al.*, 2015; Briese *et al.*, 2015; Reginensi *et al.*, 2015; T. Wang *et al.*, 2015; Yao *et al.*, 2015; Zhang *et al.*, 2015; Calafate *et al.*, 2015; Kneynsberg *et al.*, 2016; Kos *et al.*, 2016; Miranda-saksena *et al.*, 2016; Cosker *et al.*, 2016; Diefenbach *et al.*, 2016; Jia *et al.*, 2016, 2018; Bigler *et al.*, 2017; Peikon *et al.*, 2017; Sugiyama, Yao and Setou, 2017; Yap *et al.*, 2017; Jocher *et al.*, 2018; Laar *et al.*, 2018; Li *et al.*, 2018; Ohtake *et al.*, 2018; Dohner *et al.*, 2018; Kamande *et al.*, 2019; Zheng *et al.*, 2019; Lucci *et al.*, 2020; Sundaramoorthy *et al.*, 2020).

Compartmentalized devices are advantageous over the normal cultures because they allow separation of axons and cell bodies into different environments, thus replicating some key morphological aspects of neuronal function in the nervous system (Fantuzzo *et al.*, 2019). In the presence of degenerative processes in the CNS, the axons are the first part of the neuron to be lost resulting in some physical processes, such as the fragmentation of the axon. This results in breaking of connectivity between cells and eventually leads to cell death. Therefore, many researchers focused on understanding and investigating the cellular events in the axonal compartment, or testing drugs that will lead to axonal recover.

For example, *Laar et al.* (Laar *et al.*, 2018) could follow the anterograde and retrograde transport of mitochondria in the axons terminals and cell bodies individually *via* the compartmentalisation given by the microfluidic devices. Another example, of the importance of these studies for axonal regeneration was reported by *Jocher et al.* (Jocher *et al.*, 2018). Due to the compartmentalisation of the neuron cells, the molecular profile of single cell was determined by the gene expression and the quantification of the axonal growth state. Moreover, one example for investigating axonal degeneration was described by *Blizzard et al.* (Blizzard *et al.*, 2015). Here, it was shown the vulnerability of the neurons to excitotoxicity and, the compartmentalisation allowed to follow degenerative process and accurately measured the subsequent effects.

Axonal length is possible to be measured in axonal isolation devices, which is an important measurement to determine the influence of any compounds (e.g. drug or RNA interference) in the axonal growth and/or axonal regeneration. The measurement of axonal length allows researchers to determine if a compound or a treatment contribute to promote or inhibit axonal growth (Dajas-bailador *et al.*, 2012, 2014b; Blizzard *et al.*, 2015; Briese *et al.*, 2015; Yao *et al.*, 2015; Zhang *et al.*, 2015; Reginensi *et al.*, 2015; Cosker *et al.*, 2016; Kneynsberg *et al.*, 2016; Yap *et al.*, 2017; Jia *et al.*, 2018; Ohtake *et al.*, 2018; Zheng *et al.*, 2019; Lucci *et al.*, 2020). Scientists measured the axonal growth after axons cross the microgrooves and evaluate the response of axonal growth to a compound by following the axonal growth under a microscope. For example, the *Dajas-Bailador et al.* (Dajas-bailador *et al.*, 2012) overexpression of miRNA-9 leads to the decrease of the Map1b regulatory effects on axonal microtubules, which results in the reduction of axon length.

Another example was reported by *Lucci et al.* (Lucci *et al.*, 2020), which found the inhibition of miRNA-26 regulates the levels of GSK3β in polarity and neural outgrowth resulting in an axonal length reduction. Therefore, the axonal length is important for neuroscientists to study axonal events, such as axon development, regeneration and survival.

Another approach that can be employed by exploiting the neuronal compartmentalisation is the use of polymerase chain reaction (PCR) technique, that allows the amplification and identification of mRNAs in the axons or in another specific sub-cellular compartment upon RNA extraction (Dajas-bailador *et al.*, 2014b; Briese *et al.*, 2015; Yao *et al.*, 2015; Zhang *et al.*, 2015; Cosker *et al.*, 2016; Diefenbach *et al.*, 2016; Kos *et al.*, 2016; Peikon *et al.*, 2017; Jia *et al.*, 2018; Li *et al.*, 2018; Ohtake *et al.*, 2018; Zheng *et al.*, 2019; Sundaramoorthy *et al.*, 2020; Lucci *et al.*, 2020).

Immunocytochemistry is another technique used to characterise the cell morphology, which consist in staining the cells with fluorescent antibodies that allow the identification of specific cellular structures (characterising neuron's morphology), or identify location and patter of expression of proteins. The difference between this technique and the use of live-dead assays is that cells are alive during the cell viability characterisation, whilst cells are fixed when immunocytochemistry is performed. For example, the DAPI has been used to stain the nuclei of cells as reported in literature (Zhang *et al.*, 2015; Kos *et al.*, 2016; Li *et al.*, 2018; Paranjape *et al.*, 2019). The neuron structure can be stained with β-tubulin III to observe the cellular structure, which allows clear image of the axons (Reginensi *et al.*, 2015; Ryu *et al.*, 2018; Kamande *et al.*, 2019; Lucci *et al.*, 2020). F-actin (phalloidin) has been used to stain the growth cone (Zhang *et al.*, 2015; Kos *et al.*, 2016; Yap *et al.*, 2017; Ryu *et al.*, 2018).

For example, *Kos et al.* (Kos *et al.*, 2016) have treated axons with HPG and to characterise the influence of this treatment in the axons, stained the axons with Tau and quantified the fluorescence signal in axons. Another example of the use of this technique for quantification of the treatments was reported by *Lucci et al.* (Lucci *et al.*, 2020). In this study, the levels of GSK3β, which are regulated by miRNA-26, were quantified by measuring the fluorescence signal (the axons were stained with β-tubulin III and gsk) in axons after disruption of axonal transport. The β-tubulin III was also used to stain axons by *Kneynsberg et al.* (Kneynsberg *et al.*, 2016) to quantify the degeneration process in axons after applying colchicine in the axonal compartment.

Therefore, immunocytochemistry allows the quantification of modifications in the cell structures after treatment, which could be applied either in the axonal or somatodendritic compartment by using microfluidic devices. It is also possible to visualise the transport of proteins along the axons isolated from their cell bodies as reported by (Freundt *et al.*, 2012). *Freundt et al.* (Freundt *et al.*, 2012) have use the fluorescence imaging techniques (microscope + immunocytochemistry) to visualize the axonal transport of α-Synuclein.

Another technique employed to study neuronal functional and their electrical properties is electrophysiology. This approach requires electrodes to be able to measure the electrical activity of neurons. Namely, studies of neuronal activity with electrophysiology are found in non-compartmentalised devices. Normally, electrodes are patterned in glass as the micro-electrodes array (McDonald *et al.*, 2017; Deku *et al.*, 2018; Pas *et al.*, 2018) and a voltage or current is applied and the neuronal activity measured to record the neuronal communication. Although, recently some researchers reported the ability to do electrophysiology by patterning the spaces of the microgrooves with electrodes (Jokinen *et al.*, 2013; Lewandowska *et al.*, 2015; Kisiswa *et al.*, 2017) thus performing electrophysiology within a microfluidic device. This gives the possibility to understand how two different populations (plating healthy neurons in one compartment and unhealthy neurons in the other compartment) interact between each other. For example, *Jokinen et al.* (Jokinen *et al.*, 2013) reported the neuronal activity between healthy and unhealthy axons measuring the action potentials in the electrodes patterned in the microgrooves. This technique is expensive due to the patterning of electrodes that is made by using photolithography (Jokinen *et al.*, 2013; Lewandowska *et al.*, 2015).

The neuronal activity of neurons can also be measured by calcium imaging technique (Grienberger and Konnerth, 2012) using standard fluorescence microscopy techniques. Calcium imaging requires the use of fluorescence sensors that will bind to the calcium ions present in the intracellular environment. It allows to investigate the neural activity of each neuron individually, since the changes in fluorescence is related to the changes in calcium in the intracellular environment. It can be used to investigate cells respond to drugs and transmit the information between cell (Mackerron *et al.*, 2017).

Researchers have been using this technique to investigate the neuronal activity in standard 2D neural cultures (without axonal isolation) (Cichon *et al.*, 2020; Deveci, Hasna and Bouron, 2020; Yoshida and Ohki, 2020), where Fluoro-4 was used as a calcium indicator in order to visualise the neuronal activity. This technique was also employed within microfluidic device using Fluoro-4 (Mackerron *et al.*, 2017). The axons are isolated and influence of some tested compounds on intracellular processes (calcium channels) was investigated. *Mackerron et al.* (Mackerron *et al.*, 2017) investigated the neuronal response in the intracellular process (calcium channels) by adding glutamate (active compound in the central nervous system) and glutamate antagonists (such as NBQX) to the axonal compartment. Taylor et al. (Anne M. Taylor *et al.*, 2010) also measured the neuronal activity using the calcium indicator Fluor-4 to measure the changes in calcium in the cell bodies (isolated from axons) and investigating the time the cell response takes from nucleus to synapse of the neuron.

In 2D, cells are easier to manipulate due to the lack of complexity provided by the extracellular environment. Consequently, most experimental systems use a 2D configuration, which makes cell functional behaviour techniques, such as immunocytochemistry, calcium imaging, and electrophysiology easier to perform (Fantuzzo *et al.*, 2019).

However, 3D has advantages over 2D cultures, even with the limitations found in 3D cultures. One limitation of 3D cultures is the imaging of cells due to light scattering, light absorption and limited light penetration in the gel structure. These parameters limit the visualisation of cells in gels. Besides, cells within gels are out of focus (M.W. Tibbitt and Anseth, 2009; Fang and Eglen, 2017; Langhans, 2018).

Another limitation is the fact that cells in 3D systems are more difficult to characterise than in 2D cultures. For example, it is more difficult to perform immunostaining of cells in 3D or DNA/RNA extraction from gels (M.W. Tibbitt and Anseth, 2009).

Cells growing in three dimensions show more relevant physiological information. There are studies that have reported that cells can grow differently between 2D and 3D cultures, which leads to different morphology, gene level expressions, neuronal network activity and migration (Li *et al.*, 2007; Laplaca, Vernekar and Shoemaker, 2010; Lee *et al.*, 2011; Frega *et al.*, 2014b; Bosi *et al.*, 2015a; Carlson *et al.*, 2016; Chandrasekaran *et al.*, 2017; Bourke *et al.*, 2018). The difference in biological cell functional behaviour between cultures means that more researchers starts to utilise 3D cultures, since they present a culture context that more accurately reflects the conditions *in vivo* (Langhans, 2018).

A 3D culture system can provide the mechanical support in a way that is more similar to the *in vivo* environment. In 3D systems, the environment allows cells to develop as they would do in a similar native environment (Edmondson *et al.*, 2014; Antoni *et al.*, 2015; Duval *et al.*, 2017). *In vivo*, when neuron cells grow, they acquire a pyramidal shape and their neurites are able to extend in all directions (Anthony P. Barnes and Polleux, 2009). This offers a more accurate representation of the *in vivo* cytoarchitecture than for cells growing on hard substrates (Mark W Tibbitt and Anseth, 2009; Gargotti *et al.*, 2018). Thus, demonstrating the value in going from 2D to 3D studies.

2.1.5 Hydrogels

Definition

The hydrogel materials are used to investigate the cell-based processes in a more physiological structure than glass or polystyrene dishes. The cells are encapsulated within hydrogel materials during the transition of a liquid solution into a solid structure. This transition is how the hydrogel is typically formed and occurs by physical or chemical crosslinking processes, which put together all hydrogel components (Ahmed, 2015).

Hydrogels are a material consisting of a high percentage of water mixed with other components such as proteins and polysaccharides, that support cell adhesion and provide a similar environment for cells to replicate their behaviour as in vivo environments (Edmondson *et al.*, 2014; Verhulsel *et al.*, 2014; Duval *et al.*, 2017).

The hydrogel by definition is a polymeric crosslinked chain able to retain a large amount of water within its structure without dissolving. The ability of retaining water allows the transport diffusion of waste, nutrients and oxygen through its polymeric network. The ability to retain water results from the interaction of the water molecules with the main hydrogel polymeric backbone. The carboxylic acid groups attached to the main polymer backbone chain react with water forming hydrogen bonds that are released as positive ions. As a consequence, the polymeric chain becomes highly negative charged along its length. The negative charges are going to repel each other making the polymer backbone to uncoil and open up (**Figure 7**). As the polymer is in solution contacting with water, the negative charges left in the main polymeric chain are going to attract the oxygen atom from water molecules. The oxygen has a higher tendence to attract electrons, therefore is attracted by the negative charges becoming more negatively charged. While the hydrogen atoms are left more positively charged. In this way, the water is attracted to the polymeric chain network making the liquid solution becoming more viscous (Zhu and Marchant, 2012).

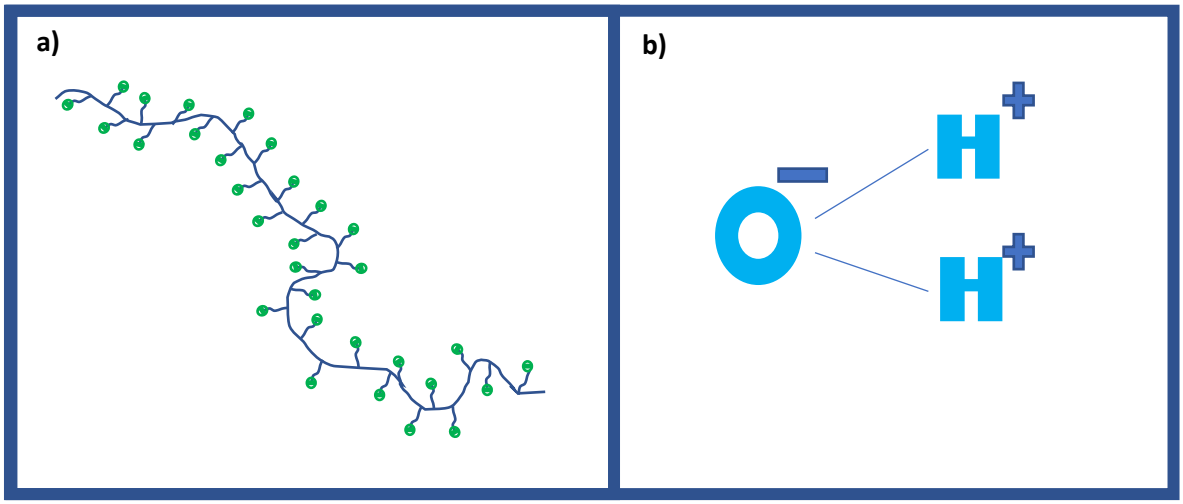


Figure 7 – Diagram showing the polymeric chain highly negatively charged after being in contact with water (**a**) and the water molecule with its oxygen and hydrogen atoms charged after being attracted to the chain (**b**).

Hydrogels offer a promising solution with the possibility to culture cells without loss of their natural properties. They offer the possibility to encapsulate cells and promote a biological environment in three dimensions, where cells can grow as they would in native tissues (Edmondson *et al.*, 2014; Verhulsel *et al.*, 2014; Duval *et al.*, 2017).

Natural and modified extracellular matrices have been used to address the desired 3D configuration and ECM environment (Frantz *et al.*, 2010). Natural hydrogels allow a more relevant cell environment, although they derived from animal sources, are time consuming and vary their composition in batch to batch (e.g. Matrigel matrix) (Rong Fan *et al.*, 2016).

Natural and Synthetic Hydrogels

Hydrogels exist in two forms: natural and synthetic (Verhulsel *et al.*, 2014), please see **Figure 8**. Examples of natural 3D hydrogels matrices based on ECM proteins for neuroscience may be found in literature, matrigel (Choi *et al.*, 2016), fibrin (Bayat *et al.*, 2016), chitosan (Crompton *et al.*, 2007), alginate (Lin *et al.*, 2017), hyaluronic acid (HA) (Broguiere, Isenmann and Zenobi-wong, 2016), polypeptides (Ren *et al.*, 2016). Despite natural hydrogels help in the evaluation of cell responses to diverse factors, they show a high level of complexity (Murphy, Lampe and Murphy, 2015; Shamloo, Mohammadaliha and Mohseni, 2015). Therefore, the range of mechanic properties and composition is huge. While natural hydrogels are bioactive, hence they already have native adhesive sites, synthetic materials are inert, therefore require the addition of integrins and signalling molecules to induce cell natural processes (Verhulsel *et al.*, 2014). Synthetic gels offer the advantage of having an environment that is known and controlled. Synthetic hydrogels provide the possibility to alter as desired the synthetic matrices. Modifying its properties is an attractive approach to researchers, since it affords in a controllable way easy access to characterize and study individual questions for each cell behaviour, which is not easily achieved in natural matrices. However, it is costly and time consuming the fabrication of synthetic gels.

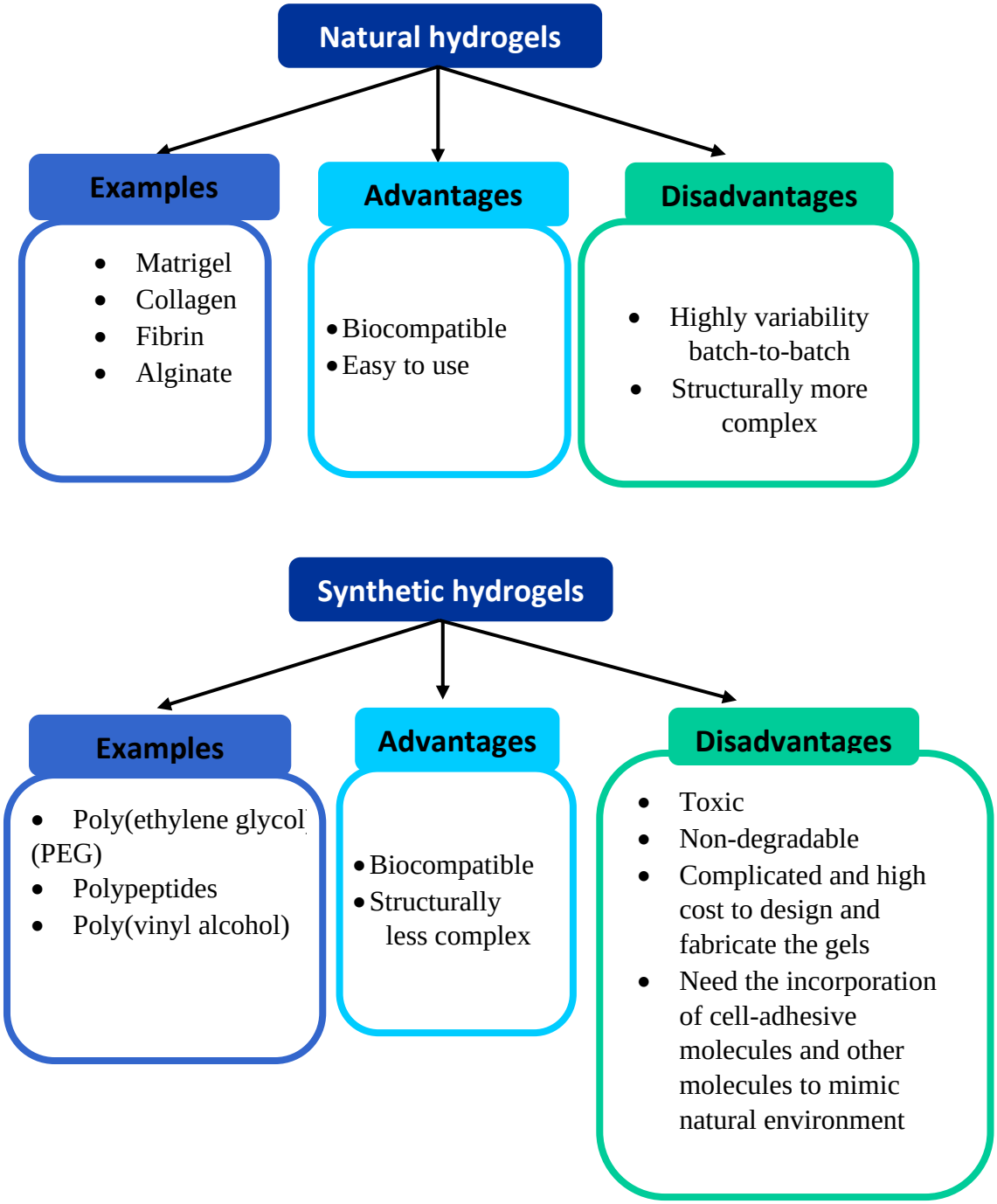


Figure 8 – Scheme with examples of natural and synthetic hydrogels, with the respective advantages and disadvantages.

Additionally, the indistinct composition of the natural matrices makes difficult to precisely know which signals promote cellular functions (M.W. Tibbitt and Anseth, 2009). The main function of natural hydrogels is to mimic the natural *in vivo* environment. That is why researchers start to use 3D cell cultures. Natural gels provide the biochemical environment that would be found in a native tissue, while synthetic gels require the incorporation of molecules to allow cell adhesion, or molecules to simulate degradation of the matrix (Verhulsel *et al.*, 2014).

Examples of natural 3D hydrogels matrices based on ECM proteins (M.W. Tibbitt and Anseth, 2009) may be found in the literature, such as Matrigel (Choi *et al.*, 2016), fibrin (Bayat *et al.*, 2016) and Hyaluronic Acid (HA) (Broguiere, Isenmann and Zenobi-wong, 2016). Matrigel is extracted from a sarcoma (mouse tumour).

Natural hydrogels have been used to better mimic the native ECM and thus makes them an important tool to investigate neurological mechanisms. Because natural gels are easy to work with and are naturally biocompatible it is a better choice to work with natural gels than with synthetic gels. One example is the protocol established by *Kim et al.* (Kim *et al.*, 2015), where human neuron cells laden in Matrigel to provide a more realistic model for Alzheimer's disease, by growing cells in a more cell relevant environment and allowing them to develop as those *in vivo*.

In this work, it is important to take into consideration the hydrogels that enable a closer cell environment, such as Matrigel or Hyaluronic Acid. The high number of hydrogels that can be used for 3D cell culture, provides a wide range of mechanical properties and composition. It has been shown that softer matrices promote maturation of embryonic neurons (growth and polarization) leading to longer neurites (Teixeira *et al.*, 2009; Zuidema *et al.*, 2014).

Regarding synthetic gels, they require more complicate methods to form the gels, since they are formed by chemical cross link to assemble the components. The chemical cross-linking methods, are for example, UV polymerization or Michaele reaction, which time consuming and expensive. The chemical cross link methods normally tend to leave free radicals when forming, and it was proven that these free radicals that present in synthetic gels are toxic for primary cells (Chen, Davis and Chem, 1999; Caliari and Burdick, 2016). Therefore, the live-dead cell assay is always required. Examples, are for example PEG combined with Hyaluronic acid to culture neurons in 3D *Broguiere et al.* (Broguiere *et al.*, 2019), or chitosan-g-oligo(L,L-lactide) copolymer *Grebenik et al.* (Grebenik *et al.*, 2020).

In contrary, natural ones require a physical cross link, such as temperature. In addition, hydrogels are commonly used in devices with simple designs, since these materials are used to act as a resistance to fluidic diffusion (Saadi, Rhee and Lin, 2007; Abhyankar *et al.*, 2008; Haessler *et al.*, 2009; Ma *et al.*, 2010; Marom *et al.*, 2015; Ahrens *et al.*, 2019). Agarose, another natural hydrogel, is commonly employed in diffusion based devices to determine the 3D gradient diffusion profiles (Mosadegh *et al.*, 2007; Abhyankar *et al.*, 2008; Haessler *et al.*, 2009).

Matrigel

The tumour is rich in biological active molecules, such as growth factors, making the Matrigel a better matrix to host cells, in particular for cell development and drug screening (Graf and Boppart, 2010; Jensen, Morrill and Huang, 2018). The main protein components from ECM present in Matrigel are laminin, collagen IV, and enactin. However, the small amounts of unknown proteins found in Matrigel cause lack of experimental consistency and make this hydrogel being criticized for the variability found in batch-to-batch (Ko and Frampton, 2016; Wu *et al.*, 2017).

Hyaluronic acid (HA)

This in turn leads some researchers to use another ECM gels. HA is another gel used for cell encapsulation, which is a polysccharide originated in the ECM (Gasperini, Mano and Reis, 2014). The HA is a major ECM component in the CNS (Wu *et al.*, 2017) and has a role in biological processes as development. Although, HA do not support cell adhesion and normally it tends to be modiefied or combined with other extracellular components or matrices (Wang *et al.*, 2012; Caliari and Burdick, 2016).

Collagen

Collagen is responsible for the mechanical support of ECM and is an organic constituent of fibrillar. In turn, the collagen is the main structural integrant of organs. The fact that collagen presents cytocompatibility and supports the matrix to resist to the different viscoelastic forces makes it an ideal gel to study cell-based processes such as migration or differentiation (Catoira *et al.*, 2019)(Caliari and Burdick, 2016)(Bonneh-barkay and Wiley, 2009). Collagen has been used due to its mechanical properties to investigate dorsal root ganglia cells for peripheral nerve injuries (Bozkurt *et al.*, 2007). However, it is a material that presents limited stability during time and shows variability batch-to-batch as many other natural hydrogels. Besides, there is less collagen in the ECM from an adult brain than an embryonic brain. Consequently, researchers combined collagen with an ECM mixture (ECM proteins; such as glycoproteins, and proteoglycans) (Lam *et al.*, 2019). For example, *Lam et al.* (Lam *et al.*, 2019) cultured primary human neurons within pure collagen and collagen mixed with ECM proteins. In this study, the neuron cell viability was higher in the ECM proteins mixture with collagen for a long-time culture, while the percentage of death cells was high in a short-term culture for neurons cultured only in pure collagen.

Fibrin

Another natural polymer used in neuronal cultures is Fibrin, which is formed from wound coagulation; it derives from blood. It is involved in wound healing and hemostasis. This polymer has been used for studying angiogenesis and another cell-based processes such as cell guidance (Li *et al.*, 2015)(Caliari and Burdick, 2016). Besides, Fibrin contains many cell ligands for the central nervous system making this gel a promiser choice for working with neurons (Navaei-nigjeh *et al.*, 2013). For example, it has been used to study neuronal differentiation of dorsal/ventral spinal neurons (Edgar, Robinson and Willerth, 2017) or for drug testing in neurons (Malheiro *et al.*, 2020). On other hand, Fibrin is not suitable for long-term cultures because of its properties has an inclination to fast degrade (Caliari and Burdick, 2016). Fibrin is combined with other gels to slow its degradation rate.

Alginate

Neuronal cells have been also encapsulated in Alginate, which consist in a polysaccharide that comes from algae. The Alginate gel has a rapid time to set, is very biocompatible and easy to use. However, this polymer lacks reproducibility of results and it is dimensional not stable and requires the combination with other cell ligands to allow the cell adhesion (Sun and Tan, 2013)(Lee and Mooney, 2012). Although its disadvantages, it has been used for neurite outgrowth studies (Matyash *et al.*, 2012), where it was reported the support and an improvement in neurite outgrowth. Besides, it has been used as scaffolds to study neuro-regeneration and nerve-regrowth (Prang *et al.*, 2006).

Polypeptides

Polypeptides are a range of synthetic hydrogels with tunable properties, that can be manipulated and defined to become suitable for encapsulation of cells. Although, they are very expensive, which is not cost-effective for large scale cell cultures. This type of Polypeptides hydrogels is normally produced by self-assembly of the molecular structures. One example of the polypeptides hydrogels used in neuron cultures is the PuraMatrix The PuraMatrix is a nanofibrous polypeptide gel that is composed with amphiphilic peptide repeating arginine-alanine-aspartate-alanine sequence (Ylä-outinen *et al.*, 2014)(Caliari and Burdick, 2016)(M.W. Tibbitt and Anseth, 2009). PuraMatrix has been build and used to investigate differentiation the gene expression in astrocytes (as mentioned in section 2.1 Neuronal development, astrocytes are the second most abundant cell in the brain) (Knight and Serrano, 2017) and the peripheral nerve (Mcgrath *et al.*, 2010). It has been also employed to investigate matrix-neuron cell interaction in comparison to Collagen type I and Matrigel (Frimat *et al.*, 2015). In this study, neurite outgrowth was compared in both 2D and 3D systems within non-compartmentalised cell cultures. Non-compartmentalised means that there was no fluidic isolation between cell bodies and axon terminals.

Polyethylene glycol (PEG)

Another synthetic hydrogel is the Polyethylene glycol (PEG), which can also be modified as the polypeptides hydrogels to provide a more suitable environment for cell encapsulation. These modifications are based on chemical alterations to modify its properties. The modifications consist in alternate the different functional groups by polymerisation techniques. This hydrogel has been used to encapsulate neuronal cells resenting advantages of being bioinert and biocompatible (Naghdi *et al.*, 2014)(Caliari and Burdick, 2016)(M.W. Tibbitt and Anseth, 2009). As typical in synthetic gels, PEG needs to be mixed with cell ligands that allow the cell attachment/adhesion to the matrix (Caliari and Burdick, 2016)(Broguiere *et al.*, 2019)(M.W. Tibbitt and Anseth, 2009). PEG hydrogel was used to study viability and neurite outgrowth of primary rat neurons within different PEG scaffolds by *Broguiere et al.* (Broguiere *et al.*, 2019). The neurite outgrowth of primary neurons with PEG gel was also investigated by *Saneinejad et al.* (Saneinejad and Shoichet, 1998), where PEG modified surfaces contributed for cell guidance in this study.

Poly(vinyl alcohol)

Another synthetic hydrogel is the Poly(vinyl alcohol) (PVA) a water soluble hydrophilic polymer formed by non-natural molecules (Ahmed, 2015)(M.W. Tibbitt and Anseth, 2009). This gel type is nontoxic, biocompatible and have good elasticity and strength properties (Fahmy *et al.*, 2015)(Mastrangelo *et al.*, 2020). As typical in synthetic hydrogels, PVA also involves chemical crosslinker process that can affect biological integrity of the proteins, drugs and cells entrapped. However, PVA is not toxic because does not require toxic compounds used in the chemical crosslink. Although, it is difficult to provide high porosity PVA scaffolds make this gel adhere to rough surfaces (Fahmy *et al.*, 2015)(Mastrangelo *et al.*, 2020).

PVA gels are normally combined with other gels or modified with other molecules to make the gel more suitable for neuronal encapsulation studies. For example, PVA was combined with Hyaluronic Acid (Ylä-outinen *et al.*, 2019) or chitosan (Alhosseini *et al.*, 2019) gels. Human pluripotent stem neuronal cells were encapsulated in PVA combined with Hyaluronic Acid and collaged to investigate cell adhesion and neurite spreading (Ylä-outinen *et al.*, 2019). In this study the mechanical characterisation of the gel was investigated.

PVA gel was also modified with tyramine, which resulted in a more soft gel for neuron encapsulation (Aregueta-robles *et al.*, 2018). In this study, the mechanical and swelling properties were characterised and the cell viability of neuroglial cells (rat Schwan cell line) was investigated.

Hydrogel formation process

In an attempt to recreate the ECM environment, hydrogels have been used, which achieve the desired 3D cell configuration (Frantz *et al.*, 2010). Hydrogels have been widely used for cell encapsulation because it is a relatively easy and biocompatible technology to recreate a 3D configuration (Gasperini, Mano and Reis, 2014). This technology has the advantage of allowing cells to receive biochemical signals from the cell surroundings, since cells grow in three dimensions. Cell encapsulation with hydrogels consists of a solution of hydrogel mixed with a cell suspension that is quickly gelled (Lambert *et al.*, 2018), thus forming the matrix structure replicating the ECM environment, as shown in **Figure 9**. The 3D neuron culture, where neurons are encapsulated in hydrogel, is also known as neuron laden hydrogel. These neuron cultures are used to study migration (Gil and del Río, 2012; Hellwig *et al.*, 2018) and morphology (Dewitt *et al.*, 2009; Frimat *et al.*, 2015) of neurons in three dimensions.

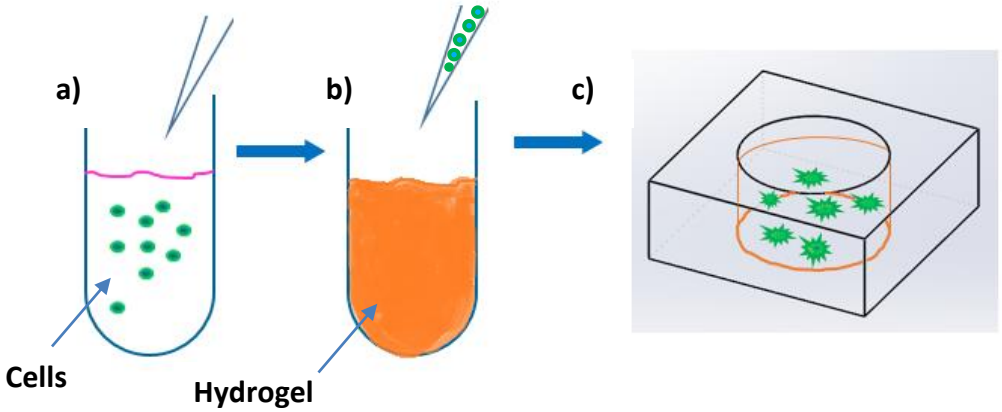


Figure 9 – Schematic of hydrogel technique for cell culture. Cells in suspension (**a**) are added to a hydrogel material in a liquid state (**b**). After mixing cells in hydrogel, the solution is added to the cell culture system and the matrix is cross linked in order to immobilise cells in a 3D matrix, where they start to develop (**c**).

3D Cortical neuron cell culture functional experiments within hydrogels

Cells in the native tissue are exposed to a 3D environment exposing cells to other cells, to circulating molecules, to the ECM. Researchers have used other type of neural cells, such as glia cells and dorsal root ganglia, in 3D and they have accessed the cell functionality, please see **Figure 10**. The 3D environments studies always report the cell viability and visualise cell growth. There are a few studies using primary mouse cortical neurons in 3D cultures, which is the type of cells that this work is going to use. As the use of 3D cell cultures is recent compared to 2D cell cultures and there is a lot of variability in the hydrogels that can be used and the different cells that are used, there is not a standarised protocol. This leads to an increased need for a standard protocol, allowing a better comparison of results between studies reported in literature. However, no one has done these cell functional behaviour experiments in a 3D axonal isolation environment, please see **Figure 10**.

O'Conner et al. (Connor *et al.*, 2001) used primary rat neuron cells in 3D to investigate neurite outgrowth. They cultured the neural cells within agarose and collagen type I, which allowed them to visualise differences between cells being cultured in 2D. They have accessed the neuronal cell viability and compared the cell survival and neurite outgrowth within the two matrices.

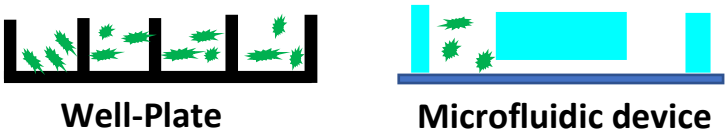
The cell viability was done using calcein acetoxymethyl ester (AM) to label live cells and to label the dead cells they have used ethidium homodimer (EthD-1). They have reported that neurons in agarose seemed to be present shorter neurites and round, as found here in the PhD work. Neuron cell viability in primary cortical neurons was also reported by *Laplaca et al.* (Laplaca, Vernekar and Shoemaker, 2010). They have used the same dyes as *O'Conner et al.* (Connor *et al.*, 2001) (live cells were labelled with calcein AM, while dead cells were labelled with EthD-1). In this study, they say they have performed immunocytochemistry even if the data was not shown. They reported to be possible to stain the cells for immunocytochemistry using 3.7% formaldehyde and using HOESCH to stain the nucleus, Tau-5 to label all the cellular structure by targeting the microtubules of the cell and, synapsin I was used to stain synapses.

Another cell functional study with 3D neuronal cells was reported by *Choi et al.* (Choi *et al.*, 2014), where DAPI was used to stain the nucleus, where neural cell lines cultured in matrigel to investigate the mutation that neural cells suffer onset Alzheimer's disease conditions. They have labelled the cells using immunocytochemistry and using PCR to investigate the gene expression levels. Cortical rat neurons were cultured in matrigel, where the axons were stained with III β-Tubulin within Matrigel and for immunocytochemistry by *Jang et al.* (Jang *et al.*, 2015).

Another example of primary cortical neurons in 3D was performed by Cao et al. (Cao and He, 2010), however they used chicken as the animal model. Here, the neurons from chicken embryos were cultured within chitosan composites, which were combined with agarose. These gels were incorporated with neuro-adhesive molecules to investigate the neurodegeneration; therefore, cell response was evaluated by labelling cells with Calcein AM and measuring the neurites (axons) outgrowth.

1. Clean the surfaces with Ethanol

2. Plate the cells mixed with hydrogel onto a well-plate or in a microfluidic device



Well-Plate **Microfluidic device**

3. Characterisation of the functional behaviour of cells

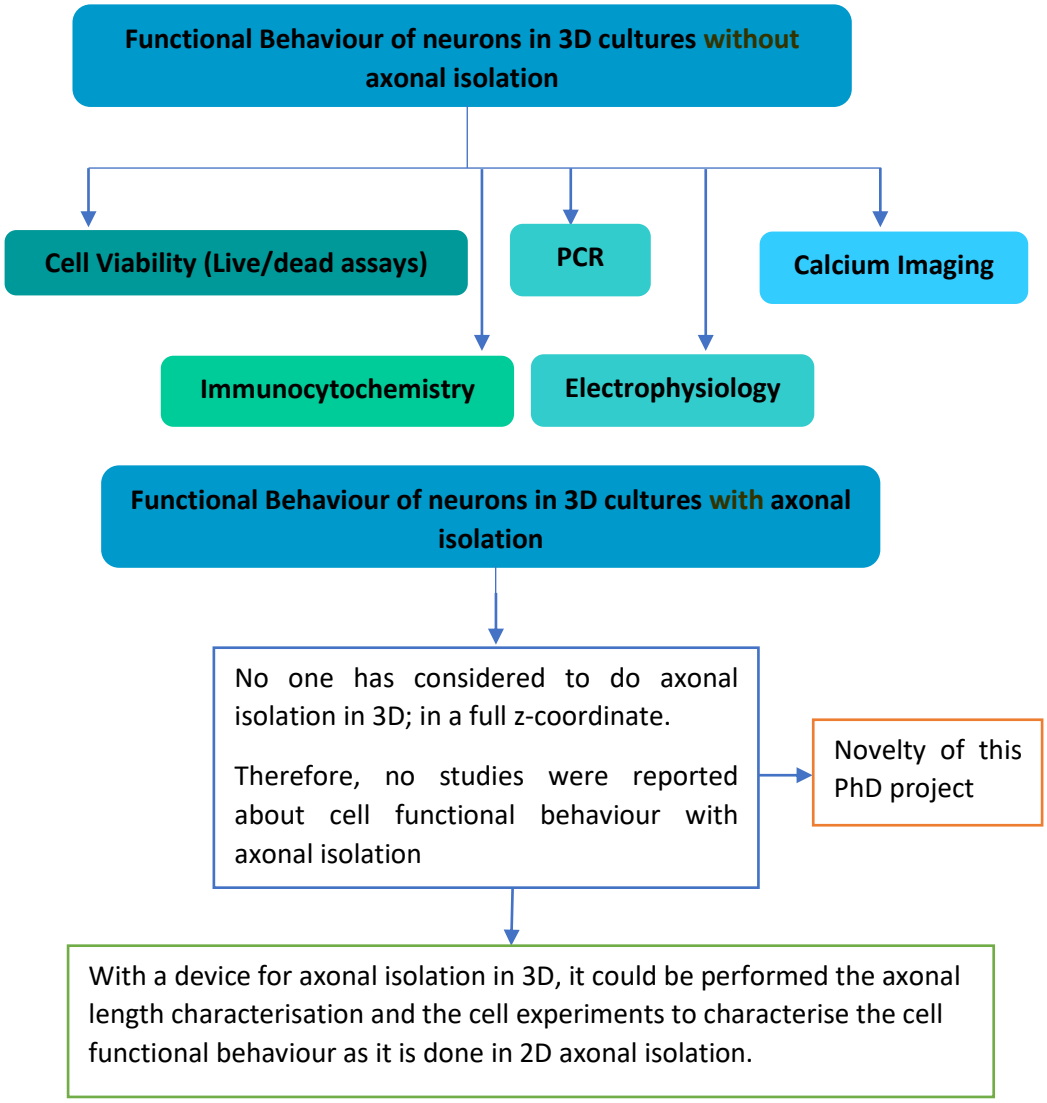


Figure 10 – Scheme showing 3D cell cultures procedure. The substrates, such as glass coverslips and the plastic surfaces (polysterene) of the petridishes, where cells are going to grow need to be clean and sterile. The cells are platted within a 3D matrix and cells develop. The functional behaviour of cells in 3D may be assessed using the following techniques: cell viability assay, immunocytochemistry, PCR, electrophysiology and calcium imaging.

However, the protocols for immunocytochemistry differ in terms of the alcohol used to kill the cells before staining, the dies to stain and the times of incubation. For example, *Laplaca et al.* (Laplaca, Vernekar and Shoemaker, 2010) used 3.7% formaldehyde for fixing the primary rat cortical neurons in the immunocytochemistry experiment, while *Boutin et al.* (Boutin and Hoffman-kim, 2015) used 4% paraformaldehyde in primary cortical rat neurons in agarose spheroids gels. They even reported than longer times of incubation steps in the immunocytochemistry do not improve the clearing of the background (that is still fluorescent). Besides, they reported shrinkage of the spheroids when performing the immunocytochemistry, labelling the nucleus with DAPI. The problem of 3D cultures relies on the fact that it is a new area, and there is not a standard protocol for immunostaining. Additionally, the fact that there is a large choice of hydrogels to use for 3D cultures and different cortical neurons (from different animal model) increase the difficulty to standardize a protocol.

Regarding, calcium imaging for primary cortical neurons within 3D culture the following studies were found. O'Connor (O'Connor *et al.*, 2000), has reported the neuronal cell response to glutamate within collagen by loading the cells with Fluo-3. The cell response can be detected in 2 minutes. Another study reported by *Wevers et al.* (Wevers *et al.*, 2016), reported the spontaneous induced calcium response in 3D neural cultures. Here, the cells were iPSC-derived mature neurons and astrocytes cultured within a scaffold device, called OrganoPlate. In the Organoplate neurons were platted within wells mixed with Matrigel. They showed the transmission of calcium response between two cells at 41 seconds and at 46 seconds using Fluoro-4 dye. Similar study where calcium imaging was employed to evaluate the spontaneous calcium response was reported by *Grebenik et al.* (Grebenik *et al.*, 2020). Here, chitosan-g-oligo (L,L-lactide) copolymer was the hydrogel used to culture primary rat cortical neurons in 3D. Furthermore, the 3D neural activity was also assessed by researchers (Xu *et al.*, 2006; Lozano *et al.*, 2015; Broguiere *et al.*, 2019; Evans, Al-Shakli and Chari, 2020) with electrophysiology, which was performed using electrodes via patch clamping or MEAS. However, the cell functional assays were performed in wells or in another devices or structures without axonal isolation.

2.2 Manufacturing and Rapid prototyping Techniques

Manufacturing processes and associated materials are important for the development and improvement of medical devices, sensors and displays, among others. A wide range of manufacturing processes have been developed to fabricate devices able to control and mimic cellular environments, as well as the ability to couple different analyses. The development of new devices improves the understanding of biological processes in neuroscience (Halldorsson *et al.*, 2015). In the literature, microfabrication techniques were employed in several studies for the development of µFDs to understand the neuronal networks. It is popular to employ microvalves (Links, 2011) and micropumps systems (Hu *et al.*, 2016), microgaps or microchannels (Taylor *et al.*, 2005), integration of porous membranes (Kim *et al.*, 2016), micro-wells (Nyoung *et al.*, 2016) and micropattern substrates with cell-adhesion and cell-repellent regions (Joo, Kang and Nam, 2015) into µFDs for neuroscience research. Examples where these devices can be applied are, for example, in cell-based microarrays (Rothbauer *et al.*, 2015), screening of drugs (Ting *et al.*, 2013), specifically for isolation of axons and its mRNA analysis (J. Wang *et al.*, 2015), control of flux gradients without disturbing cells (Xue *et al.*, 2016) and blood barriers models (Booth and Kim, 2012). Moreover, organ-in-a-chip devices rose from the integration in microfluidic platforms of complex tissues growth, for example the brain or liver cells (Rothbauer *et al.*, 2015). Integration of 3D architectures within microchambers for *in vitro* systems enable research into neurological disorders (Yang *et al.*, 2013; Meyer and Kaspar, 2016). Mainly, 3D configuration has great advantages over 2D, whereas provide the simulation mechanisms and biomimetic environment as *in vivo*. There are published research works combining 3D cell culture and µFDs devices (Li *et al.*, 2016; Yamada and Descroix, 2016), although the author of this thesis is unaware of any 3D cell culture device with a physical barrier designed for axons isolation.

The standard method to fabricate the devices used for axonal isolation are developing the microgrooves by photolithography and replicate them using soft lithography. This type of devices are fabricated by the researchers or bought to the XONA company (Dajas-bailador *et al.*, 2014b; Blizzard *et al.*, 2015; Lewandowska *et al.*, 2015; Briese *et al.*, 2015; Reginensi *et al.*, 2015; T. Wang *et al.*, 2015; Yao *et al.*, 2015; Zhang *et al.*, 2015; Calafate *et al.*, 2015; Kneynsberg *et al.*, 2016; Kos *et al.*, 2016; Miranda-saksena *et al.*, 2016; Cosker *et al.*, 2016; Diefenbach *et al.*, 2016; Jia *et al.*, 2016, 2018; Bigler *et al.*, 2017; Peikon *et al.*, 2017; Sugiyama, Yao and Setou, 2017; Yap *et al.*, 2017; Jocher *et al.*, 2018; Laar *et al.*, 2018; Li *et al.*, 2018; Ohtake *et al.*, 2018; Dohner *et al.*, 2018; Kamande *et al.*, 2019; Zheng *et al.*, 2019; Lucci *et al.*, 2020; Sundaramoorthy *et al.*, 2020). The normally have microgrooves with lengths varying between 450 to 900 µm of length, 10 µm of width and 3 µm height. These dimensions are enough to allow the passage of axons without cell bodies.

For this work we focus on the material used to create the 3D culture device considering the micro-assays that it must allow to perform and in the microfluidic network fabrication to build the barrier structure. Primary requirements are that the intended device must have the reservoirs and a physical barrier incorporating channels of a height between 2-4 µm for isolation of axons whilst allowing the passage of cell bodies between the two compartments. The aim of this project is to design a 3D device, incorporating a physical barrier that will allow only developing axons to cross, but prevent the passage of their soma between compartments. The physical barrier should contain features, such as a square or circle, with a minimum size of 10 µm (the size of a cell body) and should be biocompatible, please see **Figure 11**. The device should also be easy to fabricate and affordable, taking into account the cost of manufacturing processes and materials.

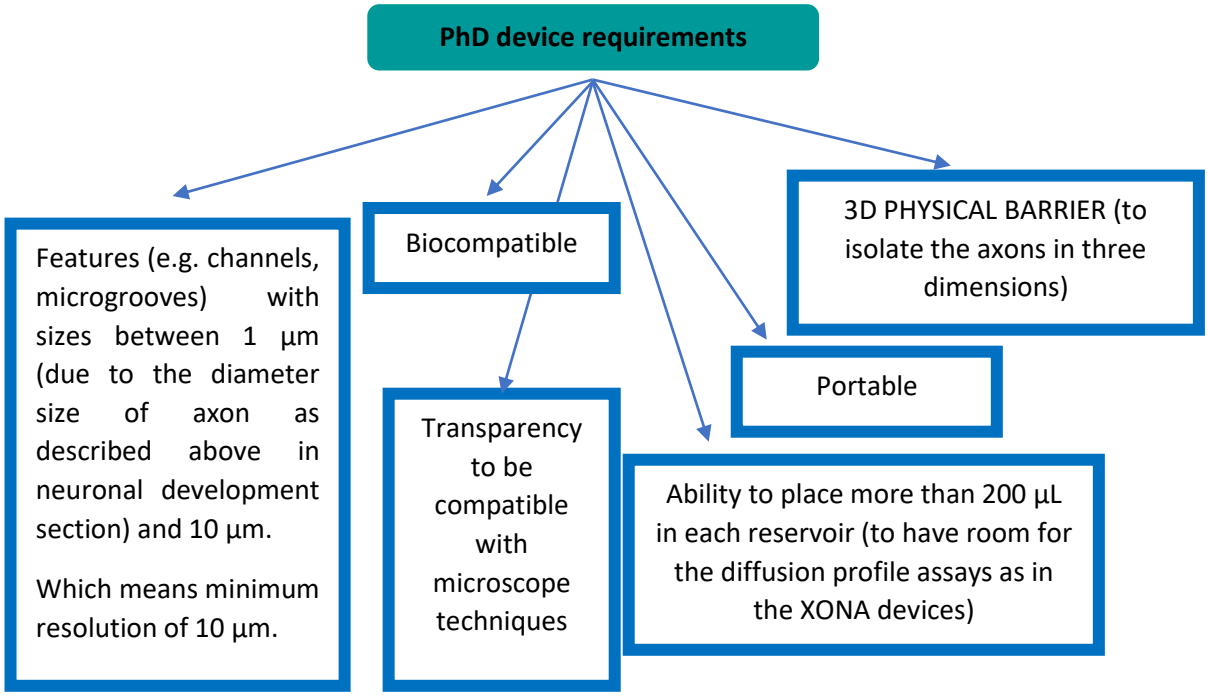


Figure 11 - Scheme with the requirements for the device that is proposed to develop in this work.

A brief introduction about the manufacturing processes for fabrication of devices is presented below. When manufacturing these devices, there are many aspects to take into consideration, such as the material properties and the resolution of the fabrication technique. The main categories of manufacturing techniques for building medical devices as their resolution and material employed are shown in **Table 1**. Microfabrication which can be divided in writing and replication techniques, including lithography methods, rapid prototyping, nanoimprint, micromachining and additive manufacturing approaches. Diverse technologies were taken in consideration for the development of the 3D cell culture device this works aims to build. For this work we focus on the material used to create the 3D culture device considering the micro-assays that it must allow to perform and in the microfluidic network fabrication to build the barrier structure. Primary requirements are that the intended device must have the reservoirs and a physical barrier incorporating channels of a height between 2-4 µm for isolation of axons whilst allowing the passage of cell bodies between the two compartments. The barrier could be manufactured by scratching and/or micro-drilling technology, FIB and E-beam technology or additive manufacturing. As well, the material of the device must be transparent and biocompatible, hence, PDMS is the material chosen for the cell culture device.

Table 1 – Summary of main techniques applied in the development of medical devices, as well as associated resolution and the materials typically used.

Categories	Technique	Resolution	Material	References
Lithography methods	Photolithography	~ 22 nm Realistically 1 µm (depends on the equipment)	Inorganic (AlF3, etc.), organic and hybrid resists. Few examples of the most common used are PMMA, Hydrogen silsesquioxane (HSQ). Diamond and silicon substrates	(Pease and Chou, 2008)
	X-ray lithography	<15 nm		(Maldonado and Peckerar, 2016)
	E-beam	<5 nm	Polymers Inorganic materials SAMS, nanotubes of carbon PMMA, Hydrogen silsesquioxane (HSQ) and ZEP resists	(Deng *et al.*, 2016)
	FIB	<5 nm	Silicon, little restriction in materials	(Gierak, Madouri and Biance, 2007)
	AFM – Dip pen lithography	< 50 nm	Small organic molecules, biological polymers, colloidal particles, metal ions	(Engstrom *et al.*, 2017)
Nanoimprint	Room-temperature NI UV-cured NI Reverse NI Soft-lithography	< 10 nm	Thermoplastics polymers and Elastomeric polymers	(Xia and Whitesides, 1998) (Biswas *et al.*, 2012)
Micromachining *	Scratching (Cutting)	~ 49 nm [a]	Metals, alloys, polymers, composites, technical ceramics, glasses	(Rahman *et al.*, 2010) (Huo and Cheng, 2013)
	Milling (Cutting)	~ 30 µm [b]		
	Drilling (Cutting)	~ 8µm [c]		
	Laser Beam Drilling	< 5 µm		
Additive Manufacturing	Stereolithography	≥50 µm – commercial <5 µm Micro high resolution	Photocurable polymers; hydrogels; ceramics; organic/inorganic hybrids, metals	(Skoog, Goering and Narayan, 2014)
	two- and multiple-photon polymerization	<100 nm		(Marino *et al.*, 2015)
	laser-induced forward transfer	~100 nm to 100 µm	Polymers; hydrogels, biomolecules	(Koo *et al.*, 2017)

	inkjet printing	50 µm	Hydrogels	(Xia and Whitesides, 1998)
	robotic dispensing	200 µm		(Malda *et al.*, 2013)
Rapid Prototyping Alternative technique	Xurography	10 µm	Tapes, polycarbonate membranes	(Bartholomeusz, Boutté and Andrade, 2005)

*, a,b,c – The resolution is referred as the depth achieved by cutting tools can achieve.

Lithographic and scanning probes processes

Lithography based techniques belong to the 'Top-down' methodology and are extended to achieve small sizes, allowing the ability to create master molds for fabrication of nanochannels, for example. Patterning lithography techniques use irradiation to transfer patterns onto a substrate. The irradiation crosses the photomask and promotes chemical changes in the substrate material exposed to the light. These chemical changes will enable the material to be selectively removed during the development. Lithography masters normally are also known as hard molds, generally made of silicon (Si) or by dielectric materials, which are going to be employed for nanoimprinting. The ability to transfer complex geometries patterns onto substrates is a worth value for microbiology, since developing nanostructures for biology has enable to answer questions in diverse research areas. In patterning lithography based methods the minimum feature size is determined by the type of illumination (Ito and Okazaki, 2000). There are different types of lithography, including UV, deep UV (DUV), extreme UV (EUV), x-ray, electrons and ions beam, accordingly to the different types of wavelength light as presented on **Table 2**. Lithography technology involves a photomask for the transmission of patterns to the substrates, although direct writing technology is in contact with the substrate. After the substrate being patterned wet and chemical etching are fabrication processes that take place to fabricate nanostructures.

Table 2 – Range of wavelengths for the respective lithography technique.

Lithography technique	Source type	Source length	References
UV lithography	Hg arc lamp (G-line, H line, I line)	365nm-436nm	(Pease and Chou, 2008) (Levinson, 2005)
DUV lithography	KrF and ArF excimer lasers	193nm-250nm	(Pease and Chou, 2008) (Levinson, 2005)
VUV lithography	F2 excimer laser	157 nm	(Levinson, 2005)
EUV lithography	Laser Plasma sources	10nm-14nm	(Stulen, Sweeney and Attwood, 1998)
X-ray Lithography	X-ray tube, synchrotron	<1nm	(Maldonado and Peckerar, 2016)(Bourdillon *et al.*, 2000)

Photolithography is also known as optical lithography and UV lithography, and it is the technique most commonly employed in the fabrication of biomicrofluidic devices (Pease and Chou, 2008). Basically, consists in the transference of a pattern to a substrate, normally a silicon wafer coated with a photoresist material, by exposing it to electromagnetic radiation (UV, DUV, EUV or X-rays). During the exposure the photoresist is suffering chemical changes, which accordingly to the type of photoresist (positive or negative) the regions exposed or not to the radiation are developed during the etching, leaving the pattern desired as designed in the photomask (Xia *et al.*, 1999). This approach requires a high number of expensive specialized steps, although presents high resolution. Photolithography has been employed in the fabrication electrodes for neuronal interfaces (Ware *et al.*, 2012), in the production of a negative photoresist (SU-8) master mold with pillars with 20 µm space between each others of 25 µm height with a 5 µm diameter for culturing hippocampal neurons in poly (lactic-co-glycolic acid) nanofibers (Wei *et al.*, 2017) and, it was employed to fabricate hydrogel structures for encapsulate dorsal root ganglia (DGR) neurons (Horn-ranney *et al.*, 2013). In addition, it was also used for developed hydrogel blocks containing human cells within microfluidic platform (Gao *et al.*, 2010).

Likewise, lithography either uses charged particles, such as ions or electrons, in the same way as photolithography. Lithography with charged particles can be either employed as direct writing technology, where a focused beam is in contact with the substrate and therefore “writing” the pattern. Electron-beam lithography (Pease and Chou, 2008) uses a beam of electrons that can be applied for generation of pillars, nanochannels or nanowells in neuroscience to investigate cells response to SU-8 material (Beckwith *et al.*, 2015), migration of Schwann cells (Jacchetti *et al.*, 2014), and neuronal polarization in response to physical and chemical cues (Gomez, Chen and Schmidt, 2007). Besides focused ion beam (FIB) is employed in the fabrication of structures at nano-scale with a beam of ions. FIB can be applied to repair photomasks and masters, to write directly into the hard surfaces (FIB milling), acting as additive technique (Duan, Wang and Xie, 2013). Also can be combined with SEM technology as characterization technique and imaging acquisition for detection of synapses (Bosch *et al.*, 2015). Nanostructures for DNA manipulation have been manufactured with FIB milling technology (Angeli *et al.*, 2011). FIB can be either be applied to create different types of structures by deposition of material, such as high aspect ratio walls (Reyntjens *et al.*, 2000) with a height between 3 µm.

Non-lithographic techniques

Replication of patterns identical to those designed in the hard mould is possible with a set of techniques which are cost-effective, have high resolution, are versatile as regards materials and do not require projection or beam lithography. These techniques include replica moulding soft-lithography and different types of nanoimprint lithography (Guo, 2007). Nanoimprint lithography is the imprinting on the resist by mechanical deformation and subsequent processes. It was proposed in 1995 by *Chou et al.* (Chou *et al.*, 1995), where sub-25 nm holes in PMMA were developed with an imprinting mould. Nanoimprint technology by replication incorporates an imprint step allowing patterns to be reproduced from moulds in mass production and then processed at room-temperature (RT) with UV-cured NI (Guo, 2004; Miebori, Unno and Taniguchi, 2014).

Micromachining

Micromachining technologies are considered as non-lithography manufacturing processes and the major fabrication techniques are involved in cutting approaches, including scratching, milling, turning, drilling and grinding. These techniques have not been used to design micro structures onto the master surface of a silicon wafer that later could be used in soft lithography, thus creating new chips for neuroscience devices. Therefore, an opportunity of research is the study of these cutting techniques in the fabrication of robust masters for future biomedical devices. It is to take into consideration that the resolution of these cutting tools depends on the size of the tip (Huo and Cheng, 2013). In addition to cutting methods, micro-injection moulding and laser machining are other two micromachining techniques that have been employed in the development of neuroscience devices.

Additive Manufacturing

A large number of different 3D printing techniques are currently being used for neuroscience applications, offering capabilities for the fabrication of accurate 3D structures, they diverge on their features, such as resolution, working principle and the materials that can be employed. 3D printing is becoming an alternative to the conventional lithography processes for microfluidic platforms fabrication (Barata, Van Blitterswijk and Habibovic, 2016). This review compiles five additive manufacturing methodologies that have demonstrated promise for biomedical applications, such as stereolithography, two-photon polymerisation, laser-induced forward transfer, inkjet printing and robotic printing. In general, despite high costs and difficulties with consistency between layers, additive manufacturing techniques are good for prototyping devices.

Chosen techniques

As a first step to build the device for this work, is to think how to fabricate the 3D physical barrier that will allow axonal isolation. Normally, the fabrication of a master mould is required, followed by its pattern replication. Precisely to build the 3D physical barrier needs to contain the features (e.g. channels or microgrooves) that will allow the axonal isolation. Therefore, the manufacturing processes, such as lithography and micromachining, were also considered for the development of a master mould. The master mould would contain specific features for axonal growth and isolation.

The master mould of the microfluidic devices for axonal isolation are normally made of glass and silicon. However, these materials are employed in lithography techniques (e.g. photolithography), which are expensive, slow and involve many steps, including spin-coating, soft- and post-bake, exposure, development and cast mould. Additionally, the lithography techniques require photomasks with high-resolution to produce the structure desired (Liu *et al.*, 2016). Consequently, these techniques were not used for the development of a master mould to generate the 3D physical barrier.

Regarding the micromachining techniques to develop a master mould with channels with a small resolution to allow axonal isolation would be experimental, because there the author of this thesis was not able to find any article where a master mould was developed by micromachining to develop a device for axonal isolation. Furthermore, the additive manufacturing techniques were also taken into consideration to build the device, in particular the 3D physical barrier. Some of the techniques do not have the right resolution (as seen in **Table 1**) or the materials are not transparent, and the techniques that have the right resolution are so expensive as lithography techniques, time consuming and there is no way to ensure the consistency between layers. As a consequence, these techniques were not further considered for the development of the device.

Therefore, a polycarbonate membrane was chosen to be the 3D physical barrier of the device that would allow axonal isolation. The polycarbonate membrane contains pores with the dimensions required for allow only the passage of axons, which is the only dimension defined and required for the development of the new device. The polycarbonate membrane can be incorporated in the fabrication of devices by xurography technique (Bartholomeusz, Boutté and Andrade, 2005), which is going to be explained bellow in section 2.2.3. The polycarbonate membrane contains pores that will allow the passage of axons between compartments, and xurography allows to cut the membrane with the right dimensions to be incorporated in devices. Besides, this technique is very inexpensive and easy to employ. In contrast to the expensive techniques, replica moulding soft lithography use polymers, which due to their physical and bio-chemical properties are low-cost. The most common polymer used in soft lithography is PDMS (Rothbauer *et al.*, 2015). An interesting review on materials used in the manufacture of microfluidic devices is given by *Ren et al.* (Ren, Zhou and Wu, 2013).

To develop the new 3D cell culture device, soft-lithography was chosen to be combined with xurography; another low-cost technique. This choice was based on the requirements, technological capabilities (**Table 1**) and facilities access. Soft lithography is the standard technique used by researchers to fabricate biological devices as easy to develop in any laboratory without access to clean rooms. Xurography is a rapid low-cost technique that allows rapid prototyping with low cost materials (Bartholomeusz, Boutté and Andrade, 2005). Combining these techniques allows for rapid and low-cost prototyping in achieving the device fabrication requirements, such as biocompatibility and transparency. Xurography is used to seal different materials using tape (Bartholomeusz, Boutté and Andrade, 2005; Kim *et al.*, 2014; Neuville *et al.*, 2017).

As explained in the hydrogels section, after the device being fabricated it is going to be used to insert hydrogel with mixed cells. As the hydrogel will have the molecules for cell adhesion, molecules and mechanical structure that will support cell growth. Moreover, due to the hydrogel the cells will develop and the axons will growth and cross between compartments through the membrane pores.

2.2.1 Materials

In the literature, silicon (Worthington *et al.*, 2015; Khalili *et al.*, 2016; Tolstik *et al.*, 2016; Yang *et al.*, 2016), glass (Stubbe *et al.*, 2015; Tang *et al.*, 2017), polymers (Yu *et al.*, 2016; Immich *et al.*, 2017), both elastomeric (Wang *et al.*, 2017) and water based polymers (Marrella *et al.*, 2017; Pensal *et al.*, 2017) have been used in the fabrication of cell culture devices.

Glass and silicon have been the main choice materials over the years, due to wide use in microelectronics industry. Silicon is a hard material, fragile and opaque that has been used to fabricate high resolution features for master moulds (Taylor *et al.*, 2005; Yamada *et al.*, 2016; Schurink *et al.*, 2017). However, these materials are time consuming, expensive and require a cleanroom laboratory. Material science research has increased to seek new low cost materials, such as polymers (Faustino *et al.*, 2016).

Polymer materials have many advantages in overcoming the issues found for hard materials (i.e. silicon). Having flexibility, ease of process, low costs and desirable optical, mechanical and chemical properties (Weibel, Diluzio and Whitesides, 2007; Faustino *et al.*, 2016; Lembong, 2018), make them the preferred choice for pattern replication.

PDMS is normally the preferred material choice for soft-lithography, which is also a good technique for rapid prototyping. PDMS has been widely used in the design and fabrication of devices, due to its biocompatibility, optically transparency, flexibility and excellent sealing properties (Faustino *et al.*, 2016)(Kim *et al.*, 2007). In contrast, thermoplastic materials (such as PMMA and PC) are more rigid and they are not gas permeable leading to incompatibility issue in the study of cell cultures devices with in microchannels or microchambers (Mou and Jiang, 2017). Thermoplastics present better solvent compatibility than PDMS making them a popular choice for the commercial production of biodevices (Becker and Locascio, 2002)(Mou and Jiang, 2017).

2.2.2 Soft-lithography

Soft-lithography is a simple, popular and inexpensive method used for the in fabrication of microfluidic devices. This technique involves the transfer of pattern from the mould by using polymeric materials, such as elastomeric polymers or thermoplastics, shown schematically in **Figure 12** (Xia and Whitesides, 1998). Soft-lithography is widely used for the replication of patterns in the development of biological devices. This mainly due to its simplicity of use with limited specialist knowledge, requiring only a gas-desiccator and a hot-plate or oven. Furthermore, polymers are typically used in soft-lithography as they are low cost due to their physical and bio-chemical properties (Rothbauer *et al.*, 2015). Polydimethylsiloxane (PDMS) is considered the standard material for biological devices (Millet *et al.*, 2010), making it an attractive material choice project. The PDMS material is deposited onto the substrate or master mould, cured and peeled off. By casting the PDMS, the features are reproduced in relief on its surface (Tobergte and Curtis, 2013). Soft-lithography is widely employed by many research groups with PDMS being the most commonly used polymer (Rothbauer *et al.*, 2015). PDMS is ideal for manufacturing the new device due to its greater flexibility, transparency and biocompatibility (Tobergte and Curtis, 2013).

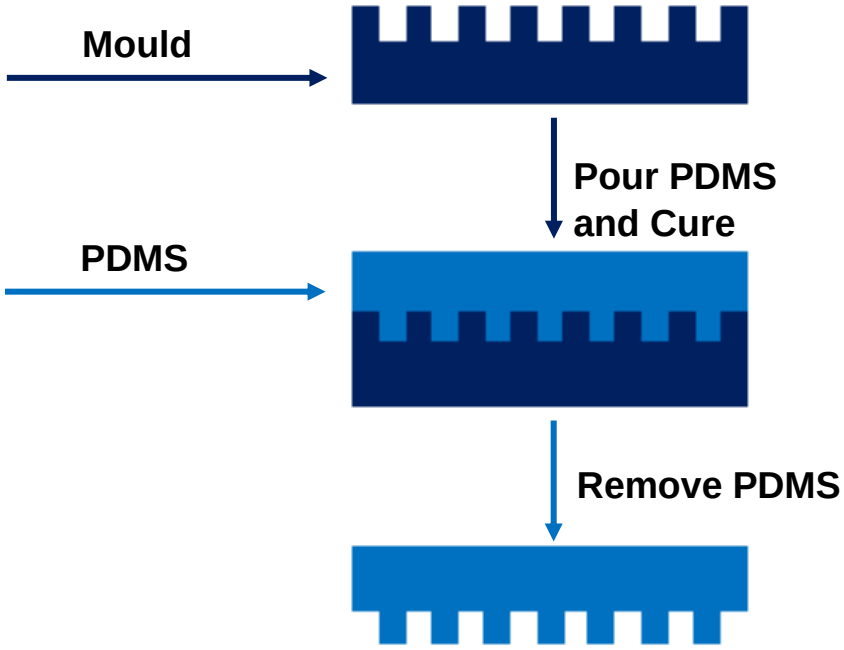


Figure 12 – Schematic of the soft-lithography process, with the replication of a pattern from a mould. Typically, for biological devices, replicas are made of PDMS, which are poured on the mould, cured and removed.

2.2.3 Xurography

Xurography is a prototyping technique that uses a sharp blade or a knifer plotter to design stryuctures onto films. This technique is a great solution to overcome the drawback of lithographic techniques such as photolithography. Since lithography techniques require the photomasks and clean rooms, also they are time-consuming and expensive. Xurography is a low-cost technique that are easy to employ and quick to test different designs as it is a rapid to fabricate different designs. It is used to accurately cut tape to the required dimensional tolerance of a given PDMS structure as described by *Pinto et al.* (Pinto *et al.*, 2015).

This inexpensive and rapid prototyping technique is widely used for the fabrication and development of channels for microfluidic research. Using a cutting plotter, complex geometries can be fabricated (Bartholomeusz, Boutté and Andrade, 2005; Santana *et al.*, 2013; Islam, Natu and Martinez, 2015; Faustino *et al.*, 2016; Martínez-lópez *et al.*, 2016). Basically, it consists in designing a sketch in a software such as CAD, connecting to a cutting plotter and a blade follows a cutting path of the features designed in the CAD draw as it moves, please see **Figure 13**.

Xurography has been used for adhesive vinyl films to generate moulds and seal thermoplastics for the manufacture of microfluidic devices (Nath *et al.*, 2014). In applying this technique, the materials used are required to have smooth, flat surfaces to achieve precise sealing (Bartholomeusz, Boutté and Andrade, 2005; Kim *et al.*, 2014; Neuville *et al.*, 2017). Therefore, it is crucial to ensure that the surfaces are flat and smooth that the tape will attach the surfaces of the film and to other compartments of the device.

For this work, the polycarbonate and double adhesive silicone are going to be cut, requiring minimum dimension of 3 mm. *Bartholomeusz et al.* (Bartholomeusz, Boutté and Andrade, 2005) reported structures with many dimensions from 100 µm to 6 mm widths and lengths of 25 mm. Smaller dimensions were reported for the a microfluidic device, which showed rectangles and triangles with crossections with minimum 20 µm in PDMS sheets (Cosson *et al.*, 2014). The limitation resolution of this technique depends on the material that is cutting and the thickness of the material (Charmet *et al.*, 2020). This technique also developed to design channels with 100 um channels on double tape with 25 um thickness, channels for DNA analysis (Greer *et al.*, 2007).

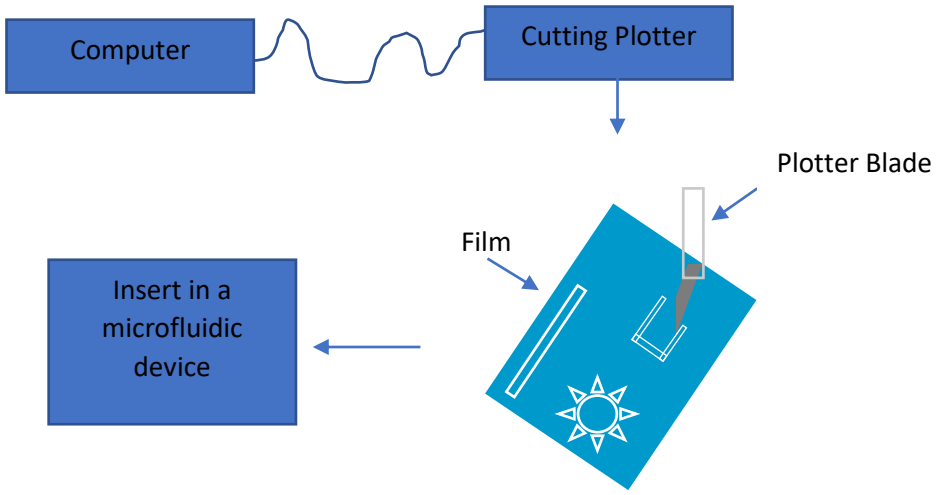


Figure 13 – Scheme of Xurography technique, which consists in designing the features desired in a CAD software connected to the cutting plotter. The blade cuts the film to replicate the design drawn in the CAD design. Later the film that was cut is collected and incorporated into the device.

2.3 Rheology

In the quest to replicate the *in vivo* environment conditions, there are not only the biochemical requirements (e.g. nutrients and components of the ECM) to take into consideration, but also biomechanical (e.g. stiffness and viscosity). The mechanical properties of the hydrogels are important in the understanding of their influence on cell behaviour. The cellular environment directly affects cells phenotypes, highlighting the importance of hydrogel selection for the culturing of cells or for the interface of cells with hydrogel material (Kotov *et al.*, 2009; Saracino, Cigognini and Silva, 2013).

The requirements of hydrogel are to be biocompatible or at least able to mimic the cellular, chemical (Shari *et al.*, 2016) or physical (Scholl and Spro, 2000) environment. Neurite growth is known to be influenced by hydrogel stiffness, since the use of softer hydrogels (i.e. hydrogel) will also improve cell phenotype and promote neurite extensions. (Zuidema *et al.*, 2014)(Navaei-nigjeh *et al.*, 2013)(Previtera, Langhammer and Firestein, 2010)(Crompton *et al.*, 2007)(Balgude *et al.*, 2001)(Dillon *et al.*, 1998). For example, using 2% Agarose presents a higher mechanical stiffness than 0.75% (Balgude *et al.*, 2001). *Balgude et al*. (Balgude *et al.*, 2001) showed that longer dorsal root ganglia neurite extensions in 0.75% Agarose.

Rheology is the science that investigates the deformation and flow behaviour of different material types when forces are applied (Mezger, 2014). Oscillation tests has been widely applied to analyse the viscoelastic properties of a biomaterial. An amplitude oscillatory sweep is used to obtain the stiffness of the gel and is applied as a strain, measuring the sine and cosine function. Corresponding to the elastic and viscous properties of the material (Qian *et al.*, 2019)(Mezger, 2014).

Oscillation tests are performed using a rheometer and are based on the principles of Hooke's Law (further information about the theory are given in **Appendix 1**. The storage modulus (G') describes the elastic behaviour of the biomaterials, while the loss modulus (G'') describes the viscous behaviour of the biomaterials. Thus, the viscoelastic behaviour of materials is characterised by determining the viscous and elastic portions of the material response. In the amplitude sweep, the structural character of the biomaterial is characterised by analysing the viscoelastic parameters, which correspond to the G' and G'' moduli in the linear viscoelastic (LVE) region, as shown in **Figure 14**.

This region describes the deformation that the material can withstand without promoting a structural breakdown of the material (Mezger, 2014). As a rule of thumb the structural characteristics of a material can be classified by:

1. If G'> G'', the structure exhibits the characteristics of a gel or solid
2. If G''> G', the structure exhibits the characteristics of a liquid or a fluid.

The G' modulus is also described as the rigidity modulus or gel strength. Typical G' values for viscoelastic gels are between 50 to 5000 Pa (Mezger, 2014). Within the LVE region, as shown in **Figure 14**, the viscoelastic parameters G′ and G″ remain constant to the applied strain.

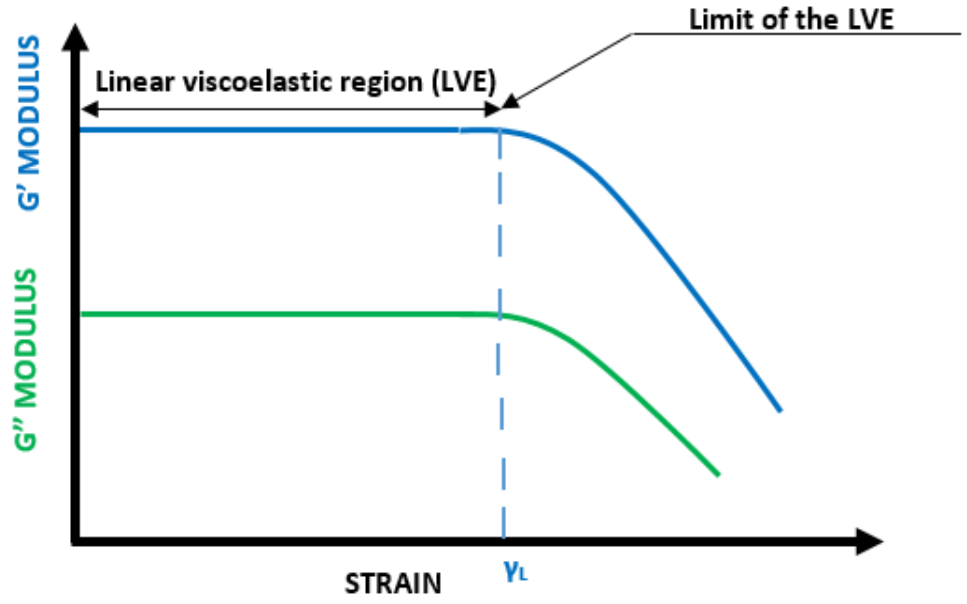


Figure 14 – The linear viscoelastic region of a sample measured using a rheometer, where the storage modulus and the viscous modulus are plotted as a function of the strain. The linear viscoelastic region is determined by the strain dependence of the G' and G'' moduli.

The limit of the LVE range indicates the amplitude response of the structure, where the sample remains without significate structural damage. The limit of the LVE value is obtained in the G' modulus curve. In this work, the viscoelastic behaviour was obtained with an Anton Paar Rheometer, using the manufactures operational guidelines.

A protocol using the same methodology is also described by *Zuidema et.al* (Zuidema *et al.*, 2014), where they obtained stiffness values for a variety of natural gels.

Including values of 90 Pa and 2.5 kPa for Matrigel and Agarose gels, respectively. Recently, *Koppes et al.* (Koppes *et al.*, 2016) followed the same methodology presented by *Zuidema et al.* (Zuidema *et al.*, 2014), to measure the stiffness of collagen-matrigel hydrogel samples. Here, they calculated the storage modulus by averaging the linear region of the strain sweep at the limit of the LVE. This methodology has also been used in the characterisation of viscoelastic properties and the calculation of the gel stiffness (or gel strength) of other materials, such as cement (Qian *et al.*, 2019), nanocomposite gels (Ivana *et al.*, 2019) and nucleoside gelators (Johnson *et al.*, 2018).

Frequency sweeps can also be performed within the LVE region to distinguish the type of material characterisation, as shown in **Figure 15**. Typically for gels, the storage modulus is higher than the loss modulus over all the range of frequencies. In a frequency sweep, a sinusoidal oscillation is applied at a fixed strain but the frequency is varied. The output is the G' and G'' components as a function of frequency.

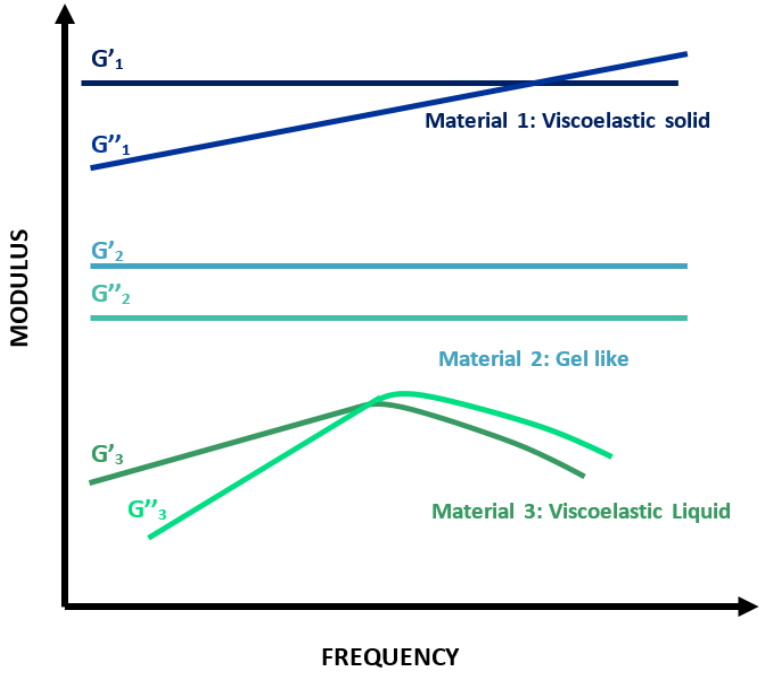


Figure 15 – Rheological frequency sweep tests for materials showing the storage modulus (G') and the loss modulus (G'').

2.4 *In Vitro* Neuron Culture Devices for Axon Isolation

In the twentieth century the hanging drop method was successfully carried out by Harrison (Harrison, 1907), where it was possible to culture neuronal cells *in vitro*. Since then alternative neuronal culture methods have been introduced, such as cell culture flasks. However, these methods did not take into consideration the compartmentalisation "concept" in studying sub cellular compartment and neuronal communication between different cell types (Millet and Gillette, 2012b). Later in the 1970s, appeared the first fluidic multicompartment chamber for neuron isolation, known as a Campenot chambers (Campenot, 1977). Campenot chambers are widely used for culturing neurons in an isolated environment at the microscale (Curanović *et al.*, 2009; Natera-naranjo *et al.*, 2010).

These culture devices are made of Teflon chambers attached to silicon grease on a petri dish and were used to study signalling transport and synapse formation, among others, and in axon growth studies (Taylor *et al.*, 2005). The disadvantages of Campenot chambers are that they are not transparent and require a hydrophobic sealing. Their fabrication is time-consuming and they are not suitable for CNS neurons; cortical neurons do not grow enough for the length of the channels of Campenot chambers (Taylor *et al.*, 2003; Park *et al.*, 2006). Despite these drawbacks, Campenot chambers are still used for the study of peripheral nervous system neurons (Gervasi *et al.*, 2016), and they can be considered the precursors of the new generation of compartmentalised devices.

In the 1990s, the concept of patterned surfaces as described by (Britland *et al.*, 1992; Kim, Park and Kang, 1995; Chen *et al.*, 1998) starts to be applied for *in vitro* devices, where cell adherent molecules, such as extracellular matrix (ECM) proteins, are deposited onto surfaces, such as glass or plastics substrates. This is achieved by manufacturing techniques like microcontact printing or laser patterning (Sciancalepore *et al.*, 2016). The advantages of surface patterning is that they are easy to employ, inexpensive and allow the control of cell behaviour; such as migration and differentiation (Hassanzadeh-barforoushi *et al.*, 2016). However, this technique by itself does not provide fluidic control and axonal compartmentalisation. Thus, a new generation of compartmentalized devices, specifically designed for axonal isolation, were developed by *Taylor et al.* (Taylor *et al.*, 2003).

A reference to the design of these new compartmentalised devices, also known by XONA devices (XONA Microfluidics Inc., U.S.), is shown in **Figure 16**. These 2D compartmentalised devices, unlike Campenot chambers, are based on PDMS chambers fabricated by soft-lithography and are used in biological studies of central CNS neurons. These new compartmentalised devices are also compatible with high-resolution imaging techniques and with immunocytochemistry (Park *et al.*, 2006). Enabling the capture of cellular behaviour over time, for example during differentiation and neurite outgrowth. These devices can be used to study axonal growth and regeneration after damage. As previously mentioned in other sections of this thesis, they consist of two compartments separated by microgrooves, where cells can be plated in one of the two comportments, whereas axons are allowed to extend and cross the microgrooves to the other one, please see **Figure 16**.

After approximately four days in culture, axons start crossing the microgrooves (150 µm length and 3 µm height) and reaching the axonal compartment. This generates a compartmentalised culture, where axons are separated from the cell bodies of the neurons. This type of compartmentalised neuronal cultures are fluidically isolated and allow the application of treatment in individual cell compartments, such as soma and axon, by applying fluidic isolation (Taylor *et al.*, 2005).

Fluidic isolation is achieved by applying a volume difference between the two chambers. This hydrostatic pressure (Taylor *et al.*, 2003), relies on applying a higher media volume to one side of the chamber, generating a flow of media from the higher to the lower chamber volume. This difference in volume prevents the passage of neurons or molecules between compartments. The time of isolation depend in the molecule size, for example Texas red dextran (3,000 Da) for 20 hours *Taylor et al.* (Taylor *et al.*, 2005) and Fluorescein (400 Da) for 15 hours (Taylor *et al.*, 2003). For instance, Park et al. (Park *et al.*, 2006) established the use of 30 µl volume difference between compartments for molecules larger than 1kDa and 50 µl volume difference for molecules smaller than 1 kDa.

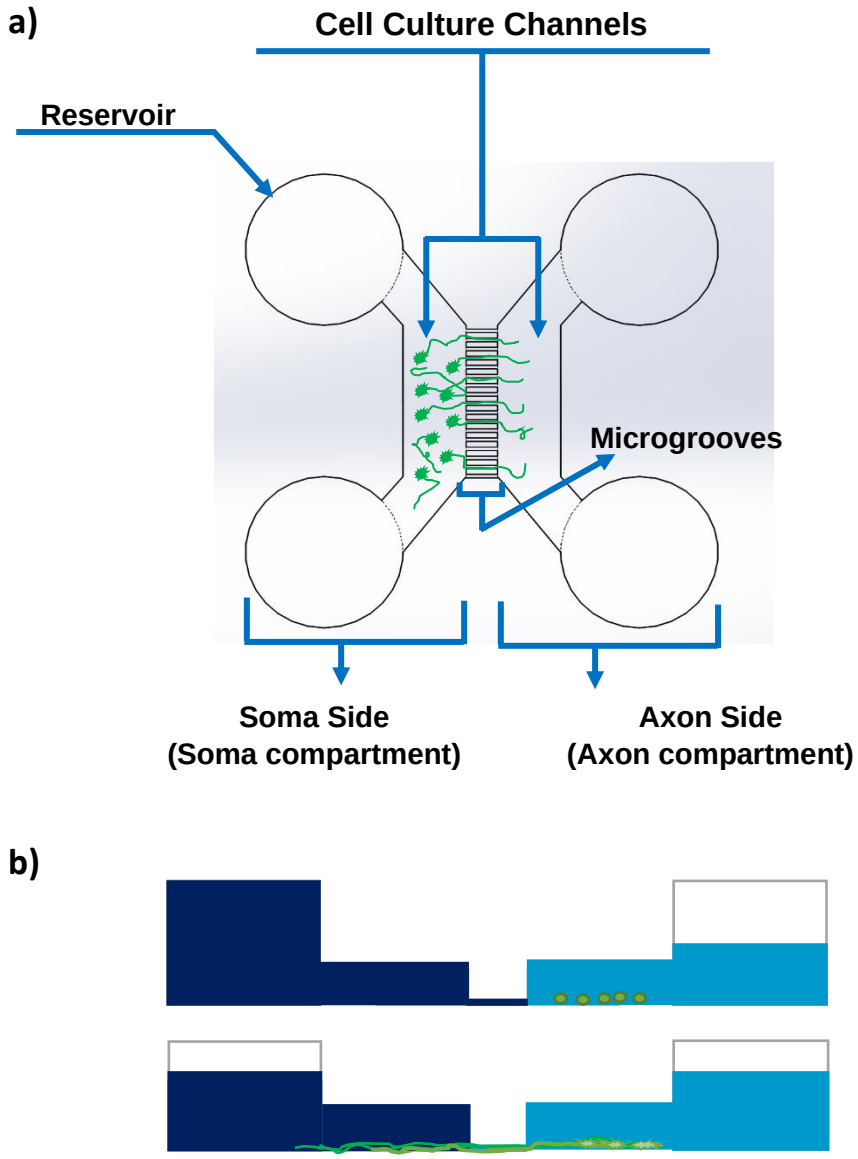


Figure 16 – Schematic design of microfluidic cell culture devices for axon isolation. **a**) Top view of the compartmentalised XONA device, showing the soma compartment where the neurons are seeded. The cells begin to polarize and its neurites grow. The axons cross to the axon side through the microgrooves. **b**) Section view: fluidic isolation of cell bodies from the soma side is achieved by applying an asymmetric media volume (hydrostatic pressure) between the two sides.

Hydrostatic pressure leads to a continuous flow that precludes the diffusion of soluble compounds into the chamber with higher volume over the microgrooves. It is possible to add small volumes in the chambers and maintain the fluidic isolation (Taylor *et al.*, 2003, 2005). Hence, it is possible to obtain pure axonal material from one compartment and perform localised biochemical analysis (Taylor *et al.*, 2005). The length of microgrooves can be adapted depending on the neuronal cell type and the duration of the experiments as required.

After the axons cross the microgrooves, experimental analysis can be carried out, such as axotomy, imaging and screening of regeneration processes, etc. (Taylor, Rhee and Jeon, 2006; Park *et al.*, 2009; Yang *et al.*, 2010; Poon *et al.*, 2011; Howard *et al.*, 2013; Southam *et al.*, 2015; Hengst *et al.*, 2016; Al-ali *et al.*, 2017). Another example of the use of microgrooves is the radial array based on PDMS presented by *Park et al.* (Park *et al.*, 2014).

2.5 Summary

There is an increasing need to investigate the cellular and molecular processes that define the biology of the axon, both in normal conditions and in axon injury, transport and regeneration. One requirement for these studies is axonal isolation, since is it important to study pure axonal material without the cell bodies. Nowadays, namely due to the success in isolating axons from soma, Taylors's devices have become the standard and are being used to address a diverse range of questions in neurological disorders (Dajas-bailador *et al.*, 2012, 2014a; Ueno *et al.*, 2012; Dixon and Philbert, 2015; Bomba-warczak *et al.*, 2016; Eitan *et al.*, 2016; Kebschull *et al.*, 2016; Kos *et al.*, 2016; Garcez, Guillemot and Dajas-bailador, 2017). These devices are mainly used to investigate axonal events (Taylor *et al.*, 2005), for example the influence of miRNAs in axon growth (Dajas-bailador *et al.*, 2012)(Zhang *et al.*, 2013) or to investigate how a virus is transmitted between neurons, by isolating the virus in one compartment of the device (Liu *et al.*, 2008). Using the same strategy of isolating a virus in one compartment, the neural activity has been investigated by *Jokinen et al.* (Jokinen *et al.*, 2013).

Other example is the induction of axonal damage and the investigation of how axons regenerate after injury (Hellman *et al.*, 2010). As well as, the possibility to investigate the interactions between neurons and astrocytes (Gao *et al.*, 2016). Despite these contributions in the study of neurons using compartmentalised devices, cells do not exhibit similar growth as cells *in vivo* and present a different cell shape, which affects cell bioactivities in native tissues (Jensen, Morrill and Huang, 2018)(Duval *et al.*, 2017). It is also noted that these studies are based on standard cell cultures, which rely on seeding cells on hard surfaces with high stiffness.

The fact that cells grow on glass or polystyrene surfaces, is the result of two-dimension devices, where cells can adapt into a different shape than in *in vivo* tissue. This in turn leads to the loss of cell phenotype resulting in a different cell response than that given by cells in their native environment. Cells were also seeded on to scaffolds or biomaterials (i.e. hydrogels) to provide a better mechanical support and a closer biological environment to reality (Caliari and Burdick, 2016; Kornev *et al.*, 2018).

Recently, a device consisting of a pillar array to allow axonal growth to be in the same direction of the Matrigel fibers was reported by *Bang et al.* (Bang *et al.*, 2016). The hydrostatic pressure influenced the orientation of Matrigel fibers, which allow the alignment of neurites outgrowth. This study only considered axonal growth in a limited Z coordinate direction and the axons were not completely isolated from their cell bodies. This study reinforces the need for research to move from 2D to 3D studies; able to isolate axons more similar environment to the native tissue.

2.6 Knowledge Gap

The knowledge gap identified in this literature review is the lack of an effective device that allows the compartmentalised culture of neurons in a three-dimensional manner, with methods that efficiently isolate axons in 3D, thus adding a more physiological layer to the current technologies.

Indeed, as already mentioned in previous sections of this thesis, the ability to compartmentalise and grow axons in an isolated fluidic environment, is fundamental to study processes and mechanisms leading to axon formation and the establishment of connectivity, ultimately delivering the ability to evaluate neuronal response to axonal stimulation/damage due to normal or disease/injury conditions. The tantalising possibility to replicate and study the same mechanisms into a three-dimensional environment, would only add a further significance and relevance to the aforementioned cellular processes, thus taking us a step closer to the comprehension of the mechanisms underlying axon development, maintenance and degeneration. After all, neurons are the most compartmentalized and interactive of all cell types, and this specialized structure requires that homeostasis is sustained over the long distances that separate a cell body from its axon terminus.

Given this long distance and an axonal volume that is many times that of the cell body, decades of research have focused on the understanding of how such a compartment can grow during development, re-grown after injury, and maintain itself throughout adulthood. Even if early evidences focused on the local environment or the cell soma as supplying the needs of the axon, it is now well-established that the axon has some unique needs that can only be met from within (Spaulding and Burgess, 2017).

In fact, several studies have focused throughout the years on the axonal compartments for the investigation of several cellular processes, such as axonal growth/regeneration, axonal transport and axonal guidance, (Dajas-bailador *et al.*, 2014b; Jia *et al.*, 2016; Kneynsberg *et al.*, 2016; Miranda-saksena *et al.*, 2016; Bigler *et al.*, 2017; Lucci *et al.*, 2020) exploiting 2D cell culture as methods. For example, Bigler and colleagues have isolated axons of human embryonic stem cells from their cell bodies in 2D compartmentalised devices for gene expression studies (Bigler *et al.*, 2017). Specifically, they identified the axonal mRNAs presents in local translation for axon guidance, signalling and regeneration (Bigler *et al.*, 2017). Furthermore, using compartmentalised microfluidic chambers, Dajas-Bailador and colleagues investigated the role of two specific proteins JIP1 and AKT in the regulation axon development (Dajas-bailador *et al.*, 2014b). Here, the axons were treated separately from their cell bodies and it was found that these proteins colocalises in axonal growth cones of cortical neurons and collaborated to promote axon growth of cortical neurons (Dajas-bailador *et al.*, 2014b). Similar, *Jia et al.* (Jia *et al.*, 2016) manipulated the axons in a compartmentalised device to investigate the role of a single microRNA, miRNA-146a in neuronal development. showing how it could influence axonal growth. *Miranda-Saksena et al.* (Miranda-saksena *et al.*, 2016) using investigated the axonal transport of neurons from their axons up to soma. Here, they evaluated the role of a protein (pUS9) involved with the Herpes virus in axon growth and in axonal transport (Miranda-saksena *et al.*, 2016). The gene expression on axons under herpes virus conditions was investigated by *Donher et al.* (Dohner *et al.*, 2018) using the same XONA chambers (with microgrooves of 450 µm length).

Understanding the mechanisms underlying the formation of the axon and the establishment of connectivity with post-synaptic targets, would ultimately also shed light on the events that lead to progressive neurodegeneration that implicate axonal dysfunction and damage as an early manifestation of disease pathology, diseases such as Alzheimer's disease, Parkinson's disease. In the CNS, once axons are damaged, they are unable to regenerate successfully, and any pathological processes affecting their function and viability could lead to impairment of connectivity and ultimately neuron death (Lingor *et al.*, 2012; Li and Chen, 2016; Hilton and Bradke, 2017). Therefore, therapies that can prevent or delay axonal degeneration and loss of function are expected to have substantial clinical impact on numerous disorders where axonopathy has a major role in disease progression. Toward this aim, the development of new and effective methods to physically and functionally separate the axons from their soma becomes crucial to study specific molecular and signalling events happening in the axons.

As a conclusion, an efficient method to characterise the localised events on the different subcellular compartments (e.g. axons, cell bodies; dendrites) is using compartmentalised devices. For example, isolating axons from cell bodies allow researchers to investigate the local mechanisms behind axon polarisation, axon transport, axon growth, axonal guidance and/or axon regeneration. The fluidic isolation allows researchers to study specifically the axon mechanisms without influence of the mechanisms from cell bodies, which without isolation would not be possible to achieve. For example, would not be possible to distinguished protein expression levels from axons and cell bodies. It is important to understand the neuron development or the mechanisms in the axons, how they growth, how they polarise, in order to further elucidate mechanisms and potential clues in the understanding of neuronal and brain function. For instance, axons are critical to maintain neuronal connectivity so it is important to be able to study this neuron cell part individually from the others. After understanding the axonal development (i.e. growth, polarisation), we can understand the different intracellular pathways involved in the development of neuronal morphology. This is important to extended our knowledge to axonal degeneration (Kneynsberg *et al.*, 2016). For example, *Kneynsberg et al.* (Kneynsberg *et al.*, 2016) were able to quantify the axonal degeneration by measuring axonal length in compartmentalised chambers.

Despite all the new insights and evidences generated by using 2D cell cultures, the isolation of the axons in 3D has not been successfully attempted. Considering that cells in 3D present different morphology, gene expression levels and phenotypes all the current studies should also be replicated in 3D, thus obtaining more realistic outcomes and more relevant results. In this way, drugs that might be developed for neurologic disorders would not fail in pre-clinical studies, as many drugs currently developed and tested on 2D methods are still failing in pre-clinical studies (Langhans, 2018).

Normally, the percentage of live cells is higher in 3D neuron cultures than in 2D (Chandrasekaran *et al.*, 2017). Additionally, morphological changes are visible between neurons growing in 2D and 3D (Laplaca, Vernekar and Shoemaker, 2010). *Li et al.* (Li *et al.*, 2007) reported morphological differences between 2D and 3D in retinal non-compartmentalised neuronal cultures, where neurons in collagen showed more extensions. Similar morphological changes between 2D and 3D neuron cultures were obtained by *Chandrasekaran et al.* (Chandrasekaran *et al.*, 2017), where the neurite extensions in non-compartmentalised systems were larger in 3D cultures than in 2D.

Another difference was found in gene expression levels, which tend to be higher in 3D cultures than in 2D cultures (Lee *et al.*, 2011; Carlson *et al.*, 2016). These studies were also performed in non-compartmentalised devices. Besides, differences in the neuronal network activity was also reported between 3D and 2D neuronal cultures within non-compartmentalised devices, where in 3D there are more random spontaneous spikes of neuronal activity (Frega *et al.*, 2014b; Bosi *et al.*, 2015a; Bourke *et al.*, 2018).

The studies carried out in 3D neuronal cultures are performed in non-compartmentalised devices that do not provide axon isolation. Therefore, the novelty is creating a new device for scientists to perform 3D neuronal culture studies in compartmentalised devices that allow axonal isolation, please see **Figure 17**. The addition of a 3D space provides a more physiological mean of culture, by allowing neurons to grow reproducing the physiological state that cells would be *in vivo*. The combination of 3D cell culture and 3D physical barrier for axonal isolation enables to monitor and evaluate the axonal length in 3D, which is an important step for future research.

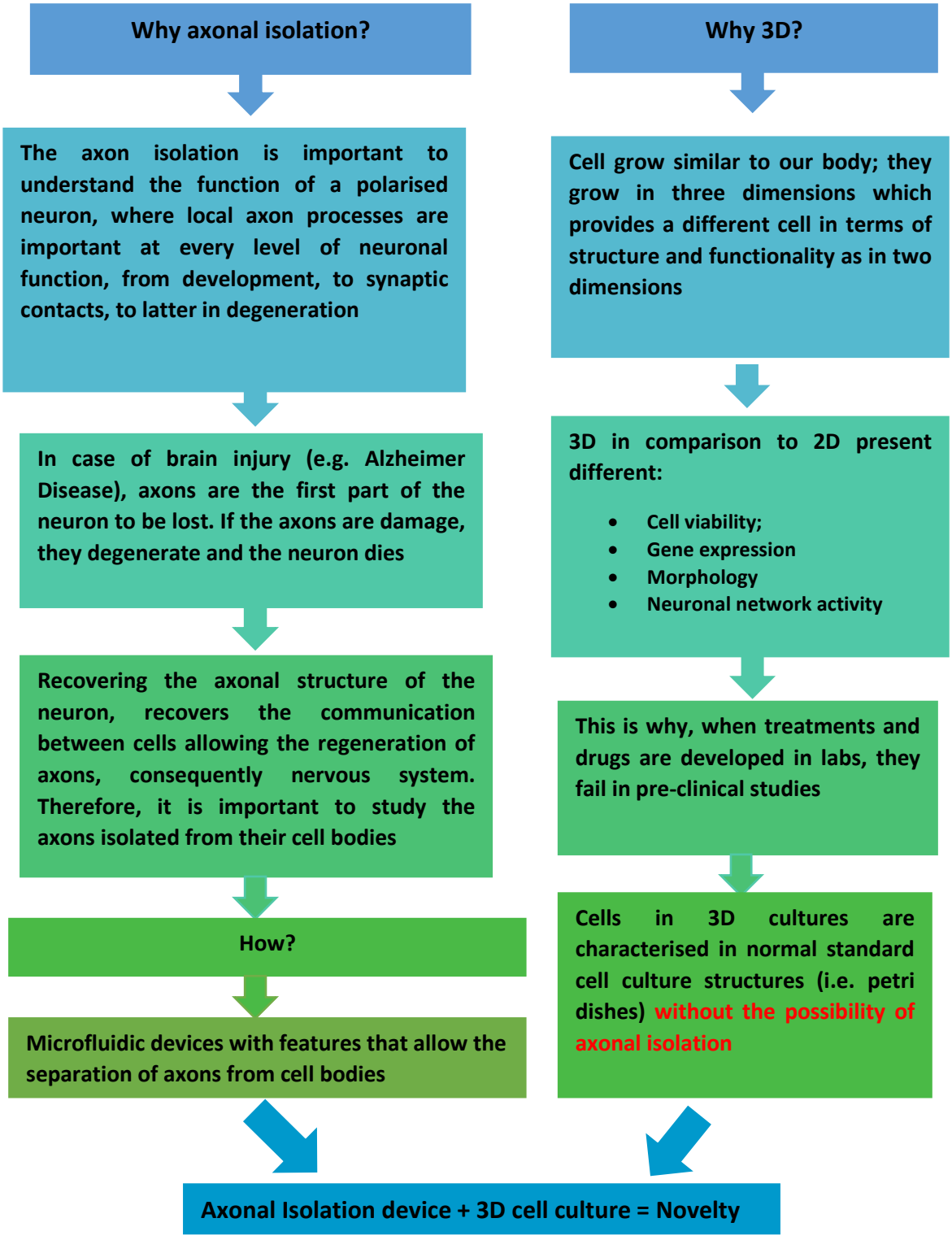


Figure 17 – Diagram showing why axonal isolation is important and why cells should be studied in 3D.

Chapter 3 Methodology

This section describes the experimental methodology for the design, fabrication and validation of the device. The device was designed to allow the separation of axons from their cell bodies within a 3D environment between compartments. It was manufactured using soft-lithography and xurography techniques. The efficiency of the device was characterised by determining the length of time a molecule is isolated in one compartment and if any leakage occurs. The validation of the device was obtained by allowing the passage of axons between compartments. The list of materials, equipment and software can be found in **Appendix 2** and **3**.

3.1 Microfluidic devices Fabrication

3.1.1 Design

The device design was created in SolidWorks Pro (2015), detailing the design, assembly and intended mode of operation. The proposed device allows the isolation of axons in a 3D environment to enable a better approximation of the processes occurring *in vivo*. A schematic representation of the biological process in the current 2D cell culture devices and what is expected to happen in the new 3D cell culture device is shown in **Figure 18**. The device consists of two polydimethylsiloxane (PDMS) blocks, where each block contains a reservoir and one channel, sealed to a polycarbonate membrane (Whatman®; 5 µm pore; 47 mm) with silicone adhesive transfer tape (3M).

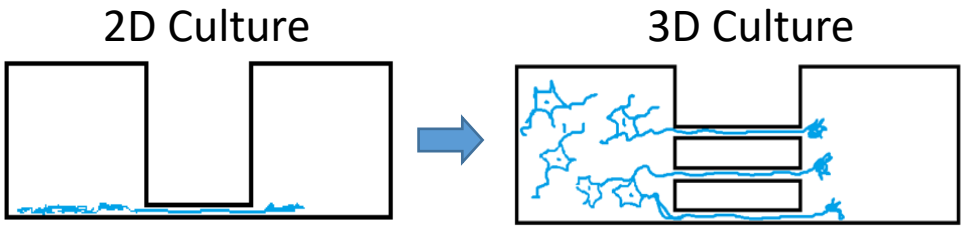


Figure 18 – Schematic of axonal isolation in a 2D environment (left) and in a 3D environment (right), where neuron development is represented in blue. In the 2D culture, neurons have a limited growth with a flattened shape attached to the surface, whereas for the 3D culture neurons are unrestricted with axonal isolation possible in 3D.

3.1.2 Soft-Lithography

Pre-polymer PDMS (Farnell) was mixed with a curing agent (weight ratio 10:1) within a plastic cup. After stirring the mixture, it was de-gassed in a vacuum desiccator for 30 minutes, poured onto the moulds and cured for 3 hours at 60°C. After curing, the PDMS was peeled off from the moulds revealing the PDMS structure, as shown in **Figure 19**. Finally, the PDMS structures were punched with a biopsy punch (5mm) to create the reservoirs.

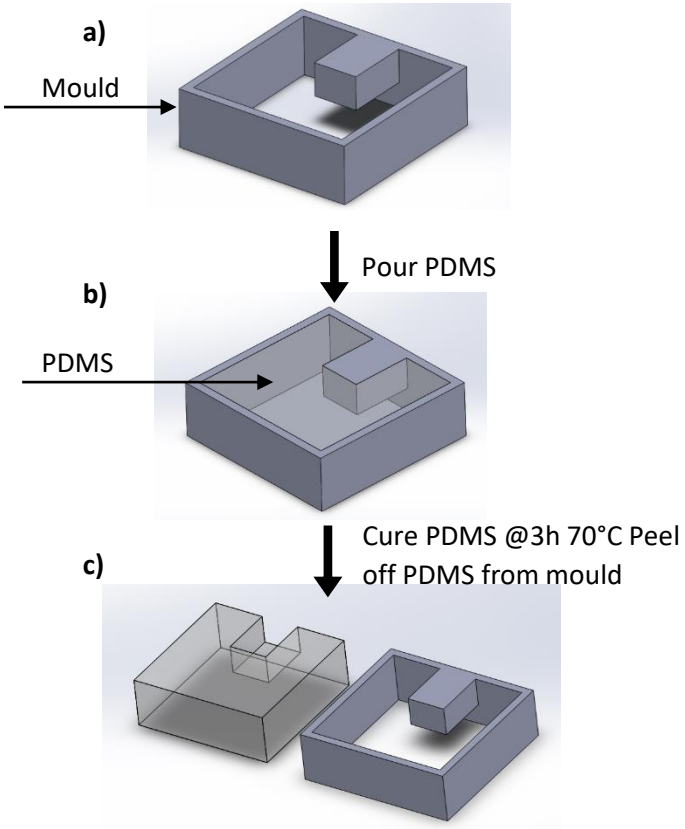


Figure 19 – Schematic representation of the process of the soft-lithography. A mould containing desired features (**a**) is used to replicate those features onto PDMS. Replicas are made of PDMS, which is first poured onto a mould (**b**) and then cured for 3 hours at 70° C (**c**). After curing, the PDMS is removed by peeling it off from the mould.

3.1.3 Xurography

The silicone adhesive transfer tape dimensions were designed in CAD and imported in the plotter cutter software (Silhouette Cameo, Graphtec) and then the tape was excised. The tape has adhesive on both sides; hence one side of the tape was sealed to the polycarbonate membrane and the other to the PDMS structure. The platform PDMS-tape-membrane-tape-PDMS was developed.

3.1.4 Materials cleaning

The materials used for the device were kept clean and sterile during fabrication. The PDMS blocks were rinsed in 70% ethanol and submersed in Hanks Balanced Salt Solution (HBSS, Ca^{2+}, Mg^{2+}, Gibco) on a petridish and placed in the incubator at 37˚ for overnight. After curing, the PDMS structures and the 22x50 mm glass coverslips (Menzel Glaser) were sonicated in sterile deionised (DI) water for 10 minutes and rinsed again in 70% ethanol for a further 10 minutes. Lastly, the PDMS blocks and glass coverslips were left inside the hood to dry overnight.

3.1.5 Reversible sealing

The sealing of different parts of the device was performed inside the hood. One side of the tape was sealed to the first PDMS structure, while the other side of the tape was sealed to the polycarbonate membrane. The un-taped side of the membrane was sealed to a second layer of tape, which was sealed to a second PDMS structure. In this way, it is possible to obtain a platform (PDMS-tape-membrane-tape-PDMS), as shown in **Figure 20**. This platform was reversibly sealed onto the glass coverslips, by pressuring the bottom surface of the platform against the coverslip with tweezers.

3.2 Leakage Tests

In order to investigate if any leakage occurs between the platform and the glass coverslip, the device was tested with a liquid solution. One reservoir of the device was filled with Ponceau (Fisher Scientific; glacial acetic acid; red dye) and the other reservoir was filled with Coomassie (Thermo Scientific; glacial acetic acid, methanol; blue dye). The device was left for 15 minutes and no leakage of fluid was observed by eye.

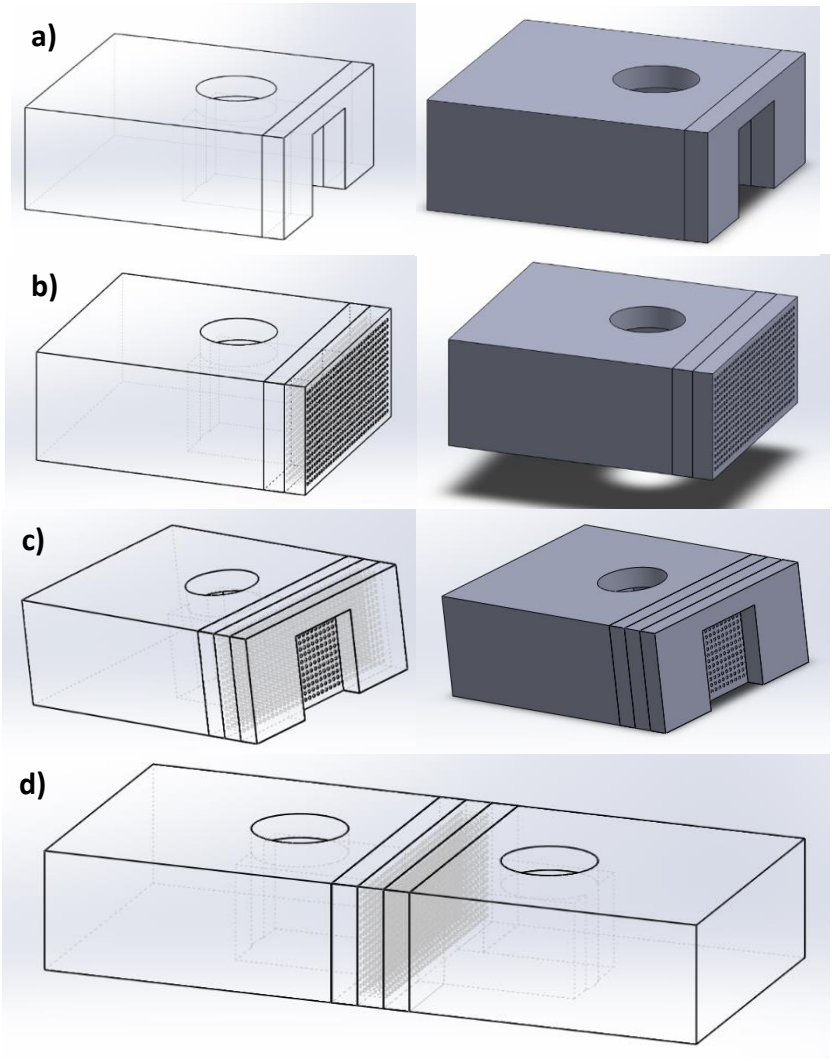


Figure 20 – PDMS block is sealed to double adhesive tape (**a**). The opposite side of the tape is sealed to the membrane (**b**). The other side of the membrane is sealed to tape (**c**) and the free side of tape is sealed to other PDMS block (**d**).

3.3 Diffusion Profiles of the Devices

3.3.1 Fluorescein Solution

Fluorescein was used to determine the time a molecule was isolated in one side of the device. First, a stock solution of fluorescein was made by measuring 40 mg Fluorescein powder (Sigma-Aldrich) in a scale and placing it in a falcon tube. 20 mL of phosphate buffered saline (PBS; Thermofisher) was added to the falcon tube, dissolving the fluorescein. Second, the molarity of the stock solution was calculated (0.0056 $mol \cdot L^{-1}$), and aliquots of 1 µM concentration were prepared and stored in the dark. The flow characterisation was performed using the Fluorescein aliquots in both 2D and 3D environment conditions within the device.

3.3.2 Diffusion Profiles in XONA device for 2D conditions

For the 2D flow characterisation XONA (SND150; XONA microfluidics) devices were used. 160 µL of PBS was placed in the soma side and 100 µL of fluorescein was added to the axonal side. Both solutions were added in the top reservoirs of the device, as shown in **Figure 21**.

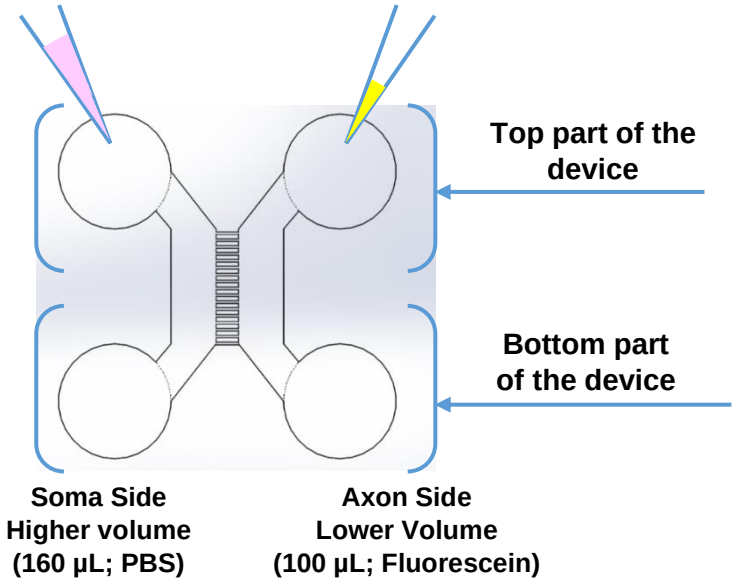


Figure 21 – Schematic representation of methodology used to determine the diffusion profiles in XONA devices for 2D environment conditions.

3.3.3 Diffusion Profiles in XONA device for 3D conditions

The diffusion of fluorescein in the XONA device was also investigated with the 3D conditions by adding a hydrogel, as seen in **Figure 22**. 160 µL of Matrigel (5 mg/ml) was added to the soma compartment and 100 µL of Matrigel was added to the axon compartment, the device was then placed in the incubator at 37˚C for 30 minutes. 160 µL of PBS was then added to the soma side and 100 µL of fluorescein added to the axonal side.

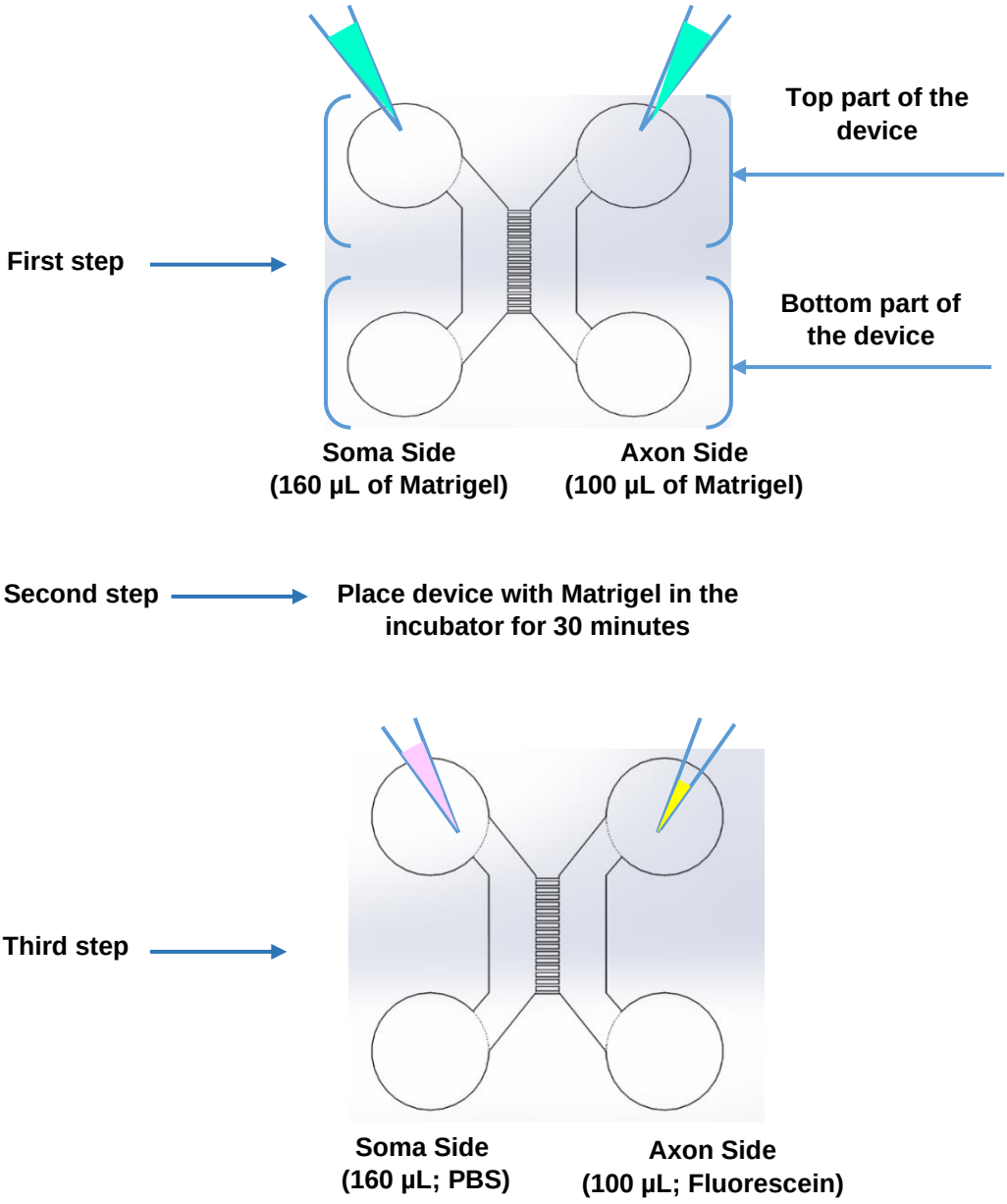


Figure 22 – Schematic representation of the methodology used to determine the diffusion profiles in XONA devices for 3D conditions. First step, Matrigel to the device in pre-gel solution. Second, the gel is formed by placing the device in the incubator, following the addition of fluorescein and PBS to the device.

3.3.4 Diffusion Profiles in the new device for 3D conditions

For the new device, 3D diffusion profiles were obtained using two different hydrogels, Agarose and Matrigel (**Figure 23**). For Agarose, 250 µL of 0.5% Agarose was added to the soma compartment and 200 µL of 0.5% Agarose was added to the axon compartment. After 30 minutes, 160 µL of PBS was added to the soma side and 50 µL of fluorescein in axon side. For Matrigel, the device was placed in the cold room at 4˚C overnight. 250 µl of 5mg/ml Matrigel was added to the soma side and 200 µl to the axon side. The device was placed in the incubator at 37˚C for 30 minutes. After which, 160 µL of PBS was added to the soma side and 50 µL of fluorescein in the axon side.

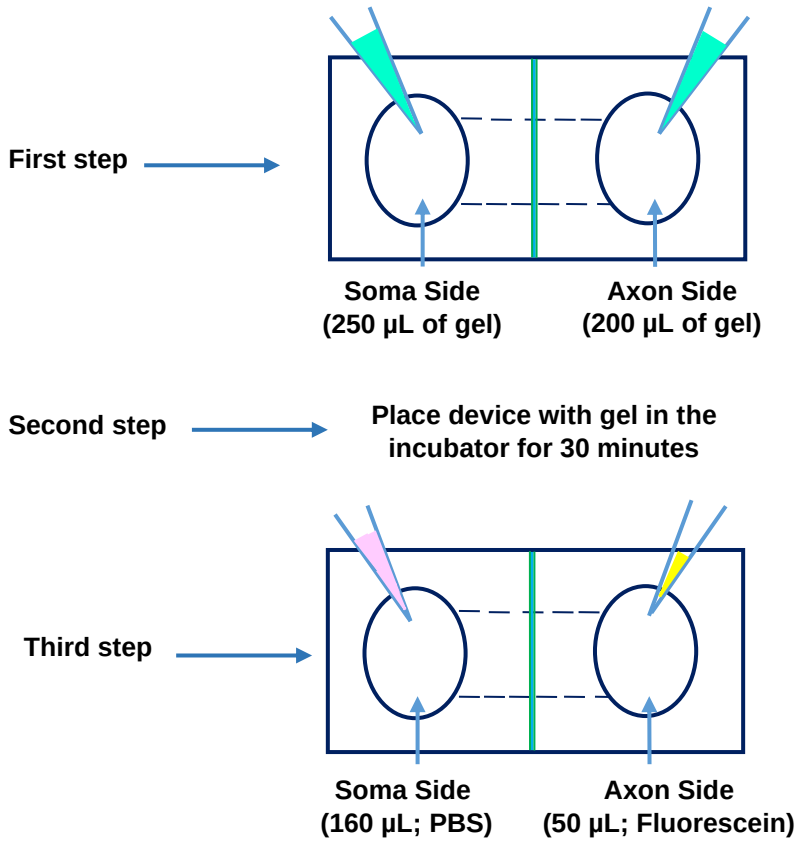


Figure 23 – Schematic representation of the methodology used to determine the diffusion profiles in the new 3D device. First step, a pre-gel solutions of Agarose or Matrigel was introduced in the device. Second, the gel is formed by placing in the incubator, following the addition of fluorescein and PBS to the device.

3.3.5 Image Analysis

Images were captured to measure the fluorescein intensity in the soma and the axon sides to assess the fluidic isolation, see **Figure 24**. The fluorescein intensity was measured in both sides by taking the average of fluorescein intensity in three different regions selected in the axon side (green squares) and in three different regions in the soma side. The fluorescence images were taken with a time exposure of 200 ms every 15 minutes over a 15 to 48 hour period. This experiment was performed using three different microfluidic devices, and repeating three times the experiment in each device. The data was normalised to the maximum fluorescence intensity using Origin Pro (version 9.1) and ImageJ (Fiji) software. This method to determine the fluorescence intensity is also described by *Taylor et al.* (Taylor *et al.*, 2003; Anne M Taylor *et al.*, 2010).

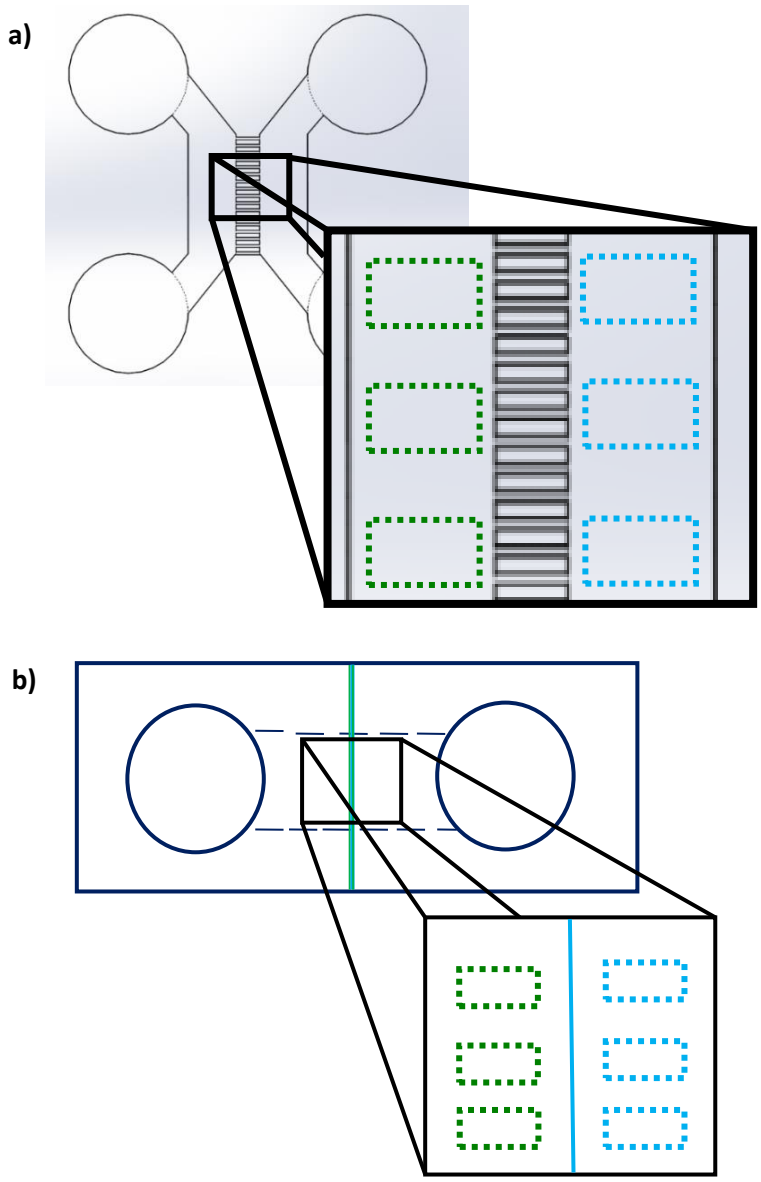


Figure 24 – Schematic representation of the regions of interest in the axon side (blue dotted lines) and soma side (green dotted lines) in the XONA device (**a**) and in the new device (**b**).

3.4 Rheology

Oscillatory rheology was performed using an Anton Paar Rheometer (MCR302, Austria) with two parallel plates (25 mm). The samples were placed on the bottom plate in pre-gel solutions. The temperature of the bottom plate was controlled to 37°C with the samples in rest for 30 minutes, allowing time for gel formation. The G' storage modulus was determined and the viscoelastic behaviour was characterised.

The Rheoplus software (version 3.6) was used and the storage (G') and loss (G'') moduli were measured in amplitude sweep performed in the strain range of 0.1% to 100% at a constant angular frequency of 10 rad/s. Frequency sweeps were performed in the linear viscoelastic region at 1% strain from 0.1 to 100 rad/s. The samples were 5 mg/ml Matrigel and 0.5% Agarose. These measurements were repeated 3 times.

3.5 Cell culture of cortical neurons

3.5.1 Ethics

All primary neural cells used for experiments were obtained in accordance with guidelines set out in the code of practice for humane killing under Schedule 1 of the UK Home Office Animals (Scientific Procedures) Act 1986, and approved by the University of Nottingham Animal welfare and Ethical Review body.

3.5.2 Dissociation

C57 mouse embryos in the E16-E17 stage of development were culled and their brains removed. Under a microscope, the meninges were extracted and the cortices dissected. After dissection, the cortices were dissociated in a petridish with 2ml Hanks Balanced Salt Solution (HBSS, Ca^{2+}, Mg^{2+}, Gibco) with 1 mg/ml trypsin (Sigma-Aldrich) and 5mg/ml DNAseI (Sigma-Aldrich), and placed at 37°C for 30 minutes in the incubator. 0.05% (v/v) trypsin inhibitor (Life Technologies) was dissolved in the petridish, containing the transferred tissue, and 6 mL Neurobasal medium (Gibco) supplemented with 2% (v/v) B27 supplement (Gibco) and 1x glutamax (Gibco). Mechanical dissociation was performed by gently triturating the tissue with a pipette. After which the dissociated cells were placed in a centrifuged at 250x g for 5 minutes. Neuronal cells were resuspended in neurobasal supplement to a final cell suspension of 25 x 10^6 cells/ml.

3.5.3 Cell plating

3.5.3.1 2D Cell Cultures

Coverslips were sterilised in 70% ethanol and left in the hood to dry. After drying, the coverslips were placed inside 24 well-plates (Corning). The surfaces of the wells and coverslips were coated with a 50 µg/ml Poly-L-Ornithine (PLO) (Sigma-Aldrich) and placed in the incubator overnight.

Once removed from the incubator, the PLO was removed from the surfaces and the wells were rinsed twice in sterile DI water. The wells were left in the hood to dry for 2 hours and primary cortical neurons were platted with a cell density of 4 x 10^5 cells/mL.

3.5.3.2 3D Agarose Cell Cultures

The coverslips and the PDMS wells were sterilised in 70% ethanol and left in the hood to dry. After which, the devices were gently pressed against the coverslips using tweezers.

Agarose low-melting (Invitrogen) was dissolved in sterile PBS using a flask, which was placed inside a microwave and heated for 2 minutes in a microwave. Agarose solutions were prepared with 0.5% (wt/v) concentration. The flask was placed in a water bath at 37°C for 15 minutes to cool down.

Cortical neurons were mixed gently using a pipette in Agarose gel inside the hood. The cell density used was 3.75 x 10^6 cells/ml. The neuron-Agarose solutions were platted in PDMS wells and placed inside the incubator at 37°C for 30 minutes. After 30 minutes, the gelatinisation occurred and the neuron laden Agarose cultures were topped up with Neurobasal supplemented media. Neuron laden Agarose cultures were maintained in the incubator at 37°C.

3.5.3.3 3D Matrigel Cell Cultures

The coverslips and platforms (PDMS-tape-membrane-tape-PDMS) were sterilised in 70% ethanol and left in the hood to dry. The devices were developed by gently pressing the platforms against the coverslips with tweezers. Matrigel (Corning) was defrosted into aliquots and placed on ice in the fridge overnight. Since Matrigel manipulation requires a cold environment, all the Matrigel experiments were performed on ice (**Appendix 4**).

Mouse primary cortical neurons were added to pre-gel solutions prior to gelation occurring. The neuron laden Matrigel solutions were made by gently adding the cells to the Matrigel mixed with Neurobasal media. These solutions had a cell density of 3.75 x10^6 cells/ml and a Matrigel concentration of 5 mg/ml. The solutions were platted onto the devices and incubated for 30 minutes at 37°C. After the 30 minutes, a gel is formed and the neuron-Matrigel cultures were topped up with media. Neuron laden Matrigel cultures were maintained in the incubator at 37°C.

3.5.4 Cell Staining

3.5.4.1 2D Neuron Cell Cultures

Neuron cultures were labelled with Calcein acetoxymethyl ester (AM; 2 µM; Sigma-Aldrich) and Propidium Iodide (4 µM) (PI; Sigma-Aldrich). The living cells were stained with Calcein AM and identified with green, while the dead cells were stained red by the PI. The cultures were incubated at 37°C for 30 minutes. After which, the Calcein AM and the PI were removed and the neuron cultures were washed 3 times with Neurobasal media. The neuron cultures were imaged in a Wide Fluorescent Light Field Microscopy (Zeiss 200 M) microscope with a with CoolSNAP MYO camera. The 2D neuron cultures were assessed in DIV 2, 5 and 7.

The quantification of axonal length can be found in any article regarding 2D neuronal cultures, for example (Taylor *et al.*, 2003; Taylor, Rhee and Jeon, 2006)(Kneynsberg *et al.*, 2016). Taylor et al. (Taylor *et al.*, 2003) was the researcher that developed this method allowing researchers to be able to isolate axons and quantify them. Her group published this method in *Nature Methods* (Taylor *et al.*, 2005) and in *Nature Protocols* (Park *et al.*, 2006). The axons growth, typically they are treated accordingly to the study and the axon length is followed under a microscope and images are acquired of the axons isolated starting from point they cross the microgroove until the axon terminal. The Fiji software was used to trace the axonal length from the edge of the microgroove to the growth cone. An average of 100 axons were traced in each repeat from three independent experiments. The tracing was made in three different time points in each chamber, the first time point corresponds to t0, the second time point is after 24 hours (t24) and the third time point is after 48 hours (t48). The data was normalised to the time point t0 and presented as a percentage of respective controls (mean±s.e.m).

3.5.4.2 3D Neuron Cell Cultures

Cell survival in neuron-Agarose cultures and the neuron-matrigel cultures was obtained in DIV 2, 5 and 7. The neuron laden hydrogel cultures were rinsed for imaging in 3% BSA and labelled with Calcein AM (2 µM) and PI (4 µM). The neuron cultures were incubated for 30 minutes at 37°C. After which the Calcein AM and PI were gently removed to avoid disturbing the 3D matrices. The cultures were rinsed 3 times with 3% BSA for 10 minutes time. The 3D neuron cultures were imaged using a Wide Fluorescent Light Field Microscopy (Zeiss 200 M) microscope with a with CoolSNAP MYO camera and Micro-Manager software 1.4.21 (Edelstein *et al.*, 2010).

The deconvolution of images was made using Huygens Pro software. For 3D axonal growth, Z-stacks (distance between each stack were 6 µm or 10 µm) were obtained to follow and measure the axonal length. To measure one axonal length in 3D it could take in some axons 5 images to follow its length, while in 2D it can take maximum 3 images to follow up its length.

3.5.5 Statistical Analysis

Data analysis was carried out using Prism v7.0 (GraphPad Software) and all data groups shown are expressed as mean±s.e.m. The probability distribution of the data set was analysed before further statistical analysis (Shapiro–Wilk test). Statistical evaluation between two groups was performed using unpaired Student's t-test. Analyses of more than two groups were carried out using one-way ANOVA with Bonferroni post-hoc analysis. Kruskal–Wallis' test followed by a Dunn's multiple comparisons test was used for non-parametric distributions.

In all statistical tests, *n* refers to the number of independent experimental repeats, which were 3 and in each independent experiment 5 replicas were made. Other researchers also used n=3 for cell viability (Carlson *et al.*, 2016)(Lam *et al.*, 2020)(Li *et al.*, 2007), for measuring the G' modulus and G'' modulus (Li *et al.*, 2007)(Broguiere *et al.*, 2019)(Zuidema *et al.*, 2014) as well as for diffusion profiles (Taylor *et al.*, 2003). Measurements of axonal length to proof the concept were done with 3 samples as reported by Taylor (Taylor *et al.*, 2003)(Taylor *et al.*, 2005). Here, per average 100 axons where measured in each experiment. For all tests, $P<0.05$ was used as threshold for significant difference. For all tests, *P* values are two-tailed.

Below there are tables expressing materials (**Table 3**), equipment (**Table 4**) and software (**Table 5**), although equipment is always expressed in the text.

Table 3 – List of the materials used in this PhD work.

Materials	Company
Glass coverslips	Menzel Glaser
XONA devices	XONA
PDMS	Farnell
Polycarbonate porous membrane 5 µm pore x 47 mm	Whatman Cyclopore
Biopsy punch	Williams Medical
Neurobasal buffer solution	Gibco
Neurobasal B27 Supplement	Gibco
Glutamax	Gibco
Poly-O-Lysine (POL)	Sigma-Aldrich
Fluorescein	Sigma-Aldrich
Paraformaldehyde	Thermofisher
Agarose Low melting	Invitrogen
Matrigel	Corning
Hanks Balanced	Gibco
Trypsin	Sigma-Aldrich
Trypsin inhibitor	Life Technologies
DNAseI	Sigma-Aldrich
24 well plates	Corning

Table 4 – List of the equipment used in this PhD work.

Equipment	
Widefield fluorescent microscope	Axiovert 200M, Zeiss
CCD camara	Photometrics CoolSnap MYO
Dissection microscope	Brunel Microscopes; IMXZ
Plotter Cutter	Graphtec America; Silhouette Cameo
Desiccator	Home made
Confocal microscope	Zeiss LSM 880
Rheometer	Anton Paar (MCR302, Austria)

Table 5 – List of the software used in this PhD work**.**

Software	**Version**
SolidWorks	2016
Graphpad Prism	7.0
ImageJ	FIJI
MatLab	2016
OriginPro	9.1
Huygens	Scientific volume imaging
Rheoplus software	3.6
Micro-Manager software	1.4.21

Chapter 4 2D and 3D Neuronal Cell Culture

4.1 Introduction

The work in this chapter will aim to ascertain the conditions required to define if cells are viable when cultured in 3D cultures. It is an optimisation chapter of the conditions required for growth and development of neurons. First it is needed to understand the reequipments of cortical neurons in 3D. After, the aim is to move into 3D devices. Considering how difficult compartmentalised 3D cultures are, it is important to investigate the matrix properties and cells viability. Because it is important to have cells alive for them to be able to grow and develop across the physical barrier in 3D.

Using 3D neuronal system, cells can still adopt their natural shape and morphology similar to that acquired by neurons *in vivo* (Arimura and Kaibuchi, 2007; Anthony P. Barnes and Polleux, 2009). Making 3D cell culture systems a valuable tool in predicting *in vivo* cell responses to external stimuli, compared to cells growing in two-dimensional (2D) cultures (Edmondson *et al.*, 2014). With the aim to investigate 3D primary cortical neuron cultures, the optimisation of cell density, the best hydrogel to host neurons and the hydrogel rigidity, were determined. These 3D neuron cultures were validated by quantifying neuron survival and evaluating neuron morphology within the different hydrogels. The first approach to evaluate this model was to choose the most suitable cell density and quantify neuronal viability. Primary cortical neuron cultures were imaged and stained within 7 days *in vitro* (DIV) at DIV 2, 5 and 7. Second, the mechanical properties of each hydrogel were characterised by evaluating its viscoelastic behaviour and determining the gel strength.

4.2 2D and 3D neuronal cultures

4.2.1 Neuronal Density

The Matrigel is very expensive (approximately £400 for 10 mL) and the stock Matrigel would be spend to quickly if it was used at its initially concentration (8mg/mL). Therefore, the idea of dilute the Matrigel was taken into consideration. It was shown that also by diluting the gel concentration, the cells have a preference by lower concentration, leading to higher pore gel sizes. This allows a higher transport of nutrients, cell wastes, etc., around the matrix. It has been reported that cells prefer more soft gels (Zuidema *et al.*, 2014), which was also proven by cell viability and survival in this work as presented in the cell plating density work. The cell density was based on the work published by *LaPlaca et al.* (Laplaca, Vernekar and Shoemaker, 2010), which shown primary neurons in matrigel using a cell density of 3.75×10^6 cells/ml. Accordingly, to the cell stock available and the gel concentration, using the formula $C_1V_1=C_2V_2$, we got different cell densities for the specific gel concentration.

The neurons were plated in 2D and 3D cell cultures, with the same plating density in a 24 well-plate as detailed in **Table 6**. In 2D cultures, neurons were grown in neurobasal media, whilst in 3D cultures neurons were grown within hydrogel. Matrigel was diluted in media to a final concentration of 7 and 5 mg/ml. **Figure 25** shows images of primary cortical neurons in laden Matrigel and the respective images of cortical neurons cultured in 2D with the same plating density after 2 days in culture. Neuron cells died when plated with the higher Matrigel concentration but at lower cell density, **Figure 25a** (7mg/ml Matrigel final concentration, 1.0×10^6 cells/ml plating density). A possible explanation for the observed phenotype is that the cell density per ml was likely too low to guarantee their survival. It is known that cortical neurons have higher chances of survival when cultured at higher densities (Lu, Piechowicz and Qiu, 2016). This can be the reason why cells growing in a higher cell density with the same Matrigel concentration, **Figure 25c** (7mg/ml Matrigel final concentration, 1.97x106 cells/ml plating density), showed a similar development to 2D (**Figure 25d**;1.97x106 cells/ml plating density).

Table 6 – Different cell and Matrigel concentrations were investigated. The respective concentrations of cells were applied in media and in Matrigel to compare neurites survival and polarisation between 2D and 3D environments.

Environment configuration	Final Concentration of Matrigel	Plating density
3D	7 mg/ml	1.97×10^6 cells/ml
		1.0×10^6 cells/ml
	5 mg/ml	3.75×10^6 cells/ml
		1.97×10^6 cells/ml
2D	–	1.97×10^6 cells/ml
		1.0×10^6 cells/ml
		3.75×10^6 cells/ml

However, cells grew with longer axons and started extending their axons, with lower Matrigel concentration, as seen in **Figure 25e** (5mg/ml Matrigel final concentration, 1.97×10^6 cells/ml plating density) and **Figure 25g** (5mg/ml Matrigel final concentration, 3.75×10^6 cells/ml plating density) than in **Figure 25c**. This means that with a lower concentration of Matrigel cells were able to survive and develop. After 4 DIV, further images were acquired to analyse their development (**Figure 26**), with the only exception of cells that died at 7mg/ml Matrigel and 1.0×10^6 cells/ml plating density (**Figure 25a**), as they were dead when imaged at the previous time point. In **Figure 26a** (7mg/ml Matrigel final concentration, 1.97×10^6 cells/ml plating density), cortical neurons showed shorter axons compared to the neurons growing in lower matrigel concentration (**Figure 26c**, **e**). Also, it can be observed that some cortical neurons started to die at this stage of the experiment. Growth factors and nutrients are easily transported within a 5 mg/ml Matrigel compared to a 7mg/ml Matrigel. This explanation is reinforced by the fact that a lower concentration of Matrigel (**Figure 26c**, **e**), neurons shown better development than a higher concentration of Matrigel (**Figure 26a**). The combination of a low concentration of Matrigel with a higher cell density (**Figure 26e**; 5mg/ml Matrigel final concentration, 3.75×10^6 cells/ml plating density) showed longer axons and enabled the assessment of their morphology. Compared to results in **Figure 25** and **Figure 26** for 2D cultures, where cell density is too high to be able to evaluate the neuronal structure.

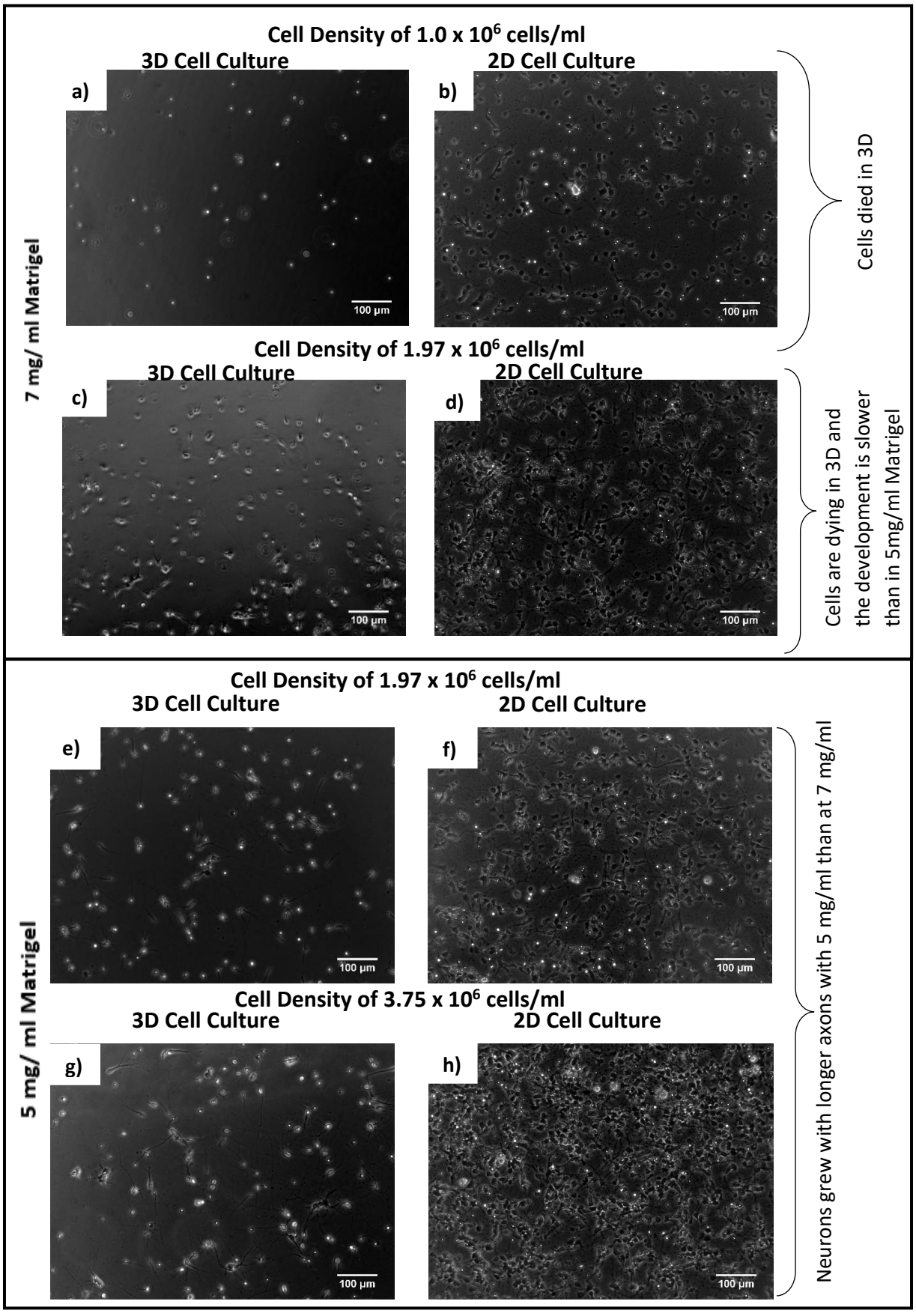


Figure 25 – Representative phase contrast images (10x) of neurons cultured in both 2D growth media and Matrigel after two days in vitro.

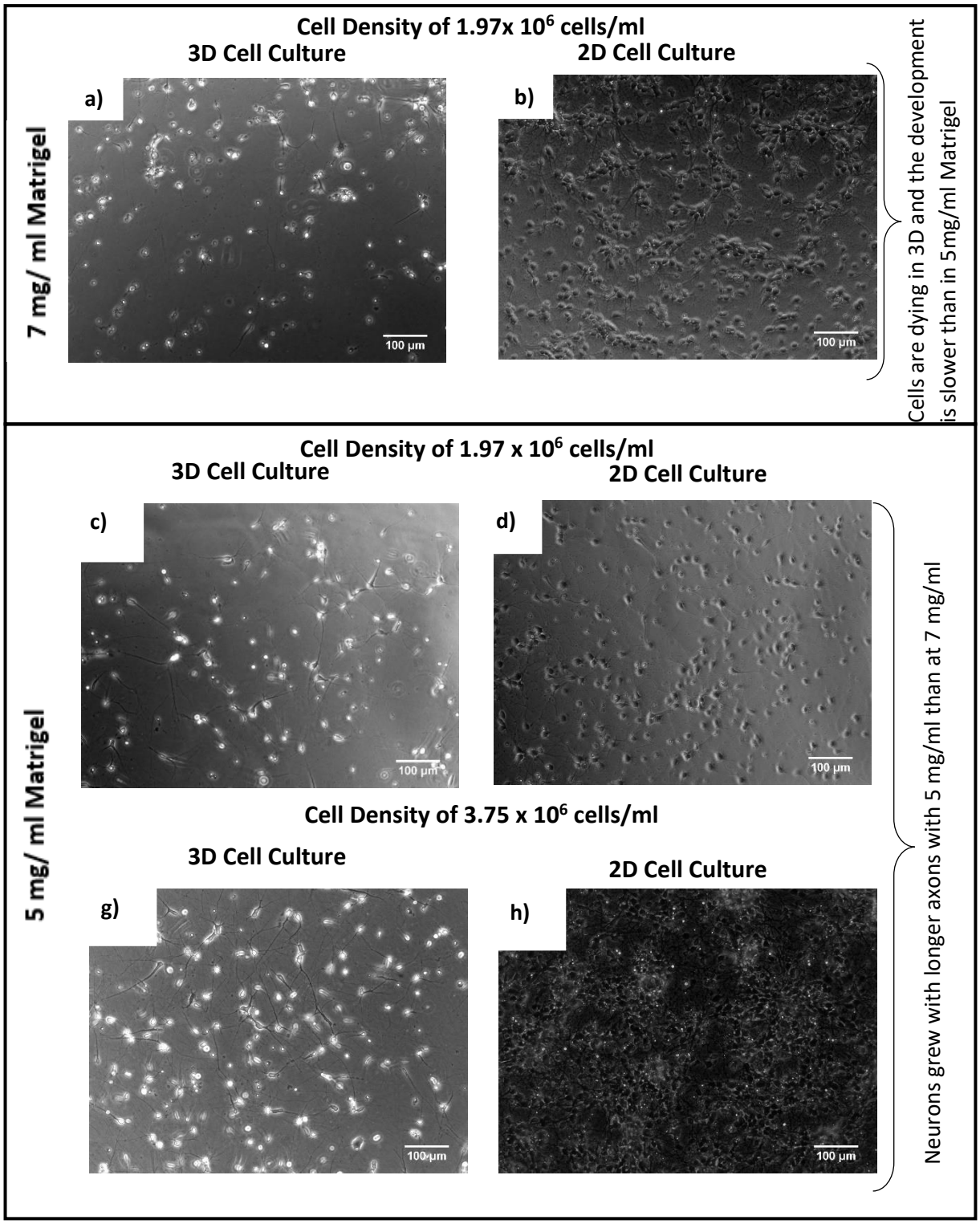


Figure 26 – Representative phase contrast images of neurons cultured in both 2D growth media and Matrigel after four days *in vitro.*

This is related to the fact that in 2D environment the cells settle at the surface and if they have the same density as in the 3D environment, it is not possible to distinguish individual neuron morphology within the highly dense network.

Neurons for 2D cultures were plated with a different cell density than the ones for 3D, avoiding the cells to agglomerate. Therefore, neurons in the 2D environment were assessed with a cell density of $4x10^5$ cells/ml, while the 3D cultures had a cell density of $3.5x10^6$ cells/ml. There is a clear difference in morphology between cells seeded in media and cells seeded in hydrogel. Cells in hydrogel have a pyramidal shape which is closer to the physiological morphology of the cortex, as well as having longer axons and higher polarisation than cells in media.

4.2.2 Neuronal Morphology

The morphology of a neuron can be identified by indicating the neuro cell parts (e.g. axons) and normally can be evaluated by neurite outgrowth and cell viability (Wevers *et al.*, 2016; Fantuzzo *et al.*, 2019). If the cells are cultured as small spheres, and they have the ability to grow and polarize it is a good indication that they retain their phenotype and are differentiating according to expected parameters (add some references to key methods).

After optimal cell viability was found, the next step towards the validation of the 3D culture system was to examine the morphology and to determine if Matrigel is a more suitable model compared to Agarose. Since previous studies reported that an increased axonal growth was observed with lower Agarose concentrations of 0.75% (Balgude *et al.*, 2001) and 0.5% (Bellamkonda and Bouche, 1995), the lower 0.5% Agarose concentration was used.

Initially, cells were plated as a population of spherical cells in Matrigel and Agarose cell cultures (**Figure 27 – DIV0**). After 4 – 5 hours neurons started to extend their processes and after DIV 2 some neurites were observed (**Figure 27 – DIV2**). Neurons showed restricted growth within the Agarose, while in Matrigel the neurons had longer neurite extensions. After DIV 5, neuros laden with Agarose had shorter neurites than neurons laden Matrigel, (**Figure 27 – DIV5**). Neurons growing in Matrigel showed a more pyramidal shape, confirming that their natural shape and they appear to have longer neurites within a few days (**Figure 27 – DIV7**).

Agarose had a low concentration of molecules, while Matrigel is extracted from a rat chondrosarcoma (tumour). The tumour is rich in biological active molecules, such as growth factors, making the Matrigel a better matrix to host neurons. **Figure 28** shows a z-stack of a 3D neuronal culture of 10 DIV, showing neurons growing in 3D matrigel matrix with a height of 210 µm. Higher magnification images are given in **Figure 29**. There are more neurons in the bottom of the z-stacks due to the fact that when cells are plated they are in a liquid solution and they are only immobilized in 3D, after the gel formation.

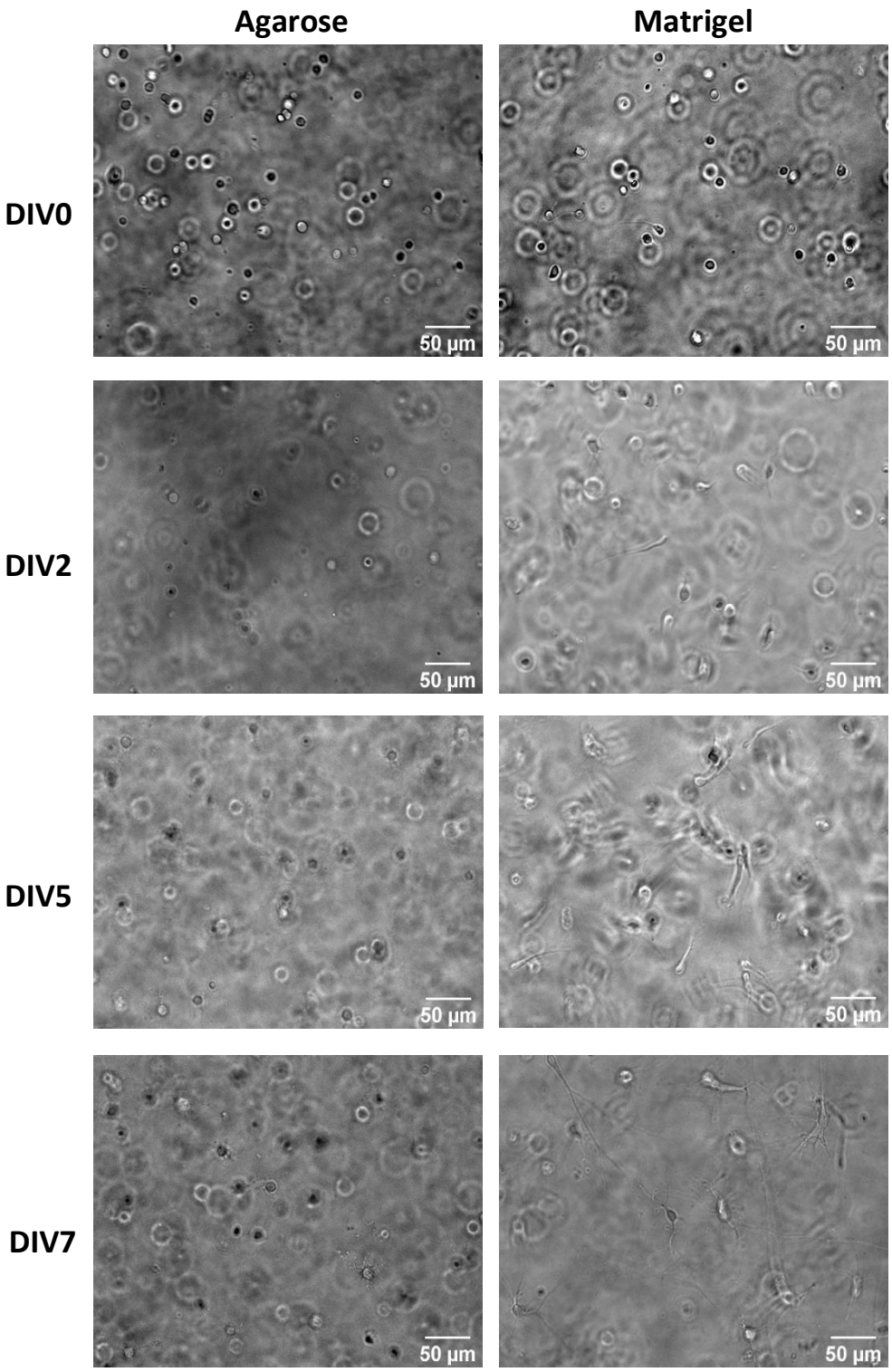


Figure 27 – Representative phase contrast images 20x of primary cortical neurons in 0.5% (v/v) Agarose and 5 mg/ml Matrigel acquired at DIV 0, 2, 5 and 7, to evaluate their morphology.

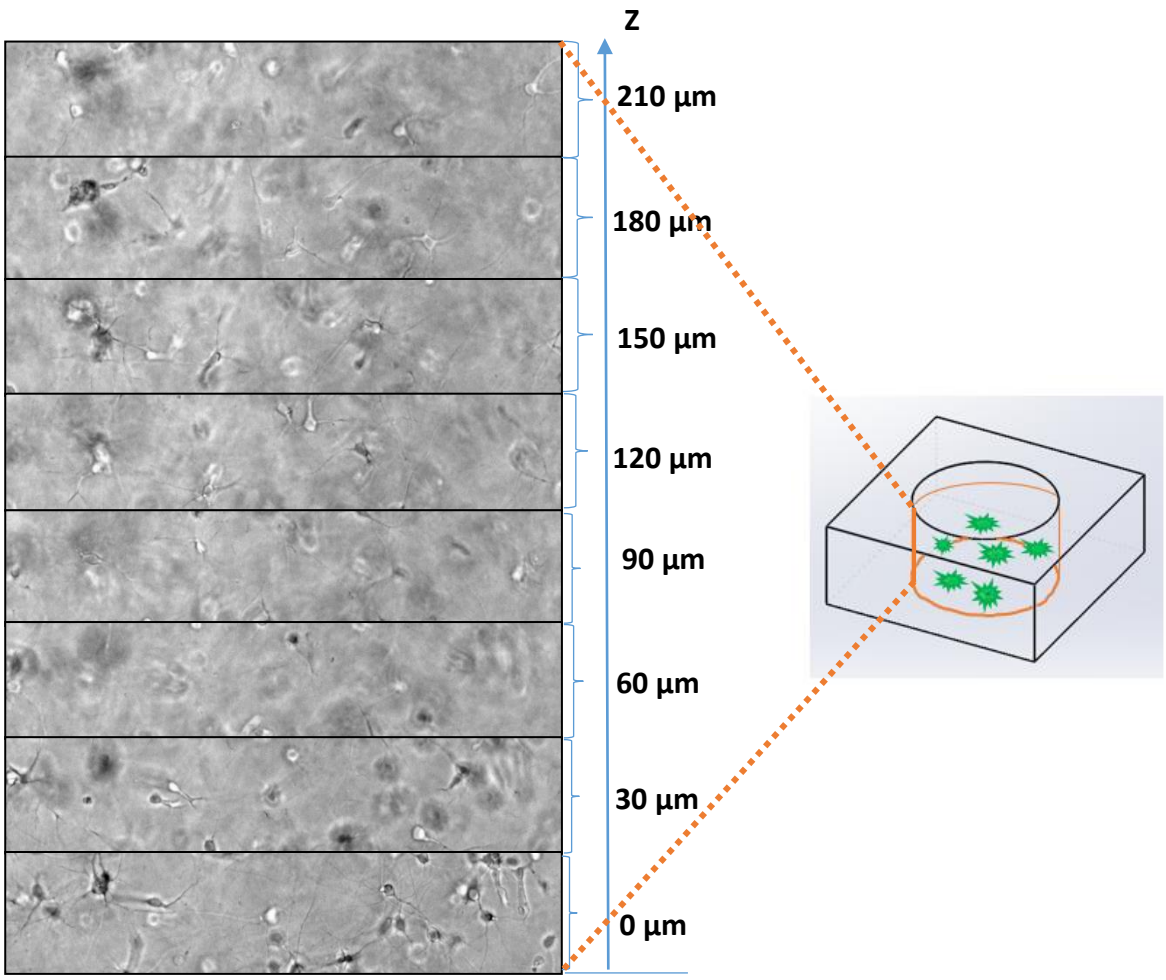


Figure 28 – Diagram of phase contrast images of neurons growing in 3D Matrigel in different dimensions, 10 days after plating achieving a gel thickness of 210 µm. It is possible to visualise neurons growing at a 3D structure.

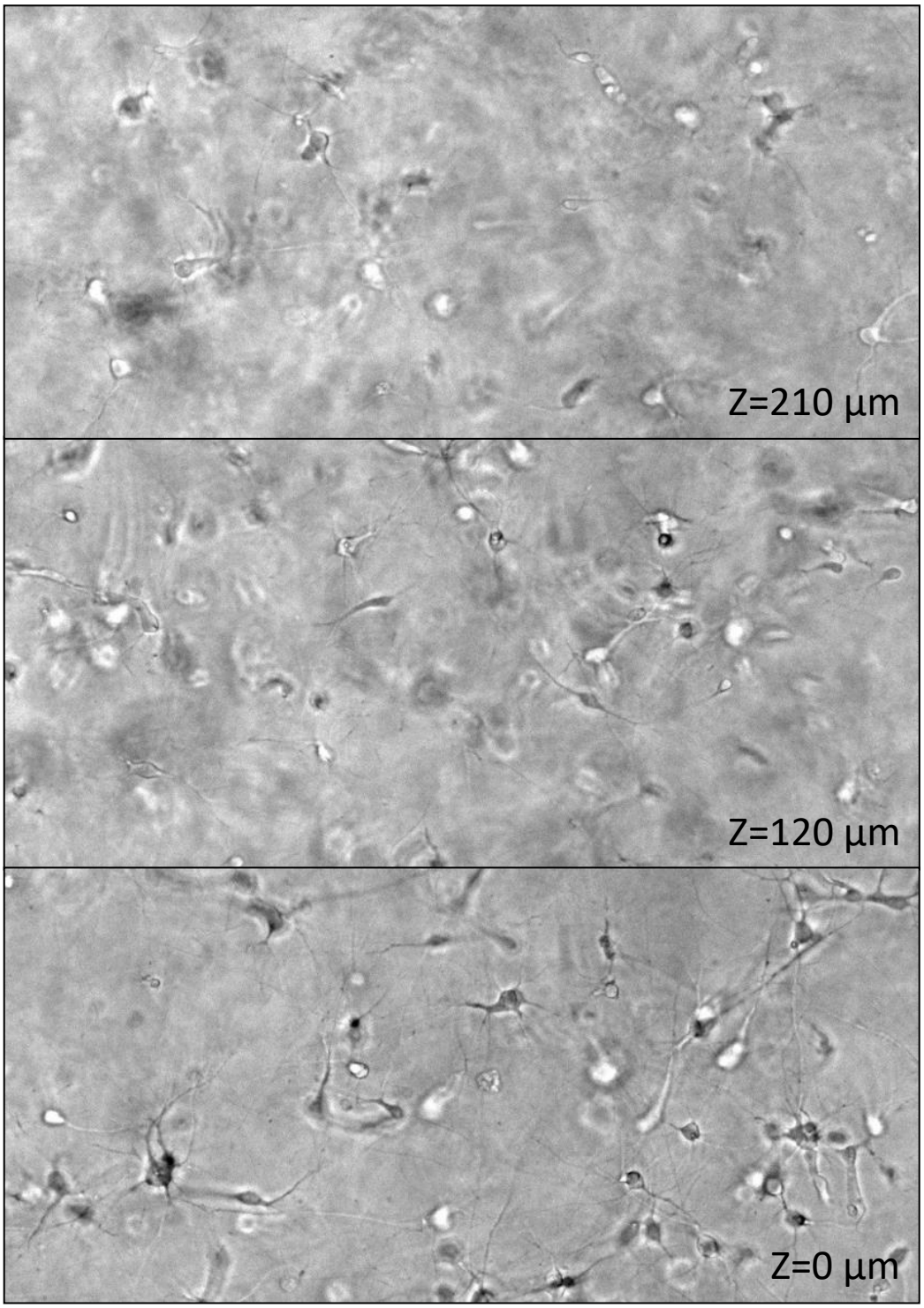


Figure 29 – Phase contrast images of a 3D Matrigel matrix with neurons cultured in 10 DIV, in the same position with different Z plan.

4.2.3 Assessment of cell functionality using fluorescence techniques

No one in our labs work with 3D cultures, being the first time in our lab to introduce 3D neuronal cultures so there is important to know and understand how cells are cultured how they behave on 3D. One objective of this project was to be able to keep cells alive and wait for them to growth and be able to isolate them in 3D. Nevertheless, we tried to perform immunocytochemistry following the same protocols as reported in literature (Lee *et al.*, 2011; Choi *et al.*, 2014; Frega *et al.*, 2014a; Bosi *et al.*, 2015b; Carlson *et al.*, 2016; Chandrasekaran *et al.*, 2017; Aiuto *et al.*, 2018), where they use 4% paraformaldehyde to fix neuronal cells for immunocytochemistry within gels. However, when we used 4% paraformaldehyde to fix the cells within Matrigel, the matrix always depolymerized. During the washes (of the immunocytochemistry) as referred in the protocols of immunocytochemistry the matrix completely depolymerized was washed away. Thus, there was nothing left to image under microscope. We tried to decrease the concentration of paraformaldehyde to 2% as same articles reported (Liz *et al.*, 2014; Koss *et al.*, 2017). However, the matrix still had some depolymerization even if now it was possible to visualize something, please see **Figure 30**. However, because it was not the scope of this thesis further experimental optimization work with immunocytochemistry was not performed.

What we can conclude is that the articles, probably did something different or there are details, such as times of incubation of the immunocytochemistry experiment, that were not reported in the articles. Additionally, there are reports of immunocytochemistry with different fixing, instead of paraformaldehyde they use formaldehyde (Laplaca, Vernekar and Shoemaker, 2010; Wevers *et al.*, 2016). For example, *La Placa et al.* (Laplaca, Vernekar and Shoemaker, 2010) used 3.7% of formaldehyde to fix cells and they say it works, however the data was not shown in their work. The paraformaldehyde was used in this work because is the fixing alcohol used in our labs. It is noteworthy, that all the articles of immunocytochemistry here cited have reported works in different neuronal cell types and different gel types. For example, 4% paraformaldehyde in cortical neurons within collagen was reported by Lee et.al (Lee *et al.*, 2011). Another example is reported by Chandrasekaran et al. (Chandrasekaran *et al.*, 2017), instead of primary cortical neurons used stem neuronal cells. Or, Liz et al. (Liz *et al.*, 2014), that used dorsal root ganglia neuronal cells instead of cortical neurons.

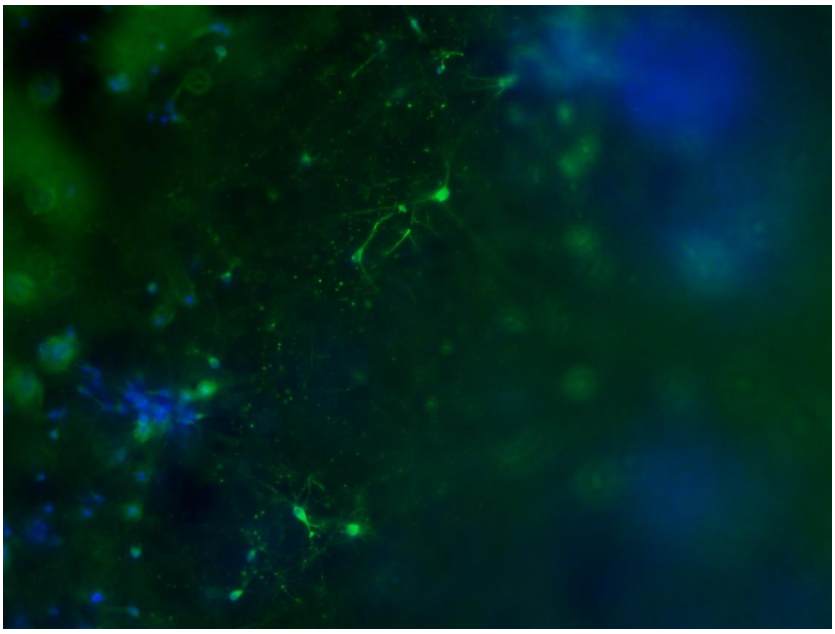


Figure 30 – Trial of immunocytochemistry in primary cortical neurons within Matrigel matrix at a concentration of 5 mg/ml. Where the matrix was still depolymerised and it was not possible to visualise the neuron cell networks in 3D, even because cells were also washed away with some part of the part of the matrix. Neurons were fixed with 2% paraformaldehyde and stained with DAPI to label the nucleus and to stained with βIII-Tubulin. Imaged in a widefield fluorescence microscope with 10x**.**

Therefore, optimization is always important, especially when in our lab no one has never worked with gels before. Increasing the difficult of working with 3D by not having a standard protocol for culturing cells in 3D. If working with immunocytochemistry is difficult, trying to do cell assays using more complicated methods would be more challenge, requiring more time and materials, and as it was not the scope of the thesis, we focused on the scope of this project; ensure that cells are alive in 3D and being able to identify morphology and cells to polarize; axons able to grow. Regarding imaging, it is possible to visualize well neurons growing in 3D if we use confocal microscopy with a high ability to identify the neuron cells, please see **Figure 31**.

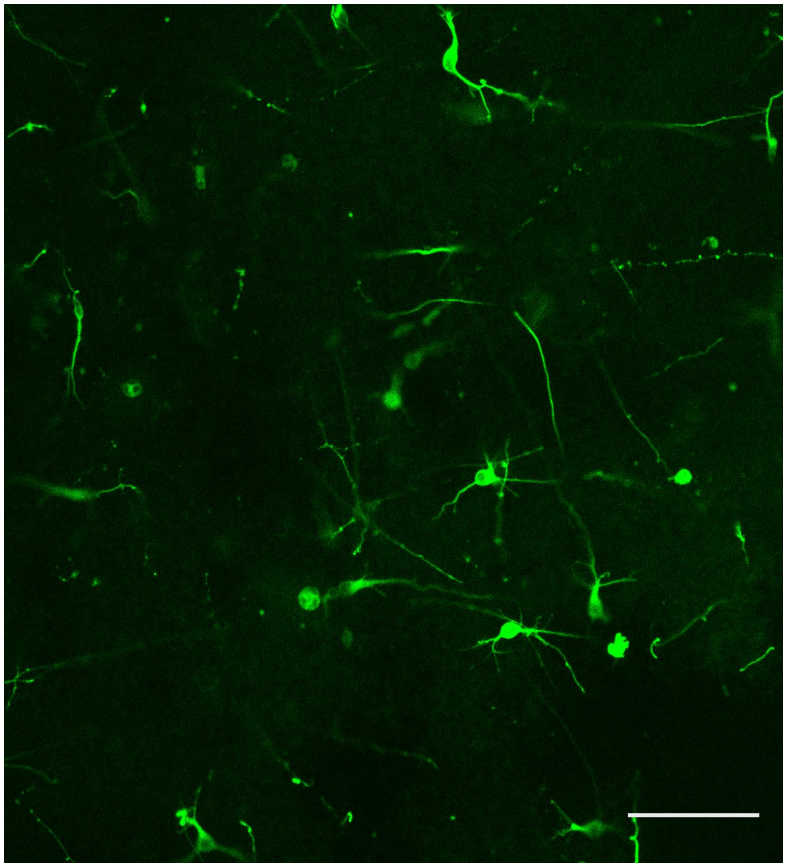


Figure 31 – Confocal image of neurons growing within Matrigel labelled with Calcein AM at DIV2. Scale bar 50 µm.

Unfortunately, as confocal equipment is extremely expensive, we just used it to prove and be able to visualize axons in 3D isolated on the device. Therefore, for cell viability a widefield fluorescent microscope was to image neurons growing in 3D cultures, however, there is a lot of background when imaging as shown in **Figure 32**. This microscope is not as good as a confocal to eliminate the background (high level of fluorescence). However, we can always use a 3D software to remove background, such as Huygens software or Volocity software. The disadvantage is that by removing the background we also remove the cell information, by removing the background we also remove fluorescence in the cells.

Another issue found in imaging 3D neuronal cells with fluorescence is when we tried to image with higher resolution images; if the resolution is higher the background is higher, and when the images are deconvoluted the loss of information of neuron morphology is even higher. The images for fluorescence are images at 10X for cell viability because it was possible to image cells and identifying them. A higher resolution would have been useful; however, this was not possible because when we increase the magnification of the microscope, the level of fluorescence was higher and we could only see green. In this case cells could not be well identified. However, to perform cell survival/ cell viability, it is possible to perform because we just need to count the number of green and red cells.

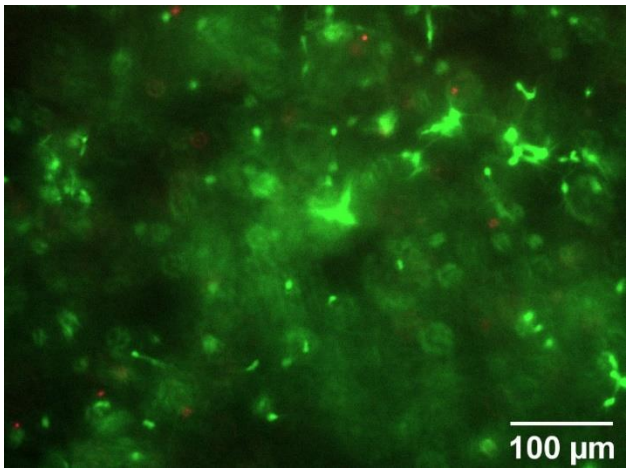


Figure 32 – Images of labelling neurons in 3D with Calcein AM, where neurons are labelled with green at DIV 2 at 10x with a widefield microscope.

Despite the challenges found, to achieve the scope of this thesis the aim is to see the growth of axons. Although it was not possible to directly measure cell phenotype, the fact that the axons were growing is a good indication of neuronal differentiation occurring in vitro, and hence a partial phenotypic test.

4.2.1 Neuronal Viability

In order to further characterise the 3D culture system, neuron cell viability was investigated to ensure that neurons are able to grow during a time of culture. Primary cortical neurons were cultured in Agarose and Matrigel matrices to grow in 3D, mimicking the cortical neurons growing *in vivo* tissue. These 3D neuron cultures were characterised by determining the neuron viability in Agarose and in Matrigel. The neuronal survival found in 2D neuron cultures, as shown in **Figure 33**. These images are in 10x to compare to the 10x images of 3D cultures, because images of 3D cultures in 20x were not possible to obtain due to the high background levels with the increase of magnification. Unfortunately, the level of background was higher with the increase of magnification, hence images of 10x were taken for 3D cultures and then deconvoluted with Huygens software to remove background. The fact that the background was being removed also information about cells were removed, however for cell viability it only needed to count the dots of live and dead cells. One image of 20x of 2D live dead assay is shown in **Figure 34**. The 3D neuron viability was evaluated by assessing neuronal survival for 2, 5 and 7 (**Figure 35**). To test neuron viability, both Propidium Iodide (PI), and Calcein acetoxymethyl ester (AM), were added to the neuron cultures, as markers for cell death and viability respectively. The living cells were stained with Calcein AM and identified with green, while the dead cells were stained red by the PI.

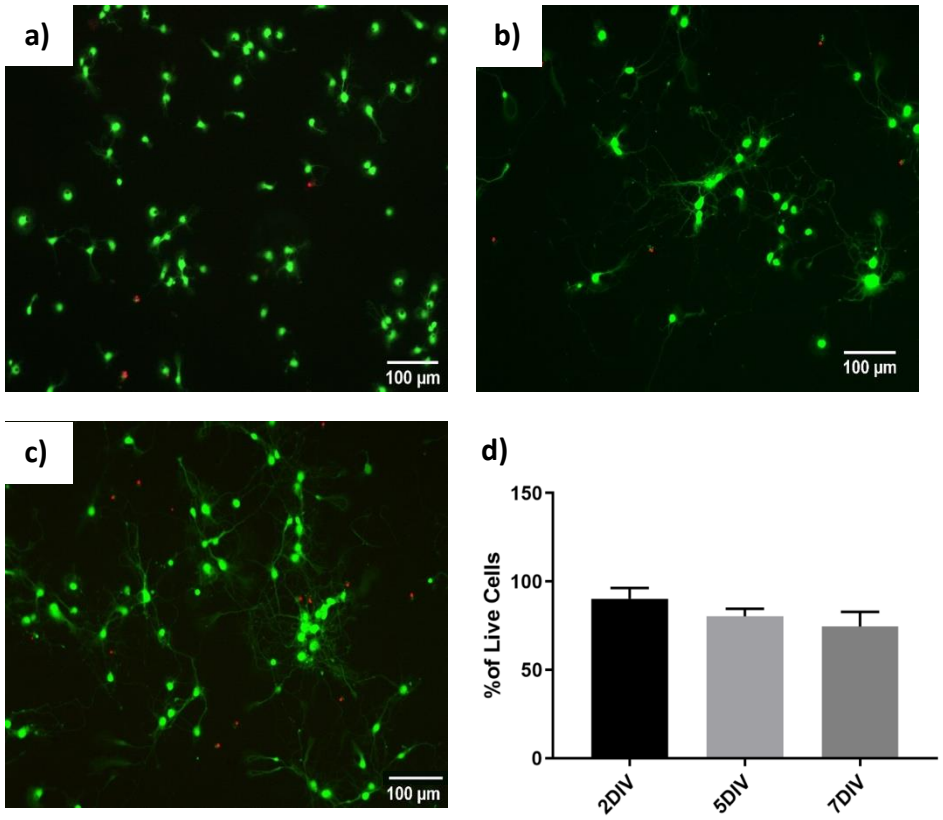


Figure 33 – Representative images of live/dead assay in 2D neuron cultures at 2DIV (**a**), 5 DIV (**b**) and 7 DIV (**c**). The percentage of living cells for DIV 2, 5 and 7. The data shown mean± SEM (n=3).

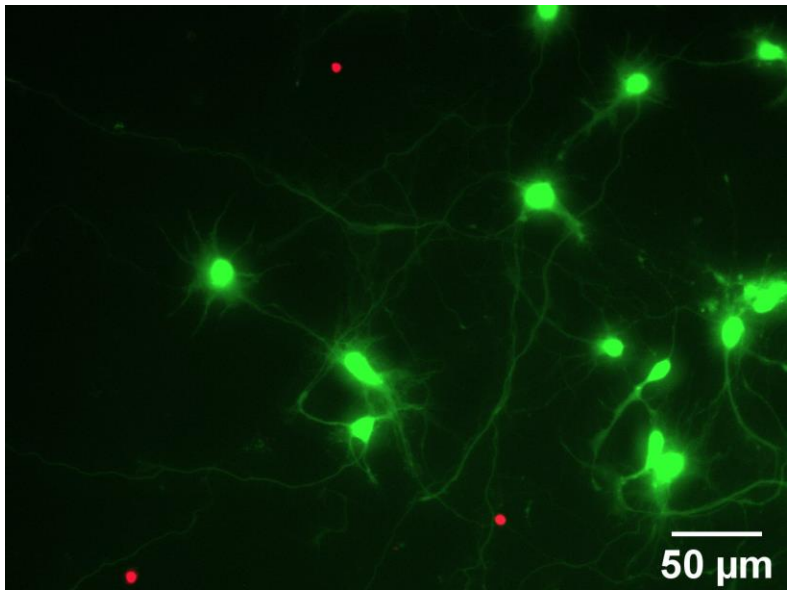


Figure 34 – Representative images of live/dead assay in 2D neuron cultures at 7 DIV at 20x.

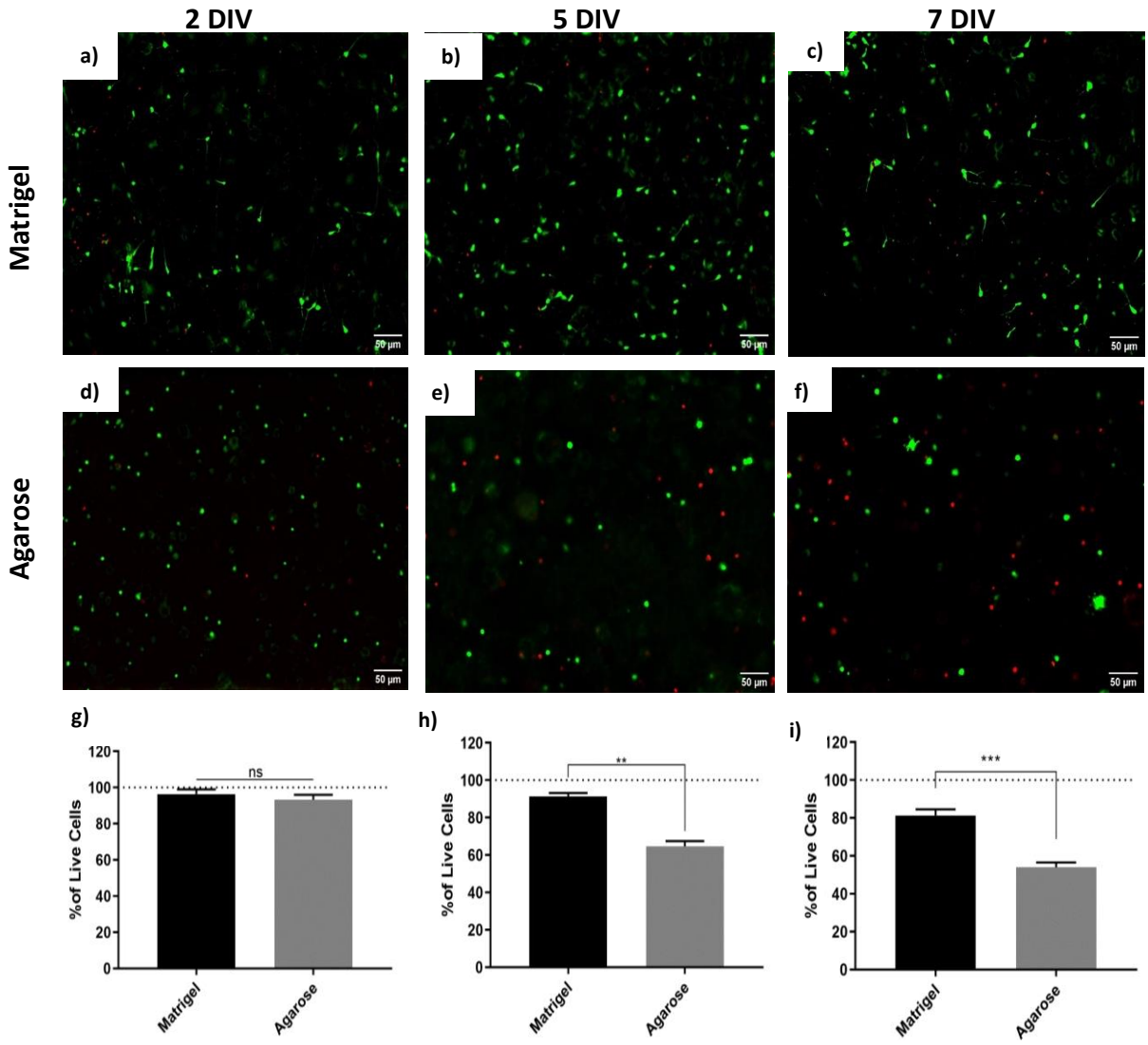


Figure 35 – Neuronal survival assessed at DIV 2, 5 and 7, in Matrigel and in Agarose. Live cells were labelled with Calcein AM (shown in green) and the dead cells stained with Propidium Iodide (shown in red). The percentage of living cells is shown at DIV 2 (g), DIV 5 (h) and at DIV 7 (i). The data shown mean± SEM (n=3), using one way-ANOVA with Tukey's test (c), with ** $p < 0.01$ and with *** $p < 0.001$. Images were deconvoluted with Huygens Software.

The same images from **Figure 35** are presented for better visibility separately for matrigel 2DIV (**Figure 36**), for Agarose 2DIV (**Figure 37**), for Matrigel 5DIV (**Figure 38)**, for Agarose 5DIV (**Figure 39**), for Matrigel 7DIV (**Figure 40**) and for Agarose 7DIV (**Figure 41**).

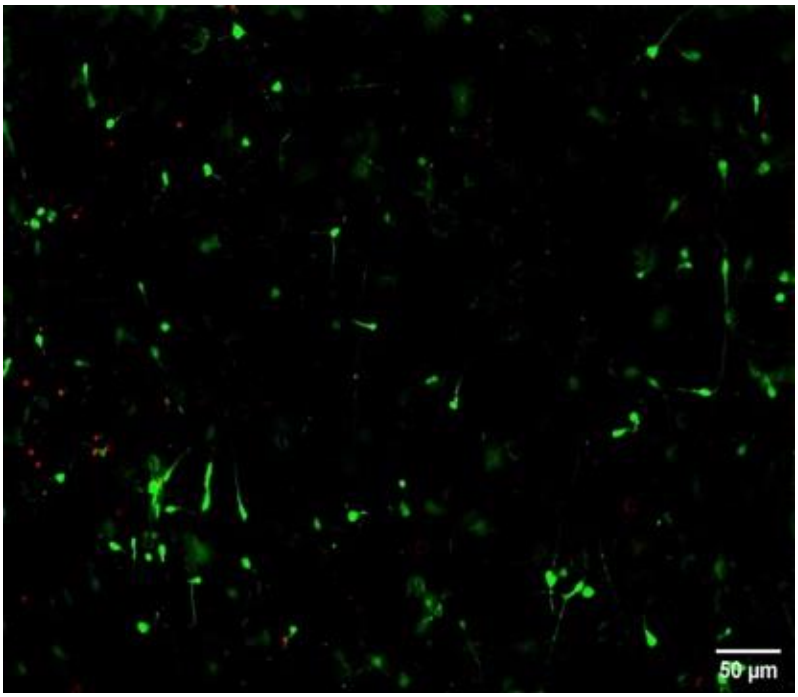


Figure 36 – Deconvoluted imaged of live/dead assay in neurons laden Matrigel (5 mg/mL) within 2DIV, neurons are labelled with Calcein AM (live cells) and P.I. (dead cells). Huygens was the software used to remove background.

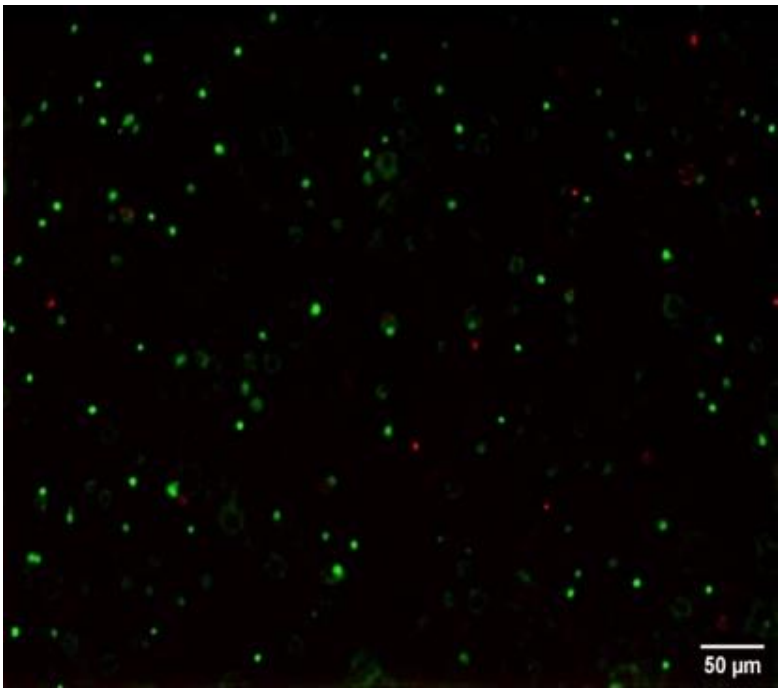


Figure 37 – Deconvoluted imaged of live/dead assay in neurons laden Agarose (0.5%) within 2DIV, neurons are labelled with Calcein AM (live cells) and P.I. (dead cells). Huygens was the software used to remove background.

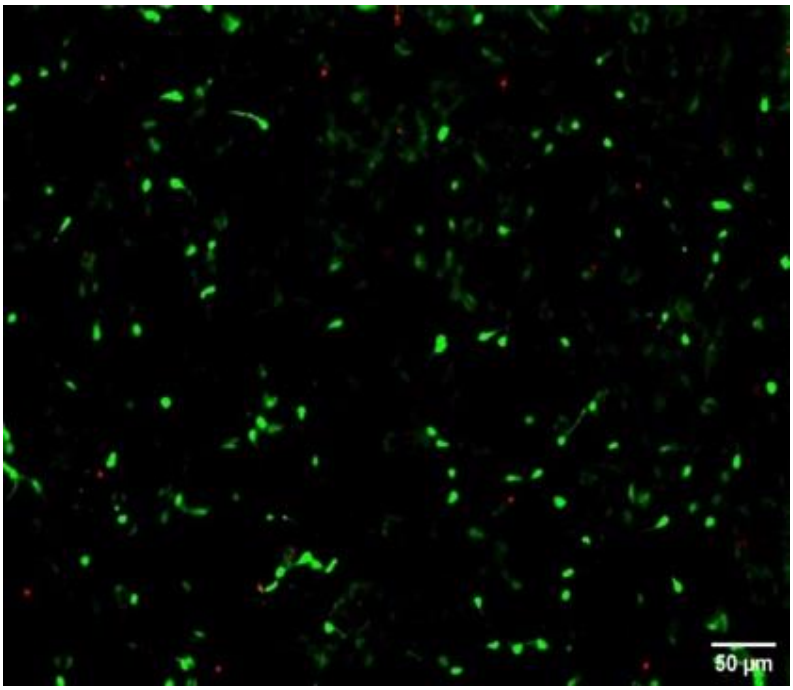


Figure 38 – Deconvoluted imaged of live/dead assay in neurons laden Matrigel (5 mg/mL) within 5DIV, neurons are labelled with Calcein AM (live cells) and P.I. (dead cells). Huygens was the software used to remove background.

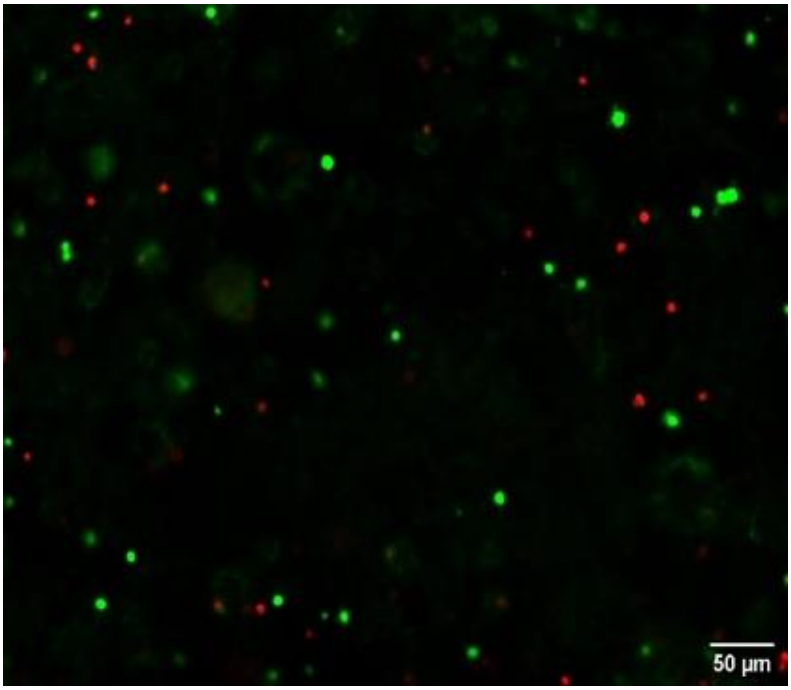


Figure 39 – Deconvoluted imaged of live/dead assay in neurons laden Agarose (0.5%) within 5DIV, neurons are labelled with Calcein AM (live cells) and P.I. (dead cells). Huygens was the software used to remove background.

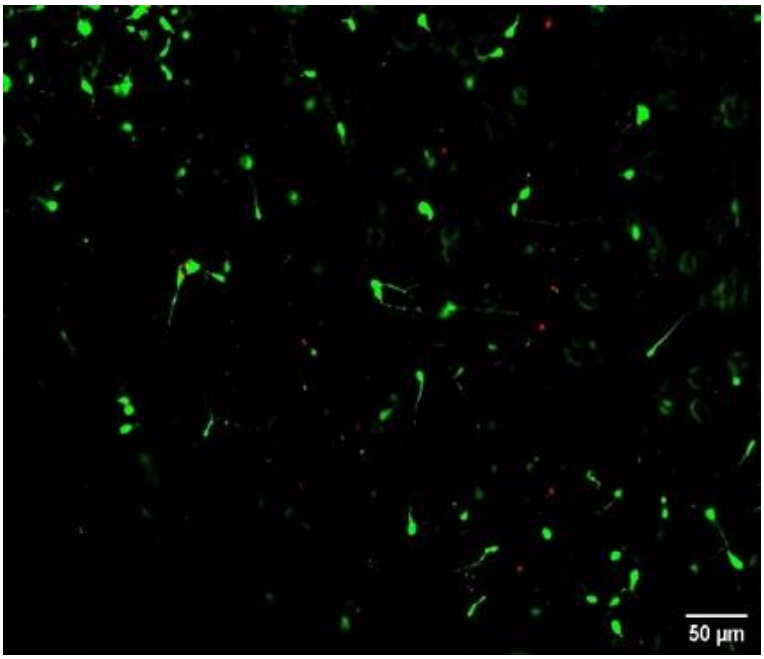


Figure 40 – Deconvoluted imaged of live/dead assay in neurons laden Matrigel (5 mg/mL) within 7DIV, neurons are labelled with Calcein AM (live cells) and P.I. (dead cells). Huygens was the software used to remove background.

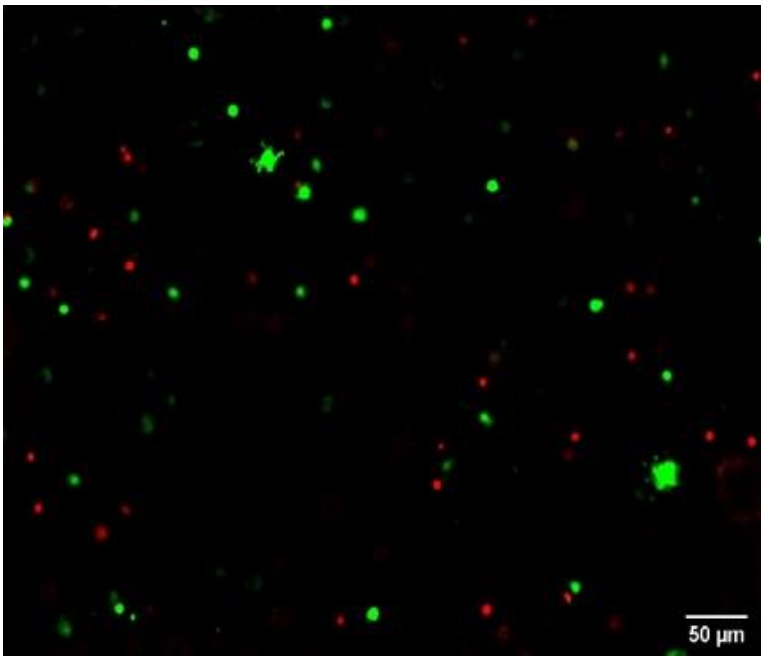


Figure 41 – Deconvoluted imaged of live/dead assay in neurons laden Agarose (0.5%) within 7DIV, neurons are labelled with Calcein AM (live cells) and P.I. (dead cells). Huygens was the software used to remove background.

At day 2 the staining showed a higher percentage of living cells in both 3D cultures compared to 2D. It is worth noting that when neurons were included within Matrigel the whole process was performed at a temperature of 4°C, whilst the Agarose inclusion was performed at 37°C. This suggests that neurons showed a greater resistance to low temperatures. At day 5, neuronal cell survival remained over 90% for Matrigel, whilst there was a decrease of 11% in 2D cultures and a 28% decrease in Agarose. At day 7, neurons cultured in both media and Matrigel continued to develop and showed a live cells viability over 70%. Whereas, Agarose cultures stopped developing and cell survival further decreased. The percentage of live cortical neurons cells for 2D and 3D culture systems is shown in **Figure 42**.

All the environments showed similar percentage of live cells at 2DIV. However, neurons laden Agarose shows a decay in cell survival in the following days of experiment. In contrast, Matrigel is able to maintain high cell viability similar to the results shown in 2D up to 7 days in culture. It is clear that Matrigel is better at supporting cell survival. While in comparison Agarose showed poor cell survival, showing it to be a toxic environment for neuron development. This assay demonstrated the viability of growing neurons in a 3D environment, where the support for neurite outgrowth and polarisation of neurons with a high cell survival could be provided.

For the cells to be able to growth they need to have a high degree of functionality. Although to evaluate neurons functionality further cell functional assays should be performed. As explained before, attempts to perform immunocytochemistry were unsuccessful, because the matrix was depolymerized when cells were fixed as reported in literature. Many researchers first do the live cell assays before perform further cell experiments that would investigate further cell functionality, such as calcium imaging or immunocytochemistry, as explained in Chapter 2.

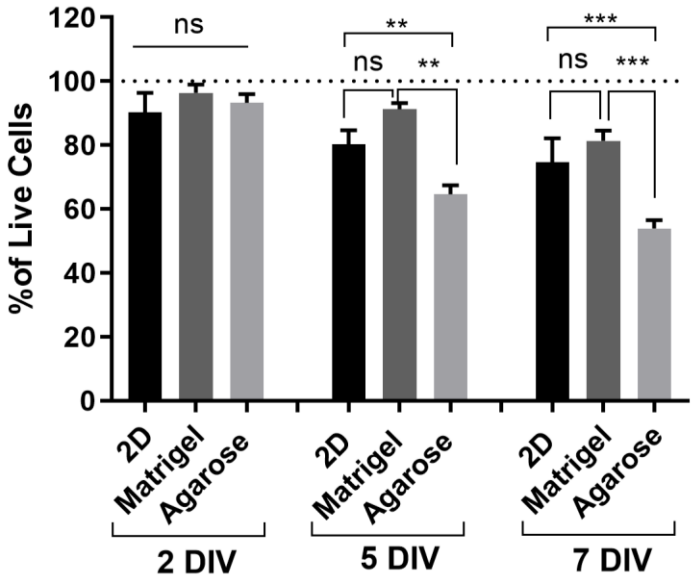


Figure 42 – The percentage of viable cells assessed as a function of cell culture environment (2D culture, Matrigel culture, Agarose culture) at DIV 2, 5, 7. The data shows mean ± SEM (n=3). One way NOVA with Tukey's test where ** $p < 0.01$ and *** $p < 0.001$.

Even if Agarose is known to not support cell culture many researchers employ agarose in studies to compare with more biocompatible gels, as agarose is simple and because of their mechanical properties can be used for further comparisons in terms of gel strength (Connor *et al.*, 2001)(Balgude *et al.*, 2001) or combined with another natural gels to give them the mechanical support needed (the mechanical support that more biocompatible gels lack). For example, agarose was combined with chitosan (Cao and He, 2010), combined with alginate (Kunze *et al.*, 2011), or combined with Matrigel (R. Fan *et al.*, 2016).

4.3 Mechanical properties of Matrigel and Agarose Matrices

The validation of the 3D systems included the mechanical characterisation of the gels. An Anton Paar Rheometer was used to characterise the viscoelastic behaviour of the hydrogels and measure the storage modulus (G') and the loss modulus (G''). A strain sweep was applied from 0.1 up to 100% at 1 Hz, at a temperature of 37°C, **Figure 43** (**a-b**). The G' and G'' were measured as a function of strain to determine the linear viscoelastic region (LVE), **Figure 43** (**a-b**). The limit of the LVE indicates the range in which the test can be carried out without destroying the sample (Zuidema *et al.*, 2014).

After acquiring the limit of the LEV region, frequency sweeps were carried out at a constant maximum strain amplitude value (1% strain) between 0.01 and 100 Hz, **Figure 43** (**c-d**) (Zuidema *et al.*, 2014). For the given conditions, linear behaviour was found up to 1% strain for both hydrogel matrices. It was found for all the samples that G' is higher than G'' in the LVE region, which means that the samples presented a solid/ gel structural response (Schneider *et al.*, 2002).

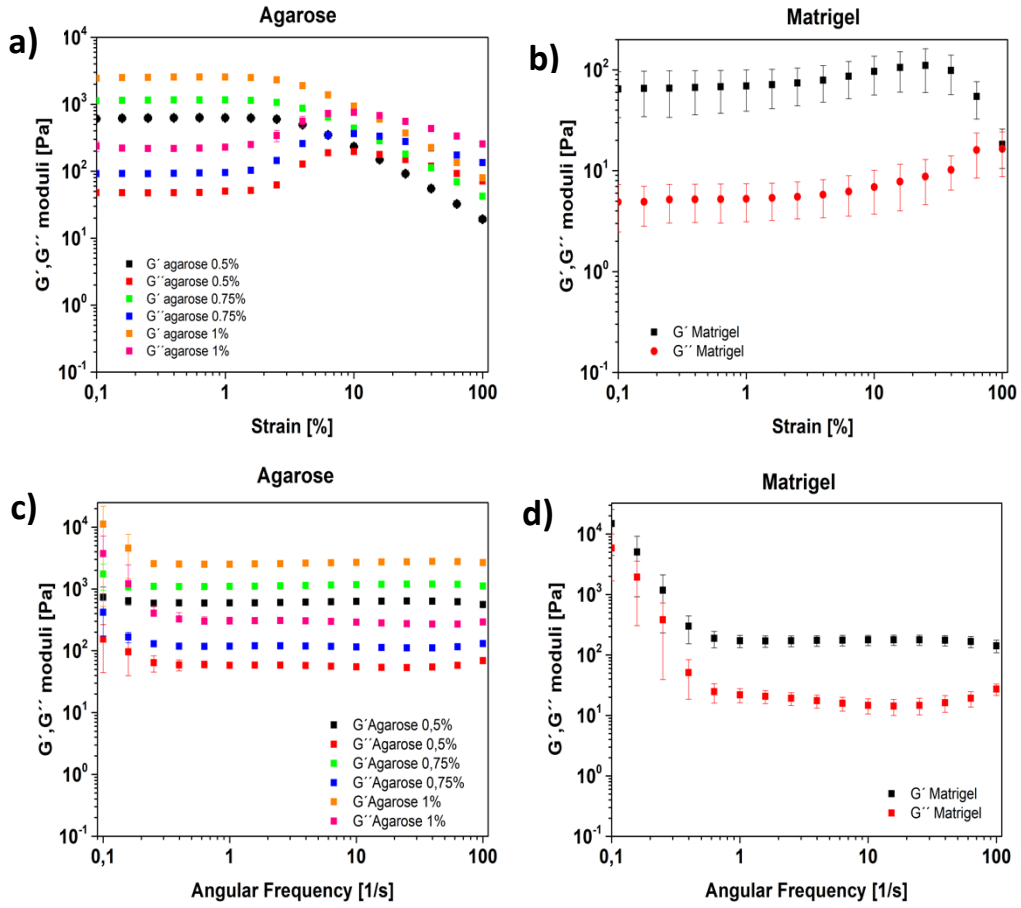


Figure 43 – Strain sweeps amplitude results for Matrigel (**a**) and Agarose (**b**) matrices to obtain the linear-viscoelastic limit, which is determined with respect to the strain. The strain sweeps were carried out with a fixed frequency of 1 Hz. Frequency sweeps results for Agarose (**c**) and in Matrigel (**d**) at 1% strain. Both oscillation tests were repeated three times.

In Agarose gels, there was an increase of G'' (for strains higher than 1% with G' > G'') which corresponds to the sample starting to form micro-cracks and fracture. However, after 3% strain the Agarose network collapsed and the sample was in a fluid state (G' < G''). The transition to fluid state was captured for the Agarose material (**Figure 43-a**).

In fact, the curves from the Agarose sample show a sharp decline in strain, implying that the fracture area increases. Whereas for Matrigel, samples show a small decrease in strain (He *et al.*, 2013; Mezger, 2014). At 100% strain the values of G' and G'' moduli are similar, indicating the start of structural collapse. It is evident that all the samples presented a typical gel behaviour, since G' is nearly predominantly higher than G'', independent of the frequency applied (Kocen *et al.*, 2017), **Figure 43** (**c-d**). The stiffness of 1% Agarose is 2.5 kPa, for 0.75% Agarose is 1.1 kPa and for 0.5% Agarose is 628 Pa. The 1% and 0.75% Agarose results exceed the brain stiffness values (150 – 1500 Pa) (Iwashita *et al.*, 2019)(Zuidema *et al.*, 2014), whereas was found for 0.5% Agarose to be between the ranges given. Nevertheless, shorter neurites and a lower cell viability were found for neurons growing in Agarose matrices.

The reasons why the primary cortical neurons growing in Agarose showed shorter neurites in comparison to the neurons growing in Matrigel, may be due to the biochemical properties of the hydrogel materials, i.e. biocompatibility and biological protein concentrations. Whereas, softer gels promote an increase in neurite growth compared to stiffer gels (Zuidema *et al.*, 2014). The 5 mg/ml Matrigel sample was shown to be the best 3D matrix to host cortical neurons, having lower stiffness values (≈ 69 Pa). *Zuidema et al.* (Zuidema *et al.*, 2014) reported higher stiffness values for Matrigel when using it at a higher concentration.

4.4 Discussion

Primary cortical neurons were cultured in 2D environment using the standard cell culture methods and in 3D environment using hydrogels. It is extremely important to choose a hydrogel that is able to support the neurons growing in 3D to achieve the most relevant cellular microenvironment as possible. This ensures a more realistic neuron culture model. Agarose and Matrigel are two natural hydrogels used to growth cells in three dimensions. A study of the neuron cell density was performed to understand which was the best cell density and concentration of hydrogel to culture neurons in three dimensions. These parameters are important to preserve the neuron structure, allowing the visualisation of neuron growth during culture.

A higher concentration of Matrigel (7mg/ml) appears to restrict neurite extension, while a lower Matrigel (5 mg/ml) concentration provided better conditions for longer neurites (**Figure 25**, **Figure 26**). The combination of lower gel concentration with the highest cell density was shown to be the best host for growing neurons in 3D; allowing the neurons to grow with longer neurites. This can be related with the pore size and stiffness of the matrix, which can be changed accordingly to the gel concentration. For instance, a lower gel concentration has more water and larger pore sizes than gels with higher concentrations (Narayanan, Xiong and Liu, 2006; Hoare and Kohane, 2008; Doyle, 2016). A lower concentration of Matrigel (**Figure 26c, e**) improves cell development and survival compared to a higher concentration (**Figure 26a**).

It is known in literature that higher gel concentration generates smaller pore size of the gel structure. The gel strength and the pore size are related (Laplaca, Vernekar and Shoemaker, 2010). The porosity is an important parameter as allows the gel to be permeable to the transport of gases, nutrients. Besides, it should be large enough for the extension of neurites. In this work, the Matrigel concentration of 7 mg/ml lead to cell death, while at a lower gel concentration (5 mg/ml) cells were alive. One of the reasons is based on the assumption that higher concentrations generate smaller pore sizes. Accordingly to this assumption, the pore size of 7 mg/ml was not large enough for the primary cortical neurons interact with other cells as the pore size should allow cell-cell interaction, migration and neurite extension (Laplaca, Vernekar and Shoemaker, 2010). In this study, the authors do not report and do not mention articles published with the pore size in Matrigel for neuronal cultures. However, it was reported that a 2 µm pore size was found for 50% matrigel concentration for cancer cells migration (Zaman *et al.*, 2006). In this study they have used Matrigel from BD Biosciences, while in this PhD project the Matrigel used was from Corning. Assuming that the Matrigel has the same concentration of proteins, the pore size in the work for this thesis would be higher, as we used 87.5% Matrigel (7 mg/mL) and 62.5% Matrigel (5 mg/mL).

The results presented in this chapter show the difference between cells growing in 2D and 3D (**Figure 25**, **Figure 26**). This difference is evident in cell morphology between the culture systems, such as in their morphology and neurite growth. As should be expected (Griffith and Swartz, 2006; Ribeiro *et al.*, 2012; Edmondson *et al.*, 2014; Jensen, Morrill and Huang, 2018; Virlogeux *et al.*, 2018) cells presented a different morphology in response to the culture method applied. Neurons growing in 3D showed a more similar shape to those living *in vivo* tissue (**Figure 29**), having a pyramidal shape, while those in 2D are flatter.

The 3D morphological shapes were maintained for 10 days demonstrating that Matrigel is a suitable neuron host able to form a 3D neuronal network. Although, morphological changes can also be seen in 2D cultures after 2 DIV, they were grown with a disparity of ECM proteins and a lack of a third dimension.

Cell viability is an important parameter to be analysed in order to maximise the conditions that allow the maintenance of cell integrity during experiments. Cell viability was determined for Agarose and Matrigel 3D cultures by investigating cell survival and the interactions between the neurons and the matrix of the biomaterials. Neuron viability was assessed between DIV2 and DIV 7, showing that Matrigel had higher cell viability than for 2D and Agarose. Although, the difference of cells survival was not shown to be significant between neurons growing in Matrigel and 2D cell cultures.

At DIV7, Matrigel showed 79% of live neurons, compared to just over 50% in Agarose. The 3D Matrigel matrix promoted neuronal development in a more realistic microenvironment, neurons started to differentiate and present neurite growth, which was visible by the length of the axons and the neurites. As a result, Matrigel provides a better 3D biocompatible support for hosting neurons, allowing high neuron viability, similar to that shown in 2D neuron cultures. Despite the advantage of biocompatibility of Matrigel to host neurons, Matrigel has the disadvantage of being time consuming, difficult to manipulate, expensive and lack of reproducibility (Hughes, Postovit and Lajoie, 2010). The fact that neurons are able to alive for a short time and still are able to differentiate, because they still growth, is a good indicator that the cells are partially functional. For confirm cell functionality further cell experiments can be performed, such as immunocytochemistry. However, the attempts to perform immunocytochemistry were not successful.

One reason for the poor neuron viability in Agarose compared to Matrigel is due to the biochemical properties of the hydrogels. Matrigel has a higher concentration of ECM proteins than in Agarose (since it is a polysaccharide hydrogel), which promotes longer axonal growth (R. Fan *et al.*, 2016)(Hughes, Postovit and Lajoie, 2010)(Tonge *et al.*, 1997). To overcome this other researchers have modified the Agarose matrix to enhance axonal growth, since it lacks sufficient proteins from the ECM (Yu, Leipzig and Shoichet, 2008).

Another reason can be due to the mechanical properties of the hydrogels. For example, stiffer matrices promote shorter neurites. Therefore, the stiffness of 0.5 Agarose and 5 mg/ml Matrigel was obtained and Agarose showed a higher stiffness than Matrigel, with both matrices having a gel-like structure even when diluted. This is confirmed by *Crompton et al.* (Crompton *et al.*, 2007), who found a large variance in gel strength when modifying its concentration. The concentration of hydrogel is an important parameter for further cell investigations. If a smaller concentration is used, the hydrogel becomes a more fluid-like structure, compared to higher concentrations that are more gel-like.

4.5 Conclusions of this Chapter

3D culture systems provide an environment for the cells to develop in three dimensions, acquiring a pyramidal shape and allowing their neurites to extend in all directions. 3D cultures offer a more accurate representation of the *in vivo* cytoarchitecture, in contrast to cells growing on hard 2D substrates. The main advantage of 3D studies over 2D is due to the loss of phenotype of cells that grow in two dimensions leading to a lack of cell-matrix interactions, limiting realistic cell growth features. Despite this, growing cells in 2D gives us the basic information about their behaviour, but does not provide cell responses as they would *in vivo,* due to their loss of native features.

This loss of *in vivo* features is explained by the lack of the structural support provided from the ECM. This confirms that the cellular environment influences cell morphology, confirming that 3D neuron cultures are important as they enable neurons to develop a similar morphology to neurons found in native tissue (**Figure 29**). Primary cortical neurons growing in Matrigel matrices are found to grow with a similar shape to the *in vivo* tissue, preserving their structure and function. Over one week of culture, neurons were able to develop and preserve their morphology and function within a more realistic environment.

The concentration of hydrogel is also an important parameter in providing the right conditions to host neurons in 3D (i.e. ability to support neuron growth). Thus, 3D cell culture models offer more realistic results adding greater accuracy to cell experimental analysis.

Chapter 5 Design and fabrication of the new 3D device

5.1 Introduction

The aim of this work is to develop a more realistic model to study axons in isolated compartments separate from their cell bodies. In particular, the isolation of each sub cellular neuron counterpart is important to improve the knowledge in axon function, degeneration and potential capacity for regeneration in the CNS. A new cell culture system has been created to allow the individualisation of neuron cell parts within a three-dimensional (3D) environment, as seen in **Figure 44**. This chapter details how the new cell culture device was designed, manufactured and validated. The design of the device was based on current microfluidic devices and prototyped fabrication techniques. The working principle was demonstrated and the performance assessed by characterising the fluorescein diffusion profiles.

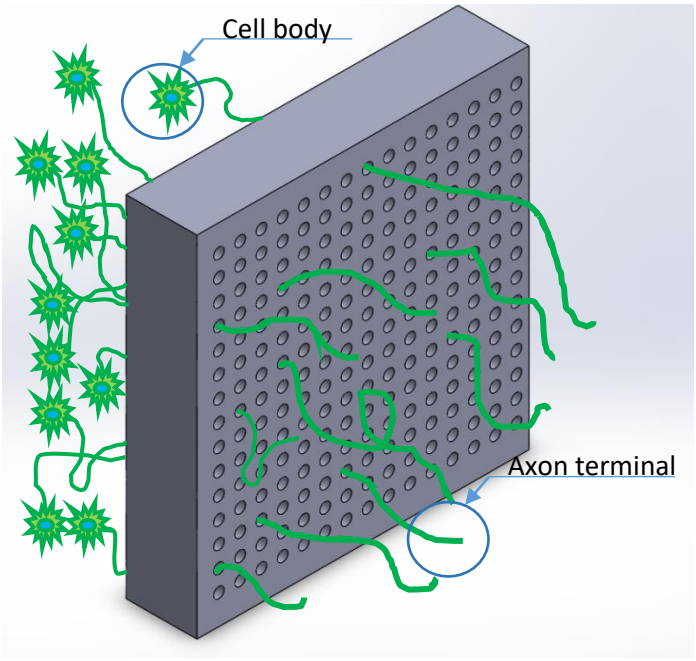


Figure 44 – Illustration of axonal isolation from cell bodies by a polycarbonate membrane with a pore diameter of 5 µm. Axons are isolated in 3D within the hydrogel, which provides the mechanical and biochemical host environment.

5.2 Design of the Device

As a first step to build the device for this work, is to think how to fabricate the 3D physical barrier that will allow axonal isolation. Normally, the fabrication of a master mould is required, followed by its pattern replication. Precisely to build the 3D physical needs to contain the features (e.g. channels or microgrooves) that will allow the axonal isolation. Therefore, the manufacturing processes, such as lithography and micromachining, were also considered for the development of a master mould. The master mould would contain specific features for axonal growth, which are replicated using the soft-lithography technique. The barrier could be manufactured by scratching and/or micro-drilling technology, FIB and E-beam technology or additive manufacturing. The microfluidic devices for axonal isolation were fabricated using glass and silicon that, when functionalized, were biocompatible for cell culture. However, these materials were employed in hard lithography, which is expensive, slow and involves many steps, including spin-coating, soft- and post-bake, exposure, development and cast mould. Also, it requires photomasks with high-resolution to produce the structure desired (Liu *et al.*, 2016). And because it requires a photomask, some designs were done taking into consideration how would be possible to create a 3D physical barrier for axonal isolation, please see **Figure 45**. By using photolithography, a sandwich structure of multilayers of PDMS chips with the microgrooves would be sealed, layer-by-layer, creating a 3D physical barrier (**Figure 46-b**). However, because it is an expensive time-consuming technique and expensive, another approach to build the 3D physical barrier was taken into consideration (**Figure 45, Figure 46-a**). This alternative would consist in building the physical barrier in one step. A trial to fabricate a 3D physical barrier by two-photon polymerization is shown in **Figure 47**. The material used was ormocer (microchem ltd.) and the ormocer 3D physical barrier was fabricated by another PhD student who uses this technique as part of their research. Here, apart from the high cost and time-consuming, there was also the problem how to seal different comparts as it is difficult to ensure the consistency between layers.

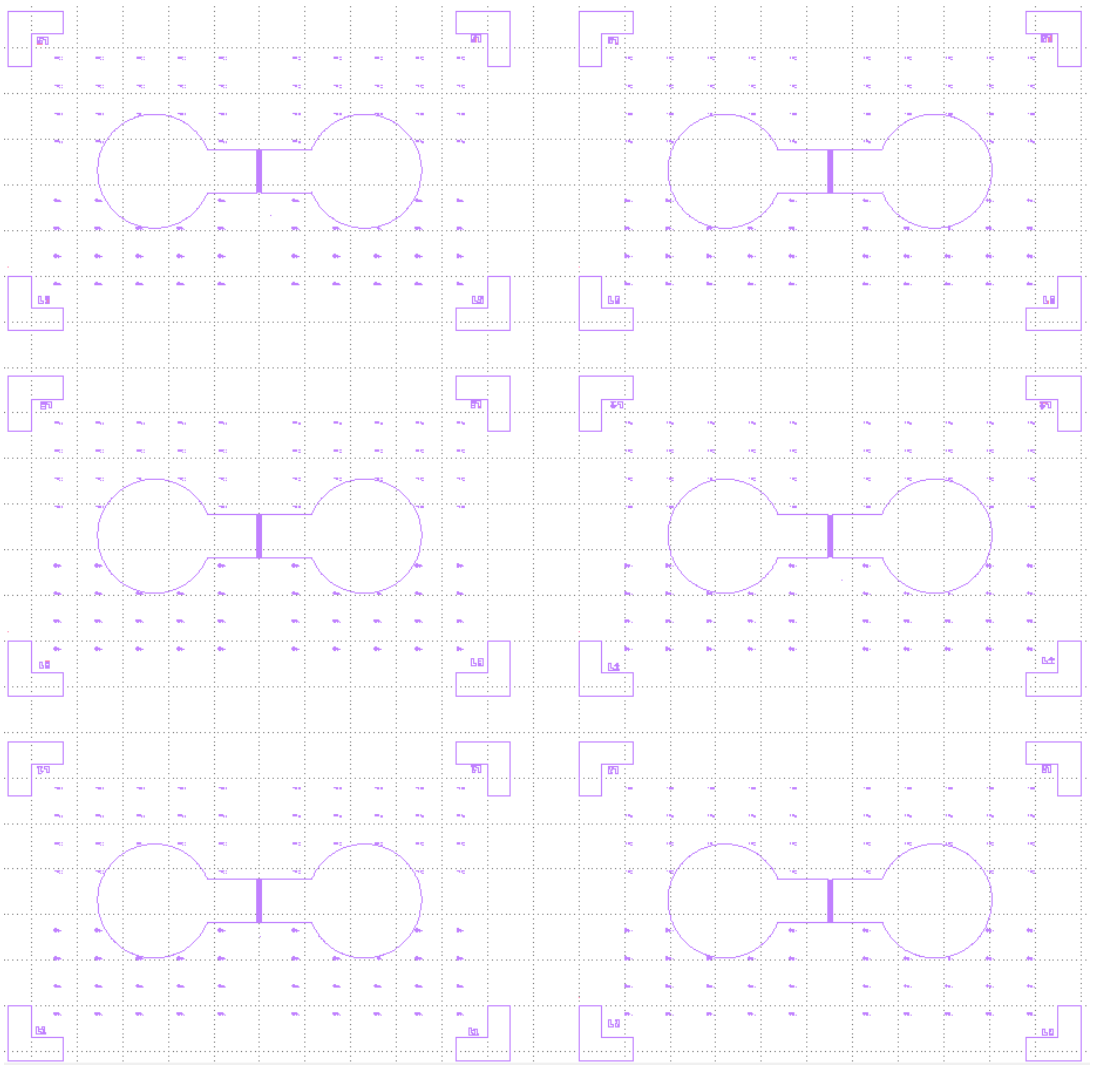


Figure 45 – Image of the design to transmit to a master mould by photolithography technique. After which, the master is employed in soft-lithography to get bulk layers of PDMS with these features. This design allows the fabrication of 6 bulk layers of PDMS that are later sealed one on top of the other.

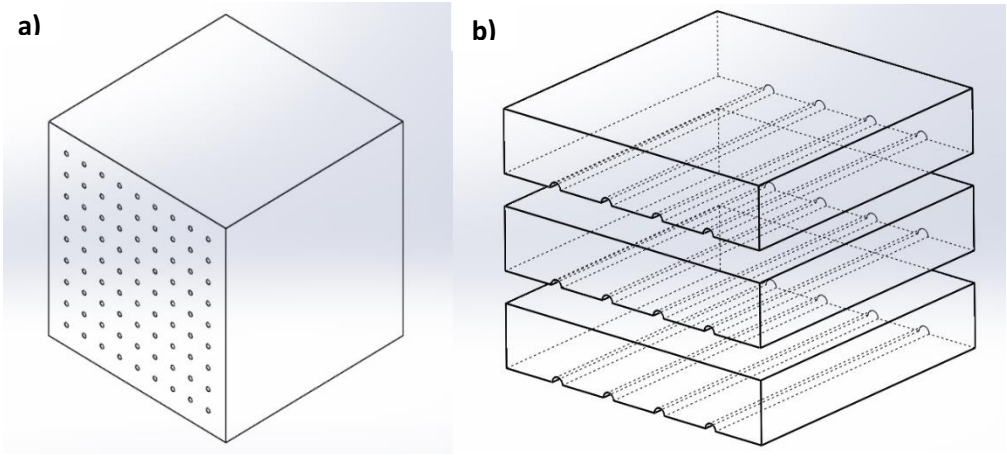


Figure 46 – Two different proposed techniques to build the 3D physical barrier for axon isolation (200 µm x 200 µm x 200 µm), which holes spaced at 20 µm intervals with 5 µm diameter: **a**) barrier fabricated with microgrooves; **b**) barrier fabrication by layers, where each layer forms the microgrooves.

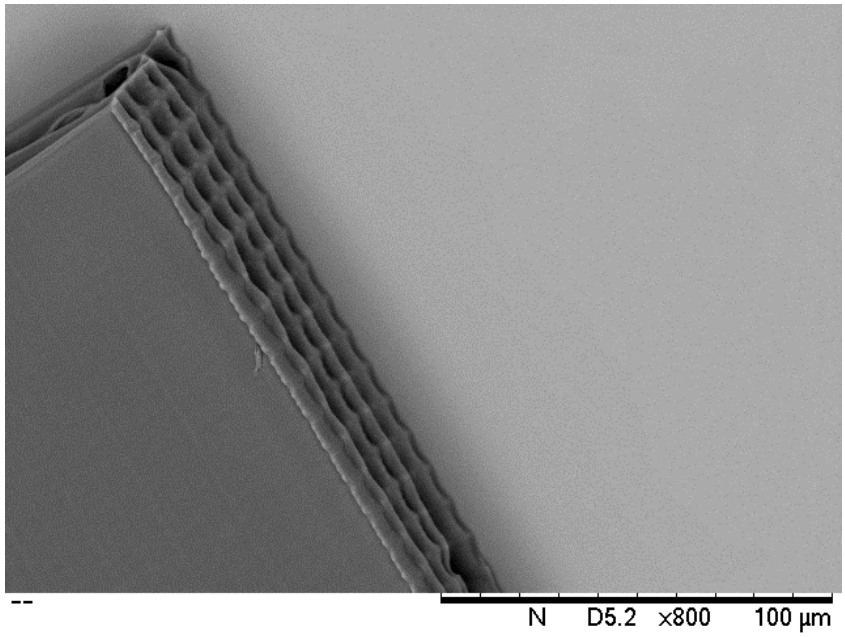


Figure 47 – SEM image of a barrier structure made of Ormocer material by two-photon polymerization.

Regarding the micromachining techniques to develop a master mould with channels with a small resolution to allow axonal isolation would be experimental, because there the author of this thesis was not able to find any article where a master mould was developed by micromachining to develop a device for axonal isolation. Furthermore, the additive manufacturing techniques were also taken into consideration to build the device. Some of the techniques do not have the right resolution (as seen in **Table 1, Chapter 2**) or the materials are not transparent, and the techniques that have the right resolution are so expensive as lithography techniques, time consuming and there is no way to ensure the consistency between layers.

The device main requirement of the device is a 3D physical barrier that will isolate axons from cell bodies by containing features with minimum size of 10 µm, to avoid the passage of cell bodies between compartments. So, techniques that could achieve a resolution of a minimum of 10 µm would be ideal. Another requirement as mentioned in chapter 2 and above, the device should be transparent to be compatible with microscopy, portable, biocompatible with cells, ability to have reservoirs that contain more than 200 µL for fluidic isolation as reported by the XONA devices and *Taylor et al.* (Taylor *et al.*, 2003, 2005; Park *et al.*, 2006). Therefore, a polycarbonate membrane was chosen to be the features of the device that would allow axonal isolation. It is easy to use, low-cost and can be biocompatible. The polycarbonate membrane contains pores with the dimensions required for allow only the passage of axons, which is the only dimension defined and required for the development of the new device. The polycarbonate membrane can be incorporated in the fabrication of devices by xurography technique (Bartholomeusz, Boutté and Andrade, 2005). The polycarbonate membrane contains pores that will allow the passage of axons between compartments, and xurography allows to cut the membrane with the right dimensions to be incorporated in devices.

We tried to culture neurons in 3D within two XONA devices to performed a 3D physical barrier as shown in **Figure 48**. From this experiment we observed that cells do not go to the area of cell culture chambers from the top device. This is explained by the fact that the cells when are platted are in a liquid solution and tend to go in the direction of the surface. Second, we could see that cells die after 1 day in the cell culture chamber of the bottom device. The fact that cells died within small spaces when cultured in Matrigel, leaded us to designed bigger dimensions for the designing the large dimensions of cell culture chambers.

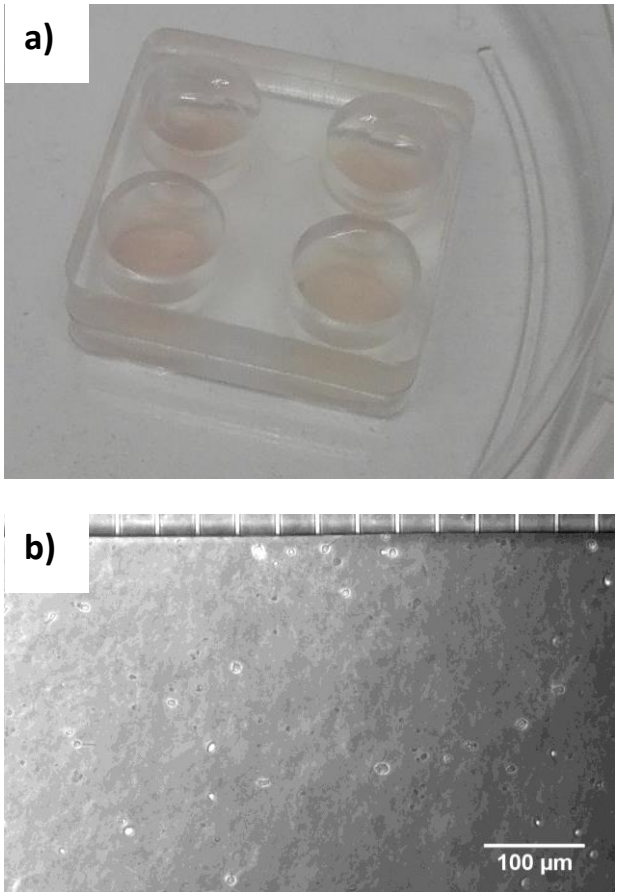


Figure 48 – Layer-by-layer of two XONA devices with neurons laden matrigel (a). Cells did settle in the direction of the surface. There is no force that will make then go inside the cell culture chamber from the top XONA device. After 1 DIV cells were dead.

The device was designed to prove that axons and cell bodies can be compartmentalised in a 3D microenvironment, providing an improved physiological method to study axonal function. In achieving this, the device must follow specific requirements, such as transparency, biocompatibility, compartmentalisation of axons from their cell bodies, with a physical barrier with pore diameter sizes equal to or lower than 5 µm.

The main challenge in manufacturing this device was the fabrication of the 3D physical barrier structure, creating both physical and spatial neuron compartments. Different manufacturing techniques, from additive manufacturing to micromachining, were considered to solve this challenge. Many of the techniques are time-consuming; and do not achieve the resolution needed; require non-transparent materials; have higher costs and/or are difficult to acquire. For these reasons, two-photon polymerisation (Ostendorf and Chichkov, 2006; Wu, Serbin and Gu, 2006) or photolithography (Pease and Chou, 2008) where not selected and the 3D physical barrier was chosen to be made from a polycarbonate membrane, as shown in **Figure 44**.

The use of a polycarbonate membrane is a more attractive approach to achieve the device aims due to its simplicity and inexpensive costs. Polycarbonate membranes have previously been used in biomedical devices for the isolation of drugs (Marom *et al.*, 2015)(Abhyankar, Lokuta and Beebe, 2006) and for axonal isolation (Cheng *et al.*, 2017), as their cheaper cost and simplicity to use has made it a popular choice for rapid prototyping. The device in this research was designed to be simple and straightforward to develop using a combination of xurography techniques (Martínez-lópez *et al.*, 2016; Mart *et al.*, 2017) and soft-lithography techniques (Y and Whitesides, 1998).

Soft-lithography is a standard technique commonly used in the fabrication of cell culture devices (Cheng *et al.*, 2017)(Qin, 2016)(Takayama *et al.*, 2012)(Han *et al.*, 2012). This technique allows the fabrication of structures, commonly made of polydimethylsiloxane (PDMS), using a material with the desirable properties that meet the device requirements, such as biocompatibility and transparency. The new device consists of two PDMS blocks incorporating a rectangular channel separated through a polycarbonate membrane with pore diameter of 5 µm. As shown in **Figure 49**, PDMS blocks have one reservoir for seeding cells and solution exchanges, and a channel for cell culture (i.e. cell culture chamber).

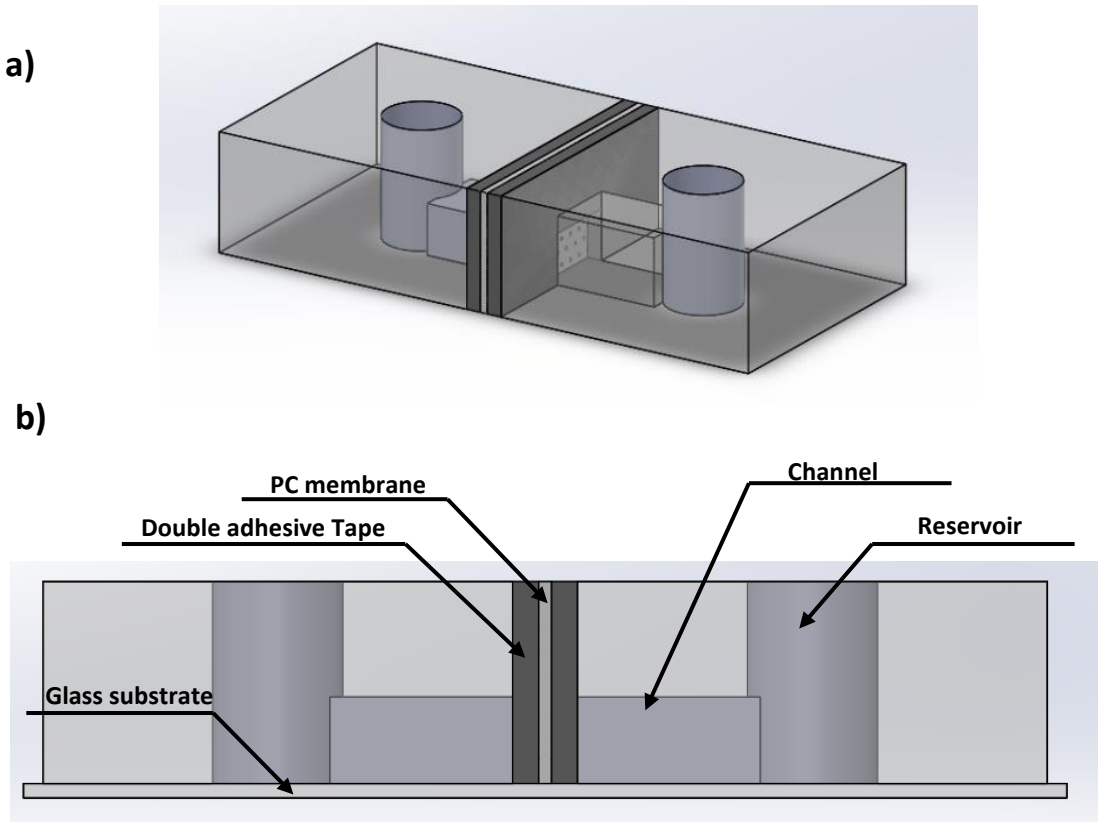


Figure 49 – 3D device (22 x 22 x 10 mm) consisting in two holes: one on top that is a reservoir (5 mm in diameter) and a second hole that corresponds to the channel (10 x 7 x 3 mm). The device consists of two PDMS blocks connected to each other, forming a long channel divided by a polycarbonate membrane (**a**). Adhesive tape is used to seal the two PDMS blocks either side of the polycarbonate membrane, resulting in the configured platform: PDMS block–tape-membrane-tape-PDMS block. The underside of the platform is sealed to the glass substrate with a reversible bonding (**b**).

5.2.1 Design Choices during Fabrication

The challenges encountered in the fabrication of the reservoirs include sealing; creation of the reservoir hole and the lateral channel. Particularly the fabrication of the holes in the PDMS blocks, ensuring a good seal is achieved without material damage during punching. Which proved to be the main problem in the fabrication of this device, this is known by trying to punch or cut PDMS the material can be damage. The reservoir hole was made by punching the PDMS blocks with a biopsy punch, avoiding the disruption of material and of the channel. The polycarbonate membrane was attached and sealed to either side of the PDMS blocks with double silicone adhesive transfer tape. Manufacturing strategies were created to generate a reservoir, a channel and to develop flat and smooth PDMS surfaces, as shown in **Figure 50**.

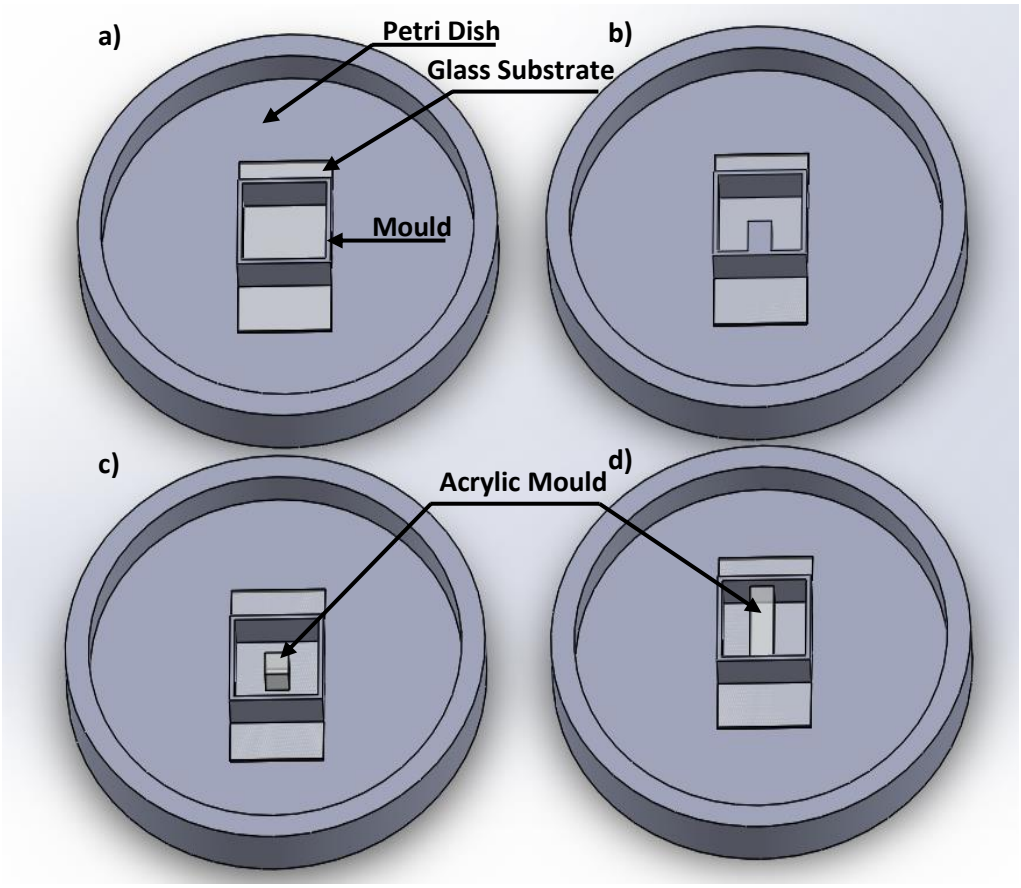


Figure 50 – Strategies to develop a lateral hole in the reservoir's block and how to ensure a smooth flat surface (a, b, c, d).

The first feature to be verified was the fabrication of the channel, since is a lateral hole in the PDMS block. A lateral on the PDMS block as shown in **Figure 51c**. Initially, it was considered that the easiest way to achieve this would be through the creation of a square PDMS block (**Figure 50a**), and subsequently punch two holes (one on top and the other on the side) using the biopsy punch. However, this strategy caused damage to the PDMS block once the second punch was made. A second strategy (**Figure 50b**) was considered, which consisted of placing a small cube and attaching it to one side of the square mould, as shown in **Figure 50b**. After curing the PDMS and its extraction from the mould might leads to a PDMS block containing already a lateral hole.

The third strategy was to place the small cube structure in the middle of the square mould (**Figure 50c**), instead of placing it close to one of the sides of the mould. However, this strategy leads to complications with cell seeding and the generation of the reservoir without damaging the material. Besides this, there was the issue that when cells were seeded, they are still in a liquid solution, and the plated cells were drawing towards the bottom of a device. Therefore, until the gel solidifies the cells would draw toward the bottom and not go in the direction of the membrane. As a result, strategy two (**Figure 50b**) is considered a better strategy than the third (**Figure 50c**). The last strategy (**Figure 50d**), consisted of a rectangular structure placed in the middle of the mould.

In this way, the resulting PDMS structure contained a square hole along the bottom surface. This long hole would have the membrane in one side and the other side would require a “plug” to avoid leakage of cells and media. The plug would be made of PDMS with a rectangular structure that would fit the lateral side, which would not be in contact with the membrane.

Using this strategy, the PDMS structure could be cut in half, sealed to the membrane and the plugs inserted in the unattached sides of the PDMS structures. However, due to the difficulty in cutting PDMS with high precision, this strategy was not continued. The PDMS replicas from these strategies presented are shown in **Figure 51**. Overall, strategy two (**Figure 50b**) proved to be the most successful. Where, after casting, the PDMS already contained the square hole (**Figure 52a**) and then the reservoir hole (**Figure 52b**) was created using the biopsy punch method. The PDMS block, with the side channel, was fixed with double adhesive tape (**Figure 53a**) and the free side of the tape was sealed to the polycarbonate membrane (**Figure 53b**).

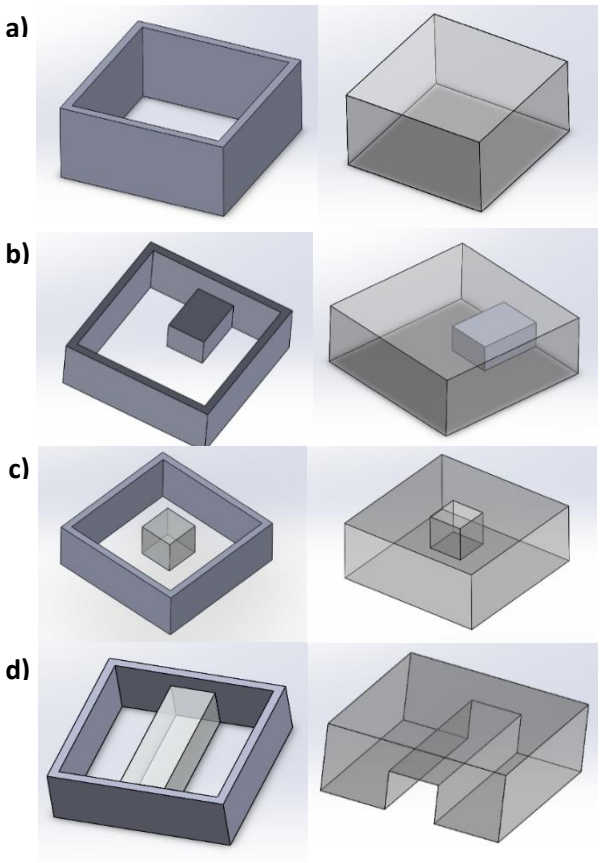


Figure 51 – PDMS blocks extracted from the moulds. **a**) Simple PDMS block, with two punches made, one for the lateral hole and the other for the reservoir (**Figure 50a**); **b**) PDMS reservoir with a lateral hole made from a cubic form located next to the mould (**Figure 50b**); **c**) A lateral hole fabricated in the middle of one of the PDMS faces (**Figure 50c**); **d**) PDMS block with a channel along its surface (**Figure 50d**).

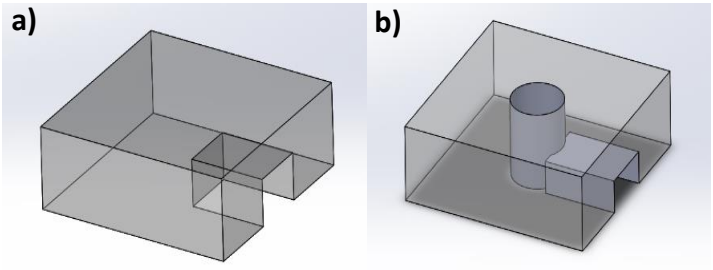


Figure 52 – Strategy used to fabricate PDMS blocks: **a**) PDMS block casted from the mould; **b**) reservoir punch in the PDMS block.

After this, the free side of the membrane was sealed to a second slice of tape and finally sealed to the second PDMS block (**Figure 53c**). The platform (PDMS-tape-membrane-tape-PDMS) was sealed onto the surface of the glass coverslip. The proposed design is based on the fact that individual cell parts can be separated by a porous membrane, allowing the isolation of axons in 3D.

The device only requires the use of a micropipetting technique to introduce and change the solutions without the need of any external equipment, such as a pump system. During the experiment the cell bodies are seeded in the soma side of the device and start developing their axons. Axonal isolation is provided by having one side that corresponds to the somatic side (containing cell bodies) and the other corresponding to the axonal side (containing only axons), separated by a polycarbonate membrane.

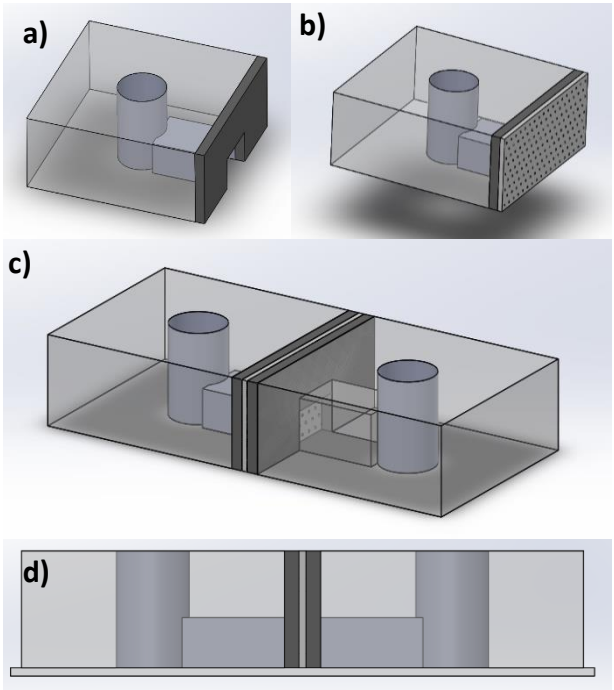


Figure 53 – Following the proposed strategy, two one compartment PDMS block are sealed by double adhesive tape (**a**). One side of the tape is sealed to the membrane (**b**), and the other side of the membrane is sealed to other tape (**c**), which is sealed to the second compartment (**d**).

5.2.2 Device Fabrication

The proposed strategy was selected as the preferred manufacturing technique as it is cost-effective, allows for rapid prototyping, the use of low-cost and transparent materials and its compatibility with microscopy techniques. The first time the PDMS blocks were used, they were submerged in a Hanks solution to promote its biocompatibility. The integration of the polycarbonate membrane to the PDMS block was achieved using double adhesive tape.

One side of the tape seals to the PDMS and the other to the polycarbonate membrane. Double adhesive tape is used between PDMS blocks and the membrane for adhesion of the device components. A platform was created consisting in PDMS-tape-membrane-tape-PDMS and it is sealed to glass coverslip 22mm x 50mm. This sealing is reversible, allowing biological devices to be reused, as t can be detached from the platform and coverslip. Allowing, experiments to be easily replicated using the same platforms.

5.3 Cell Culture Device Characterisation

For the characterisation of this novel device, diffusion profiles were investigated and the devices were checked for any leakage between the PDMS and the coverslip. Diffusion profiles are important in biological experiments, since they give an indication of the time required to maintain a molecule (e.g. drugs, chemicals, dyes) isolated in one compartment. The diffusion profiles show how long fluidic isolation can be maintained, which is the time a target molecule takes to cross from one side to the other through the membrane against the hydrostatic pressure. As demonstrated before in XONA devices, in order to control the fluidic isolation the volume in the both soma and axon compartments are adjusted, creating a hydrostatic pressure between compartments (Taylor *et al.*, 2003, 2005; Roca and Cited, 2006; Toh *et al.*, 2014; Brandenberg and Lutolf, 2017). This time is evaluated by the use of a fluorescent dye (i.e. fluorescein).

A volume difference between the soma and axon compartments is applied to provide fluidic isolation as *Taylor et al.*(Taylor *et al.*, 2003, 2005) did. Using the same volumes as a guide parameter for the experiment, a higher volume (e.g. 160 µl) is applied to the soma compartment and a lower volume to the axon compartment (e.g. 100 µl). The axon compartment contains the fluorescein and the volume difference created by hydrostatic pressure provides the isolation of molecules on one compartment. The soma compartment provides resistance against any diffusion of fluorescein from the axon compartment (Roca and Cited, 2006; Brandenberg and Lutolf, 2017) Diffusion profiles in both 2D and 3D conditions were determined in XONA devices. Results for 2D conditions in XONA devices were reported by *Taylor et al.* (Taylor *et al.*, 2003). The XONA device was used to understand the experimental protocol and compare against the diffusion profiles obtained in the new device.

The diffusion profiles in the new device were obtained only for the 3D conditions, as the device is to be used for 3D cell cultures. The fluorescence intensity images were acquired using a microscope and images analysed using MatLab Pro (2016) and ImageJ. These programmes were used to measure the fluorescence intensity in both the soma and axon compartments. The fluorescent intensity was measured for each image by calculating the average fluorescent intensity in three different regions for both the soma and the axon compartments. The data was normalised to the maximum intensity value obtained.

5.3.1 Leakage tests

One of the main issues associated with this device is achieving a good seal between the platform and the glass coverslip. This is believed to be a common problem as devices based on porous membranes are difficult to seal (Morel *et al.*, 2012), due to leakage or membrane detachment. This can cause many issues to the experimental protocols. In the case of leakage, experiments are not valid as axon isolation is no longer possible (**Figure 54c**) and a balanced hydrostatic pressure is not achievable (**Figure 54a, b**). In **Figure 54** (**a**), there is an example of a not perfect sealing, since after 2 hours period fluorescein is presented between both compartments. While, in **Figure 54** (**b**) shows fluorescein isolated in one compartment for 2 hours period, which confirms a perfect sealing. If there is no fluidic isolation, neurons can travel between compartments when they are plated, as seen in **Figure 54** (**c** – left side).

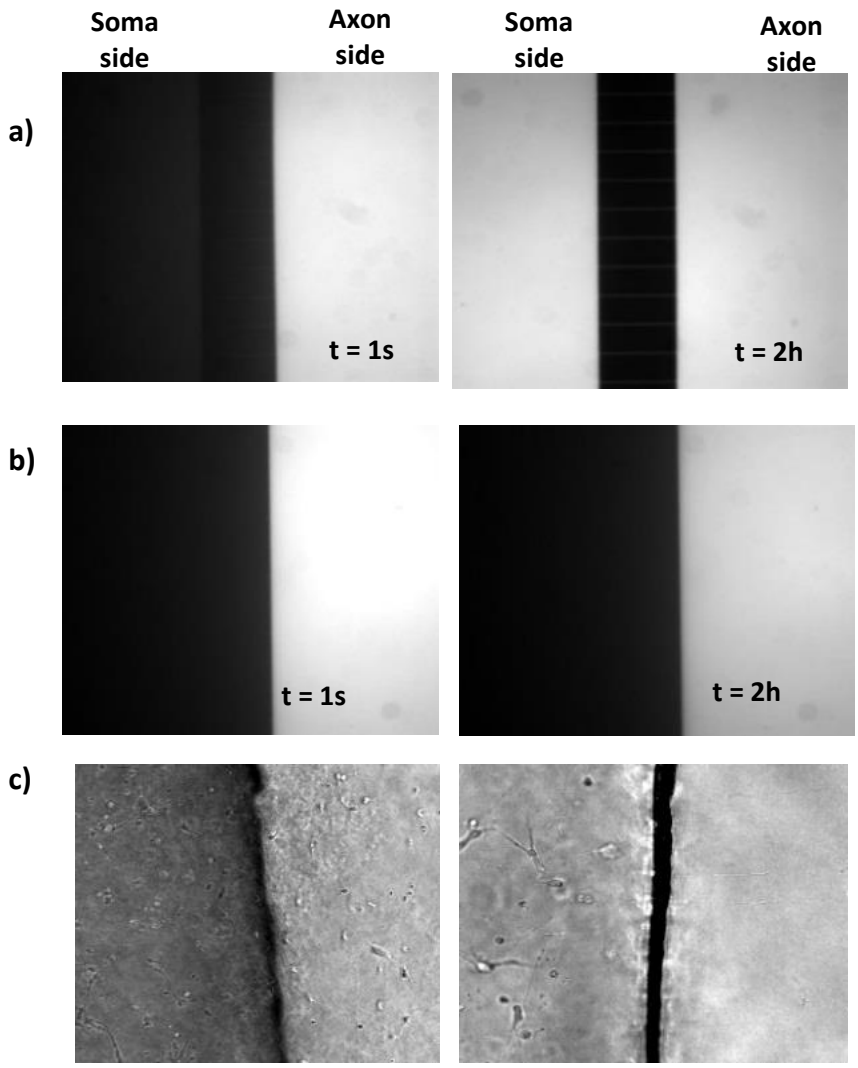


Figure 54 – Flow characterisation experiments to test the proposed sealing method (**a**) showing a perfect seal (**b**) between XONA devices and the glass substrate in the beginning of the experiment (left side) and after 2 hours of experiment (right side). The white area corresponds to the axon side, where Fluorescein is placed, whereas the black area corresponds to the soma side, which is not filled with Fluorescein. Example of sealing issues within the new device (**c** – left hand image), showing no isolation between cells and a good sealing in the new device (**c** – right hand image), where cells are isolated in one compartment.

In order to confirm that there was no leakage in the device between the PDMS and the glass coverslip, a simple test with dye was performed, as shown in **Figure 55**. First, one side was filled with 200 µL of Ponceau (red) and the other side was filled with 100 µL of Coomassie (blue). This device was successfully tested without leakages for 15 minutes. Additionally, during cell experiments (more than 5 days) no leakage was observed.

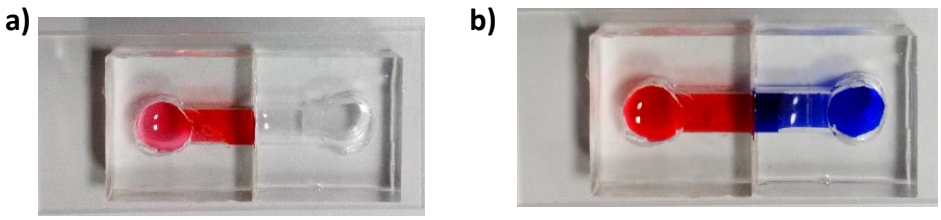


Figure 55 – Leakage test in the new cell culture device showing no leakage after top up. First, one side of the device was topped up with Ponceau dye (red) (**a**) and the other side was filled with Coomassie dye (blue) (**b**). No fluidic leakage was visible in the device, proving the device was successfully sealed.

5.3.2 Diffusion Profiles on XONA devices

Diffusion profiles were obtained in the, commercially available XONA device for 2D axonal isolation, for both 2D and 3D environment conditions. It has been reported that by applying a volume difference of 50 µl (less than 1 kDa) between soma and axonal compartment in a XONA device, results in the isolation of any component (i.e. molecule, dye, other cell types) for 15 hours (Taylor *et al.*, 2003, 2005). Here, diffusion profiles for XONA device was determined for both 2D and 3D conditions. The 2D diffusion profiles in the XONA device were obtained using the same conditions as *Taylor et al.* (Taylor *et al.*, 2003) reported.

For the 3D diffusion profiles, the volumes applied in the device started to be the same as the ones used by Taylor (Taylor *et al.*, 2003, 2005) in the XONA device. As this is a new device, the volumes were estimated to achieve fluidic isolated, hence the volume different chosen was by trial error as presented in **Table 7**. Before adding the fluorescein to de device in 3D, the gel layer was placed in different volumes in the device. There was not found a fluidic isolation for any volume's conditions below the condition 16. There is a difference of volume in the gel layer and a difference of volume when the fluorescein is added to allow fluidic isolation. From our tests, and to allow the same volumes of fluorescein as expressed in *Taylor et al.* (Taylor *et al.*, 2003) there is a need of a difference between the gel layers and a then apply the fluorescein volume different as Taylor reported (Taylor *et al.*, 2003). Besides, Matrigel is expensive to use in this experiment because it is a big volume of gel in each trial, so we used Agarose gel.

Table 7 – Volumes of gel inserted in the axon and soma compartment within Agarose.

Number assays	Vaxon	Vsoma
1	400	400
2	400	350
3	400	300
4	400	250
5	400	200
6	400	150
7	400	100
8	350	350
9	300	350
10	300	300
11	300	250
12	300	200
13	300	150
14	300	100
15	250	250
16	250	200
17	250	150
18	250	100
19	200	200
20	200	100
21	100	100

5.3.2.1 2D Diffusion Profiles for XONA devices

The 2D diffusion profiles in the XONA device was obtained by acquiring images every 15 minutes for a 15 hours period (**Figure 56**), as a replica of what *Taylor et al.* (Taylor *et al.*, 2003) did. The only difference is that in this work fluorescein was not added after 4 hours as Taylor did. A decrease in the fluorescein intensity for the 2D diffusion is visible, as the PBS solution (higher volume in the soma compartment) slowly travels to the axon compartment (lower volume compartment), diluting the fluorescein. Moreover, it is clear that the difference in volumes hinders the fluorescein entering the soma compartment. In fact, there is no perfect isolation between the compartments, since both compartments are always in "communication". A ~7% increase in fluorescence intensity was found after for 15 hours in the soma compartment, and shown to have the variability as the XONA device (Taylor *et al.*, 2003).

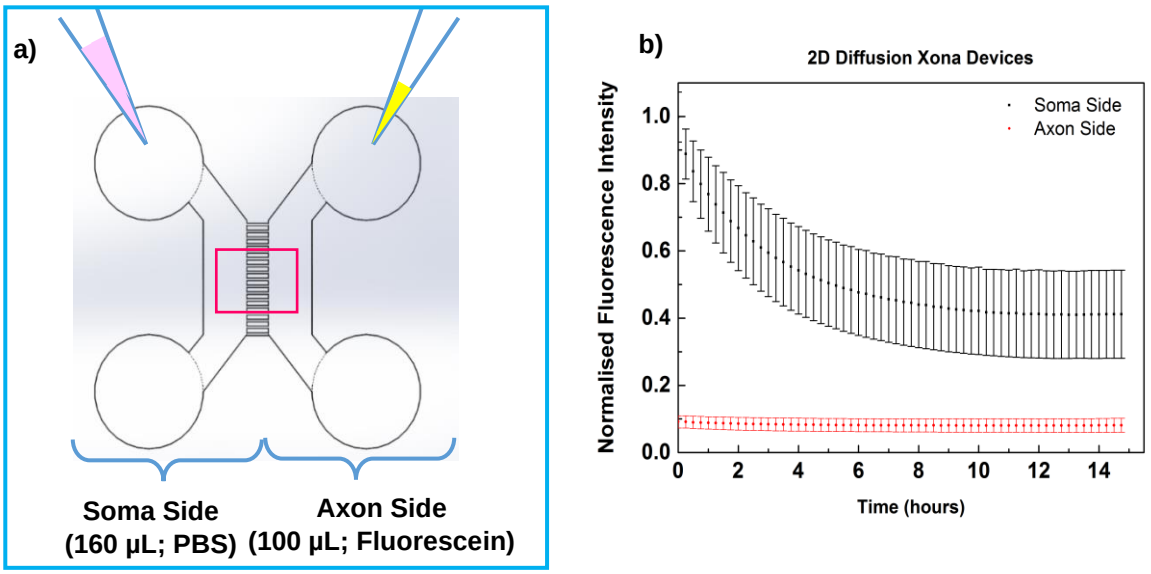


Figure 56 – 2D Diffusion profiles in the XONA device. **a**) The devices were filled with 160 µl of PBS solution added to the soma compartment and 100 µl of fluorescein (1 µM) in the axonal compartment. Square in red represent the area of image acquisition. **b**) Fluorescence intensity values are plotted as a function of time, where images were taken every 15 minutes over a 15 hours period. The fluorescence intensity was normalised to the maximum intensity value recorded. All trials were repeated three times.

5.3.2.2 3D Diffusion Profiles for XONA devices

Additionally, the XONA device was filled with 160 µl of Matrigel added to the soma compartment and 100 µl to the axon compartment. The 3D diffusion profiles were investigated for a 48 hour period, as after the initial 15 hours, the diffusion between both compartments had not yet stabilised. At the initial stages of the experiment, the fluorescence intensity was the same in both compartments, as the diffusion of fluorescein through the matrix is slower than in the 2D conditions (**Figure 57**). Since the hydrogel matrix acts as a resistant layer to fluorescein diffusion, the intensity starts to increase on the axon compartment after 1 hour. This is followed by a sharp increase in fluorescence intensity until it starts to stabilize after 20 hours. During this stabilisation period, a small increase of 16.5% fluorescence intensity is seen in the soma compartment. This small increase is related to the fact that the diffusion of fluorescein is slower compared to the 2D conditions. Which allows the fluorescein to diffuse through the matrix crossing the microgrooves and continue to flow towards the axon compartment.

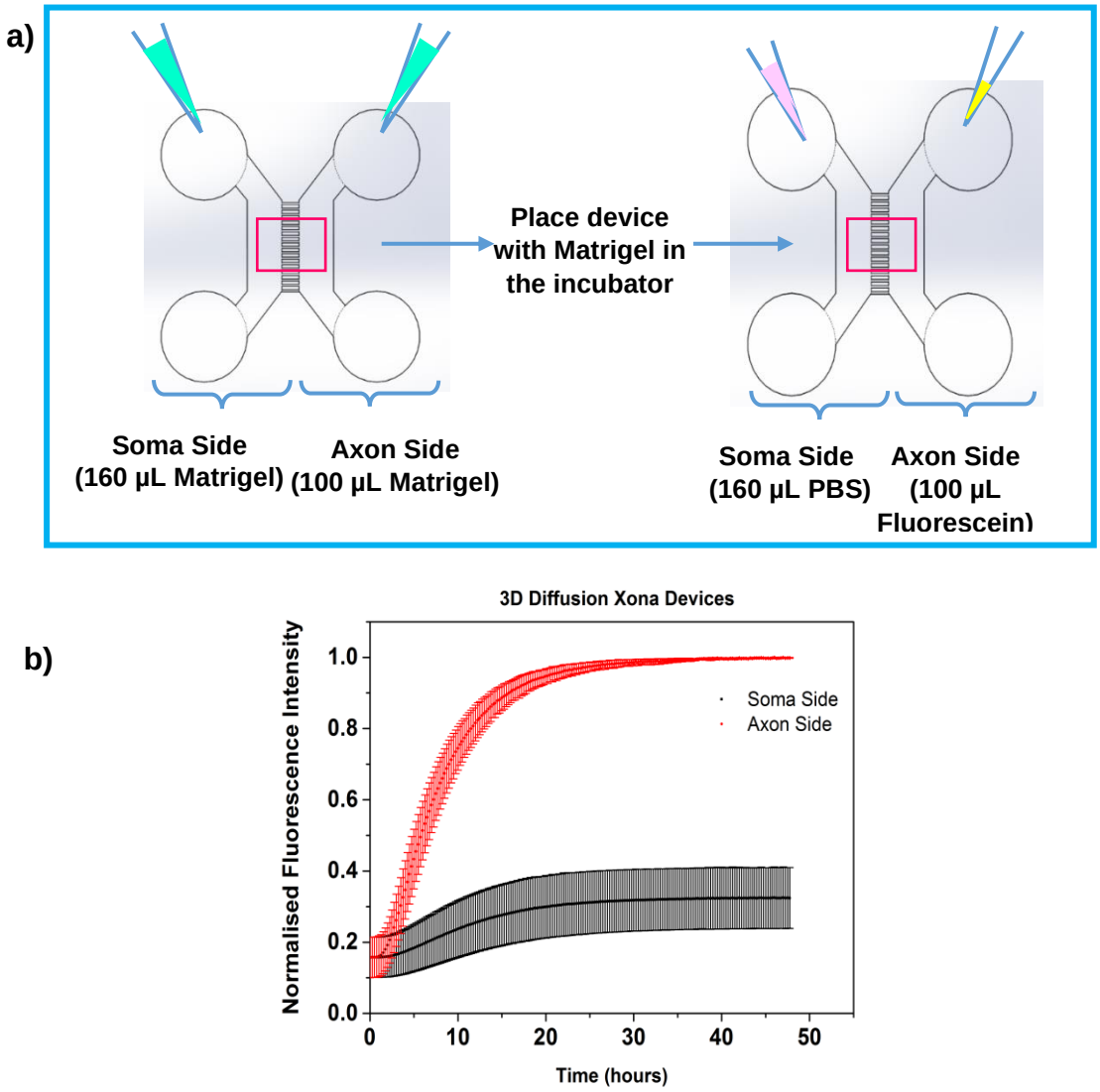


Figure 57 – 3D Diffusion profiles in the XONA device. **a**) For the 3D conditions the devices were filled with 160 µl of Matrigel (5 mg/ml) added to the soma compartment and 100 µl added to the axonal compartment. After filling the devices with Matrigel, they were placed inside the incubator at 37°C for 30 minutes. After which, 160 µl of PBS was added to the soma compartment and 100 µl of fluorescein (1 µM) to the axonal compartment. Squares in red represents the area of image acquisition. **b**) The fluorescence intensity values are plotted as a function of time, where images were taken every 15 minutes for a 48 hour period. The fluorescence intensity was normalised to the maximum intensity value recorded. All trials were repeated three times.

The experimental plots show a tendency of how the flow behaves in the XONA device, with an associated error of about 40% due to the variation of fluorescence intensity. Which is related to how fast the fluorescein travels in each XONA device.

The fluorescein intensity in the XONA device for the 3D conditions at 24 hours is shown in **Figure 58**. Showing the difference of fluorescein intensity between the two compartments, being able to prove the fluidic isolation after 1 day. The intensity presented by the red line is higher because the fluorescein in the experiment is added to the top reservoir, leading to the fluorescein travelling from the top reservoir to the bottom reservoir. Consequently, the fluorescein intensity is higher for the red line than the pink line.

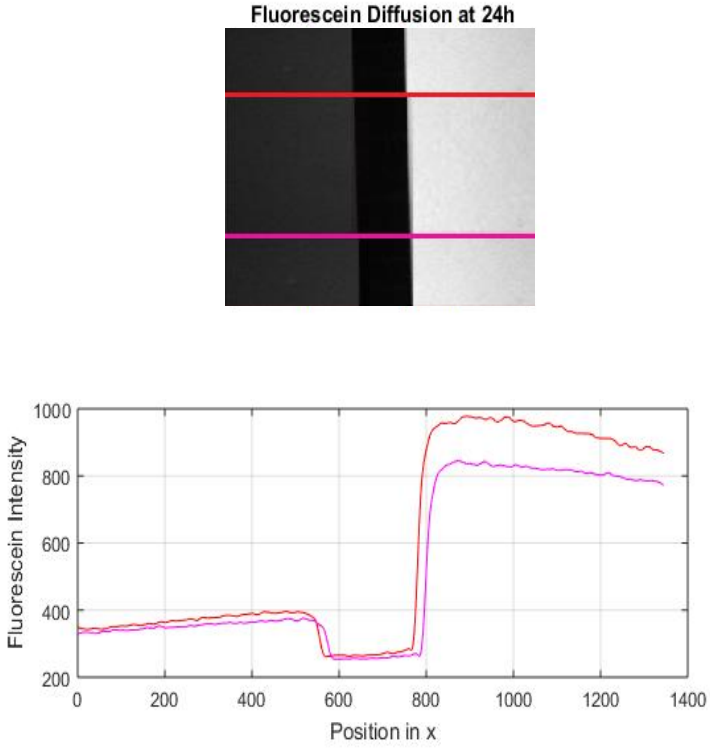


Figure 58 - Diffusion profiles for Matrigel within the XONA device at 24 hours. The micrograph images have coloured lines, which corresponds to the fluorescein intensity values in different directions. Each line is plotted as a function of the x position.

5.3.3 Diffusion Profiles in the New Device

The diffusion profiles of the new device were characterised for 3D conditions (diffusion through hydrogel). This was achieved by filling the reservoirs with hydrogel. Pre-gel solutions were introduced carefully into the reservoirs, with the soma compartment containing 250 µl of the pre-gel solution and the axon compartment 200 µl. After gelation, 200 µl of PBS was added to the soma compartment, while 50 µl of fluorescein was added to the axon compartment. Images were acquired every 2 seconds for over 1 hour. The fluorescein isolation time in the axon compartment was determined, using the same methodology as for the XONA 3D diffusion profiles. The fluorescein diffusion profile for the new device using Agarose gel is shown in **Figure 59** (**b**) and Matrigel in **Figure 59** (**c**). The data was normalised to the maximum intensity value.

There is a similar flow trend in both matrices, despite of the variability found. The variability in fluorescence intensity varied between each assay experiments. This likely caused by the way fluorescein travels along the channel and how the gel settles in each device. This variability corresponds to the large error bar range. This effect was also found in the work of *Taylor et al.* (Taylor *et al.*, 2003). Additionally, as Agarose is more viscous than Matrigel, the fluorescein travels slower (see **Appendix 6**).

In fact, fluorescein in Agarose starts is isolated in the axon compartment after 25 minutes, whereas the fluorescein in Matrigel is isolated for only 8 minutes in the axon compartment (which means that for 8 minutes there is no presence of fluorescein in the soma compartment). After which, there is a constant increase of fluorescein intensity in the axon compartment. The fluorescein has the same intensity value at the beginning of the experiment, because the fluorescein takes time to diffuse within the gel as it passes along the channel.

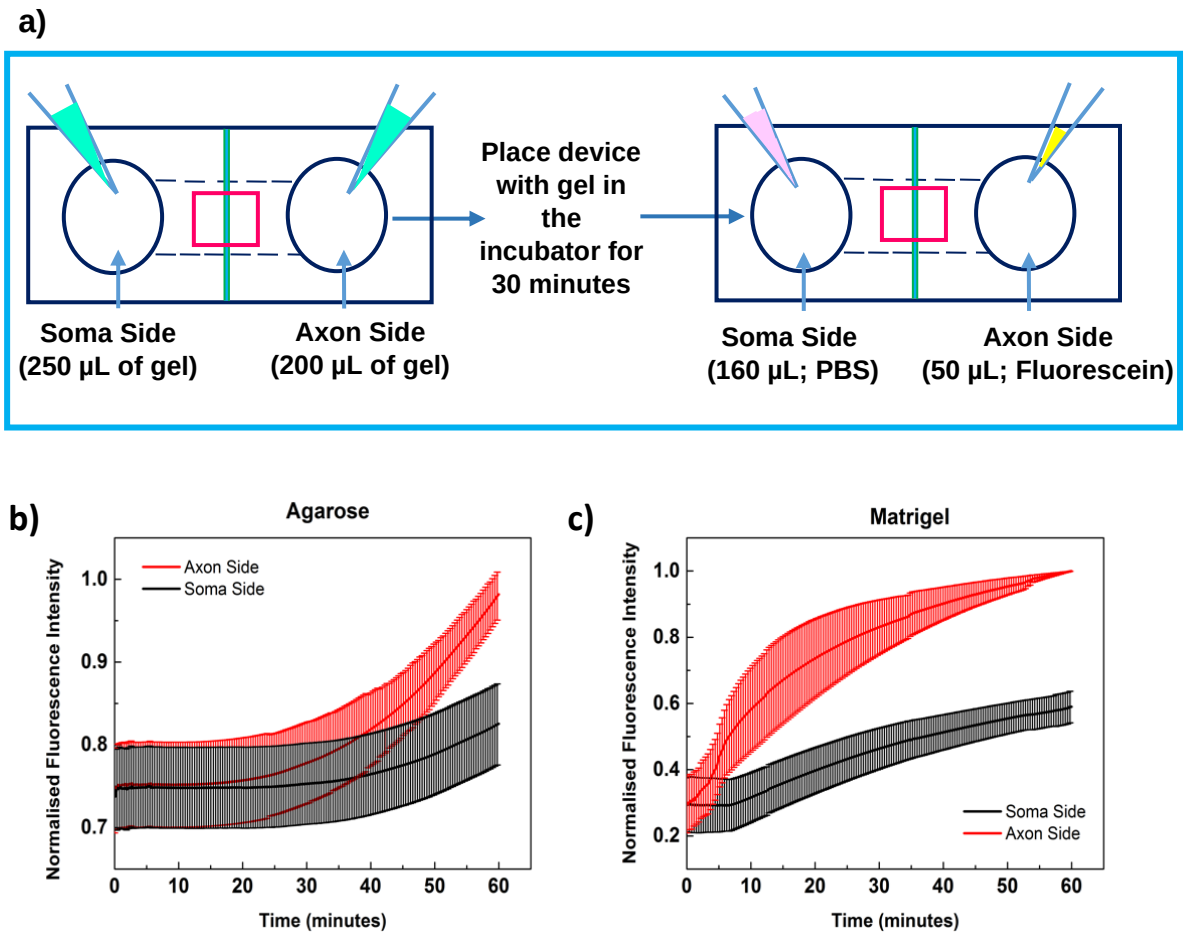


Figure 59 – 3D Diffusion profiles in the new cell culture device. **a**) For each device, the soma side was filled with 250 µl of pre-gel solution (0.5% Agarose or 5 mg/ml Matrigel), while the axon side had 200 µl of pre-gel solution. After forming a gel, 200 µl of PBS was added to the soma side and 50 µl of fluorescein (1 µM; 400 Da) to the axonal side. The squares in red represent the area of image acquisition. Diffusion profiles in the new device obtained for both the Agarose (**b**) and Matrigel (**c**) matrices. Fluorescence intensity values are plotted as a function of time. The images are taken every 2 seconds over a 1 hour period. The fluorescence intensity is normalised to the maximum intensity value, with each experiment repeated three times.

5.4 Discussion

A simple design for a new 3D cell culture device was proposed as proof of concept, aimed at isolating axons in a 3D cell configuration. This design consisted of developing a device with two compartments separated by a 3D physical barrier; allow only the passage of axons. One compartment contains neuron cell bodies (soma) and the other compartment contains axons. The 3D physical barrier consisted of a polycarbonate membrane (9 µm thick with 5 µm diameter pore size), allowing only the passage of axons and inhibiting the passage of cell bodies (soma).

As discussed in Chapter 2, axons have a diameter of 0.1 - 0.2 µm (the maximum achievable size for mice cortical neurons) and the cell bodies have a maximum size of 10 µm. The membrane separates the two compartments across the channel, which connects two 5 mm diameter reservoirs. The polycarbonate membrane is sealed to the PDMS blocks with silicone adhesive tape. The design of the new device integrates rapid prototyping techniques, such as soft-lithography and xurography, as a cheaper alternative to other expensive techniques such as photolithography. Moreover, devices fabricated using soft-lithography can also be mass produced, which would not be possible if a two-photon polymerisation technique was used. In this way, the device can be easily replicated in any lab, providing a quick and cost effective way to investigate simple biological experiments.

The proposed manufacturing strategies used to fabricate the complex channel hole by avoid material damage and ensure a smooth flat surfaces in the adhesion of the silicone tape to the PDMS. Forming the PDMS platform (PDMS-tape-membrane-tape-PDMS), which is sealed to the glass coverslip. In order to validate the biological experiments, there is a need to ensure that there is a good seal between the components.

The main aim of the device is to achieve axon isolation in three dimensions which replicates the *in vivo* environment. Providing an improved physiological approach for the investigation of biological mechanisms in pure axonal material. An example investigation is to evaluate the influence drugs have on axonal growth, where the drug is added to the axon compartment and are isolated without crossing to the soma side. From this to apply, diffusion profiles must be obtained to determine how long a molecule is held in isolation, without crossing to the opposing side.

The diffusion profiles in the new device were obtained for 3D conditions, where a fluorescent molecule is diffused thought a 3D biomatrix (hydrogel) by fluorescence microscopy. Besides offering a more realistic cell environment, 3D extracellular matrices provide improved fluidic resistance, minimising the flow along the channel. Hydrogels are commonly used in devices with simple geometric features, since they act as a resistance to fluidic diffusion (Marom *et al.*, 2015)(Saadi, Rhee and Lin, 2007)(Ma *et al.*, 2010)(Abhyankar *et al.*, 2008)(Haessler *et al.*, 2009)(Ahrens *et al.*, 2019).

Agarose has been widely used in diffusion based devices to determine the 3D gradient diffusion profiles (Haessler *et al.*, 2009)(Abhyankar *et al.*, 2008)(Mosadegh *et al.*, 2007), due its ease of use and low cost. Matrigel has had limited use in diffusion experiments due to its high costs.

Haessler et al. (Haessler *et al.*, 2009) reported a new device showing diffusion profiles for Agarose and the cell work in Collagen-Matrigel. Similar, *Abhyankar et al.* (Abhyankar *et al.*, 2008) reported diffusion profiles within Agarose and validated their device with cells contained within a Collagen matrix. Interestingly, the articles cited in this thesis present only simulation of 3D diffusion as a function of time without presenting the experimental 3D diffusion profile work. The fact that the experimental diffusion profiles are not reported can be due to the high level of variability in the results obtained. The only exception is the work of *Taylor et al.* (Taylor *et al.*, 2003), who have reported the experimental diffusion profiles, showing a similar variability as the results found in this work.

Unlike, the work of *Taylor et al.* (Taylor *et al.*, 2003), no solution was added during the 2D diffusion profile experiments. Accordingly to Taylor (Taylor *et al.*, 2003), after 4 hours of running the experiment, more fluorescein was added to avoid the decay in fluorescence intensity. The same approach was also used in the 2D XONA diffusion profiles of this work (**Figure 56**). The decay in intensity was avoided by using hydrogels (**Figure 57**), where a visible delay in the difference of fluorescein intensity between compartments, can be seen at the beginning of the experiment. Proving that the biomaterial acts as a physical barrier to the flow diffusion.

It was possible to isolate fluorescein in one side of the device for the length of the experiment, with only a small increase of 16.5% in fluorescence intensity in the XONA 3D diffusion profiles. The gradient generated is based on diffusion between the two compartments, which can be controlled by balancing the hydrostatic pressure. The volume difference allows the isolation of the fluorescein in the axon compartment. To increase the molecule time further development of the design is required. The proposed device was designed to facilitate axon isolation within a 3D neuronal network. It was successfully fabricated without fluid leakages, as shown by the validation results. After which cell fluidic isolation with two different hydrogels was investigated, with different biochemical and mechanical properties. Agarose and Matrigel were chosen as they are frequently used to mimic the ECM environments.

The fluidic isolation was characterised by recording the fluorescence intensity of fluorescein (400 Da; 1 µM) over time. A membrane separates the two compartments allowing fluidic isolation for at least 8 minutes in the Matrigel and 25 minutes in Agarose. The diffusion profile was achieved over a large distance of 7 mm for both hydrogels. The fluorescein diffusion profile can be delayed by using stiffer matrices and by increasing physical features (i.e. channels) in the design.

5.5 Conclusions

In this chapter, a novel platform suitable for conducting fast and cost-effective axon isolation, within a 3D environment, was successfully presented. A 3D physical barrier, isolating axons from their cell bodies, is achieved through a membrane. The polycarbonate membrane was used to achieve compartmentalisation within the device, acting as a physical barrier for the isolation of axons from the soma (cell bodies) and thus allowing localised cell stimulation. The key advantage of this approach is the simplicity of its manufacture using low-cost materials, with high reproducibility, portability and ease of manipulation. This approach is more attractive to researchers than using more expensive techniques, such as photolithography. Using biomaterials provides a 3D cell environment able to restrict flow by acting as a resistance to fluid diffusion. With the reservoirs facilitating the biomolecule diffusion, creating a gradient across the hydrogel.

This device is easy to operate and achieves isolation of molecules for up to 9 minutes in Matrigel (a more biocompatible matrix) and 25 minutes in Agarose (a more toxic cell matrix). By employing hydrostatic pressure, isolation of molecules in one compartment was demonstrated. Although this is insufficient time for axonal development experiments for gene targeting (which require 24 hours of fluidic isolation (Taylor *et al.*, 2005; Park *et al.*, 2006; Lucci *et al.*, 2020), there is enough time for stimulating the cells with calcium indicators for calcium imaging (Chung and Choo, 2010). Experiments of calcium imaging where performed within 3D neuronal cultures (O'Connor *et al.*, 2000; Wevers *et al.*, 2016; Grebenik *et al.*, 2020). These cell functional assays were performed in wells or in another devices or structures without axonal isolation. However, the cell response to calcium stimuli were observed after 2 minutes of loading the cells with a drug (O'Connor *et al.*, 2000; Grebenik *et al.*, 2020). In particular, *Wevers et al.* (Wevers *et al.*, 2016) showed the transmission of calcium response between two cells at 41 seconds and at 46 seconds using Fluoro-4 dye.

Chapter 6 Neuronal Culture Assessment within new 3D Cell culture devices

6.1 Introduction

The purpose of the chapter was to validate the functional performance of the device by confirming axonal isolation had been achieved in three dimensions. In **Chapter 4**, Matrigel neuron cultures results presented a similar percentage of live cells to the two-dimensional (2D) cell culture methods. This shows that Matrigel is able to host neurons, and as a hydrogel is capable of growing them in 3D. As discussed in **Chapter 5**, the focus of this project was to design and test a new 3D cell culture device to provide 3D axonal isolation, where neurons can grow within a more realistic cellular environment. This chapter presents the device validation to test the proof of concept by confirming the axonal isolation in three dimensions. Isolation of axons from neuron cell bodies is crucial in the study of understanding the growth mechanisms involved in the axon. The axons were isolated from the cell bodies between two compartments using a polycarbonate membrane containing a 5 µm pore diameter which allows only the passage of axons, and inhibiting the passage of cell bodies. The primary cortical neurons were plated on the soma compartment, after which the axons grew into the axon compartment. The assessment of axonal isolation was achieved by measuring the percentage of axonal growth and the growth rate.

6.2 3D Axonal Isolation

As mentioned on chapter 2, the axonal length measurements are only performed in 2D cell cultures within microfluidic devices, which allow the measurement of axons without the interference of cell bodies. In a normal dish, axons grow in every direction without guidance. Some researchers have employed the “stripe assay”, which consist in coating patterns onto the surfaces with repulsive (e.g. Fibronectin Leucine Rich Transmembrane Protein 2) and attractive (e.g. poly-L-lysine/laminin) molecules to control the axonal guidance (Vahidi *et al.*, 2008; Yamagishi *et al.*, 2016). However, fluidic isolation is not possible to achieve in these situations. Consequently, without fluidic isolation is not possible to study the local influence of a compound in a neuron cell’part (i.e. axon). Therefore, microfluidic devices were developed allowing a directed axonal growth and giving the possibility to have fluidic isolation, which provides the capability to investigate axonal events (e.g. influence of a miRNA in the axonal growth) (Taylor *et al.*, 2003, 2005).

The measurement of axonal length provides to researchers to determine if a compound (i.e. drug or miRNA) contribute for overexpression or inhibition of axonal growth (Dajas-bailador *et al.*, 2012, 2014b; Blizzard *et al.*, 2015; Briese *et al.*, 2015; Yao *et al.*, 2015; Zhang *et al.*, 2015; Reginensi *et al.*, 2015; Cosker *et al.*, 2016; Kneynsberg *et al.*, 2016; Yap *et al.*, 2017; Jia *et al.*, 2018; Ohtake *et al.*, 2018; Zheng *et al.*, 2019; Lucci *et al.*, 2020). Scientists measured the axonal growth after axons cross the microgrooves and evaluate the response of axonal growth to a compound by following the axonal growth under a microscope. For example, the Dajas-bailador et al. (Dajas-bailador *et al.*, 2012) overexpression of miRNA-9 leads to the decrease of the Map1b regulatory effects on axonal microtubules, which results in the reduction of axon length. Another example was reported by *Lucci et al.* (Lucci *et al.*, 2020), which found the overexpression of miRNA-26 regulates the levels of GSK3β in polarity and neural outgrowth resulting in an axonal length reduction. Therefore, by measuring the differences in axonal length, if there is a reduction or an increase in the axonal length, it is possible to investigate the effects of any treatment or any study on axons; such as investigating axonal transport (David *et al.*, 2012; Sundaramoorthy *et al.*, 2020), axonal regeneration (Ohtake *et al.*, 2018)(Taylor *et al.*, 2005) or axonal outgrowth (Lucci *et al.*, 2020)(Taylor *et al.*, 2009). For example, it was reported a protocol for the study of myelination with axonal isolation, where the electrical simulation promotes an increase in myelin formation. This result may be significant for pre-clinical studies (Yang *et al.*, 2012). The fact that axons are isolated, they are aligned and this alignment of axons allows accurate measurement of neurite length and ease of quantification.

Primary cortical neurons were platted on the soma compartment of the device. Initially, cells showed a spherical morphology at DIV 0. At this stage, the axon compartment does not show any cellular material. The neurons started to develop and extend their axons. The axons are the longer neurites that extended, a few of which crossed the membrane at DIV2, as seen in **Figure 60**. While in the XONA device, the axons cross to the axon compartment after DIV4 (Taylor *et al.*, 2005). A diagram of the 3D axonal growth is shown in **Figure 61** and **Figure 62**. The axons kept growing and crossing the membrane as shown in the **Figure 63** and in **Figure 64**, which clearly shows the isolation achieved between the axons and their cell bodies. The axons showed an average length of 447 µm for DIV4 in the new device. Morphologically, neurons growing in this device have not shown any difference from those growing in wells (seen in Chapter 4).

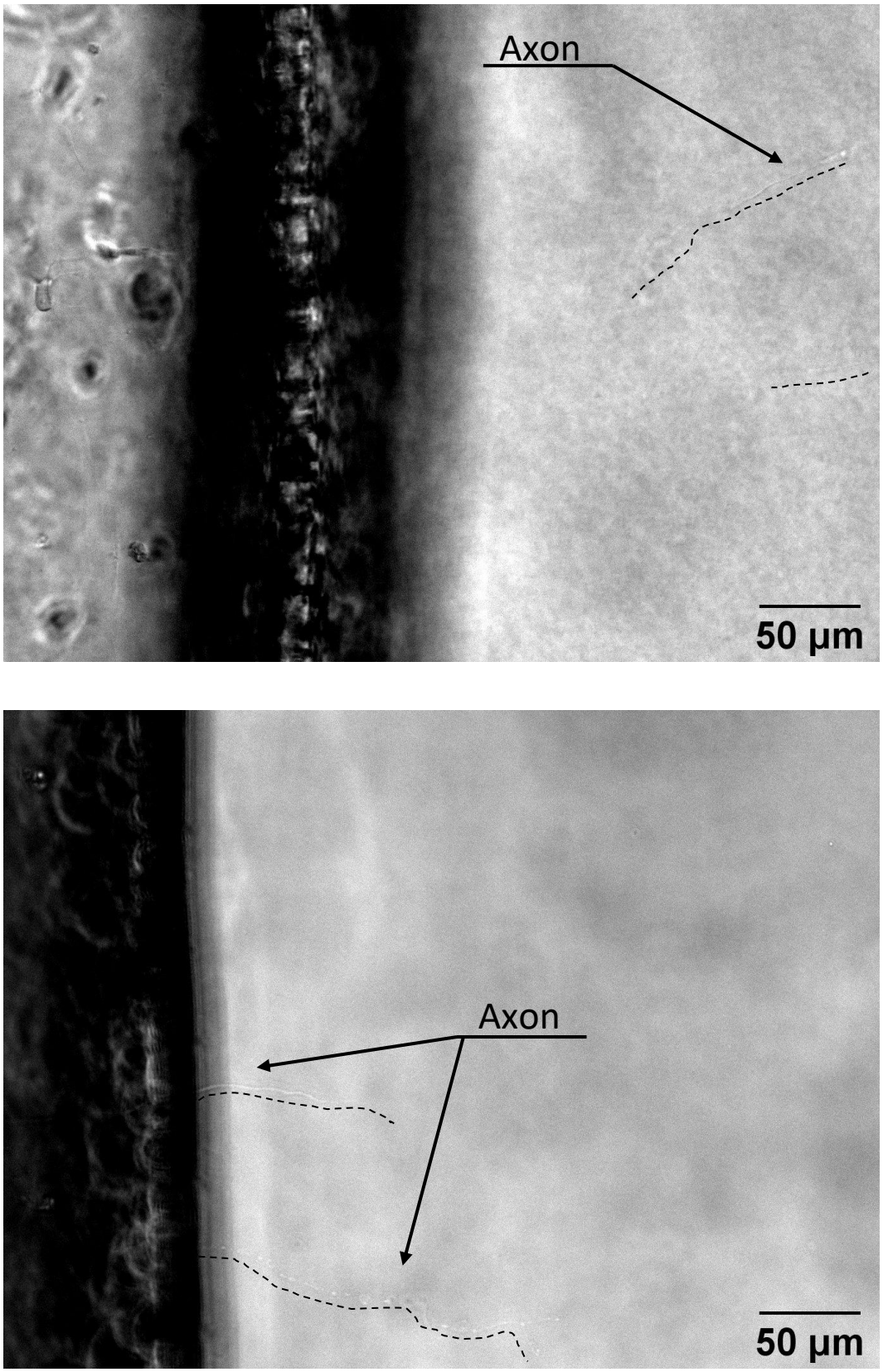


Figure 60 – Bright Field images of axons starting to cross the membrane at 2DIV.

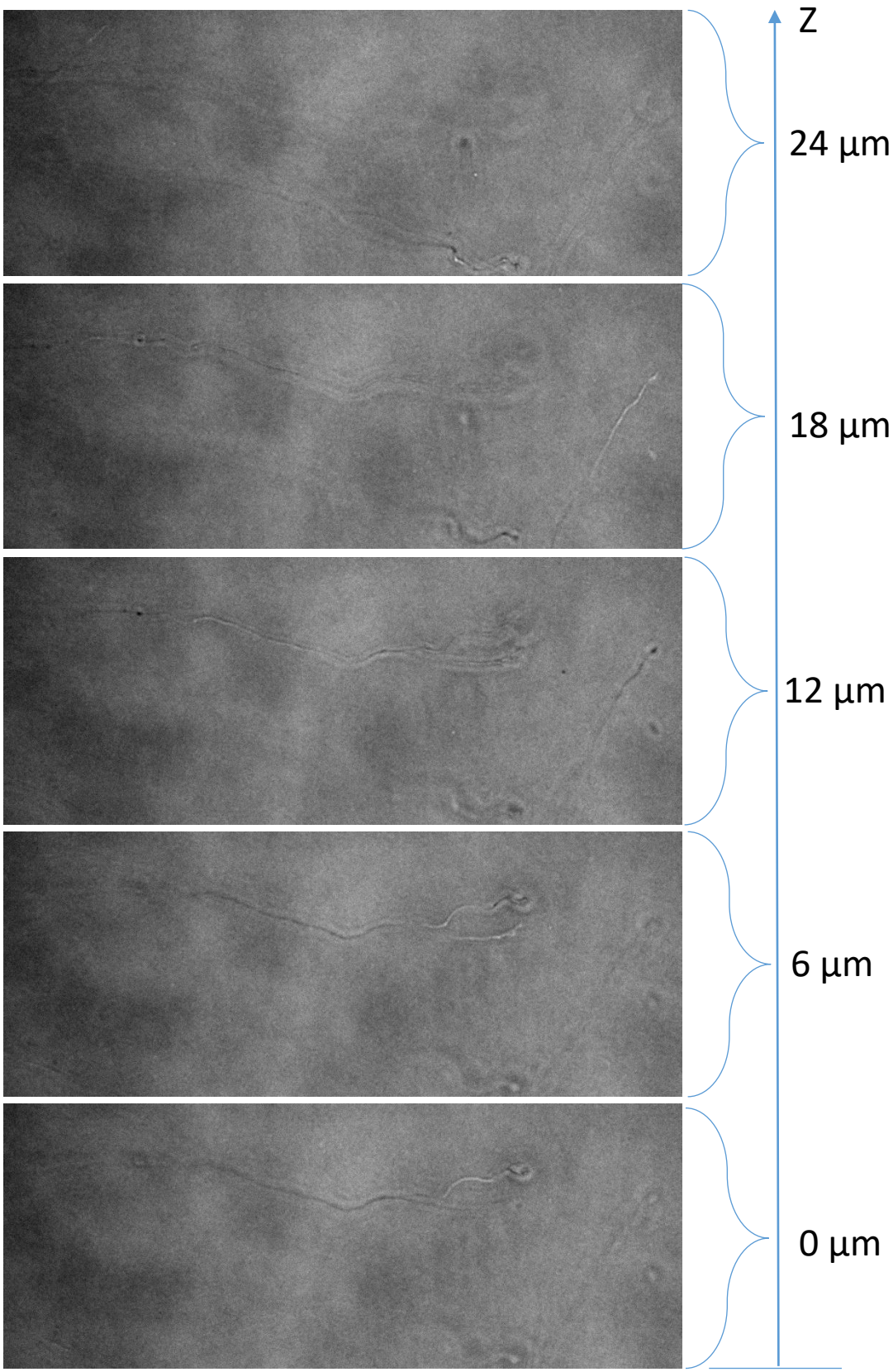


Figure 61 – Phase contrast images showing axons growing in 3D after 4 days in culture. Each frame is taken at a distance of 6 µm between each other in the z-stack.

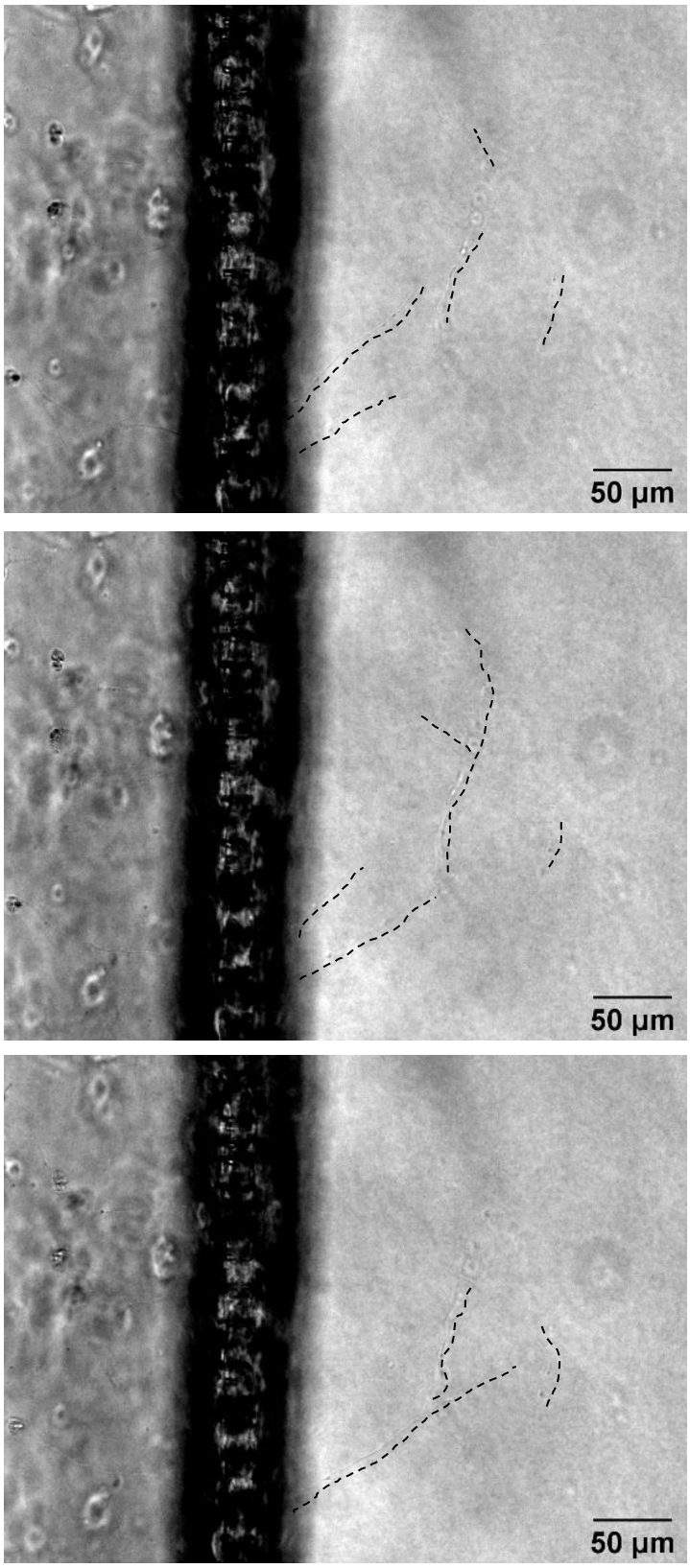


Figure 62 – Representative phase contrast image of isolated axons from their cell bodies in Matrigel within the new device at 4 days in culture. Each image is separated by 10 µm distance between each other in the stack. Higher magnification images are shown in **Appendix 7**.

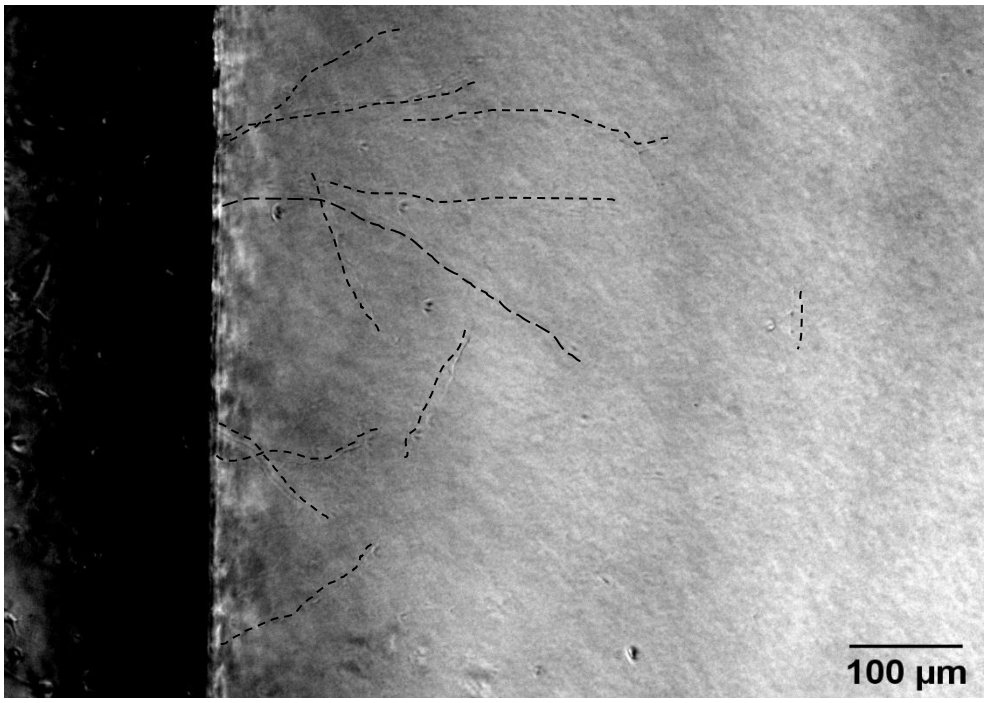


Figure 63 – Representative phase contrast image of axons crossing the membrane at DIV 4.

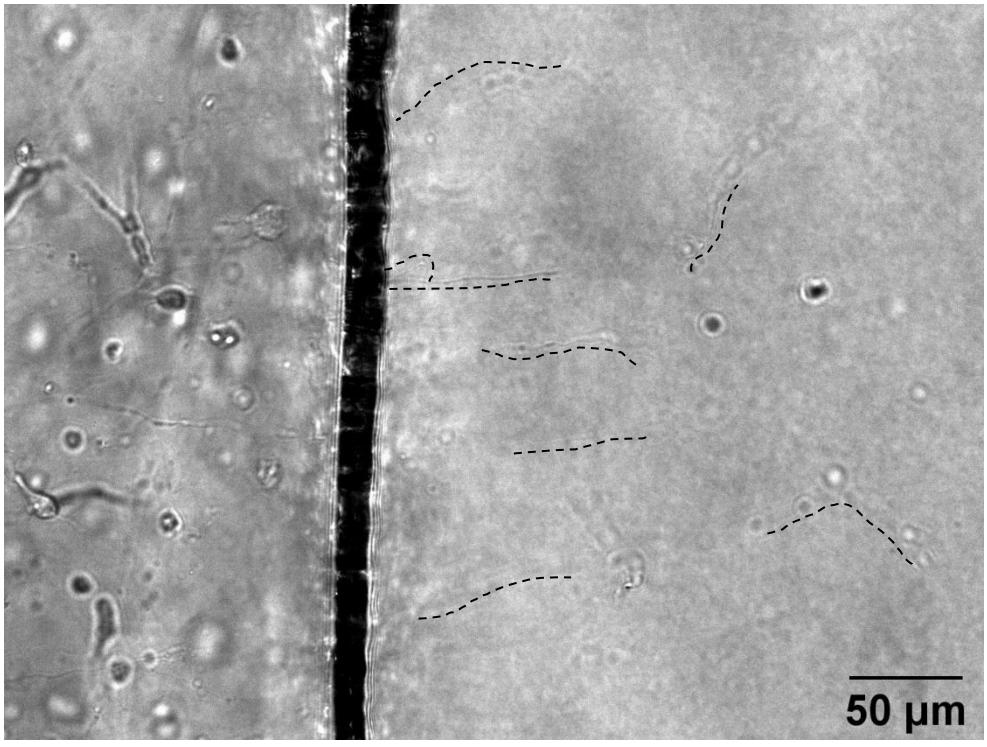


Figure 64 – Representative phase contrast image of axons crossing the membrane without cell bodies at DIV 4.

In the XONA device, the axons are only seen to cross the barrier after 4 DIV, in contrast to the neurons within the new device, which start to cross the membrane at 2 DIV. The percentage of axonal growth and the growth rate are shown for both the XONA and the new device, as shown in **Figure 65** and **Figure 66**, respectively.

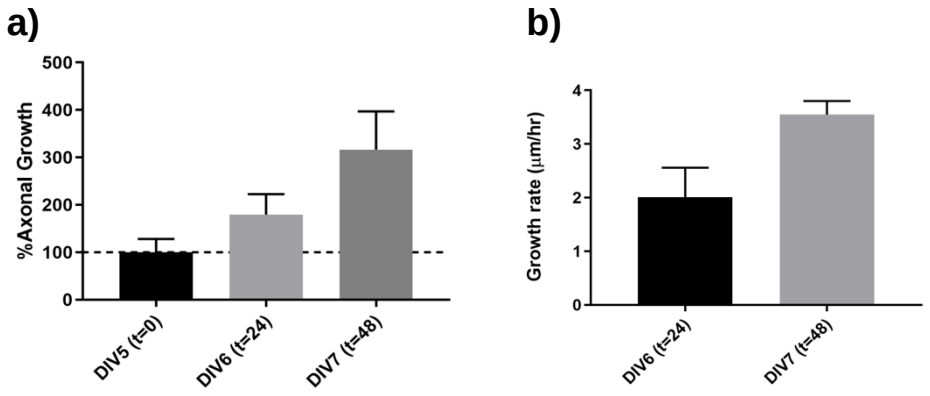


Figure 65 – Percentage of axonal growth at t=0 (**a**) and measurement of axonal growth rate (**b**) in the XONA device. The data was normalised to the mean value at DIV 5, with an axonal growth of 1.54 µM per day. The data show mean ± SEM (n=3).

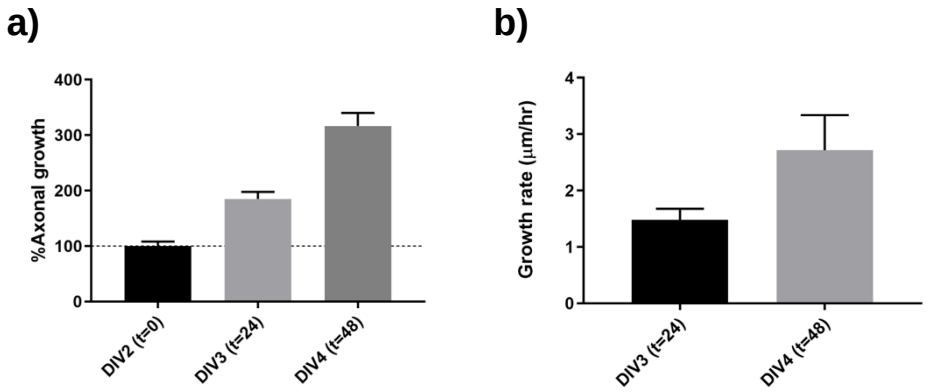


Figure 66 – Percentage of axonal growth at t=0 (**a**) and measurement of axonal growth rate (**b**) in the new 3D device. The data was normalised to the mean value at DIV2, with an axonal growth rate of 1.74 µM per day. The data shown mean ± SEM (n=3).

This experiment was performed until 5 DIV in the XONA device and 2 DIV in the new device, the time point at which the axons crossed the physical barrier. In the XONA device the neurons need to cross through 145 µm thickness (channels length) and 9 µm thickness (membrane) in the new device.

An axonal growth rate of 1.54 µm/hour was determined for the XONA device and an axonal growth rate of 1.74 µm/hour in the new 3D cell culture device. The higher growth rate is likely due to with the 3D environment provided by the Matrigel, which contains a high concentration of molecules promoting axon growth.

In 2D all axonal measurements performed after the axons cross the barrier, they have reported axonal growth rate under conditions, such as axotomy (Taylor *et al.*, 2005) or stimulation of miRNAs where axons, in control groups, extended themselves 24.5±0.58µm every 6h (Lucci *et al.*, 2020). However, a study comparing 3D with 2D neuronal cultures without axonal isolation reported that the length of neurites are longer in 3D than 2D (Chandrasekaran *et al.*, 2017). No one have never done axonal isolation in 3D, as explained on Chapter 2. The only article that study axonal alignment, to simulate axons isolated from their soma have not reported the axonal rate. Because they could not totally isolate the cell bodies from their axons, there was no fluidic isolation provided. Therefore, any compound added to axonal side would always pass to the soma side, hence fluidic isolation was not achieved in this study (Bang *et al.*, 2016). In this project fluidic isolation is achieve with cell bodies totally isolated from their axons.

Calcein AM was carefully added to the axonal side do not to disturb the 3D cell cultures, diffused in the matrix. A volume difference was applied to ensure that Calcein AM was isolated in one side, as seen in **Figure 67**, showing the axons on one side. This device is able to achieve axon isolation in a more realistic cell environment, providing analysis in pure axonal fraction as the device is made from a transparent material it is possible to label and observe the neurons under a fluorescence microscope.

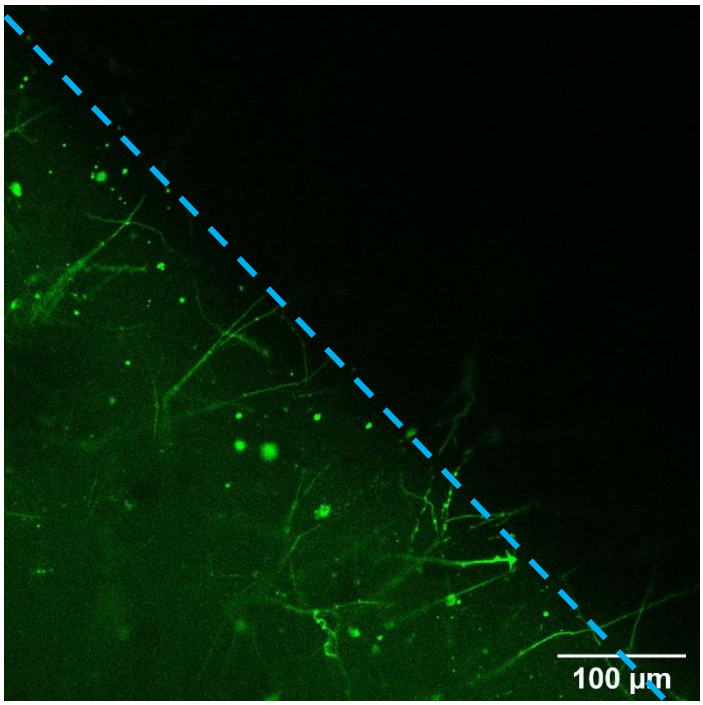


Figure 67 – Representative confocal image of axons isolated in the new 3D device at DIV 5. The line in blue represents a membrane.

6.3 Discussion

A new cell culture device is presented to provide axonal isolation in a 3D environment. The device is compatible with microscopy techniques, can be reused and it does not require any specific external equipment, only the use of micropipetting, offering easy usage for the generation of simple protocols.

The device consists of two PDMS chambers separated by a polycarbonate membrane, which provides isolation of axons within a 3D environment. Allowing cells to grow in a more realistic environment, enabling a better approximation to those processes occurring *in vivo*. By creating a more accurate representation of in vivo cellular behaviour model, a more viable correlation between cellular responses can be made. Offering the opportunities to further develop systems to be able to study neurons and obtain more realistic results in environments which are able to better mimic the brain cytoarchitecture. For example, the influence microRNA on axonal growth can be better investigated, as well as cell-cell interactions and communication with specific local targets.

The function of the novel new device is to allow 3D axonal isolation, able to better represent the 3D neuronal network cytoarchitecture. This has been successfully achieved as shown in **Figure 60–64**, **67**. These images provide experimental evidence for the demonstration that axons can be isolated from their cell bodies within the 3D matrix. Neurons are able to grow and are able to extend their axons, with axons shown to have crossed the membrane.

A good indication that cells are functional is the fact that they are alive and they are growing their axons, although further cell experiments would be needed to confirm it. As proof of concept, it was crucial to first demonstrate their viability and capacity for axonal growth, as proxi for normal neuronal differentiation. The fact that axons could be continually measured in three consecutive days is a good indicator that cells are functional across the whole experimental timeline.

After 2 days of culture the primary cortical neurons start to cross the membrane and axons are isolated in one compartment. The neurons within the device can be labelled and observed under a confocal microscope. Even with the use of a confocal microscope, fluorescent images need to be deconvoluted to remove the background fluorescence. This device allows the monitoring of neuron survival, neurite's growth in three-dimensions (3D) and axonal isolation (**Figure 67**). The measurements of axonal growth and growth rate in 3D cultures showed a higher growth compared to the 2D cultures. The higher growth rates in new devices is due to the 3D environment provided by the Matrigel, which contains a high concentration of molecules promoting the axonal growth and a more physiological presentation of growth cues.

Further cell functional assays would have added further confirmation to the functionality of the device, but this was beyond the scope of this project. Because of the time constraints of the project and costs, the focus centred on achieving isolation of axons in 3D within a 3D physical barrier.

6.4 Conclusions and Questions addressed

The aim of this chapter was to test and evaluate the novel device for axon isolation in a 3D to better represent a more realistic *in vivo* environment. This device has shown to be easily reproducible, fabricate and use as well as being cost effective to operate. The experimental work provides the recognition that neurons growing within matrigel mimic the neurons of an *in vivo* environment, achieving isolation for several minutes. This device allows neuron organisation and formation of a neuronal networks in a more physiological cell environment.

Overall, a new novel 3D cell culture device has been designed and validate, in achieving neuron and axons development in a 3D environment. Able to establish morphological phenotypes in a 3D matrix, adding value and relevance to the experimental analysis (i.e. cell-cell communication).

Chapter 7 Conclusions and Future work

This chapter summarises the aims and outcomes from this work and the overall conclusions. Recognising the potentials of the device as well as its limitations. Lastly, recommendations for future work are also given.

7.1 Conclusions

In chapter 2, I discussed how despite the notable advances in research that have been provided by 2D cell culture systems, even compartmentalised ones, they cannot model brain cytoarchitecture. In the case of 3D cell cultures, despite their early stages of development, can theoretically achieve this level of complexity in the future. In chapter 4, it is shown that Matrigel was proven to be a better matrix for growing neurons than Agarose. The neuron cell survival in Matrigel was as high as the survival rate in 2D culture methods. In chapter 5, it was proven that fluidic isolation for molecules of 400 Da size (fluorescein) can be achieved for over 8 minutes in Matrigel and 25 minutes in Agarose. Even if this means it is not possible to study axonal developmental processes over long periods, it is still possible to do Calcium Imaging in the cell body of cortical neurons grown in 3D after acute stimulation of the axon compartment. This could provide important information about neuronal activity in 3D and the similarities/differences with current 2D models. In chapter 6, I provide proof of concept for the achievement of axon isolation in 3D. This is an initial step towards the development of new cell culture devices that could improve studies into compartmentalised 3D culture conditions.

Although proof of concept was achieved, there is still room for improvement, for example, there are possible experimental approaches that can be used to increase the time of isolation of a molecule in one side. One is to use an alternative hydrogel with higher storage modulus, as suggested in chapter 5. This will increase the resistance of the molecule diffusion, while the other approach is to create a new design with resulting features to delay the fluid flow. The device can be developed using photolithography, a sandwich structure of multilayers of PDMS chips with the microgrooves would be sealed, layer-by-layer, creating a 3D physical barrier. Another suggestion for future work is the development of master moulds using micromachining.

In addition to the above mentioned advantages, this device is inexpensive, easy to fabricate and can be replicated as many times as the researchers wish. There is the potential to employ the same methodology in devices with more complex designs, which can increase the time a molecule can be fluidically isolated. Despite the great potential of the new 3D cell culture device, there are a few recognised drawbacks: Leakage, future work could be done by using an irreversible sealing between the PDMS and the glass coverslip; besides the advantages of culturing cells in 3D, there is still some restrictions in using this method in some research labs for the use of 3D cell cultures. One of the reasons for this is due to the use and variety of extracellular matrices which vary in their structures and composition. This leads to a lack of reproducible data for statistical analysis. Furthermore, it is not yet feasible for large-scale experiments due to higher costs and lack of reproducibility in hydrogels. As there is a lot of variability in the choice of materials and the cells type being used, leads to a diverse range of protocols. Hydrogel is difficult to view with imaging tools and still remains a challenge for imaging studies, which for 3D, will always have a fluorescence background. A solution to this is to do a deconvolution in the images using 3D software, such as Huygens or Volocity. However, in doing this cell structure information can be lost.

In the brain, neuron cells grow spatially distributed in three dimensions. This device combines axonal isolation and 3D cell environments, providing a more realistic physiological model which can improve the understating of development, and neurodegeneration models; cell behaviours and functions. Moreover 3D can improve research in drug testing; while allowing the more efficient co-culture different brain cell types, such as microglia and astrocytes. For example, culturing astrocytes or microglia in the axon side, in order to investigate their influence in axon function and or development/survival, as seen in **Figure 68**. This neuron laden Matrigel 3D cultures may also be useful for brain injury; neuron biology; and cell-cell communications studies in *in vitro* models: since neuron cultures can be maintained for short and long periods of time. Besides the fact that it is already complex to assess 3D neuron cultures, this model can be improved by culturing neurons with other cell types, providing a closer brain environment.

In order to obtain meaningful data for more advanced research proposals (i.e. neurodegeneration models), greater multidisciplinary work between engineers, physicists and biologists is required, which could then address the huge theoretical and practical challenges in developing novel compartmentalised 3D neuronal culture devices.

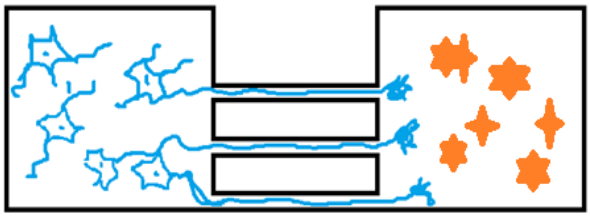


Figure 68 – Schematic representation of the new device with axons shown in blue and astrocytes shown in orange growing in a 3D environment.

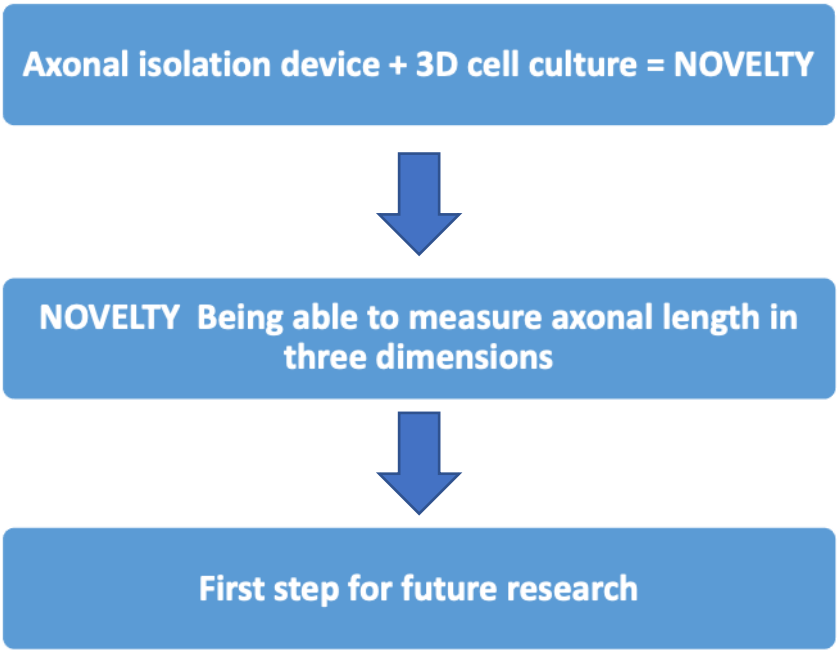


Figure 69 – The novelty of the project, as no one has never considered to isolate axons from cell bodies in 3D, with different Z-coordinates, which mimics the brain cytoarchitecture. As expressed above in neuronal development, the ability to isolate the axons allow to study the proteins that regulate the mechanisms for axonal regeneration.

Chapter 8 References

Abhyankar, V. V *et al.* (2008) 'A platform for assessing chemotactic migration within a spatiotemporally defined 3D microenvironment', *Biomedical Engineering*, 8(9), pp. 1507–1515. doi: 10.1039/b803533d.A.

Abhyankar, V. V, Lokuta, M. A. and Beebe, D. J. (2006) 'Characterization of a membrane-based gradient generator for use in cell-signaling studies', *Lab on a Chip*, 6(3), pp. 389–393. doi: 10.1039/b514133h.

Ahmed, E. M. (2015) 'Hydrogel : Preparation , characterization , and applications : A review', *Journal of Advanced Research*. Cairo University, 6(2), pp. 105–121. doi: 10.1016/j.jare.2013.07.006.

Ahrens, L. *et al.* (2019) 'Generation of 3D Soluble Signal Gradients in Cell-Laden Hydrogels Using Passive Diffusion', *Advanced Biosystems*, 3(1). doi: 10.1002/adbi.201800237.

Aiuto, L. D. *et al.* (2018) 'Generation of three-dimensional human neuronal cultures : application to modeling CNS viral infections', *Stem Cell Research and Therapy*. Stem Cell Research & Therapy, 9(1).

Al-ali, H. *et al.* (2017) 'In vitro models of axon regeneration', *Experimental Neurology*. Elsevier Inc., 287, pp. 423–434. doi: 10.1016/j.expneurol.2016.01.020.

Alhosseini, S. N. *et al.* (2019) 'Improved cellular response on functionalized polypyrrole interfaces', *Journal of Cellular Physiology*, 234(9), pp. 15279–15287. doi: 10.1002/jcp.28173.

Amor, S. *et al.* (2010) 'Inflammation in neurodegenerative diseases', *Immunology*, 129(2), pp. 154–169. doi: 10.1111/j.1365-2567.2009.03225.x.

Angeli, E. *et al.* (2011) 'DNA manipulation with elastomeric nanostructures fabricated by soft-moulding of a FIB-patterned stamp', *Lab on a Chip*, 11(15), pp. 2625–2629. doi: 10.1039/c1lc20411d.

Antoni, D. *et al.* (2015) 'Three-Dimensional Cell Culture : A Breakthrough in Vivo', *International Journal of Molecular Sciences*, 16(3), pp. 5517–5527. doi: 10.3390/ijms16035517.

Aregueta-robles, U. A. *et al.* (2018) 'Tailoring 3D Hydrogel Systems for Neuronal Encapsulation in Living Electrodes', pp. 273–287. doi: 10.1002/polb.24558.

Arimura, N. and Kaibuchi, K. (2007) 'Neuronal polarity : from extracellular signals to intracellular mechanisms', *Nature Reviews Neuroscience*, 8(3), pp. 194–205. doi: 10.1038/nrn2056.

Bae, H. *et al.* (2010) 'In Vitro Models for Biomechanical Studies of Neural Tissues', *Biomaterials As Stem Cell Niche*, 2(September 2010), pp. 153–171. doi: 10.1007/8415.

Balgude, A. P. *et al.* (2001) 'Agarose gel stiffness determines rate of DRG neurite extension in 3D cultures', *Biomaterials*, 22(10), pp. 1077–1084.

Bang, S. *et al.* (2016) 'Engineering-Aligned 3D Neural Circuit in Microfluidic Device', *Advanced Healthcare Materials*, 5(1), pp. 159–166. doi: 10.1002/adhm.201500397.

Barata, D., Van Blitterswijk, C. and Habibovic, P. (2016) 'High-throughput screening approaches and combinatorial development of biomaterials using microfluidics', *Acta Biomaterialia*. Acta Materialia Inc., 34, pp. 1–20. doi: 10.1016/j.actbio.2015.09.009.

Barnes, Anthony P and Polleux, F. (2009) 'Establishment of Axon-Dendrite Polarity in Developing Neurons', *Annual Review of Neuroscience*, 32(June 2009), pp. 347–381. doi: 10.1146/annurev.neuro.31.060407.125536.

Barnes, Anthony P. and Polleux, F. (2009) 'Establishment of Axon-Dendrite Polarity in Developing Neurons', *Annual Review of Neuroscience*, 32(1), pp. 347–381. doi: 10.1146/annurev.neuro.31.060407.125536.

Bartholomeusz, D. A., Boutté, R. W. and Andrade, J. D. (2005) 'Xurography : Rapid Prototyping of Microstructures Using a Cutting Plotter', *Journal of Microelectromechanical Systems*, 14(6), pp. 1364–1374.

Bayat, N. *et al.* (2016) 'Differentiation of Human Endometrial Stem Cells into Schwann Cells in Fibrin Hydrogel as 3D Culture', *Molecular Neurobiology*. Molecular Neurobiology, 53(10), pp. 7170–7176. doi: 10.1007/s12035-015-9574-7.

Becker, H. and Locascio, L. E. (2002) 'Polymer microfluidic devices', *Talanta*, 56(2), pp. 267–287.

Beckwith, K. S. *et al.* (2015) 'Tunable high aspect ratio polymer nanostructures for cell interfaces', *Nanoscale*. Royal Society of Chemistry, 7(18), pp. 8438–8450. doi: 10.1039/c5nr00674k.

Bellamkonda, R. and Bouche, N. (1995) 'Hydrogel-based three-dimensional matrix for neural cells', 29, pp. 663–671.

Bigler, R. L. *et al.* (2017) 'Messenger RNAs localized to distal projections of human stem cell derived neurons', *Scientific Reports*. Springer US, 7(1), pp. 1–11. doi: 10.1038/s41598-017-00676-w.

Biswas, A. *et al.* (2012) 'Advances in top – down and bottom – up surface nanofabrication : Techniques , applications & future prospects', *Advances in Colloid and Interface Science*. Elsevier B.V., 170(1–2), pp. 2–27. doi: 10.1016/j.cis.2011.11.001.

Blizzard, C. A. *et al.* (2015) 'Identifying the primary site of pathogenesis in amyotrophic lateral sclerosis – vulnerability of lower motor neurons to proximal excitotoxicity', *DMM Diases Models and Mechanisms*, 8(3), pp. 215–224. doi: 10.1242/dmm.018606.

Bomba-warczak, E. *et al.* (2016) 'Interneuronal Transfer and Distal Action of Tetanus Toxin and Botulinum Neurotoxins A and D in Central Neurons', *CellReports*. The Author(s), 16(7), pp. 1974–1987. doi: 10.1016/j.celrep.2016.06.104.

Bonneh-barkay, D. and Wiley, C. A. (2009) 'Brain Extracellular Matrix in Neurodegeneration', 19, pp. 573–585. doi: 10.1111/j.1750-3639.2008.00195.x.

Booth, R. and Kim, H. (2012) 'Characterization of a microfluidic in vitro model of the blood-brain barrier (mBBB)', *Lab Chip*, 12(10). doi: 10.1039/c2lc40094d.

Bosch, C. *et al.* (2015) 'FIB/SEM technology and high-throughput 3D reconstruction of dendritic spines and synapses in GFP-labeled adult-generated neurons', *Frontiers in Neuroanatomy*, 9(May). doi: 10.3389/fnana.2015.00060.

Bosi, S. *et al.* (2015a) 'From 2D to 3D: novel nanostructured scaffolds to

investigate signalling in reconstructed neuronal networks', *Scientific Reports*, 5. doi: 10.1038/srep09562.

Bosi, S. *et al.* (2015b) 'From 2D to 3D: novel nanostructured scaffolds to investigate signalling in reconstructed neuronal networks', *Scientific Reports*, 5, p. 9562. doi: 10.1038/srep09562.

Bourdillon, A. J. *et al.* (2000) 'X-ray imaging: applications to patterning and lithography', *Journal of Physics D: Applied Physics*, 33(12), pp. R103–R116.

Bourke, J. L. *et al.* (2018) 'Three-dimensional neural cultures produce networks that mimic native brain activity', *Journal of Tissue Engineering and Regenerative Medicine*, 12(2), pp. 490–493. doi: 10.1002/term.2508.

Boutin, M. E. and Hoffman-kim, D. (2015) 'Application and Assessment of Optical Clearing Methods for Imaging of Tissue-Engineered Neural Stem Cell Spheres', *Tissue Engineering - Part C: Methods*, 21(3), pp. 292–302.

Bozkurt, A. *et al.* (2007) 'In Vitro Assessment of Axonal Growth Using Dorsal Root Ganglia', 13(12). doi: 10.1089/ten.2007.0116.

Brandenberg, N. and Lutolf, M. P. (2017) 'Employing Microfluidic Devices to Induce Concentration Gradients', in *Biology and Engineering of Stem Cell Niches*. Elsevier Inc., pp. 431–444. doi: 10.1016/B978-0-12-802734-9.00027-5.

Briese, M. *et al.* (2015) 'Whole transcriptome profiling reveals the RNA content of motor axons', *Nucleic Acids Research*, 44(4). doi: 10.1093/nar/gkv1027.

Britland, S. *et al.* (1992) 'Micropatterning Proteins and Synthetic Peptides on Solid Supports: A Novel Application for Microelectronics Fabrication Technology', *Biotechnology Progress*, 8(2), pp. 155–160.

Broguiere, N. *et al.* (2019) 'Macroporous hydrogels derived from aqueous dynamic phase separation', *Biomaterials*. Elsevier, 200, pp. 56–65. doi: 10.1016/j.biomaterials.2019.01.047.

Broguiere, N., Isenmann, L. and Zenobi-wong, M. (2016) 'Biomaterials Novel enzymatically cross-linked hyaluronan hydrogels support the formation of 3D neuronal networks', *Biomaterials*. Elsevier Ltd, 99, pp. 47–55. doi: 10.1016/j.biomaterials.2016.04.036.

Budday, S., Steinmann, P. and Kuhl, E. (2015) 'Physical biology of human brain development', *Frontiers in Cellular Neuroscience*, 9(July), pp. 1–17. doi: 10.3389/fncel.2015.00257.

Burry, R. W. (2010) *Immunocytochemistry : A Practical Guide for Biomedical Research*. doi: 10.1007/978-1-4419-1304-3.

Calafate, S. *et al.* (2015) 'Synaptic Contacts Enhance Cell-to-Cell Tau Pathology Propagation', *Cell Reports*. The Authors, 11(8), pp. 1176–1183. doi: 10.1016/j.celrep.2015.04.043.

Caliari, S. R. and Burdick, J. A. (2016) 'A practical guide to hydrogels for cell culture.', *Nature methods*. Nature Publishing Group, 13(5), pp. 405–14. doi: 10.1038/nmeth.3839.

Campenot, R. B. (1977) 'Local control of neurite development by nerve growth factor', *Proc. NatI. Acad. Sci.*, 74(10), pp. 4516–4519.

Cao, Z. and He, W. (2010) 'Neuronal responses to simply prepared chitosan composite gels', in *Proceedings of the 2010 Biomedical Science and Engineering Conference, BSEC 2010: Biomedical Research and Analysis in Neuroscience, BRAiN*. IEEE, pp. 1–4. doi: 10.1109/BSEC.2010.5510825.

Carlson, A. L. *et al.* (2016) 'Generation and transplantation of reprogrammed human neurons in the brain using 3D microtopographic scaffolds', *Nature Communications*. Nature Publishing Group, 7(March), pp. 1–10. doi: 10.1038/ncomms10862.

Catoira, M. C. *et al.* (2019) 'Overview of natural hydrogels for regenerative medicine applications', *Journal of Materials Science: Materials in Medicine*. Springer US. doi: 10.1007/s10856-019-6318-7.

Chandrasekaran, A. *et al.* (2017) 'Comparison of 2D and 3D neural induction methods for the generation of neural progenitor cells from human induced pluripotent stem cells', *Stem Cell Research*. The Authors, 25, pp. 139–151. doi: 10.1016/j.scr.2017.10.010.

Charmet, J. *et al.* (2020) 'Low-Cost Microfabrication Tool Box', *Micromachines*, 11(2), pp. 1–16. doi: 10.3390/mi11020135.

Chen, A., Davis, B. H. and Chem, D. J. B. (1999) 'UV irradiation activates JNK and increases αI(I) collagen gene expression in rat hepaticStellate Cells', *Journal of Biological Chemistry*, 274(1), pp. 158–164.

Chen, C. S. *et al.* (1998) 'Micropatterned Surfaces for Control of Cell Shape, Position, and Function', *Biotechnology Progress*, 7938(98), pp. 356–363.

Cheng, M. Y. *et al.* (2017) 'A compartmentalized culture device for studying the axons of CNS neurons', *Analytical Biochemistry*. Elsevier Inc, 539, pp. 11–21. doi: 10.1016/j.ab.2017.09.013.

Chiu, H., Alqadah, A. and Chang, C. (2014) 'The role of microRNAs in regulating neuronal connectivity.', *Frontiers in cellular neuroscience*, 7(January), p. 283. doi: 10.3389/fncel.2013.00283.

Choi, S. H. *et al.* (2014) 'A three-dimensional human neural cell culture model of Alzheimer's disease', *Nature*. Nature Publishing Group, 515(7526), pp. 274–278. doi: 10.1038/nature13800.

Choi, S. H. *et al.* (2016) '3D culture models of Alzheimer's disease: a road map to a "cure-in-a-dish"', *Molecular Neurodegeneration*. Molecular Neurodegeneration, pp. 1–11. doi: 10.1186/s13024-016-0139-7.

Chou, S. Y. *et al.* (1995) 'Imprint of sub-25 nm vias and trenches in polymers', *Applied Physics Letters*, 67(1995), pp. 3114–3116. doi: 10.1063/1.114851.

Chung, B. G. and Choo, J. (2010) 'Microfluidic gradient platforms for controlling cellular behavior', *Electrophoresis*, 31(18), pp. 3014–3027. doi: 10.1002/elps.201000137.

Cichon, J. *et al.* (2020) 'Imaging neuronal activity in the central and peripheral nervous systems using new Thy1.2-GCaMP6 transgenic mouse lines', *Journal of Neuroscience Methods*. Elsevier, 334. doi: 10.1016/j.jneumeth.2019.108535.

Connor, S. M. O. *et al.* (2001) 'Survival and neurite outgrowth of rat cortical neurons in three- dimensional agarose and collagen gel matrices', *Neuroscience Letters*, 304(3), pp. 189–193.

Cosker, K. E. *et al.* (2016) 'The RNA-binding protein SFPQ orchestrates an RNA regulon to promote axon viability', *Nature Neuroscience*. Nature Publishing

Group, 19(5), pp. 690–696. doi: 10.1038/nn.4280.

Cosson, S. *et al.* (2014) 'Ultra-rapid prototyping of flexible, multi-layered microfluidic devices via razor writing', *Lab on a Chip*. Royal Society of Chemistry, 15(1), pp. 72–76. doi: 10.1039/C4LC00848K.

Crompton, K. E. *et al.* (2007) 'Polylysine-functionalised thermoresponsive chitosan hydrogel for neural tissue engineering', *Biomaterials*, 28(3), pp. 441–449. doi: 10.1016/j.biomaterials.2006.08.044.

Curanović, D. *et al.* (2009) 'Compartmented Neuron Cultures for Directional Infection by Alpha Herpesviruses', *Current Protocols in Cell Biology*. doi: 10.1002/0471143030.cb2604s43.Compartmented.

Dajas-bailador, F. *et al.* (2012) 'microRNA-9 regulates axon extension and branching by targeting Map1b in mouse cortical neurons', *Nature Neuroscience*, 15(5), pp. 697–699. doi: 10.1038/nn.3082.

Dajas-bailador, F. *et al.* (2014a) 'Regulation of axon growth by the JIP1 – AKT axis', *Journal of Cell Science*, 127(1), pp. 230–239. doi: 10.1242/jcs.137208.

Dajas-bailador, F. *et al.* (2014b) 'Regulation of axon growth by the JIP1 – AKT axis', *Jurnal of Cell Science*, 127(1), pp. 230–239. doi: 10.1242/jcs.137208.

David, A. T. *et al.* (2012) 'A herpes simplex virus 1 (McKrae) mutant lacking the glycoprotein K gene is unable to infect via neuronal axons and egress from neuronal cell bodies.', *mBio*, 3(4), pp. 1–10. doi: 10.1128/mBio.00144-12.

Debanne, D. (2004) 'Information processing in the axon', *Nature Reviews Neuroscience*, 5(4), pp. 304–316. doi: 10.1038/nrn1397.

Deku, F. *et al.* (2018) 'Amorphous silicon carbide ultramicroelectrode arrays for neural stimulation and recording', *Journal of Neural Engineering*. IOP Publishing, 15(1).

Deng, J. *et al.* (2016) 'Acceleration of e-beam lithography by minimized resist exposure for large scale nanofabrication', *Microelectronic Engineering*. Elsevier B.V., 166, pp. 31–38. doi: 10.1016/j.mee.2016.09.002.

Dermutz, H. *et al.* (2017) 'Paper-based patterned 3D neural cultures as a tool to study network activity on multielectrode arrays', *RSC Advances*, 7(62), pp.

39359–39371. doi: 10.1039/c7ra00971b.

Deveci, A., Hasna, J. and Bouron, A. (2020) ‘Inhibition of store-operated calcium channels by N-arachidonoyl glycine (NAGly): no evidence for the involvement of lipid-sensing G protein coupled receptors’, *Scientific Reports*. Springer US, 10(1), pp. 1–10. doi: 10.1038/s41598-020-59565-4.

Dewitt, D. D. *et al.* (2009) ‘Collagen I-Matrigel Scaffolds for Enhanced Schwann Cell’, *Tissue Engineering - Part A*, 15(10), pp. 2785–2793.

Diefenbach, R. J. *et al.* (2016) ‘The Basic Domain of Herpes Simplex Virus 1 pUS9 Recruits Kinesin- 1 To Facilitate Egress from Neurons’, *Journal of virology*, 90(4), pp. 2102–2111. doi: 10.1128/JVI.03041-15.Editor.

Dillon, G. P. *et al.* (1998) ‘The influence of physical structure and charge on neurite extension in a 3D hydrogel scaffold’, *Journal of biomaterials science. Polymer edition*, 9(10), pp. 1049–1069. doi: 10.1163/156856298X00325.

Dixon, A. R. and Philbert, M. A. (2015) ‘Morphometric assessment of toxicant induced neuronal degeneration in full and restricted contact co-cultures of embryonic cortical rat neurons and astrocytes: Using m-Dinitrobezene as a model neurotoxicant’, *Toxicology in Vitro*. Elsevier Ltd, 29(3), pp. 564–574. doi: 10.1016/j.tiv.2014.12.015.

Dohner, K. *et al.* (2018) ‘Importin α1 is required for nuclear import of herpes simplex virus proteins and capsid assembly in fibroblasts and neurons’, *PLoS Pathogens*, 14(1), pp. 1–35.

Dotti, C. G., Sullivan, C. A. and Banker, G. A. (1988) ‘The Establishment of Polarity by Hippocampal Neurons in Culture’, *Journal of Neuroscience*, 8(4), pp. 41454–1468.

Doyle, A. D. (2016) ‘Generation of 3D collagen gels with controlled, diverse architectures’, *Current Protocols in Cell Biology*, 2016, pp. 10.20.1-10.20.16. doi: 10.1002/cpcb.9.Generation.

Duan, C., Wang, W. and Xie, Q. (2013) *Review article: Fabrication of nanofluidic devices*, *Biomicrofluidics*. doi: 10.1063/1.4794973.

Duval, K. *et al.* (2017) ‘Modeling Physiological Events in 2D vs. 3D Cell Culture’,

Physiology, 32(4), pp. 266–277. doi: 10.1152/physiol.00036.2016.

Edelstein, A. *et al.* (2010) 'Computer control of microscopes using manager', *Current Protocols in Molecular Biology*, SUPPL.92(October 2010), pp. 14.20.1-14.20.17.

Edgar, J. M., Robinson, M. and Willerth, S. M. (2017) 'Fibrin Hydrogels Induce Mixed Dorsal / Ventral Spinal Neuron Identities During Differentiation of Human Induced Pluripotent Stem Cells V5Z1M9', *Acta Biomaterialia*. doi: 10.1016/j.actbio.2017.01.040.

Edmondson, R. *et al.* (2014) 'Three-Dimensional Cell Culture Systems and Their Applications in Drug Discovery and Cell-Based Biosensors', *Assay and Drug Development Technologies*, 12(4), pp. 207–218. doi: 10.1089/adt.2014.573.

Eitan, E. *et al.* (2016) 'Probing extracellular Sonic hedgehog in neurons', *Biology Open*, 5(8), pp. 1086–1092. doi: 10.1242/bio.019422.

Engstrom, D. S. *et al.* (2017) 'Additive nanomanufacturing – A review', *Journal of Materials Research*, 29(17). doi: 10.1557/jmr.2014.159.

Evans, M. G., Al-Shakli, A. and Chari, D. M. (2020) 'Electrophysiological properties of neurons grown on soft polymer scaffolds reveal the potential to develop neuromimetic culture environments', *Integrative Biology*, 11(11), pp. 395–403. doi: 10.1093/intbio/zyz033.

Fahmy, A. *et al.* (2015) 'Poly(vinyl alcohol)-hyaluronic Acid Membranes for Wound Dressing Applications: Synthesis and and in vitro Bio-Evaluations', 26(7), pp. 1466–1474.

Fan, R. *et al.* (2016) 'Bio-printing cell-laden Matrigel-agarose constructs', *Journal of Biomaterials Applications*, 31(5), pp. 684–692. doi: 10.1017/S0950268814002131.Tuberculosis.

Fan, Rong *et al.* (2016) 'Bio-printing cell-laden Matrigel – agarose constructs', 31(5), pp. 684–692. doi: 10.1177/0885328216669238.

Fang, Y. and Eglen, R. M. (2017) 'Three-Dimensional Cell Cultures in Drug Discovery and Development', *SLAS Discovery*, 22(5), pp. 456–472. doi: 10.1177/1087057117696795.

Fantuzzo, J. A. *et al.* (2019) 'Compartmentalized devices as tools for investigation of human brain network dynamics', *Development Dynamics*, 248(1), pp. 65–77. doi: 10.1002/dvdy.24665.Compartmentalized.

Faustino, V. *et al.* (2016) 'Biomedical microfluidic devices by using low-cost fabrication techniques: A review', *Journal of Biomechanics*, 49(11), pp. 2280–2292. doi: 10.1016/j.jbiomech.2015.11.031.

Frantz, C. *et al.* (2010) 'The extracellular matrix at a glance', 2010, pp. 4195–4200. doi: 10.1242/jcs.023820.

Frega, M. *et al.* (2014a) 'Network dynamics of 3D engineered neuronal cultures : a new experimental model for in-vitro electrophysiology', *Scientific Reports*, 4. doi: 10.1038/srep05489.

Frega, M. *et al.* (2014b) 'Network dynamics of 3D engineered neuronal cultures: a new experimental model for in-vitro electrophysiology.', *Scientific reports*, 4, p. 5489. doi: 10.1038/srep05489.

Freundt, E. C. *et al.* (2012) 'Neuron-to-neuron transmission of α-synuclein fibrils through axonal transport', *Annals of Neurology*, 72(4), pp. 517–524. doi: 10.1002/ana.23747.

Frimat, J. *et al.* (2015) 'Advances in 3D neuronal cell culture', *Journal of Vacuum Science and Technology B: Nanotechnology and Microelectronics*, 33(6). doi: 10.1116/1.4931636.

Gallo, V. and Deneen, B. (2014) 'Glial Development: The Crossroads of Regeneration and Repair in the CNS', *Neuron*, 83(2), pp. 283–308. doi: 10.1016/j.neuron.2014.06.010.Glial.

Gao, D. *et al.* (2010) 'A microfluidic approach for anticancer drug analysis based on hydrogel encapsulated tumor cells', *Analytica Chimica Acta*. Elsevier B.V., 665(1), pp. 7–14. doi: 10.1016/j.aca.2010.03.015.

Gao, Y. *et al.* (2016) 'Functional imaging of neuron–astrocyte interactions in a compartmentalized microfluidic device', *Microsystems & Nanoengineering*, 2. doi: 10.1038/micronano.2015.45.

Garcez, P. P., Guillemot, F. and Dajas-bailador, F. (2017) 'Study of miRNA

function in the developing axons of mouse cortical neurons: Use of compartmentalized microfluidic chambers and in utero electroporation', *Neuromethods*, 128, pp. 59–71. doi: 10.1007/7657.

Gargotti, M. *et al.* (2018) 'Comparative studies of cellular viability levels on 2D and 3D in vitro culture matrices', *Cytotechnology*. Springer Netherlands, 70(1), pp. 261–273. doi: 10.1007/s10616-017-0139-7.

Gasperini, L., Mano, F. and Reis, R. L. (2014) 'Natural polymers for the microencapsulation of cells', *Journal of the Royal Society Interface*, 11(100).

Geckil, H. *et al.* (2011) 'Engineering hydrogels as extracellular matrix mimics', *Nanomedicine (London, England)*, 5(3), pp. 469–484. doi: 10.2217/nnm.10.12.Engineering.

Gervasi, N. M. *et al.* (2016) 'The local expression and trafficking of tyrosine hydroxylase mRNA in the axons of sympathetic neurons', *RNA*, 22(6), pp. 883–895. doi: 10.1261/rna.053272.115.agent.

Gierak, J., Madouri, A. and Biance, A. L. (2007) 'Sub-5 nm FIB direct patterning of nanodevices', *Microelectronic Engineering*, 84(5–8), pp. 779–783. doi: 10.1016/j.mee.2007.01.059.

Gil, V. and del Río, J. A. (2012) 'Analysis of axonal growth and cell migration in 3D hydrogel cultures of embryonic mouse CNS tissue.', *Nature Protocols*, 7(2), pp. 268–280. doi: 10.1038/nprot.2011.445.

Gomez, N., Chen, S. and Schmidt, C. E. (2007) 'Polarization of hippocampal neurons with competitive surface stimuli : contact guidance cues are preferred over chemical ligands', *Journal of the Royal Society Interface*, 4(13), pp. 223–233. doi: 10.1098/rsif.2006.0171.

Graf, B. W. and Boppart, S. A. (2010) 'Imaging and Analysis of Three-Dimensional Cell Culture Models', *Methods in molecular biology*, 591, pp. 211–227. doi: 10.1007/978-1-60761-404-3.

Grebenik, E. A. *et al.* (2020) 'Chitosan-g-oligo(L,L-lactide) copolymer hydrogel for nervous tissue regeneration in glutamate excitotoxicity: In vitro feasibility evaluation', *Biomedical Materials (Bristol)*, 15(1).

Greer, J. *et al.* (2007) 'Comparison of glass etching to xurography prototyping of microfluidic channels for DNA melting analysis', *Journal of Micromechanics and Microengineering*, 17(12), pp. 2407–2413. doi: 10.1088/0960-1317/17/12/003.

Grienberger, C. and Konnerth, A. (2012) 'Imaging Calcium in Neurons', *Neuron*. Elsevier Inc., 73(5), pp. 862–885. doi: 10.1016/j.neuron.2012.02.011.

Griffith, L. G. and Swartz, M. A. (2006) 'Capturing complex 3D tissue physiology in vitro.', *Nature reviews Molecular cell biology*, 7(3), pp. 211–224. doi: 10.1038/nrm1858.

Gullberg, D. and Ekblom, P. (1995) 'Extracellular matrix and its receptors during development', 854, pp. 845–854.

Gumy, L. F. *et al.* (2011) 'Transcriptome analysis of embryonic and adult sensory axons reveals changes in mRNA repertoire localization', *RNA (New York, N.Y.)*, 17(1), pp. 85–98. doi: 10.1261/rna.2386111.

Guo, B. L. J. (2007) 'Nanoimprint Lithography : Methods and Material Requirements', *Advanced Materials*, 19(4), pp. 495–513. doi: 10.1002/adma.200600882.

Guo, L. J. (2004) 'Recent progress in nanoimprint technology and its applications', *JOURNAL OF PHYSICS D: APPLIED PHYSICS*, 37. doi: 10.1088/0022-3727/37/11/R01.

Haessler, U. *et al.* (2009) 'An agarose-based microfluidic platform with a gradient buffer for 3D chemotaxis studies', *Biomedical Microdevices*, 11(4), pp. 827–835. doi: 10.1007/s10544-009-9299-3.

Haggerty, A. E., Marlow, M. M. and Oudega, M. (2016) 'Extracellular matrix components as therapeutics for spinal cord injury', *Neuroscience Letters*. Elsevier Ireland Ltd. doi: 10.1016/j.neulet.2016.09.053.

Halldorsson, S. *et al.* (2015) 'Advantages and challenges of microfluidic cell culture in polydimethylsiloxane devices', *Biosensors and Bioelectronics*. Elsevier, 63, pp. 218–231. doi: 10.1016/j.bios.2014.07.029.

Han, S. *et al.* (2012) 'Three-dimensional extracellular matrix-mediated neural stem cell differentiation in a microfluidic device', *Lab on a Chip*, 12(13), p. 2305.

doi: 10.1039/c2lc21285d.

Harrison, R. G. (1907) ‘Observations on the living developing nerve fiber’, *The Anatomical Record*, pp. 116–128.

Hassanzadeh-barforoushi, A. *et al.* (2016) ‘A rapid co-culture stamping device for studying intercellular communication’, *Scientific*. Nature Publishing Group, 6, pp. 1–11. doi: 10.1038/srep35618.

He, J. *et al.* (2013) ‘Autonomous self-healing of poly(acrylic acid) hydrogels induced by the migration of ferric ions’, *Polymer Chemistry*, 4(17). doi: 10.1039/C3PY00692A.

Hellman, A. N. *et al.* (2010) ‘Examination of axonal injury and regeneration in micropatterned neuronal culture using pulsed laser microbeam dissection’, *Lab on a Chip*, 10(16), pp. 2083–2092. doi: 10.1039/B927153H.

Hellwig, C. *et al.* (2018) ‘Culture of human neurospheres in 3D scaffolds for developmental neurotoxicity testing’, *Toxicology in Vitro*. Elsevier, 52(October 2018), pp. 106–115. doi: 10.1016/j.tiv.2018.06.002.

Hengst, U. *et al.* (2009) ‘Axonal elongation triggered by stimulus-induced local translation of a polarity complex protein’, *Nature Cell Biology*, 11(8), pp. 1024–1030. doi: 10.1038/ncb1916.

Hengst, U. *et al.* (2016) ‘Axonal elongation triggered by stimulus-induced local translation of a polarity complex protein’, *Nat Cell Biol.*, 21(3), pp. 193–201. doi: 10.1016/j.molmed.2014.11.008.Mitochondria.

Hilton, B. J. and Bradke, F. (2017) ‘Can injured adult CNS axons regenerate by recapitulating development?’, *Development (Cambridge)*, 144(19), pp. 3417–3429. doi: 10.1242/dev.148312.

Hoare, T. R. and Kohane, D. S. (2008) ‘Hydrogels in drug delivery: Progress and challenges’, *Polymer*. Elsevier Ltd, 49(8), pp. 1993–2007. doi: 10.1016/j.polymer.2008.01.027.

Horn-ranney, E. L. *et al.* (2013) ‘Structural and molecular micropatterning of dual hydrogel constructs for neural growth models using photochemical strategies’, *Biomedical microdevices*, 15(1), pp. 49–61. doi: 10.1007/s10544-012-9687-y.

Howard, L. *et al.* (2013) 'ProNGF promotes neurite growth from a subset of NGF-dependent neurons by a p75NTR-dependent mechanism.', *Development (Cambridge, England)*, 140(10), pp. 2108–17. doi: 10.1242/dev.085266.

Hu, L. *et al.* (2016) 'An on-demand gas segmented flow generator with high spatiotemporal resolution for in vivo analysis of neuronal response in C . elegans', *Lab on a Chip*. Royal Society of Chemistry, 16, pp. 4020–4027. doi: 10.1039/C6LC00948D.

Hughes, C. S., Postovit, L. M. and Lajoie, G. A. (2010) 'Matrigel : A complex protein mixture required for optimal growth of cell culture', *Proteomics*, 10(9), pp. 1886–1890. doi: 10.1002/pmic.200900758.

Huo, D. and Cheng, K. (2013) *Micro-Cutting: Fundamentals and Applications*. Wiley.

Hur, M. *et al.* (2011) 'Destination of the C4 Component of the Prefixed Brachial Plexus', *Clinical Anatomy*, 24(6), pp. 717–720. doi: 10.1002/ca.21161.

Hussain, R. *et al.* (2018) 'Neurodegenerative Diseases: Regenerative Mechanisms and Novel Therapeutic Approaches', *Brain Sciences*, 8(9). doi: 10.3390/brainsci8090177.

Immich, A. P. S. *et al.* (2017) 'Improved tympanic membrane regeneration after myringoplastic surgery using an artificial biograft A.P.S.', *Materials Science and Engineering C*. Elsevier B.V., 73, pp. 48–58. doi: 10.1016/j.msec.2016.12.007.

Islam, M., Natu, R. and Martinez, R. (2015) 'A study on the limits and advantages of using a desktop cutter plotter to fabricate microfluidic networks', *Microfluidics and Nanofluidics*. Springer Berlin Heidelberg, 19(4), pp. 973–985. doi: 10.1007/s10404-015-1626-9.

Ito, T. and Okazaki, S. (2000) 'Pushing the limits of lithography', *Nature*, 406(6799), pp. 1027–1031.

Ivana, Š. *et al.* (2019) 'A novel low molecular weight nanocomposite hydrogel formulation for intra-tumoural delivery of anti-cancer drugs', 565(April), pp. 151–161. doi: 10.1016/j.ijpharm.2019.04.070.

Iwashita, M. *et al.* (2019) 'Brain-stiffness-mimicking tilapia collagen gel promotes

the induction of dorsal cortical neurons from human pluripotent stem cells', *Scientific Reports*. Springer US, 9(1). doi: 10.1038/s41598-018-38395-5.

Jacchetti, E. *et al.* (2014) 'Microstructured polydimethylsiloxane membranes for peripheral nerve regeneration', *MICROELECTRONIC ENGINEERING*. Elsevier B.V., 124(60), pp. 26–29. doi: 10.1016/j.mee.2014.04.014.

Jang, J. M. *et al.* (2015) 'Engineering Controllable Architecture in Matrigel for 3D Cell Alignment', *ACS Applied Materials and Interfaces*, 7(4), pp. 2183–2188. doi: 10.1021/am508292t.

Jensen, G., Morrill, C. and Huang, Y. (2018) '3D tissue engineering , an emerging technique for pharmaceutical research', *Acta Pharmaceutica Sinica B*. Elsevier B.V., 8(5), pp. 756–766. doi: 10.1016/j.apsb.2018.03.006.

Jia, L. *et al.* (2016) 'MicroRNA 146a locally mediates distal axonal growth of dorsal root ganglia neurons under high glucose and sildenafil conditions', *Neuroscience*, 329, pp. 43–53. doi: 10.1016/j.neuroscience.2016.05.005.MicroRNA.

Jia, L. *et al.* (2018) 'Exosomes derived from high-glucose – stimulated Schwann cells promote development of diabetic peripheral neuropathy', *FASEB journal*, 32(12), pp. 6911–6922. doi: 10.1096/fj.201800597R.

Jocher, G. *et al.* (2018) 'Microfluidics of Small-Population Neurons Allows for a Precise Quantification of the Peripheral Axonal Growth State', *Frontiers in cellular neuroscience*, 12(June), pp. 1–12. doi: 10.3389/fncel.2018.00166.

Johnson, L. *et al.* (2018) 'Low Molecular Weight Nucleoside Gelators: A Platform for Protein Aggregation Inhibition', *Molecular Pharmaceutics*. American Chemical Society, 16, pp. 462–467. doi: 10.1021/acs.molpharmaceut.8b01013.

Jokinen, V. *et al.* (2013) 'A microfluidic chip for axonal isolation and electrophysiological measurements', *Journal of Neuroscience Methods*. Elsevier B.V., 212(2), pp. 276–282. doi: 10.1016/j.jneumeth.2012.10.013.

Joo, S., Kang, K. and Nam, Y. (2015) 'In vitro neurite guidance effects induced by polylysine pinstripe micropatterns with polylysine background', pp. 2731–2739. doi: 10.1002/jbm.a.35405.

Kamande, J. W. *et al.* (2019) 'Multi-compartment Microfluidic Device Geometry and Covalently Bound Poly-D-Lysine Influence Neuronal Maturation', *Frontiers in Bioengineering and Biotechnology*, 7, pp. 1–9. doi: 10.3389/fbioe.2019.00084.

Kane, K. I. . *et al.* (2018) 'Determination of the rheological properties of Matrigel for optimum seeding conditions in microfluidic cell cultures', *AIP Advances*, 8(12). doi: 10.1063/1.5067382.

Kebschull, J. M. *et al.* (2016) 'A New Defective Helper RNA to Produce Recombinant Sindbis Virus that Infects Neurons but does not Propagate', *Frontiers in Neuroanatomy*, 10(May), pp. 1–7. doi: 10.3389/fnana.2016.00056.

Khalili, V. *et al.* (2016) 'Characterization of mechanical properties of hydroxyapatite – silicon – multi walled carbon nano tubes composite coatings synthesized by EPD on NiTi alloys for biomedical application', *Journal of the Mechanical Behavior of Biomedical Materials*, 59, pp. 337–352. doi: 10.1016/j.jmbbm.2016.02.007.

Kim, H. H. *et al.* (2016) 'Identification of precursor microRNAs within distal axons of sensory neuron', *HHS Public Access*, 134(2), pp. 193–199. doi: 10.1111/jnc.13140.Identification.

Kim, Jitae *et al.* (2014) 'Chemical Rapid prototyping of multifunctional microfluidic cartridges for electrochemical biosensing platforms', *Sensors & Actuators: B. Chemical*. Elsevier B.V., 202, pp. 60–66. doi: 10.1016/j.snb.2014.05.009.

Kim, L. *et al.* (2007) 'A practical guide to microfluidic perfusion culture of adherent mammalian cells.', *Lab on a chip*, 7(6), pp. 681–694. doi: 10.1039/b704602b.

Kim, S., Park, J. and Kang, K. (1995) 'Micropatterned biocompatible materials with applications for cell cultivation', *Journal of Micromechanics and Microengineering*, 5(2), pp. 172–174.

Kim, Y. H. *et al.* (2015) 'A 3D human neural cell culture system for modeling Alzheimer ' s disease', *PROTOCOL*, 10(7). doi: 10.1038/nprot.2015.065.

Kisiswa, L. *et al.* (2017) 'T-type Ca 2+ channels are required for enhanced sympathetic axon growth by TNF a reverse signalling', *Open Biology*, 7(1).

Kneynsberg, A. *et al.* (2016) 'Quantitative and semi-quantitative measurements

of axonal degeneration in tissue and primary neuron cultures', *Journal of Neuroscience Methods*, 266, pp. 32–41. doi: 10.1016/j.jneumeth.2016.03.004.Quantitative.

Knight, V. B. and Serrano, E. E. (2017) 'Hydrogel scaffolds promote neural gene expression and structural reorganization in human astrocyte cultures'. doi: 10.7717/peerj.2829.

Ko, K. R. and Frampton, J. P. (2016) 'Developments in 3D neural cell culture models: the future of neurotherapeutics testing?', *Expert Review of Neurotherapeutics*, 7175(May), pp. 1–3. doi: 10.1586/14737175.2016.1166053.

Kocen, R. *et al.* (2017) 'Viscoelastic behaviour of hydrogel-based composites for tissue engineering under mechanical load', *Biomedical Materials (Bristol)*, 12(2).

Koo, S. *et al.* (2017) 'Laser-assisted biofabrication in tissue engineering and regenerative medicine', *Journal of Materials Research*, 32(1), pp. 128–142. doi: 10.1557/jmr.2016.452.

Koppes, A. N. *et al.* (2016) 'Robust neurite extension following exogenous electrical stimulation within single walled carbon nanotube-composite hydrogels', *Acta Biomaterialia*. Acta Materialia Inc., 39, pp. 34–43. doi: 10.1016/j.actbio.2016.05.014.

Kornev, V. A. *et al.* (2018) 'Hydrogel-assisted neuroregeneration approaches towards brain injury therapy : A state-of-the-art review', *Computational and Structural Biotechnology Journal*. The Authors, 16, pp. 488–502. doi: 10.1016/j.csbj.2018.10.011.

Kos, A. *et al.* (2016) 'Monitoring mRNA Translation in Neuronal Processes Using Fluorescent Non-Canonical Amino Acid Tagging', *Journal of Histochemistry & Cytochemistry*, 64(5), pp. 323 –333. doi: 10.1369/0022155416641604.

Koss, K. M. *et al.* (2017) 'Improved 3D Hydrogel Cultures of Primary Glial Cells for In Vitro Modelling of Neuroinflammation', (December), pp. 1–11. doi: 10.3791/56615.

Kotov, N. A. *et al.* (2009) 'Nanomaterials for neural interfaces', *Advanced Materials*, 21(40), pp. 3970–4004. doi: 10.1002/adma.200801984.

Kunze, A. *et al.* (2011) 'Micropatterning neural cell cultures in 3D with a multi-layered scaffold', *Biomaterials*. Elsevier Ltd, 32(8), pp. 2088–2098. doi: 10.1016/j.biomaterials.2010.11.047.

Laar, V. S. Van *et al.* (2018) 'Evidence for Compartmentalized Axonal Mitochondrial Biogenesis : Mitochondrial DNA Replication Increases in Distal Axons As an Early Response to Parkinson ' s Disease-Relevant Stress', *Journal of Neuroscience*, 38(34), pp. 7505–7515. doi: 10.1523/JNEUROSCI.0541-18.2018.

Lam, D. *et al.* (2019) 'Optimizing cell encapsulation condition in ECM-Collagen I hydrogels to support 3D neuronal cultures', *Journal of Neuroscience Methods*. Elsevier B.V., p. 108460. doi: 10.1016/j.jneumeth.2019.108460.

Lam, D. *et al.* (2020) 'Optimizing cell encapsulation condition in ECM-Collagen I hydrogels to support 3D neuronal cultures', *Journal of Neuroscience Methods*. Elsevier, 329(October 2019), p. 108460. doi: 10.1016/j.jneumeth.2019.108460.

Lambert, C. R. *et al.* (2018) 'Hydrogels with reversible chemical environments for in vitro cell culture', *Biomedical Materials (Bristol)*. IOP Publishing, 13(4). doi: 10.1088/1748-605X/aab45d.

Langhans, S. A. (2018) 'Three-Dimensional in Vitro Cell Culture Models in Drug Discovery and Drug Repositioning', *Frontiers in Pharmacology*, 9(January), pp. 1–14. doi: 10.3389/fphar.2018.00006.

Laplaca, M. C., Vernekar, V. N. and Shoemaker, J. T. (2010) 'Three-Dimensional Neuronal Cultures', in *Methods in Bioengineering: 3D Tissue Engineering*, pp. 187–204.

Lee, J. H. *et al.* (2011) 'Collagen gel three-dimensional matrices combined with adhesive proteins stimulate neuronal differentiation of mesenchymal stem cells', *Journal of the Royal Society Interface*, 8(60), pp. 998–1010.

Lee, K. Y. and Mooney, D. J. (2012) 'Alginate : properties and biomedical applications', *Progress in Polymer Science*, 37(1), pp. 106–126. doi: 10.1016/j.progpolymsci.2011.06.003.Alginate.

Lembong, J. (2018) 'The Evolution of Polystyrene as a Cell Culture Material', *Tissue Engineering - Part B: Reviews*, 24(5), pp. 359–372. doi:

10.1089/ten.teb.2018.0056.

Levinson, H. J. (2005) *Principles of Lithography*. Second. SPIE Press - The International Society for Optical Engineering.

Lewandowska, M. K. *et al.* (2015) 'Recording large extracellular spikes in microchannels along many axonal sites from individual neurons', *PLoS ONE*, 10(3), pp. 1–24. doi: 10.1371/journal.pone.0118514.

Li, C. *et al.* (2018) 'Distal Axonal Proteins and Their Related MiRNAs in Cultured Cortical Neurons', *Molecular Neurobiology*. Molecular Neurobiology, 56(4), pp. 2703–2713.

Li, G. N. *et al.* (2007) 'Genomic and Morphological Changes of Neuroblastoma Cells', *Tissue Engineering*, 13(5), pp. 1035–1047. doi: 10.1089/ten.2006.0251.

Li, H. and Chen, G. (2016) 'In Vivo Reprogramming for CNS Repair: Regenerating Neurons from Endogenous Glial Cells', *Neuron*, 91(4), pp. 728–738. doi: 10.1016/j.neuron.2016.08.004.In.

Li, Y. *et al.* (2015) 'Fibrin Gel as an Injectable Biodegradable Scaffold and Cell Carrier for Tissue Engineering', *Scientific World Journal*, 2015.

Li, Z. *et al.* (2016) 'Assessment of metabolism-dependent drug efficacy and toxicity on a multilayer organs-on-a-chip', *Integrative Biology*. Royal Society of Chemistry, 8(10), pp. 1022–1029. doi: 10.1039/C6IB00162A.

Lin, S. C. *et al.* (2017) 'Production and in vitro evaluation of macroporous , cell-encapsulating alginate fi bres for nerve repair', *MSC*. Elsevier B.V., 73, pp. 653–664. doi: 10.1016/j.msec.2016.12.016.

Lingor, P. *et al.* (2012) 'Axonal degeneration as a therapeutic target in the CNS', *Cell and Tissue Research*, 349(1), pp. 289–311. doi: 10.1007/s00441-012-1362-3.

Links, D. A. (2011) 'Valve-based microfluidic compression platform : single axon injury and regrowth', *Lab on a Chip*, 11, pp. 3888–3895. doi: 10.1039/c1lc20549h.

Liu, J. *et al.* (2016) 'Direct 3D-printing of cell-laden constructs in microfluidic architectures', *Lab Chip*. Royal Society of Chemistry, 16(8), pp. 1430–1438. doi:

10.1039/C6LC00144K.

Liu, W. *et al.* (2008) 'A Microfluidic Chamber for Analysis of Neuron-to-Cell Spread and Axonal Transport of an Alpha-Herpesvirus', *Journal of Neuroscience*, 33(16), pp. 6885–6894. doi: 10.1371/journal.pone.0002382.

Liz, M. A. *et al.* (2014) 'Neuronal deletion of GSK3 β increases microtubule speed in the growth cone and enhances axon regeneration via CRMP-2 and independently of MAP1B and CLASP2', pp. 1–19.

Lowery, L. A. and Vactor, D. Van (2009) 'The trip of the tip : understanding the growth cone machinery', *Nature Reviews Molecular Cell Biology*, 10(5), pp. 332–343. doi: 10.1038/nrm2679.

Lozano, R. *et al.* (2015) '3D printing of layered brain-like structures using peptide modified gellan gum substrates', *Biomaterials*. Elsevier Ltd, 67(1), pp. 264–273. doi: 10.1016/j.biomaterials.2015.07.022.

Lu, Z., Piechowicz, M. and Qiu, S. (2016) 'A Simplified Method for Ultra-Low Density, Long-Term Primary Hippocampal Neuron Culture', *Journal of Visualized Experiments*, 2016(109), pp. 1–8. doi: 10.3791/53797.

Lucci, C. *et al.* (2020) 'Spatiotemporal regulation of GSK3 β levels by miRNA-26a controls axon development in cortical neurons', *Development*, 42, pp. 1–16. doi: 10.1242/dev.180232.

Ma, L. *et al.* (2010) 'A porous 3D cell culture micro device for cell migration study', *Biomedical Microdevices*, 12(4), pp. 753–760. doi: 10.1007/s10544-010-9429-y.

Mackerron, C. *et al.* (2017) 'A Microfluidic Platform for the Characterisation of CNS Active Compounds', *Scientific Reports*. Springer US, 7(1), pp. 1–11. doi: 10.1038/s41598-017-15950-0.

Malda, J. *et al.* (2013) '25th anniversary article: Engineering hydrogels for biofabrication', *Advanced Materials*, 25(36), pp. 5011–5028. doi: 10.1002/adma.201302042.

Maldonado, J. R. and Peckerar, M. (2016) 'X-ray lithography: Some history, current status and future prospects', *Microelectronic Engineering*. Elsevier B.V.,

161, pp. 87–93. doi: 10.1016/j.mee.2016.03.052.

Malheiro, A. *et al.* (2020) 'A three-dimensional biomimetic peripheral nerve model for drug testing and disease modelling', *Biomaterials*. Elsevier Ltd, 257(November 2019), p. 120230. doi: 10.1016/j.biomaterials.2020.120230.

Manuscript, A., Live, F. and Imaging, C. (2015) 'Fluorescence Live Cell Imaging', *Methods Cell Biology*, pp. 77–94. doi: 10.1016/B978-0-12-420138-5.00005-7.Fluorescence.

Marino, A. *et al.* (2015) 'Biomimicry at the nanoscale: current research and perspectives of two-photon polymerization', *Nanoscale*. Royal Society of Chemistry, 7(7), pp. 2841–2850. doi: 10.1039/c4nr06500j.

Marom, A. *et al.* (2015) 'Microfluidic Chip for Site-Specific Neuropharmacological Treatment and Activity Probing of 3D Neuronal "Optonet" Cultures', *Advanced Healthcare Materials*, 4(10), pp. 1478–1483. doi: 10.1002/adhm.201400643.

Marrella, A. *et al.* (2017) 'Enhanced mechanical performances and bioactivity of cell laden-graphene oxide / alginate hydrogels open new scenario for articular tissue engineering applications', *Carbon*. Elsevier Ltd, 115, pp. 608–616. doi: 10.1016/j.carbon.2017.01.037.

Mart, J. I. *et al.* (2017) 'Rapid Fabrication of Disposable Micromixing Arrays Using Xurography and Laser Ablation'. doi: 10.3390/mi8050144.

Martínez-lópez, J. I. *et al.* (2016) 'Xurography as a Rapid Fabrication Alternative for Point-of-Care Devices : Assessment of Passive Micromixers', *Sensors*, 16(5), pp. 1–21. doi: 10.3390/s16050705.

Mastrangelo, R. *et al.* (2020) 'Twin-chain polymer hydrogels based on poly (vinyl alcohol) as new advanced tool for the cleaning of modern and contemporary art', *Proceedings of the National Academy of Sciences of the United States of America*, 117(28). doi: 10.1073/pnas.2011246117.

Matyash, M. *et al.* (2012) 'Novel Soft Alginate Hydrogel Strongly Supports Neurite Growth and Protects Neurons Against Oxidative Stress', *TISSUE ENGINEERING: Part A*, 18. doi: 10.1089/ten.tea.2011.0097.

McDonald, M. *et al.* (2017) 'Diamond microelectrode arrays for in vitro neuronal

recordings', *MRS Communications*, 7(3), pp. 683–690. doi: 10.1557/mrc.2017.62.

Mcgrath, A. M. *et al.* (2010) 'BD PuraMatrix peptide hydrogel seeded with Schwann cells for peripheral nerve regeneration', *Brain Research Bulletin*. Elsevier Inc., 83(5), pp. 207–213. doi: 10.1016/j.brainresbull.2010.07.001.

Meyer, K. and Kaspar, B. K. (2016) 'Glia – neuron interactions in neurological diseases : Testing non-cell autonomy in a dish', *Brain Research*. Elsevier, pp. 1–17. doi: 10.1016/j.brainres.2015.12.051.

Mezger, T. G. (2014) *The Rheology Handbook*. 4th Editio. Hanover: Vincentz Network.

Miebori, T., Unno, N. and Taniguchi, J. (2014) 'Microelectronic Engineering Super resolution technique for sub-100 nm nanoimprint mold via mechanical deformation method', *MICROELECTRONIC ENGINEERING*. Elsevier B.V., 123, pp. 38–42. doi: 10.1016/j.mee.2014.05.022.

Millet, L. J. *et al.* (2010) 'Guiding neuron development with planar surface gradients of substrate cues deposited using microfluidic devices.', *Lab on a chip*, 10(12), pp. 1525–35. doi: 10.1039/c001552k.

Millet, L. J. and Gillette, M. U. (2012a) 'New perspectives on neuronal development via microfluidic environments', *Trends in Neurosciences*. Elsevier Ltd, 35(12), pp. 752–761. doi: 10.1016/j.tins.2012.09.001.

Millet, L. J. and Gillette, M. U. (2012b) 'Over a century of neuron culture: From the hanging drop to microfluidic devices', *Yale Journal of Biology and Medicine*, 85(4), pp. 501–521.

Miranda-saksena, M. *et al.* (2016) 'Dual Role of Herpes Simplex Virus 1 pUS9 in Virus Anterograde Axonal Transport and Final Assembly in Growth Cones in Distal Axons', *Journal of Virology*, 90(5), pp. 2653–2663. doi: 10.1128/JVI.03023-15.Editor.

Morel, M. *et al.* (2012) 'Concentration landscape generators for shear free dynamic chemical stimulation', *Lab on a Chip*, 12(7), pp. 1340–1346. doi: 10.1039/c2lc20994b.

Morelli, S. *et al.* (2019) 'Membrane bioreactor for investigation of

neurodegeneration', *Materials Science & Engineering C*. Elsevier, 103(May), p. 109793. doi: 10.1016/j.msec.2019.109793.

Mosadegh, B. *et al.* (2007) 'Generation of stable complex gradients across two-dimensional surfaces and three-dimensional gels', *Langmuir*, 23(22), pp. 10910–10912. doi: 10.1021/la7026835.

Mou, L. and Jiang, X. (2017) 'Materials for Microfluidic Immunoassays : A Review', *Advanced Healthcare Materials*, 6(15). doi: 10.1002/adhm.201601403.

Murphy, D. B. and Davidson, M. W. (2012) *Fundamentals of Light Microscopy and Electronic Imaging*. Wiley.

Murphy, N. P., Lampe, K. J. and Murphy, N. P. (2015) 'Mimicking biological phenomena in hydrogel- based biomaterials to promote dynamic cellular responses', *Journal of Materials Chemistry B*. Royal Society of Chemistry, 3, pp. 7867–7880. doi: 10.1039/C5TB01045D.

Naghdi, P. *et al.* (2014) 'Survival , proliferation and differentiation enhancement of neural stem cells cultured in three-dimensional polyethylene glycol – RGD hydrogel with tenascin'. doi: 10.1002/term.

Namba, T. *et al.* (2015) 'Extracellular and intracellular signaling for neuronal polarity', *Physiological Reviews*, 95(3), pp. 995–1024. doi: 10.1152/physrev.00025.2014.

Narayanan, J., Xiong, J. Y. and Liu, X. Y. (2006) 'Determination of agarose gel pore size: Absorbance measurements vis a vis other techniques', *Journal of Physics: Conference Series*, 28(1), pp. 83–86. doi: 10.1088/1742-6596/28/1/017.

Natera-naranjo, O. *et al.* (2010) 'Identification and quantitative analyses of microRNAs located in the distal axons of sympathetic neurons', pp. 1516–1529. doi: 10.1261/rna.1833310.1.

Nath, P. *et al.* (2014) 'Polymerase chain reaction compatibility of adhesive transfer tape based microfluidic platforms', pp. 1187–1193. doi: 10.1007/s00542-013-1901-1.

Navaei-nigjeh, M. *et al.* (2013) 'Enhancing neuronal growth from human endometrial stem cells derived neuron-like cells in three-dimensional fibrin gel for

nerve tissue engineering', *Journal of Biomedical Materials Research - Part A*, 102(8), pp. 2533–2543. doi: 10.1002/jbm.a.34921.

Neuville, A. *et al.* (2017) 'Xurography for microfluidics on a reactive solid', *Lab on a Chip*. Royal Society of Chemistry, 17(2), pp. 293–303. doi: 10.1039/C6LC01253A.

Nyoung, D. *et al.* (2016) 'Multifunctional hydrogel coatings on the surface of neural cuff electrode for improving electrode-nerve tissue interfaces', *Acta Biomaterialia*. Acta Materialia Inc., 39, pp. 25–33. doi: 10.1016/j.actbio.2016.05.009.

O'Connor, S. M. *et al.* (2000) 'Primary neural precursor cell expansion , differentiation and cytosolic Ca 2 + response in three-dimensional collagen gel', *Journal of Neuroscience Methods*, 102(2), pp. 187–195.

Ohtake, Y. *et al.* (2018) 'Axonal Activation of the Unfolded Protein Response Promotes Axonal Regeneration Following Peripheral Nerve Injury', *Neuroscience*. The Authors, 375, pp. 34–48. doi: 10.1016/j.neuroscience.2018.02.003.

Ostendorf, A. and Chichkov, B. N. (2006) 'Two-photon polymerization: A new approach to micromachining', *Photonics Spectra*, 40(10), pp. 72–80.

Paranjape, S. R. *et al.* (2019) 'Compartmentalization of Human Stem Cell-Derived Neurons within Pre- Assembled Plastic Microfluidic Chips', *Journal of Visualized Experiments*, 147(May), pp. 1–8. doi: 10.3791/59250.

Parekh, R. and Ascoli, G. A. (2013) 'Neuronal Morphology goes Digital: A Research Hub for Cellular and System Neuroscience', *Neuron*, 77(6), pp. 1017–1038. doi: 10.1016/j.neuron.2013.03.008.Neuronal.

Park, J. *et al.* (2014) 'A microchip for quantitative analysis of CNS axon growth under localized biomolecular treatments', *Journal of Neuroscience Methods*. Elsevier B.V., 221, pp. 166–174. doi: 10.1016/j.jneumeth.2013.09.018.

Park, J. W. *et al.* (2006) 'Microfluidic culture platform for neuroscience research.', *Nature protocols*, 1(4), pp. 2128–36. doi: 10.1038/nprot.2006.316.

Park, J. W. *et al.* (2009) 'Novel microfluidic platform for culturing neurons:

Culturing and biochemical analysis of neuronal components', *Biotechnology Journal*, 4(11), pp. 1573–1577. doi: 10.1002/biot.200900159.

Pas, J. *et al.* (2018) 'Neurospheres on Patterned PEDOT : PSS Microelectrode Arrays Enhance Electrophysiology Recordings', *Advanced Biosystems*, 2(1), pp. 1–11. doi: 10.1002/adbi.201700164.

Pease, R. F. and Chou, S. Y. (2008) 'Lithography and other patterning techniques for future electronics', *Proceedings of the IEEE*, 96(2), pp. 248–270. doi: 10.1109/JPROC.2007.911853.

Peikon, I. D. *et al.* (2017) 'Using high-throughput barcode sequencing to efficiently map connectomes', *Nucleic Acids Research*, 45(12), pp. 1–16. doi: 10.1093/nar/gkx292.

Pensal, M. *et al.* (2017) 'Factors affecting the mechanical behavior of collagen hydrogels for skin tissue engineering', *Journal of the Mechanical Behavior of Biomedical Materials*, 69(December 2016), pp. 85–97. doi: 10.1016/j.jmbbm.2016.12.004.

Pinto, E. *et al.* (2015) 'A Rapid and Low-Cost Nonlithographic Method to Fabricate Biomedical Microdevices for Blood Flow Analysis', pp. 121–135. doi: 10.3390/mi6010121.

Polleux, F. and Snider, W. (2010) 'Initiating and Growing an Axon', *Cold Spring Harbor perspectives in biology*, 2(4), pp. 1–19.

Poon, W. W. *et al.* (2011) 'β-Amyloid impairs axonal BDNF retrograde trafficking', *Neurobiology of Aging*, 32(5), pp. 821–833. doi: 10.1016/j.neurobiolaging.2009.05.012.

Prang, P. *et al.* (2006) 'The promotion of oriented axonal regrowth in the injured spinal cord by alginate-based anisotropic capillary hydrogels', *Biomaterials*, 27, pp. 3560–3569. doi: 10.1016/j.biomaterials.2006.01.053.

Previtera, M. L., Langhammer, C. G. and Firestein, B. L. (2010) 'Effects of substrate stiffness and cell density on primary hippocampal cultures', *Journal of Bioscience and Bioengineering*. The Society for Biotechnology, Japan, 110(4), pp. 459–470. doi: 10.1016/j.jbiosc.2010.04.004.

Price, D. J. *et al.* (2011) *Building Brains : An Introduction to Neural Development*. Edited by et al. Andrew P. Jarman. John Wiley & Sons, Incorporated.

Qian, Y. *et al.* (2019) 'Rheological characterization of the viscoelastic solid-like properties of fresh cement pastes with nanoclay addition', *Theoretical and Applied Fracture Mechanics*. Elsevier, 103(May), p. 102262. doi: 10.1016/j.tafmec.2019.102262.

Qin, J. (2016) 'Assessment of metabolism-dependent drug efficacy and toxicity on a multilayer organs-on-a-chip', *Integrative Biology*. Royal Society of Chemistry, 8(10), pp. 1022–1029. doi: 10.1039/C6IB00162A.

Rahman, M. *et al.* (2010) 'A multiprocess machine tool for compound micromachining', *International Journal of Machine Tools and Manufacture*. Elsevier, 50(4), pp. 344–356. doi: 10.1016/j.ijmachtools.2009.10.007.

Reginensi, D. *et al.* (2015) 'Increased migration of olfactory ensheathing cells secreting the Nogo receptor ectodomain over inhibitory substrates and lesioned spinal cord', *Cellular and Molecular Life Sciences*, 72(14), pp. 2719–2737. doi: 10.1007/s00018-015-1869-3.

Ren, K. *et al.* (2016) 'Injectable Polypeptide Hydrogels with Tunable Microenvironment for 3D Spreading and Chondrogenic Di ff erentiation of Bone-Marrow- Derived Mesenchymal Stem Cells', *Biomacromolecules*, 17(12), pp. 3862–3871. doi: 10.1021/acs.biomac.6b00884.

Ren, K., Zhou, J. and Wu, H. (2013) 'Materials for microfluidic chip fabrication', *Accounts of Chemical Research*, 46(11), pp. 2396–2406. doi: 10.1021/ar300314s.

Reyntjens, S. *et al.* (2000) 'Focused ion beam induced deposition: fabrication of three-dimensional microstructures and Young's modulus of the deposited material', *Journal of Micromechanics and Microengineering*, 10(2), pp. 181–188.

Ribeiro, A. *et al.* (2012) 'Substrate Three-Dimensionality Induces Elemental Morphological Transformation of Sensory Neurons on a Physiologic Timescale', *Tissue Engineering - Part A*, 18(1–2), pp. 93–102. doi: 10.1089/ten.tea.2011.0221.

Roca, S. F. and Cited, R. (2006) '(12) United States Patent', 2(12). doi:

10.1038/incomms1464.

Rothbauer, M. *et al.* (2015) 'Recent advances and future applications of microfluidic live-cell microarrays', *Biotechnology Advances*. Elsevier Inc., 33(6), pp. 948–961. doi: 10.1016/j.biotechadv.2015.06.006.

Rozario, T. and Desimone, D. W. (2010) 'The extracellular matrix in development and morphogenesis : A dynamic view', *Developmental Biology*. Elsevier Inc., 341(1), pp. 126–140. doi: 10.1016/j.ydbio.2009.10.026.

Ruoslahti, E. (1996) 'Brain extracellular matrix.', *Glycobiology*, 6(5), pp. 489–492. doi: 10.1093/glycob/6.5.489.

Ryu, J. R. *et al.* (2018) 'A monitoring system for axonal growth dynamics using micropatterns of permissive and Semaphorin 3F chemorepulsive signals', *Lab on a Chip*. Royal Society of Chemistry, 19(2), pp. 291–305. doi: 10.1039/c8lc00845k.

Saadi, W., Rhee, S. W. and Lin, F. (2007) 'Generation of stable concentration gradients in 2D and 3D environments using a microfluidic ladder chamber', *Biomedical Microdevices*, 9(5), pp. 627–635. doi: 10.1007/s10544-007-9051-9.

Saneinejad, S. and Shoichet, M. S. (1998) 'Patterned glass surfaces direct cell adhesion and process outgrowth of primary neurons of the central nervous system', *Journal of Biomedical Materials Research*, 42(1), pp. 13–19. doi: 10.1002/(SICI)1097-4636(199810)42:1<13::AID-JBM3>3.0.CO;2-R.

Santana, P. P. De *et al.* (2013) 'Fabrication of glass microchannels by xurography for electrophoresis applications', pp. 1660–1664. doi: 10.1039/c3an36540a.

Saracino, G. A. A., Cigognini, D. and Silva, D. (2013) 'Nanomaterials design and tests for neural tissue engineering', *Chem Soc Rev*, pp. 225–262. doi: 10.1039/c2cs35065c.

Schmidt, S. and Friedl, P. (2010) 'Interstitial cell migration : integrin-dependent and alternative adhesion mechanisms', *Cell Tissue Res*, pp. 83–92. doi: 10.1007/s00441-009-0892-9.

Schneider, J. P. *et al.* (2002) 'Responsive hydrogels from the intramolecular

folding and self-assembly of a designed peptide', *Journal of the American Chemical Society*, 124(50), pp. 15030–15037. doi: 10.1021/ja027993g.

Scholl, M. and Spro, C. (2000) 'Ordered networks of rat hippocampal neurons attached to silicon oxide surfaces', *Journal of Neuroscience Methods*, 104, pp. 65–75.

Schurink, B. *et al.* (2017) 'Fabrication and characterization of microsieve electrode array (μSEA) enabling cell positioning on 3D electrodes', *Journal of Micromechanics and Microengineering*. IOP Publishing. doi: 10.1088/0960-1317/27/1/015017.

Sciancalepore, A. G. *et al.* (2016) 'Micropatterning control of tubular commitment in human adult renal stem cells', *Biomaterials*. Elsevier Ltd, 94, pp. 57–69. doi: 10.1016/j.biomaterials.2016.03.042.

Shamloo, A., Mohammadaliha, N. and Mohseni, M. (2015) 'Integrative Utilization of Microenvironments , Biomaterials and Computational Techniques for Advanced Tissue Engineering', *Journal of Biotechnology*. Elsevier B.V., 212, pp. 71–89. doi: 10.1016/j.jbiotec.2015.08.005.

Shari, F. *et al.* (2016) 'Polycaprolactone Microfibrous Scaffolds to Navigate Neural Stem Cells', *Biomacromolecules*, 17(10), pp. 3287–3297. doi: 10.1021/acs.biomac.6b01028.

Shi, M. *et al.* (2013) 'Glia co-culture with neurons in microfluidic platforms promotes the formation and stabilization of synaptic contacts.', *Lab on a chip*, 13(15), pp. 3008–21. doi: 10.1039/c3lc50249j.

Skoog, S. A., Goering, P. L. and Narayan, R. J. (2014) 'Stereolithography in tissue engineering', *Journal of Materials Science: Materials in Medicine*, 25(3), pp. 845–856. doi: 10.1007/s10856-013-5107-y.

Southam, K. A. *et al.* (2015) 'Microfluidic primary culture model of the lower motor neuron–neuromuscular junction circuit', *Neuromethods*. Elsevier B.V., 103(2), pp. 181–193. doi: 10.1007/978-1-4939-2510-0_11.

Spaulding, E. L. and Burgess, R. W. (2017) 'Accumulating Evidence for Axonal Translation in Neuronal Homeostasis', *Frontiers in Neuroscience*, 11(May), pp. 1–8. doi: 10.3389/fnins.2017.00312.

Stoeckli, E. T. (2018) ‘Understanding axon guidance : are we nearly there yet ?’, *Development (Cambridge)*, 145(10). doi: 10.1242/dev.151415.

Stubbe, M. *et al.* (2015) ‘Biosensors and Bioelectronics The effect of hyperbaric air on the electric activity of neuronal in vitro networks’, *Biosensors and Bioelectronic*. Elsevier, 73, pp. 153–159. doi: 10.1016/j.bios.2015.05.052.

Stulen, C. W. G., Sweeney, D. and Attwood, D. (1998) ‘Extreme ultraviolet lithography’, *Journal of vacuum science & technology. B, Microelectronics and nanometer structures processing, measurement and phenomena*, 16(6), pp. 3142–3149. doi: 10.1116/1.590453.

Sugiyama, E., Yao, I. and Setou, M. (2017) ‘Visualization of local phosphatidylcholine synthesis within hippocampal neurons using a compartmentalized culture system and imaging mass spectrometry’, *Biochemical and Biophysical Research Communications*. Elsevier Ltd, 495(1), pp. 1048–1054. doi: 10.1016/j.bbrc.2017.11.108.

Sun, J. and Tan, H. (2013) ‘Alginate-Based Biomaterials for Regenerative Medicine Applications’, *Materials*, 6(4), pp. 1285–1309. doi: 10.3390/ma6041285.

Sundaramoorthy, V. *et al.* (2020) ‘Novel role of SARM1 mediated axonal degeneration in the pathogenesis of rabies’, *Scientific Reports*, 16(2), pp. 1–20. doi: 10.1371/journal.ppat.1008343.

Takano, T., Funahashi, Y. and Kaibuchi, K. (2019) ‘Neuronal Polarity : Positive and Negative Feedback Signals’, *Frontiers in Cell and Developmental Biology*, 7(April), pp. 1–10. doi: 10.3389/fcell.2019.00069.

Takayama, Y. *et al.* (2012) ‘Network-wide integration of stem cell-derived neurons and mouse cortical neurons using microfabricated co-culture devices’, *BioSystems*. Elsevier Ireland Ltd, 107(1), pp. 1–8. doi: 10.1016/j.biosystems.2011.08.001.

Tang, Y. *et al.* (2017) ‘Patch method for culture of primary hippocampal neurons’, *Microelectronic Engineering*. Elsevier B.V., 175, pp. 61–66. doi: 10.1016/j.mee.2017.01.012.

Taylor, A. M. *et al.* (2003) ‘Microfluidic multicompartment device for neuroscience research’, *Langmuir*, 19(5), pp. 1551–1556. doi: 10.1021/la026417v.

Taylor, A. M. *et al.* (2005) 'A microfluidic culture platform for CNS axonal injury, regeneration and transport.', *Nature methods*, 2(8), pp. 599–605. doi: 10.1038/nmeth777.

Taylor, A. M. *et al.* (2009) 'Axonal mRNA in uninjured and regenerating cortical mammalian axons.', *The Journal of neuroscience : the official journal of the Society for Neuroscience*, 29(15), pp. 4697–707. doi: 10.1523/JNEUROSCI.6130-08.2009.

Taylor, Anne M *et al.* (2010) 'Microfluidic local perfusion chambers for the visualization and manipulation of synapses', *Neuron*, 66(1), pp. 57–68. doi: 10.1016/j.neuron.2010.03.022.Microfluidic.

Taylor, Anne M. *et al.* (2010) 'Microfluidic Local Perfusion Chambers for the Visualization and Manipulation of Synapses', *Neuron*. Elsevier Ltd, 66(1), pp. 57–68. doi: 10.1016/j.neuron.2010.03.022.

Taylor, A. M., Rhee, S. W. and Jeon, N. L. (2006) 'Microfluidic Chambers for Cell Migration and Neuroscience Research', *Methods in Molecular Biology*. Humana Press, 321, pp. 167–177.

Teixeira, A. I. *et al.* (2009) 'The promotion of neuronal maturation on soft substrates', *Biomaterials*, 30, pp. 4567–4572. doi: 10.1016/j.biomaterials.2009.05.013.

Tibbitt, Mark W and Anseth, K. S. (2009) 'Hydrogels as Extracellular Matrix Mimics for 3D Cell Culture', *Biotechnology and Bioengineering*, 103(4), pp. 655–663. doi: 10.1002/bit.22361.

Tibbitt, M.W. and Anseth, K. S. (2009) 'Hydrogels as Extracellular Matrix Mimics for 3D Cell Culture', *Biotechnology and Bioengineering*, 103(4), pp. 655–663. doi: 10.1002/bit.22361.Hydrogels.

Ting, X. *et al.* (2013) 'On-chip investigation of cell – drug interactions', *Advanced Drug Delivery Reviews*. Elsevier B.V., 65(11–12), pp. 1556–1574. doi: 10.1016/j.addr.2013.02.001.

Tobergte, D. R. and Curtis, S. (2013) *Introduction to Microfabrication Techniques*, *Journal of Chemical Information and Modeling*. doi: 10.1017/CBO9781107415324.004.

Toh, A. G. G. *et al.* (2014) 'Engineering microfluidic concentration gradient generators for biological applications', *Microfluidics and Nanofluidics*, 16(1–2), pp. 1–18. doi: 10.1007/s10404-013-1236-3.

Tolstik, E. *et al.* (2016) 'Studies of silicon nanoparticles uptake and biodegradation in cancer cells by Raman spectroscopy', *Nanomedicine: Nanotechnology, Biology, and Medicine*. Elsevier Inc., 12(7), pp. 1931–1940. doi: 10.1016/j.nano.2016.04.004.

Tonge, D. . *et al.* (1997) 'Effects of Extracellular Matrix Components on Axonal Outgrowth from Peripheral Nerves of Adult Animals in Vitro', *Experimental Neurology*, 146(90), pp. 81–90.

Ueno, Y. *et al.* (2012) 'Axonal outgrowth and dendritic plasticity in the cortical peri-infarct area after experimental stroke', *Stroke*, 43(8), pp. 2221–2228. doi: 10.1161/STROKEAHA.111.646224.

Vahidi, B. *et al.* (2008) 'Microfluidic-based strip assay for testing the effects of various surface-bound inhibitors in spinal cord injury', *Journal of Neuroscience Methods*, 170(2), pp. 188–196. doi: 10.1016/j.jneumeth.2008.01.019.

Verhulsel, M. *et al.* (2014) 'A review of microfabrication and hydrogel engineering for micro-organs on chips', *Biomaterials*. Elsevier Ltd, 35(6), pp. 1816–1832. doi: 10.1016/j.biomaterials.2013.11.021.

Virlogeux, A. *et al.* (2018) 'Reconstituting Corticostriatal Network on-a-Chip Reveals the Contribution of the Presynaptic Compartment to Huntington's Disease', *Developmental Dynamics*, 22(1), pp. 110–122. doi: 10.1002/dvdy.24665.

Walker, C. A. *et al.* (2018) 'A b 1 – 42 triggers the generation of a retrograde signaling complex from sentinel mRNAs in axons', *EMBO Reports*, 19(7), pp. 1–13. doi: 10.15252/embr.201745435.

Wang, B. *et al.* (2017) 'Fabrication of elastomer pillar arrays with height gradient for cell culture studies', *Microelectronic Engineering*. Elsevier B.V., 175, pp. 50–55. doi: 10.1016/j.mee.2017.01.014.

Wang, J. *et al.* (2009) 'Microfluidics: a new cosset for neurobiology.', *Lab on a chip*, 9(5), pp. 644–652. doi: 10.1039/b813495b.

Wang, J. *et al.* (2015) 'Label-Free Isolation and mRNA Detection of Circulating Tumor Cells from Patients with Metastatic Lung Cancer for Disease Diagnosis and Monitoring Therapeutic E ffi cacy', *Analytical Chemistry*, 87, pp. 11893–11900. doi: 10.1021/acs.analchem.5b03484.

Wang, T. *et al.* (2015) 'Control of Autophagosome Axonal Retrograde Flux by Presynaptic Activity Unveiled Using Botulinum Neurotoxin Type A', *Journal of Neuroscience*, 35(15), pp. 6179–6194. doi: 10.1523/JNEUROSCI.3757-14.2015.

Wang, X. *et al.* (2012) 'Hyaluronic acid-based scaffold for central neural tissue engineering', *Interface Focus*, 2(3), pp. 278–291. doi: 10.1098/rsfs.2012.0016.

Ware, T. *et al.* (2012) 'Fabrication of Responsive, Softening Neural Interfaces', *Advanced Functional Materials*, 22(16), pp. 3470–3479. doi: 10.1002/adfm.201200200.

Watson, P. M. D. *et al.* (2017) 'Bioengineered 3D Glial Cell Culture Systems and Applications for Neurodegeneration and Neuroinflammation', *SLAS Discovery*, 22(5), pp. 583–601. doi: 10.1177/2472555217691450.

Wei, J. *et al.* (2017) 'Microelectronic Engineering Fabrication of PLGA nano fi bers on PDMS micropillars for neuron culture studies', *Microelectronic Engineering*. Elsevier B.V., 175, pp. 67–72. doi: 10.1016/j.mee.2017.01.015.

Weibel, D. B., Diluzio, W. R. and Whitesides, G. M. (2007) 'Microfabrication meets microbiology', *Nature Reviews Microbiology*, 5(3), pp. 209–18. doi: 10.1038/nrmicro1616.

Wevers, N. R. *et al.* (2016) 'High-throughput compound evaluation on 3D networks of neurons and glia in a microfluidic platform', *Scientific Reports*, 6(August), pp. 1–10. doi: 10.1038/srep38856.

Worthington, K. S. *et al.* (2015) 'Prevascularized silicon membranes for the enhancement of transport to implanted medical devices', pp. 1602–1609. doi: 10.1002/jbm.b.33506.

Wu, S. *et al.* (2017) 'Three-dimensional hyaluronic acid hydrogel-based models for in vitro human iPSC-derived NPC culture and differentiation', *Journal of Materials Chemistry B*. Royal Society of Chemistry, 5(21), pp. 3870–3878. doi: 10.1039/c7tb00721c.

Wu, S., Serbin, J. and Gu, M. (2006) 'Two-photon polymerisation for three-dimensional micro-fabrication', *Journal of Photochemistry and Photobiology A: Chemistry*, 181(1), pp. 1–11. doi: 10.1016/j.jphotochem.2006.03.004.

Xia, Y. *et al.* (1999) 'Unconventional Methods for Fabricating and Patterning Nanostructures.', *Chemical reviews*, 99(7), pp. 1823–1848. doi: 10.1021/cr980002q.

Xia, Y. and Whitesides, G. M. (1998) 'Soft Lithography', *Angewandte Chemie*, 37(5), pp. 550–575.

Xu, T. *et al.* (2006) 'Viability and electrophysiology of neural cell structures generated by the inkjet printing method', *Biomaterials*, 27(19), pp. 3580–3588. doi: 10.1016/j.biomaterials.2006.01.048.

Xu, T. *et al.* (2009) 'Electrophysiological characterization of embryonic hippocampal neurons cultured in a 3D collagen hydrogel', *Biomaterials*. Elsevier Ltd, 30(26), pp. 4377–4383. doi: 10.1016/j.biomaterials.2009.04.047.

Xue, P. *et al.* (2016) 'Isolation and retrieval of circulating tumor cells on a microchip with double parallel layers of herringbone structure', *Microfluidics and Nanofluidics*. Springer Berlin Heidelberg, 20(12), pp. 1–9. doi: 10.1007/s10404-016-1834-y.

Y, X. and Whitesides, G. M. (1998) 'Soft Lithography', in *Annual Review of Material Science*, pp. 1–33. doi: 10.1146/annurev.matsci.28.1.153.

Yamada, A. *et al.* (2016) 'In-mold patterning and actionable axo-somatic compartmentalization for on-chip neuron culture', *Lab on a chip*, 16(11), pp. 2059–2068. doi: 10.1039/x0xx00000x.

Yamada, K. M. and Cukierman, E. (2007) 'Modeling Tissue Morphogenesis and Cancer in 3D', *Cell*, 130(4), pp. 601–610. doi: 10.1016/j.cell.2007.08.006.

Yamada, S. A. and Descroix, S. (2016) 'Transient microfluidic compartmentalization using actionable microfilaments for biochemical assays, cell culture and organs-on-chip', *Lab on a Chip*. Royal Society of Chemistry, 16, pp. 4691–4701. doi: 10.1039/C6LC01143H.

Yamagishi, S. *et al.* (2016) 'Stripe Assay to Study the Attractive or Repulsive

Activity of a Protein Substrate Using Dissociated Hippocampal Neurons', *Journal of Visualized Experiments*, 2016(112), pp. 1–7. doi: 10.3791/54096.

Yamamoto, N., Tamada, A. and Murakami, F. (2002) 'Wiring of the brain by a range of guidance cues', *Progress in Neurobiology*, 68(6), pp. 393–407.

Yang, H. I. *et al.* (2012) 'Axon Myelination and Electrical Stimulation in a Microfluidic , Compartmentalized Cell Culture Platform', pp. 112–118. doi: 10.1007/s12017-012-8170-5.

Yang, K. *et al.* (2013) 'A microfluidic array for quantitative analysis of human neural stem cell self-renewal and differentiation in three-dimensional hypoxic microenvironment', *Biomaterials*. Elsevier Ltd, 34(28), pp. 6607–6614. doi: 10.1016/j.biomaterials.2013.05.067.

Yang, S. *et al.* (2016) 'Cell response on the biomimetic scaffold of silicon nano- and micro-topography', *Journal of Materials Chemistry B*. Royal Society of Chemistry, 4(Cvd), pp. 1891–1897. doi: 10.1039/C5TB02361K.

Yang, Y. *et al.* (2010) 'Pre-synaptic regulation of astroglial excitatory neurotransmitter transporter GLT1', *Neuron*, 61(6), pp. 880–894. doi: 10.1016/j.neuron.2009.02.010.Pre-synaptic.

Yao, P. J. *et al.* (2015) 'Dendrosomatic Sonic Hedgehog Signaling in Hippocampal Neurons Regulates Axon Elongation', *Journal of Neuroscience*, 35(49), pp. 16126–16141. doi: 10.1523/JNEUROSCI.1360-15.2015.

Yap, Y. C. *et al.* (2017) 'Mild and repetitive very mild axonal stretch injury triggers cystoskeletal mislocalization and growth cone collapse', *PLos ONE*, 12(5), pp. 1–19.

Yi, J. J. *et al.* (2010) 'TGF-β Signaling Specifies Axons during Brain Development', *Cell*. Elsevier Ltd, 142(1), pp. 144–157. doi: 10.1016/j.cell.2010.06.010.

Ylä-outinen, L. *et al.* (2014) 'Three-dimensional growth matrix for human embryonic stem cell-derived neuronal cells', *JOURNAL OF TISSUE ENGINEERING AND REGENERATIVE MEDICINE*, 8(May 2012), pp. 186–194. doi: 10.1002/term.

Ylä-outinen, L. *et al.* (2019) 'Screening of Hydrogels for Human Pluripotent Stem Cell – Derived Neural Cells : Hyaluronan-Polyvinyl Alcohol-Collagen-Based Interpenetrating Polymer Network Provides an Improved Hydrogel Scaffold', *Macromolecular Bioscience*, 19(7), pp. 1–13. doi: 10.1002/mabi.201900096.

Yoshida, T. and Ohki, K. (2020) 'Natural images are reliably represented by sparse and variable populations of neurons in visual cortex', *Nature Communications*. Springer US, 11(1). doi: 10.1038/s41467-020-14645-x.

Yu, L. M. Y., Leipzig, N. D. and Shoichet, M. S. (2008) 'Promoting neuron adhesion and growth', *Materials Today*. Elsevier Ltd, 11(5), pp. 36–43. doi: 10.1016/S1369-7021(08)70088-9.

Yu, S. B. *et al.* (2016) 'Polymer Thin Films with Tunable Acetylcholine-like Functionality Enable Long- Term Culture of Primary Hippocampal Neurons', *ACS nano*, 10(11), pp. 9909–9918. doi: 10.1021/acsnano.6b03527.

Zaman, M. H. *et al.* (2006) 'Migration of tumor cells in 3D matrices is governed by matrix stiffness along with cell-matrix adhesion and proteolysis', 103(29).

Zhang, Y. *et al.* (2013) 'The MicroRNA-17 – 92 Cluster Enhances Axonal Outgrowth in Embryonic Cortical Neurons', *Journal of Neuroscience*, 33(16), pp. 6885–6894. doi: 10.1523/JNEUROSCI.5180-12.2013.

Zhang, Y. *et al.* (2015) 'MicroRNAs in the axon locally mediate the effects of chondroitin sulfate proteoglycans and cGMP on axonal growth', *Developmental Neurobiology*, 75(12), pp. 1402–1419. doi: 10.1002/dneu.22292.MicroRNAs.

Zheng, Y. *et al.* (2019) 'Somatic autophagy of axonal mitochondria in ischemic neurons', *The Journal of cell biology*, 218(6), pp. 1891–1907.

Zhu, J. and Marchant, R. E. (2012) 'Design properties of hydrogel tissue-engineering scaffolds', *Expert Rev Med Devices*, 8(5), pp. 607–626. doi: 10.1586/erd.11.27.Design.

Zuidema, J. M. *et al.* (2014) 'A protocol for rheological characterization of hydrogels for tissue engineering strategies', *Journal of Biomedical Materials Research - Part B Applied Biomaterials*, 102(5), pp. 1063–1073. doi: 10.1002/jbm.b.33088.

Chapter 9 Appendices

9.1 Appendix 1

The samples are placed between two parallel plates, where the bottom plate is stationary and the upper plate moves back and forth by the shear force applied. The upper plate applies a force based on a sinusoidal shear deformation. The oscillation sweeps are based on Hooke's Law, which states that a proportional relationship exists between stress and strain. For ideal elastic solids, Hooke's Law implies that the shear stress (σ) is directly proportional to the shear strain (γ):

$$\sigma = G\,\gamma$$

The proportional constant G (Pa) is the shear modulus, a measure of the resistance to deformation. G is the vector sum that characterises the viscoelastic behaviour, being the result of storage modulus (G') and the loss modulus (G''), as shown in **Figure 70**. The viscoelastic materials consist of an elastic portion, which is represented by G' and viscous portion; represented by G'' (Mezger, 2014).

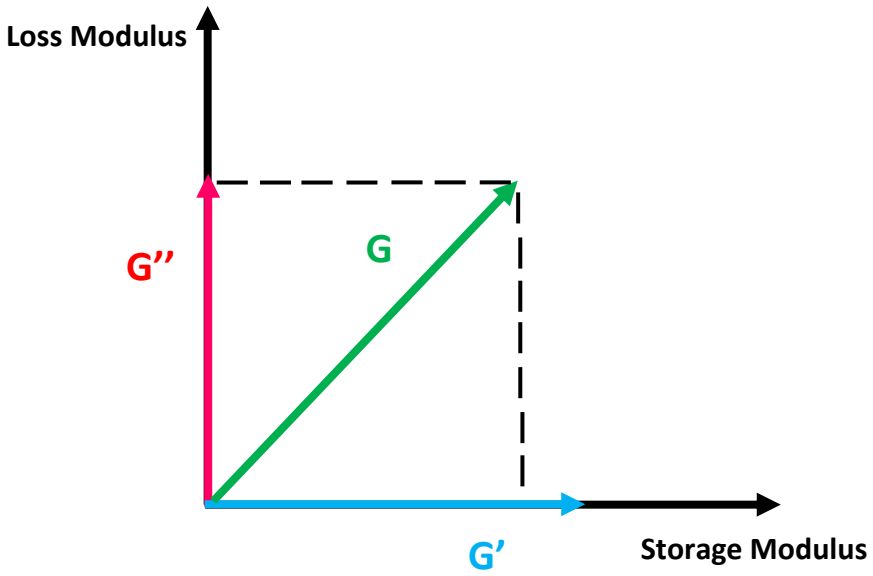


Figure 70 – Schematic representation of the vector diagram showing the components G' and G'', which result vector is the shear modulus G.

9.2 Appendix 2

Table 8 – List of the materials used in this PhD work.

Materials
Glass coverslips
XONA devices
PDMS
Polycarbonate porous membrane 5 um pore x 47 mm
Biopsy punch
Neurobasal buffer solution
Neurobasal B27 Supplement
Glutamax
Poly-O-Lysine (POL)
Fluorescein
Paraformaldehyde
Agarose Low melting
Matrigel

Table 9 – List of the equipment used in this PhD work.

Equipment
Inverted microscope
Dissection microscope
Plotter Cutter
Desiccator
Confocal microscope

9.3 Appendix 3

Table 10 – List of the software used in this PhD work.

Software
SolidWorks (2016)
Graphpad Prism (7.0)
ImageJ (FIJI)
MatLab (2016)
OriginPro (9.1)
KLayout
Huygens
Rheoplus software (3.6)

9.4 Appendix 4

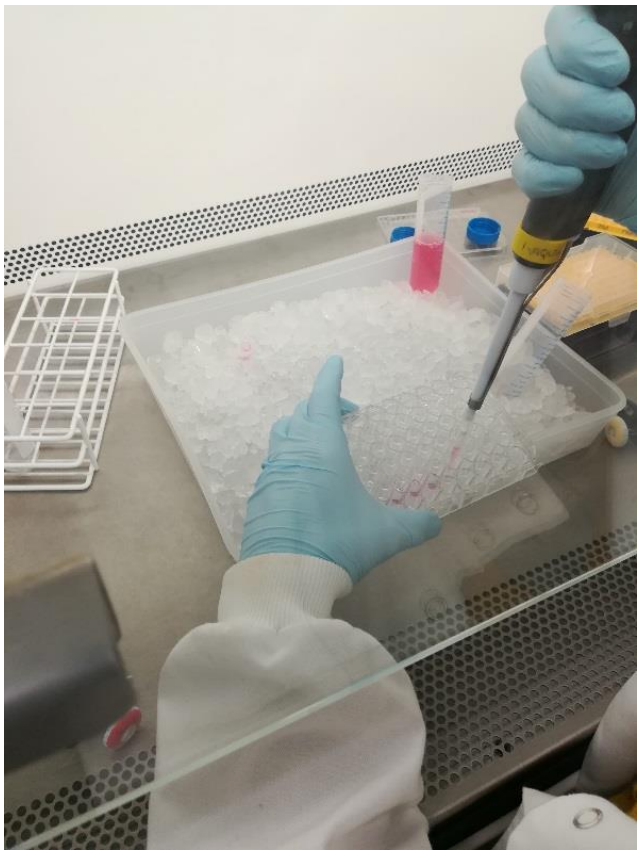


Figure 71 – Setup of Matrigel manipulation, where media, Matrigel and well plates and devices, are placed in a recipient filled with ice.

9.5 Appendix 5

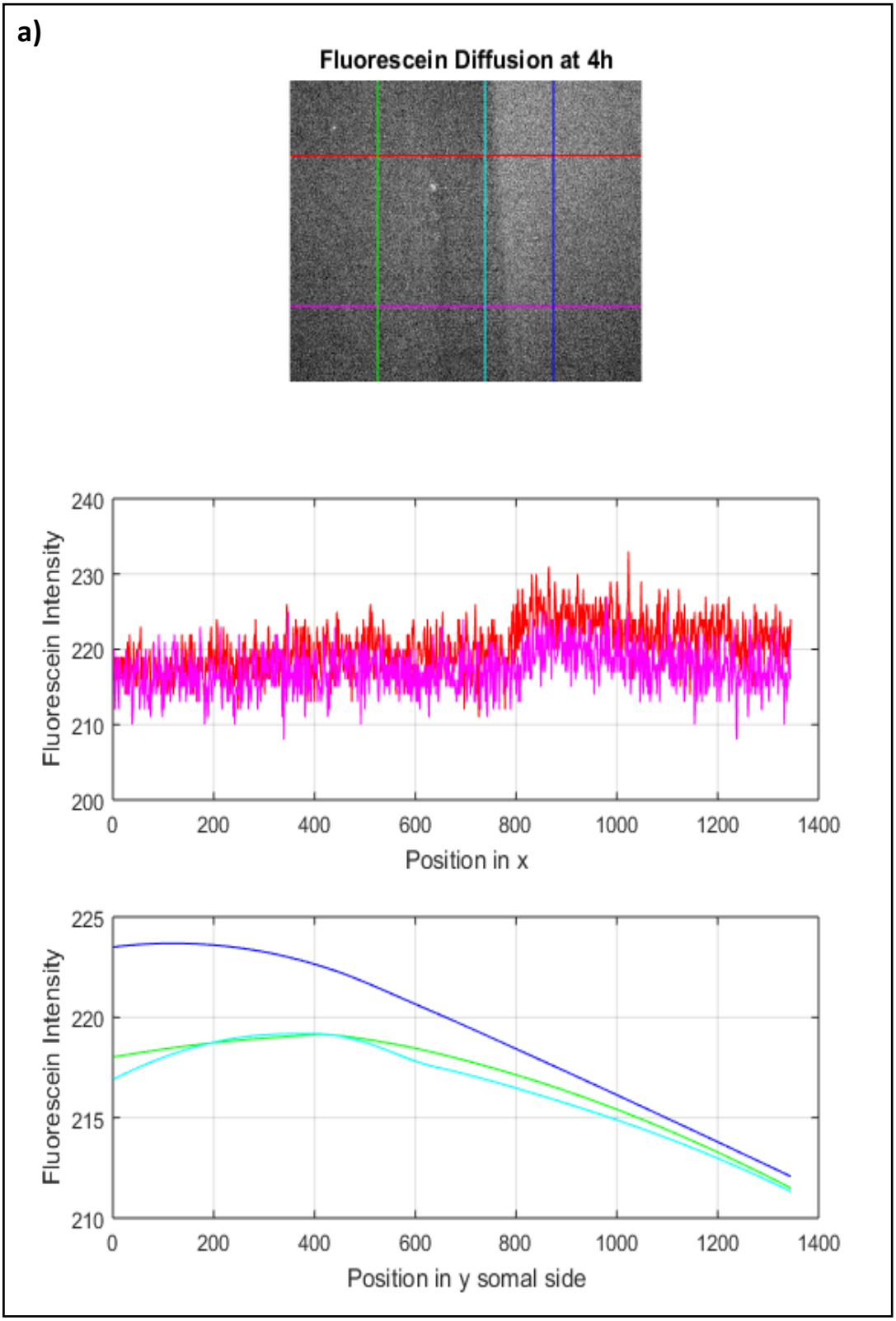


Figure 72 – Fluorescence intensity for 3D conditions in XONA devices at 4 hours.

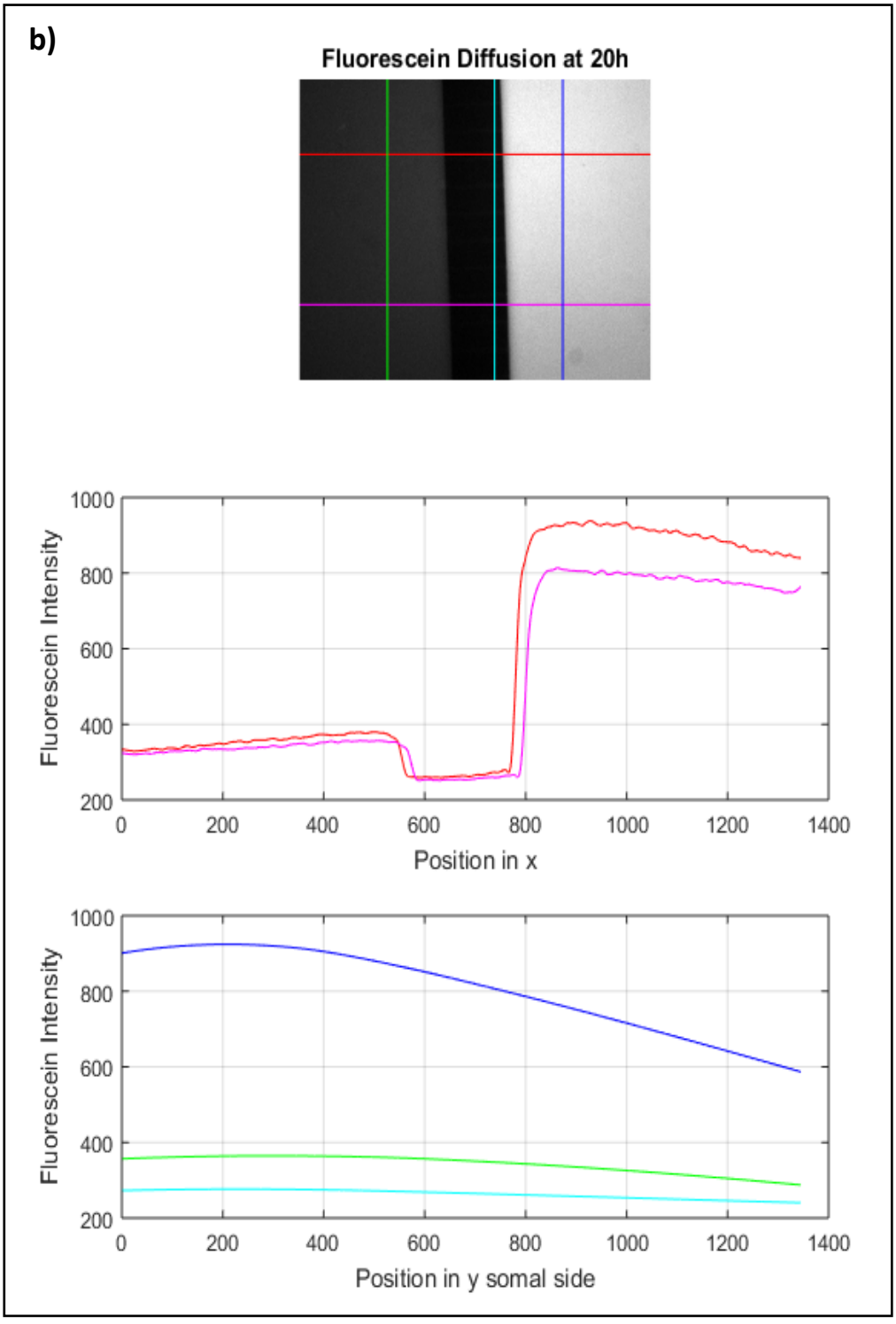


Figure 73 – Fluorescence intensity for 3D conditions in XONA devices at 20 hours.

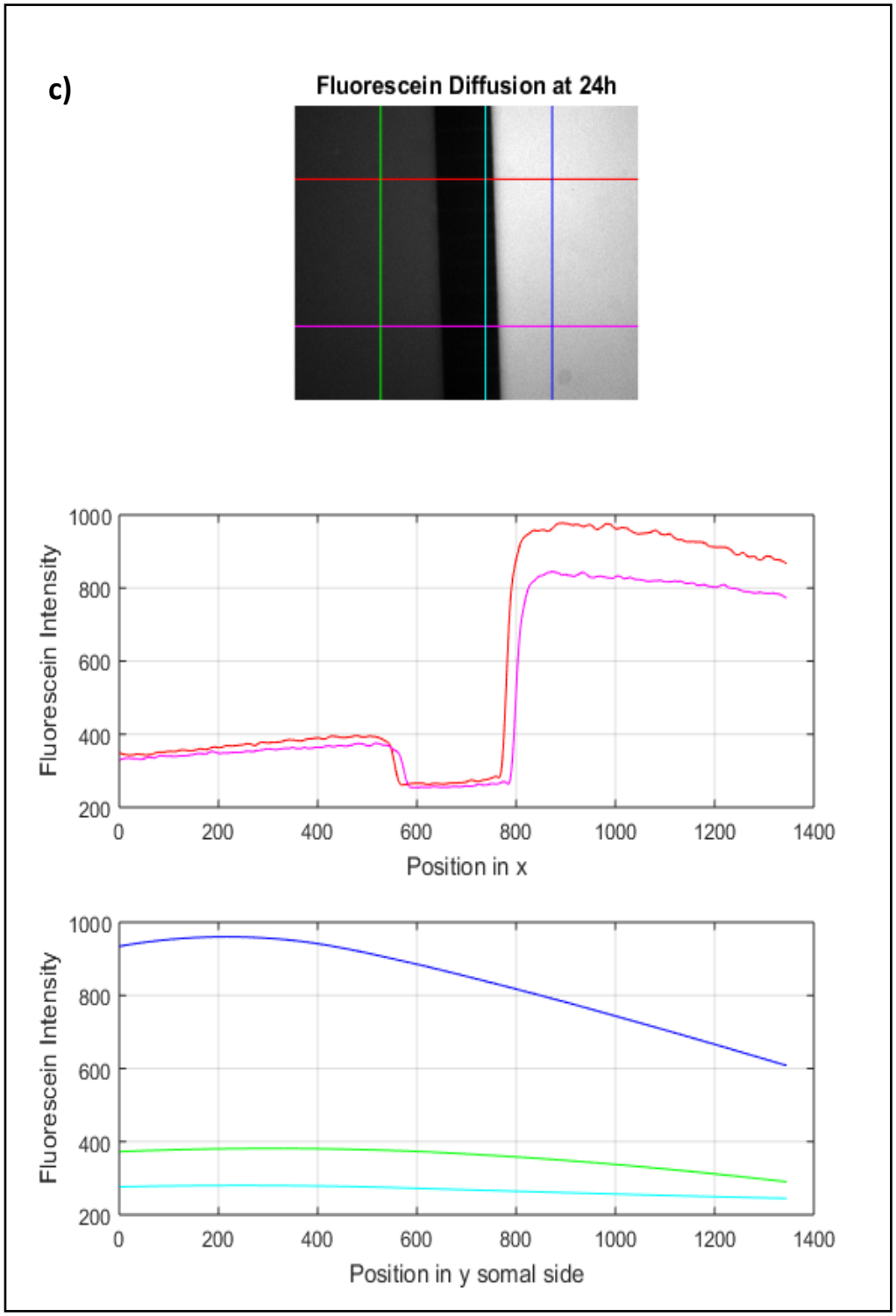


Figure 74 – Fluorescence intensity for 3D conditions in XONA devices at 24 hours.

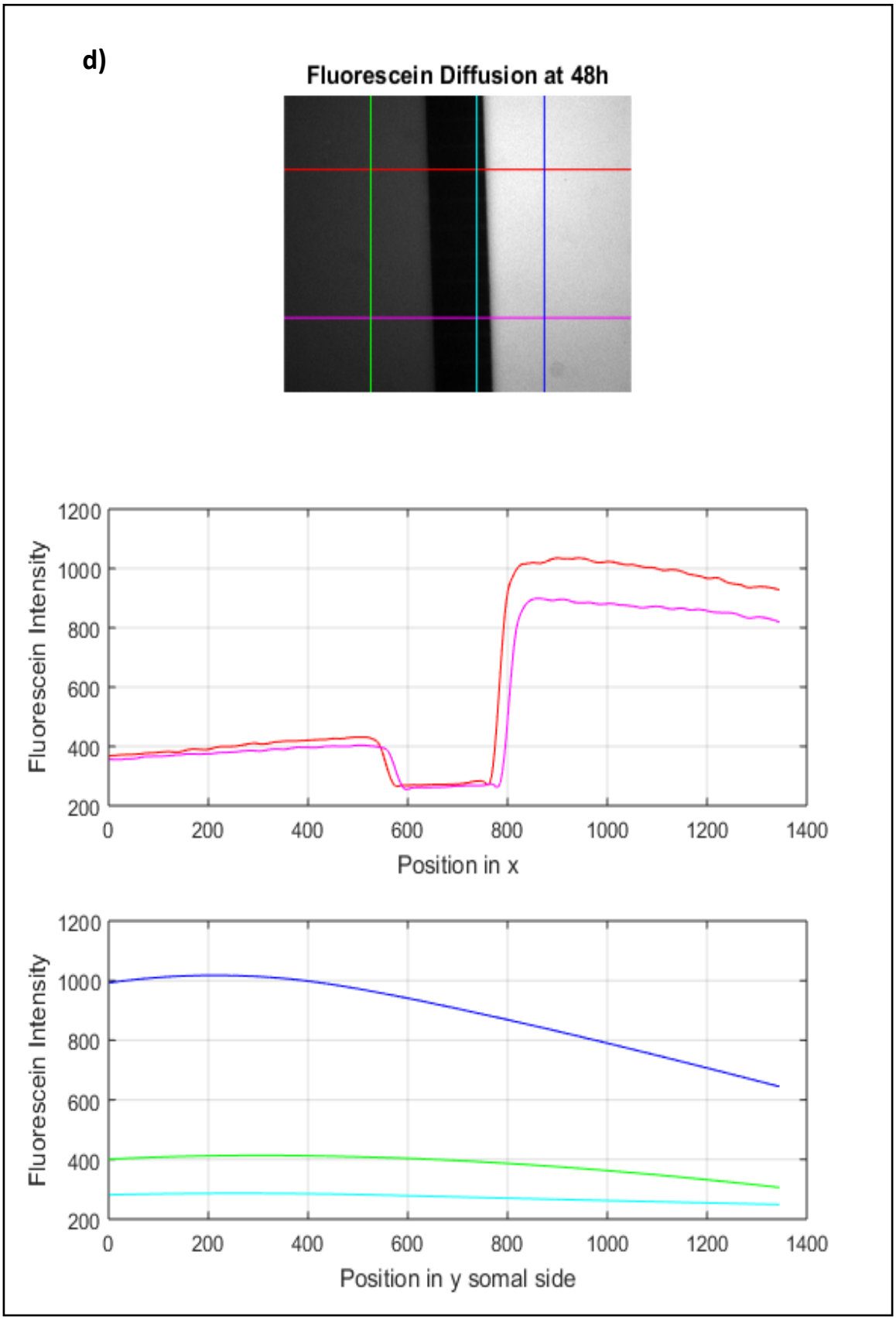


Figure 75 – Fluorescence intensity for 3D conditions in XONA devices at 48 hours.

9.6 Appendix 6

The viscoelastic behaviour was characterised for agarose (at 1%; 0.75%; 0.5%) and Matrigel (at 7mg/ml; 5 mg/ml). The viscosity was plotted in function of the applied shear rate for the different concentrations of Agarose and Matrigel, **Figure 76**. The flow curves present a shear thinning behaviour, where the viscosity decreases with the increase of shear rate, which is typical to find on polymer solutions. This behaviour was also observed in Matrigel solutions by Kane *et al.* (Kane *et al.*, 2018). The shearing is deforming the polymeric chains, which start to disentangle with the shear direction. The deformation of the chains caused by the shearing, leads to the decrease in viscosity values. Besides, the higher the hydrogel concentration value presented higher viscosity values. At rest, the Agarose and Matrigel present a solid structure with the higher viscosity value, which correspond to 249 Pa·s for the 5mg/ml Matrigel and to 348 Pa·s for 0.5% agarose.

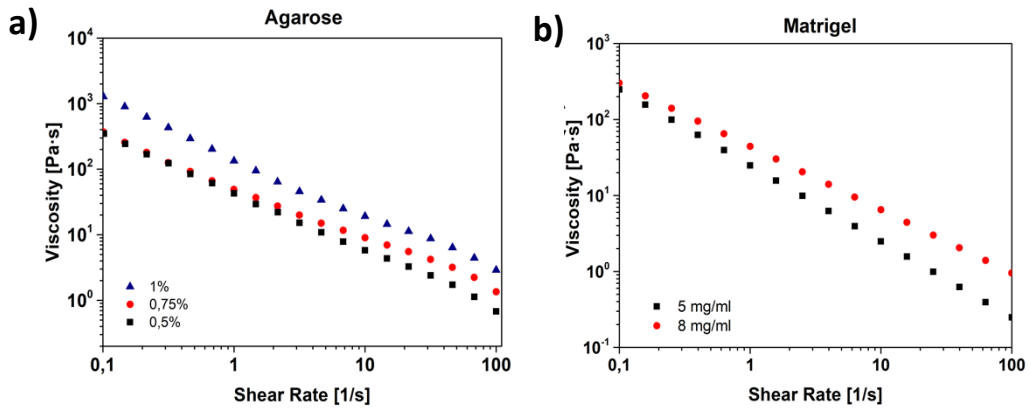


Figure 76 – Flow curves of agarose 1%, 0.75%, 0.5% (**a**) and Matrigel at 8 mg/ml and 5 mg/ml (**b**) at a constant temperature of 37°C.

9.7 Appendix 7

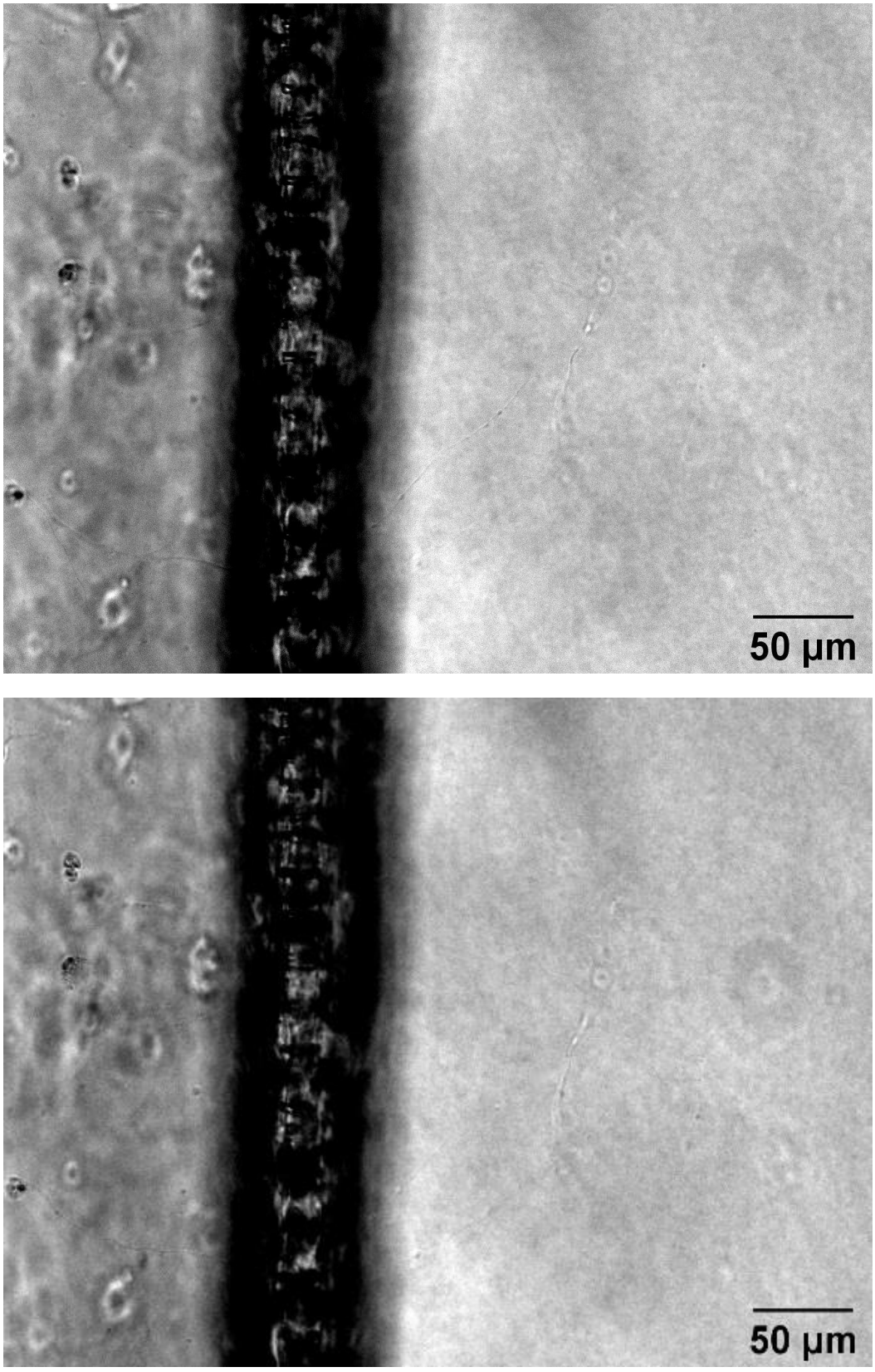


Figure 77 – Phase contrast images showing 3D axonal isolation, where axons are isolated growing in 3D.

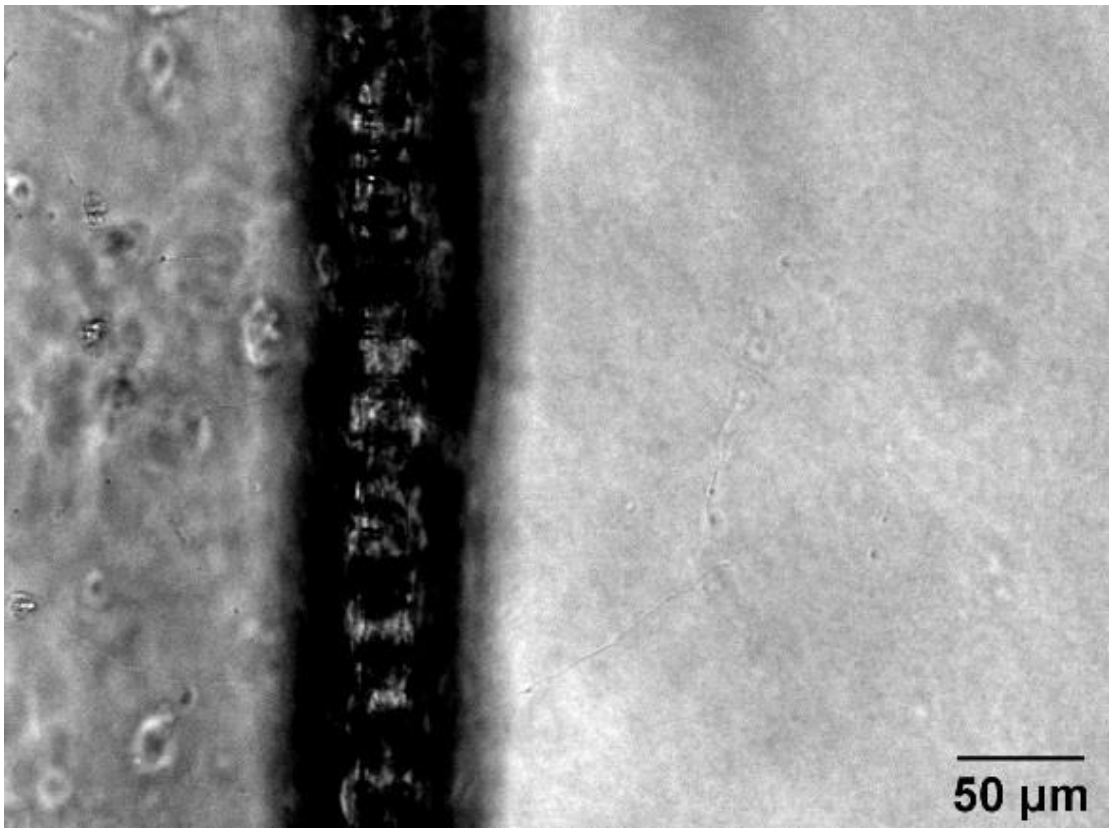


Figure 78 – Continuation of the image from **Figure 77.**